ulm university universität ulm

Controlled Supramolecular Assembly of Peptides via Chemical Reactions

Kumulative Dissertation

Zur Erlangung des Doktorgrades Dr. rer. nat.
im Fachbereich Chemie der
Fakultät für Naturwissenschaften der Universität Ulm

vorgelegt von
Michaela Pieszka (M. Sc.)
geboren in Ellwangen (Jagst)

April 2021

Dissertation der Universität Ulm

Amtierender Dekan: Prof. Dr. Thorsten Bernhardt
Erstgutachterin: Prof. Dr. Tanja Weil
Zweitgutachter: Prof. Dr. Mika Lindén
Drittgutachterin: Prof. Dr. Patricia Dankers

Datum der Verteidigung: 21. März 2022

Abstract

Peptide assembly is an emerging tool for designing novel biomaterials with extraordinary properties. Biocompatibility and biodegradability are key requirements for application in biomedicine and can often be achieved by utilizing peptide-based materials. Furthermore, the simplicity of peptide synthesis and the ease of chemical modification as well as the cost- and time efficiency and monodispersity of peptides contribute to the popularity of these compounds in recent years. The diversity of oligopeptides that form various nanostructures offers new opportunities to tailor material properties in order to accomplish many different tasks. Additionally, introducing stimuli responsive moieties can lead to greater control by using internal and external triggers *in vivo,* yielding in assembly, disassembly, degradation or rearrangement of peptide nanostructures. While some amino acids intrinsically can respond to ambient factors such as pH and redox environment, introducing non-natural amino acids and other chemical modifications expands the palette of stimulus-responsive properties of peptide assemblies.

Within this thesis, the controlled assembly and disassembly of peptides was investigated using multiple biologically relevant triggers such as pH and oxidative stress. Peptides from different classes of pro-assembling compounds were synthesized incorporating different stimulus-responsive chemical modifications or amino acids and the compounds were subsequently examined for the controlled formation of nanostructures.

In the first chapter, the self-assembly of an amphiphilic peptide KIKISQINM is prevented upon introduction of a kink into the primary sequence by replacing one amide bond in the amino acid chain with a carboxylic ester in the side chain of serine, giving a so-called *depsipeptide*. After hydrolytic removal of a protecting group from the N-terminus, a physiological pH induced *O,N*-acyl shift within the amino acid sequence leads to self-assembly into fibrillar architectures. Oxidation of methionine into methionine sulfoxide by naturally abundant hydrogen peroxide causes an imbalance between hydrophobic and hydrophilic amino acid side chains and electrostatic repulsion between peptides, which leads to partial destruction of β-sheets and subsequent disassembly of peptide fibers. This study shows how simple chemical tools can be exploited for orthogonal, controlled peptide assembly and disassembly and lays foundation for following studies on responsive peptide materials.

Subsequently, in the second project using the depsipeptide approach, assembly of short aromatic peptides is prevented by a boronic acid secured kink in the primary sequence. The boronic acid enables dynamic covalent conjugation with a salicylhydroxamate functionalized cell-penetrating peptide, which leads to uptake of two pro-assembling peptide sequences by A549 cancer cells. Depsipeptides are released into the cytosol by pH triggered hydrolytic removal of the delivery vehicle. The boronic acid caging group is removed by endogenous hydrogen peroxide which leads to an *O,N*-acyl shift unleashing the assembling peptide

sequences. Co-assembly of the peptides inside cancer cells leads to formation of fluorescent fibres that have a detrimental effect on cell morphology and viability, which opens the pathway for potential applications in high oxidative stress related diseases.

Finally, the assembly of complementary peptide strands utilizing pH-responsive boronic acid-catechol chemistry is presented. Here, various numbers of L-3,4-dihydroxyphenylalanine and L-boronophenylalanine were incorporated into peptide sequences in order to elucidate the influence of multivalency and order of amino acids in the primary sequence on binding affinity. Peptides with the possibility of divalent and trivalent binding showed significantly enhanced affinities towards each other, while no binding occurred using mismatched peptide sequences. Furthermore, trivalent binding exhibited similar affinity as binding of eight base pair long DNA strands. The enhanced binding affinity, higher backbone stability, ease of further chemical modification and molecular recognition of these sequences could be beneficial for use as synthetic DNA mimics and could further be utilized for programming macromolecular assemblies, which was shown within this study by dynamic covalent conjugation of polymers to proteins.

In summary, this thesis presents multiple approaches for controlled peptide assembly processes including disassembly using various peptide types and triggers. Here, dynamic covalent and immolation chemistry of boronic acids was utilized to assemble and disassemble peptides on demand using the biologically relevant triggers pH, salt concentration and hydrogen peroxide. The utility of such compounds for application in biomedicine was shown by intracellular assembly as well as by creating dynamic covalently bound conjugates between peptides or between proteins and polymers with biological relevance.

Table of Contents

1 Introduction

1.1 Assembly of Peptides

1.1.1 General Introduction to Peptides

Nature requires only twenty-one building blocks in the form of α-amino acids to generate peptides and proteins which offer a great variety of complex biological functions, for example, in the cardiovascular and nervous system, immunological processes and the intestines. Among other tasks, peptides are involved in cell-communication, immune response, feeling of pain, metabolism and reproduction, which makes them essential for life.[1] Besides their ubiquitous presence in living systems, peptides have gained popularity in treatment of various medical conditions such as diabetes, HIV (human immunodeficiency virus), cancer and autoimmune diseases.[2],[3],[4],[5],[6]

Peptides are built up by the formation of amide bonds between carboxy and amine groups of amino acids. Here, sequences of up to 10 monomers are classified as oligopeptides, while longer amino acids chains are called polypeptides. Amino acid sequences with more than 50 monomers are classified as proteins, which are folded into unique tertiary and quaternary structures and extend the diversity of physiological and biochemical functions of peptides.[1]

The biosynthesis of peptides and proteins starts with the transcription, where a gene is converted into messenger ribonucleic acid (mRNA) by RNA polymerases inside the cell nucleus. Afterwards, mRNA is transported into the cytoplasm, where it is read by ribosomes and translated into the amino acid sequence of the peptide or protein. Subsequently, the enzyme catalyzes the formation of amide bonds between amino acids to form the respective biomolecule.[7] Due to the growing interest in peptides for application in various fields, new methods for peptide synthesis were developed as the isolation from natural sources bears danger of contamination with viruses and suffers from low accessibility to higher quantities of tissues.[1] While ring opening polymerization offers high quantities of polypeptides, the products lack sequence precision compared to genetical engineering.[8] Besides biotechnological techniques for the synthesis of sequence-defined peptides, solid-phase peptide synthesis (SPPS) also offers the possibility of generation of high quantities of monodispersed peptides with defined sequence and functionality. SPPS was introduced by Merrifield in 1963 and was further optimized by microwave-assistance affording higher purities and reaction rates.[9],[10] Taking advantage of orthogonal protecting groups, the peptide is build-up stepwise on a polymer resin from the *C*- to the *N*-terminus and subsequently cleaved from the solid support.

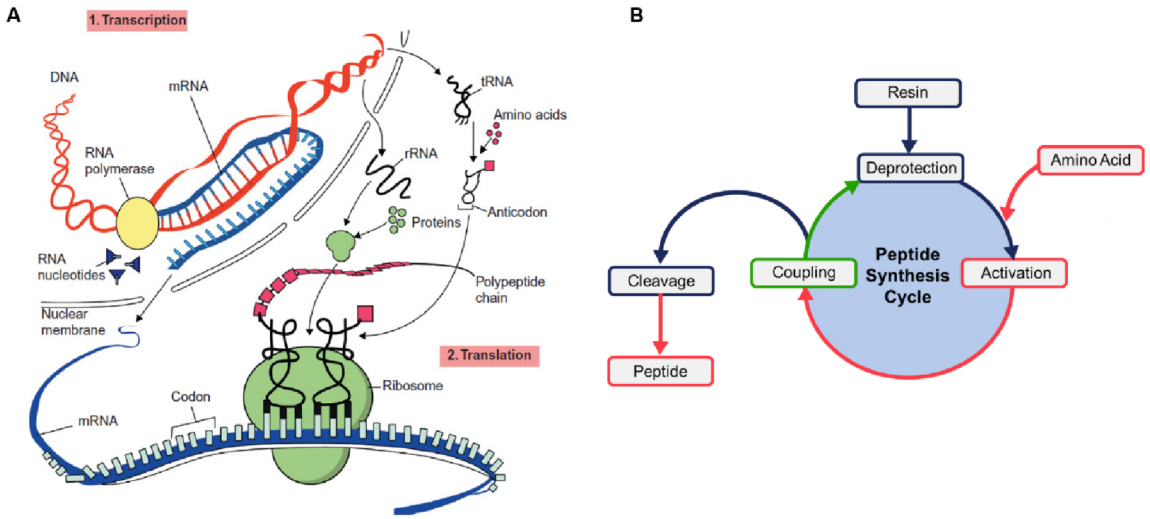

Figure 1: Schematical depiction of peptide synthesis. A) Biosynthesis, B) solid-phase peptide synthesis. A) Reprinted from "Human Biochemistry" by G. Litwack, chapter "Protein Biosynthesis", page 324, 2018, with permission from Elsevier. The image was reproduced by G. Litwack from http://www.rpdp.net/sciencetips_v3/images/L8A1_clip_image002.gif.[11] B) Reproduced from https://egbc-images.s3-eu-west-1.amazonaws.com/content/w620/171019.png "Peptide Synthesis Market Overview, Growth, Demand and Forecast Research Report to 2022".

In order to expand nature's toolbox of building blocks, non-natural amino acids as well as other modifications such as dyes, aromatic groups, polymers, fatty acids, saccharides and drugs can be incorporated into the peptide sequence using SPPS. The facile synthetic access and the versatility of peptides lays the foundation for the administration of these biomolecules as drugs or for drug delivery, where they play a role in cellular targeting. Furthermore, peptide-derived materials, generated upon formation of nanoarchitectures by self-assembly, found use in gene therapy, tissue engineering, 3D cell culture, imaging and sensing as well as many other applications.[12] Further advantages of peptide materials which contribute to their widespread use are their biodegradability, low toxicity of the degradation products and low immunogenicity.[13] The half-life of peptides which are assembled into nanostructures has been reported to be increased in comparison to their monomeric form. Additionally, assembly may enhance bioactivity of peptides by a multivalency effect.[12] Due to these benefits there has been a huge interest in developing novel peptide assembly-based materials in recent years which will be further discussed in the following chapters beginning with the foundation of peptide assembly to an in-depth view into its applications.

1.1.2 Supramolecular Interactions between Peptides

The versatility of functional groups in amino acid side chains offers the possibility for peptides to engage in various non-covalent interactions in an intra- and intermolecular fashion. Charged amino acids such as negatively charged aspartic acid (Asp, D) and glutamic acid (Glu, E) as well as positively charged histidine (His, H), lysine (Lys, K) and arginine (Arg, R) can form ionic interactions with oppositely charged ions.[14] Ionic

interactions are the strongest non-covalent interactions (200-300 kJ·mol^{-1}) and can even be stronger than some covalent bonds. They can be both attractive and repulsive and therefore have a strong influence on peptide assembly. Other electrostatic interactions can be formed between ions and dipoles (50-200 kJ·mol^{-1}) as well as dipoles with other dipoles (5-50 kJ·mol^{-1}), however these are weaker than ion-ion interactions.[15]

Hydrogen bonds are one of the most important non-covalent interactions in peptide assembly and are the predominant force in stabilizing secondary structures of peptides. For the same reason, they are also important in protein folding.[8] Amino acids which contain hydrophilic side chain functional groups like serine (Ser, S), threonine (Thr, T), glutamine (Gln, Q) and asparagine (Asn, N) can interact by forming hydrogen bonds. These interactions can also be formed in the peptide backbone by C=O and N-H residues of amide bonds.[14] Hydrogen bonds are dipole-dipole interactions (4-120 kJ·mol^{-1}) which form between a hydrogen atom and a strongly electronegative atom such as oxygen, nitrogen and sulfur.[15],[16] When hydrogen is bound to an electron-rich atom, the covalent bond is polarized which is the reason why hydrogen displays electropositive properties.

π-π interactions, which are based on the interaction of the π-electron cloud and the σ-framework of aromatic compounds, can be formed between aromatic side chain residues of tyrosine (Tyr, Y), tryptophan (Trp, W) and phenylalanine (Phe, F).[14],[15] The strength of π-π-interactions can reach up to 50 kJ·mol^{-1}. π-Systems are also able to interact with cations, which can be even stronger that π-π-interactions as they possess strengths of 5-80 kJ·mol^{-1}.[15] Formation of these non-covalent bonds is especially important in building-up the tertiary structure of proteins, where the delocalized electron density of aromatic amino acids interacts with metal ions.[16]

Lastly, hydrophobic interactions can be found between amino acids with hydrophobic side chains such as alanine (Ala, A), leucine (Leu, L), isoleucine (Ile, I), valine (Val, V) and methionine (Met, M).[14] Hydrocarbon groups can interact by exclusion of polar residues and solvents, which leads to assembly into hydrophilic and hydrophobic regions in proteins and amphiphilic peptides. This property makes them one of the main driving forces for self-assembly of peptide chains.[8]

Peptide assembly is strongly influenced by the solvent as the strength of intermolecular interactions is highly dependent on solvent polarity. While the strength of hydrogen bonds and ion-ion interactions are decreased in polar solvents like water, the hydrophobic effect is enhanced with solvent polarity. Meanwhile, π-π interactions are robust in both water and organic solvents. Therefore, combination of different non-covalent interactions provides the best solution for peptide assembly into ordered structures.[17],[18]

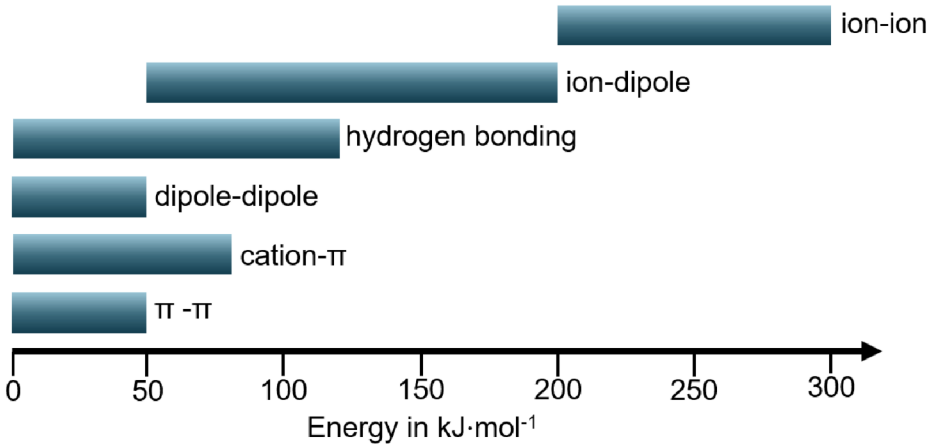

Figure 2: Representation of energies of non-covalent interactions.[15]

The above described non-covalent interactions dictate the assembly processes by intermolecular connection of peptide strands. The use of non-covalent interactions instead of covalent chemical bonds is a key advantage of supramolecular assembly of peptides into ordered structures, as the reversibility of these interactions offers the possibility for error correction in the stacking arrangement. If covalent irreversible connections were to be used, kinetically trapped mismatches would propagate and therefore could prevent formation of well-ordered structures.[19]

The stacking arrangement of the peptides influences the final supramolecular nanostructure. Inspired by protein folding, synthetic peptides can be designed to mimic the formation of β-sheets, α-helices and coiled-coils by adopting different stacking arrangements. As proteins consist of a long peptide chain, they will intramolecularly organize into their tertiary structure and might interact with other polypeptides to create a quaternary structural motif.[20] On the other hand, stacks of oligopeptides can further arrange into nanostructures such as fibres, tubes, worms, sheets, tapes and spheres like micelles and vesicles, and furthermore potentially can form hydrogels (see Figure 3).[21], [14]

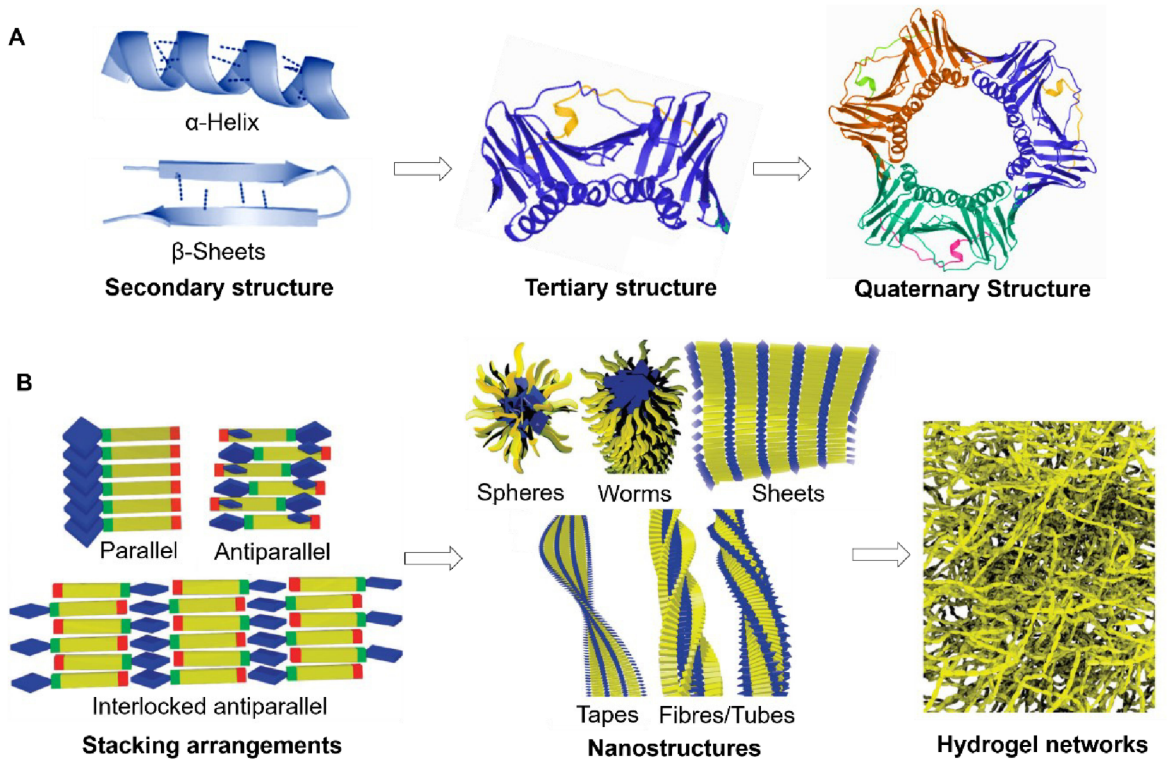

Figure 3: Secondary, tertiary and quaternary structure of proteins based on non-covalent interactions (A) and stacking arrangements of peptide amphiphiles leading to supramolecular nanostructure formation, which eventually can result in hydrogelation (B). A) Protein secondary structures were adapted from "Mechanics of proteins with a focus on atomic force microscopy" by Rico et al.[22] (https://jnanobiotechnology.biomedcentral.com/articles/10.1186/1477-3155-11-S1-S3#rightslink) with minor changes. The copyright (2013) belongs to Rico et al., licensee BioMed Central Ltd., the article was published by Springer Nature. This is an open access article under the CC BY license (https://creativecommons.org/licenses/by/2.0/). Protein tertiary and quaternary structures were adapted from the RCSB protein data bank and were found under "1AXC". B) Adapted from Ref.[14] with permission from The Royal Society of Chemistry.

Unnatural amino acids as well as chemical modifications can further extend intermolecular interactions and support peptide assembly. For example, the installation of hydrophobic head groups such as alkyl tails and aromatic systems can drive assembly processes and has been excessively used for peptide-based biomaterials. These will be discussed among other systems in chapter 1.1.3.

1.1.3 Peptide Nanostructures and their Applications

Assembly of proteins, which are essentially polypeptides, is ubiquitous in nature. Tubulin proteins assemble into filamentous structures to form microtubules, which are important for intracellular motion and positioning of organelles.[23] Another intracellular protein assembly is observed in actin filaments, which are part of the cytoskeleton and therefore contribute to the shaping of cells.[24] Taking inspiration from naturally occurring assemblies, various systems have been developed for peptide self- and co-assembly in order to create biomaterials with unique properties. Designer peptides have been developed to tune the assembly into ordered structures with various shapes depending on the desired application, for example into peptide fibers (Figure 4).

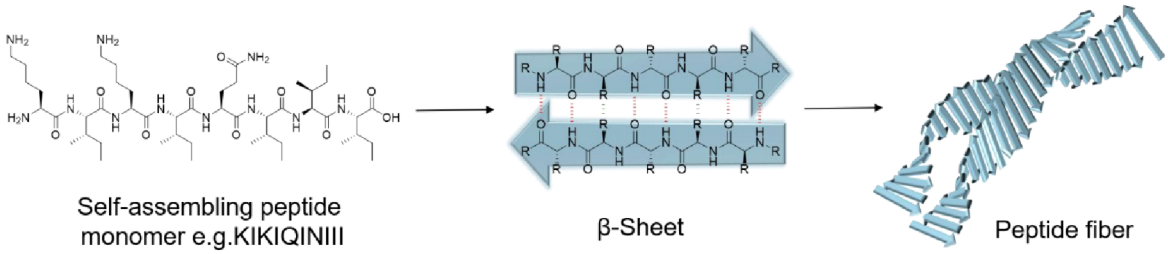

Figure 4: Intermolecular interactions between peptide strands lead to formation of β-sheets and further self-assembly into fibers.[25]

The biodegradability of peptides as well as the ease of functionalization with targeting moieties makes them highly interesting for drug delivery for example in cancer therapy.[8] Here, the ability of peptides to assemble into hollow structures like nanotubes or nanovesicles provides the possibility for drug loading which is especially useful for delivery of poorly water-soluble drugs, as they can be encapsulated inside the hydrophobic core of self-assembled peptide amphiphiles.[8],[26] Alternatively, the drug can be covalently bound to the peptides.[27] Similar to encapsulation of small molecular drugs, oligonucleotides could be encapsulated or bound to self-assembling peptides, offering the possibility of such conjugates to be used in gene therapy.[28] Furthermore, drug-loaded injectable peptide-based hydrogels can be applied locally at the tumor site which improves the safety and efficacy of treatment by a slow release at the targeted area.[8] Improved cellular uptake of peptide nanostructures and targeting of disease sites can be achieved by conjugation of cell-penetrating and targeting peptides, proteins or aptamers.

The next chapters will give an insight into different types of self-assembling peptides and their applications. Additionally, incorporation of stimulus responsive residues into the peptides can provide control over self-assembly using triggers such as changes in pH, temperature or redox environment, which also will be discussed.[29]

1.1.1.1 Short Aromatic Peptide Amphiphiles

Alzheimer's disease is a neurodegenerative disorder distinguished by plaques in the brain which mainly consist of fibrillar amyloid β-peptide. Here, aromatic π–π interactions play a crucial role in the supramolecular assembly of the 40-42 amino acid long peptide into fibrils.[30] Derived from Alzheimer's β-amyloid peptide, diphenylalanine (FF) has gained popularity as a versatile building block for peptide assembly and is the shortest known self-assembling peptide sequence.[24] Aromatic stacking between phenylalanine side chains in FF leads to self-assembly into tubes and spheres, while chemical modification of the dipeptide can alter its architecture.[24],[31],[14] Addition of a Fmoc modification on the *N*-terminus leads to formation of fibrous hydrogels with good physical properties[32], which was

shown to support the growth of cells and was used in combination with Fmoc-RGD to help cell proliferation and spreading (Figure 5).[33]

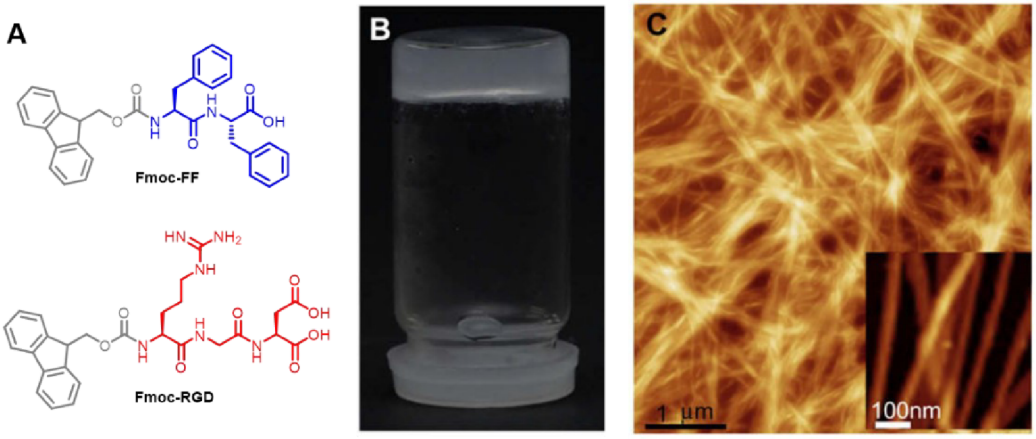

Figure 5: A) Chemical structure of Fmoc-FF and Fmoc-RGD. B) Hydrogel formed by co-assembly of the peptides and atomic force microscopy (AFM) image of the gel consisting of fibrous networks (C). Reprinted from "Self-assembled peptide-based hydrogels as scaffolds for anchorage-dependent cells" by Zhou et al.,[33] *Biomaterials*, *30* (**2009**), 2526, with permission from Elsevier.

In general, many Fmoc-capped short peptides are able to rapidly form supramolecular and stable conjugates with each other via π-π-stacking and hydrophobic interactions.[34],[35],[36],[37],[38] Aromatic amino acids can improve self-assembly as well as stability due to π-π-interactions between Fmoc and the aromatic rings in the side chains, therefore they have been studied and utilized intensively. However, peptides with non-aromatic amino acids in the peptide sequence are also frequently used for self-assembly.[39],[14] Depending on the amino acid sequence, different nanoarchitectures can be engineered. Many Fmoc protected short peptides have been reported to form fibrous hydrogels, which makes them particularly interesting for tissue regeneration and engineering. Low molecular weight hydrogelators offer many advantages for applications *in vivo* such as low bioaccumulation, facile renal clearance and requirement of only low peptide concentrations for hydrogelation.[40] Fmoc-FF hydrogel nanoparticles, which have been fabricated using an inverse-emulsion technique and stabilized by a surfactant, were envisioned to act as drug delivery systems by encapsulation of doxorubicin or 5-fluorouracil.[41] Furthermore, the ability for compound encapsulation can be exploited by utilizing the hydrophobic interior of Fmoc-peptide based assemblies for catalytic reactions.[42] While many peptide hydrogels have been reported to be biocompatible, some exhibited toxicity towards cells which can be utilized for controlling cellular growth.[43],[44],[45] While both Fmoc-FF and Fmoc-RGD can form fibrous hydrogels, other amino acids promote formation of spherical structures, for example Fmoc-FS(tBu) and Fmoc-FP.[24] This shows that self-assembly of aromatic short peptides is very susceptible to small changes in the molecular structures, where changing one functional group or sometimes even only one atom can have a severe influence on structure formation. These changes can arise from

variations in hydrophobicity or aromaticity, as well as the order of the amino acids in the primary sequence which influences intermolecular hydrogen bonds between peptides. Furthermore, enhanced flexibility of the primary sequence by incorporation of glycine next to the *N*-terminus can lead to less molecular order and therefore changes in the architecture.[14]

Besides Fmoc, other aromatic groups on the *N*-terminus can also lead to self-assembly of short peptides. Some examples of aromatics that provide the necessary hydrophobic and π-π stacking interactions, which are required for self-assembly of most short peptides, are naphthalene, pyrene, azobenzene and phenothiazine.[43],[46],[47],[48] Changing the aromatic residue can provide additional functions such as fluorescence for imaging or stimulus responsiveness. Furthermore, combination of different peptides with each other or molecules such as drugs and polymers by co-assembly offers the possibility for fine-tuning not only the physical properties of the material such as hydrogelation, fluorescence or thermo-responsiveness, but also can introduce additional functions such as anti-inflammatory activity.[49],[50]

1.1.1.2 Peptides with Alternating Hydrophobic and Hydrophilic Residues

Some proteins are able to self-assemble into insoluble amyloid fibers which exhibit remarkable resistance towards degradation. These fibers primarily consist of β-sheets which are stacked perpendicular to the fiber axis and stabilized by hydrogen bonds. Although formation of these structures has been associated to medical conditions such as Alzheimer's disease, Diabetes type 2 and Parkinson's disease, they also display beneficial characteristics which are useful for biomedical applications.[51],[52] Amyloid fibers have been successfully utilized as synthetic extracellular matrices, hydrogels, as well as for drug delivery and bioelectronic devices.[53],[54],[55],[25],[56] Similar fibers are formed by amphiphilic peptides which contain alternating hydrophobic and hydrophilic amino acids residues in their primary sequence.[57] Self-assembly of these oligopeptides is driven by shielding of the unpolar side chain functional groups from water,[58] which leads to formation of amyloid nanofibers containing a β-sheet secondary structure.[25] They have been utilized for many applications such as gene transduction, cell culture and tissue engineering.[59],[60],[61],[62] Based on the desired function, the compounds can be either positively or negatively charged and further modified using functional ligands such as fluorophors, biotin, cysteine or maleimides for further functionalization.[60],[63],[49]

Peptide sequences containing alternating hydrophobic and hydrophilic amino acids such as Fmoc-KIKIQI, CKFKFQF and RGDKIKIQIC have been shown to enhance nerve fiber growth of neurons, which were derived from the peripheral nervous system (PNS) of mice, by acting as a scaffold for cell growth and adhesion. *In vivo* studies showed that injured

facial nerves of mice, which are responsible for movement of the whiskers, could be regenerated and the ability to move the whiskers was recovered upon injection of self-assembled peptide fibers into the injury site, where they remained for several weeks due to their high tissue adhesiveness. Since the peptide fibers did not trigger an immune response and no addition of growth factors or hormones was required to enhance neuronal regrowth, this strategy might be a promising candidate for tissue engineering with low cost and has also been investigated for other cell types such as bone and stem cells.[63]

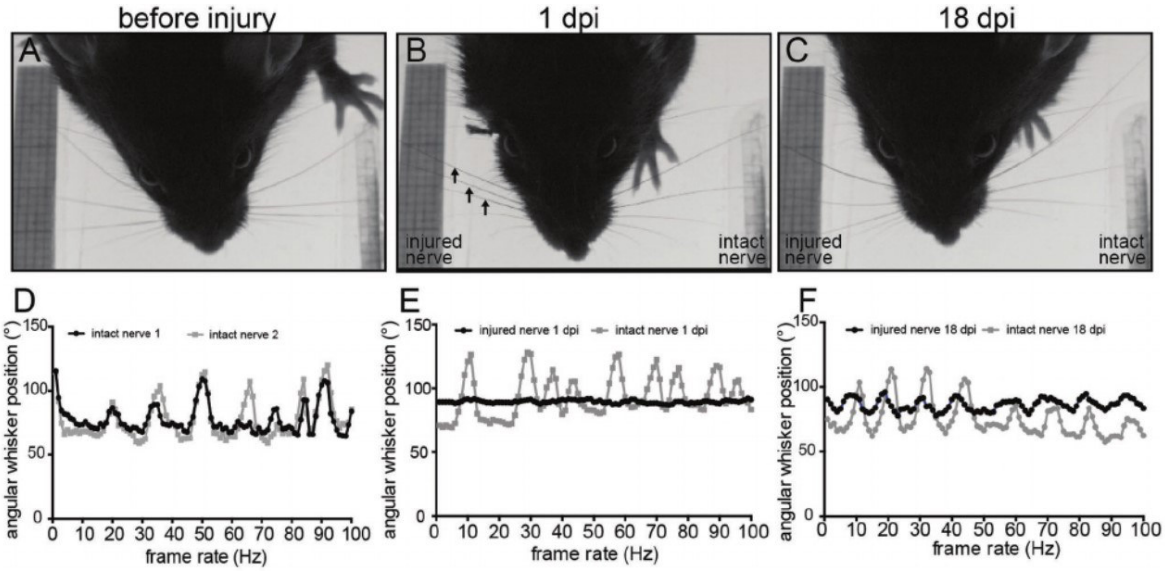

Figure 6: Position of mice whiskers before (A), one day (B) and 18 days (C) after injury of the facial nerve. Whiskers move synchronously before the injury (D) but cannot be moved one day after the injury (E). Movement is partially recovered by the help of self-assembling peptides 18 days after the injury (F).[63] The figure was reprinted from a publication by Schilling et al.[63] with permission of John Wiley & Sons, Inc. – Copyright 2019.

Similar peptide sequences have also found application for retroviral gene transfer. Here, positively charged fibers formed by the peptide QCKIKQIINMWQ were able to interact with the negatively charged surface of virions and hence act as a bridge to circumvent the electrostatic repulsion of negatively charged membranes of cells and virions. The peptide fibrils have been shown to induce transduction more efficiently than several other transduction enhancers, while displaying lower cytotoxicity and were equally efficient as the most used system RetroNectin, while being more cost- and time-efficient. The described peptide sequence is a fragment of the HIV-1 glycoprotein gp120. A similar but extended amino acid sequence NTLQCKIKQIINMWQEVG was found to enhance viral infectivity within a study on interactions between HIV-1 and cellular receptors.[59]

1.1.1.3 Peptide Amphiphiles with an Alkyl Chain

Many bacteria express bioactive lipopeptides, which serve them many purposes such as protection against viruses, fungi and other bacteria. Naturally produced lipopeptides contain an alkyl chain that is bound to a cyclic peptide due to the enhanced stability of cyclic peptides *in vivo.* A prominent example for an antimicrobial active lipopeptide is daptomycin,

which has been approved for treatment of bacteria-caused infections.[64] The anti-bacterial activity derives from the ability of the alkyl chain to insert into the cell wall. Aggregation of daptomycin into micelles leads to formation of holes resulting in ion leakage from the cell, which causes depolarization and inhibition of DNA, protein and RNA synthesis.[65]

In contrast to naturally expressed lipopeptides, synthetic lipopeptides typically contain a linear peptide chain.[64] They are often referred to as peptide amphiphiles and are a prominent example for self-assembling peptides which are serving a valuable contribution in designing materials for biomedical applications. Consisting of a hydrophobic alkyl tail which is bound to an linear oligopeptide, hydrophobic collapse of the peptides leads to formation of β-sheets and self-assembly into cylindrical or ribbon-like nanofibers which are stabilized by hydrogen bonding.[66] Peptide amphiphile based biomaterials have been used for building-up artificial extracellular matrices. Here, simple modifications of self-assembling peptides with cell adhesion peptide motifs such as RGDS or IKVAV were used for promoting cell binding to the peptide scaffolds by interactions with integrin receptors on the cell surfaces. Such systems have not only been able to support cell growth, but also improved the survival of neural stem cells by their encapsulation before injection into the brain of rats.[67],[68],[69]

Peptide-based biomaterials are also highly attractive for tissue engineering. Here, presentation of growth factors on the surface of supramolecular assemblies can support cell signaling and this way leads to replacement and repair of tissue. For this task a hydrogel was designed based on a peptide amphiphile mimicking the structure of heparin, a molecule that is known to stabilize growth factors and enhance their interactions with receptors for signaling angiogenesis. Improved growth of capillary structures was observed when the hydrogel was used for culturing HUVEC cells. Furthermore, the same peptide was able to improve bone regeneration.[70],[71]

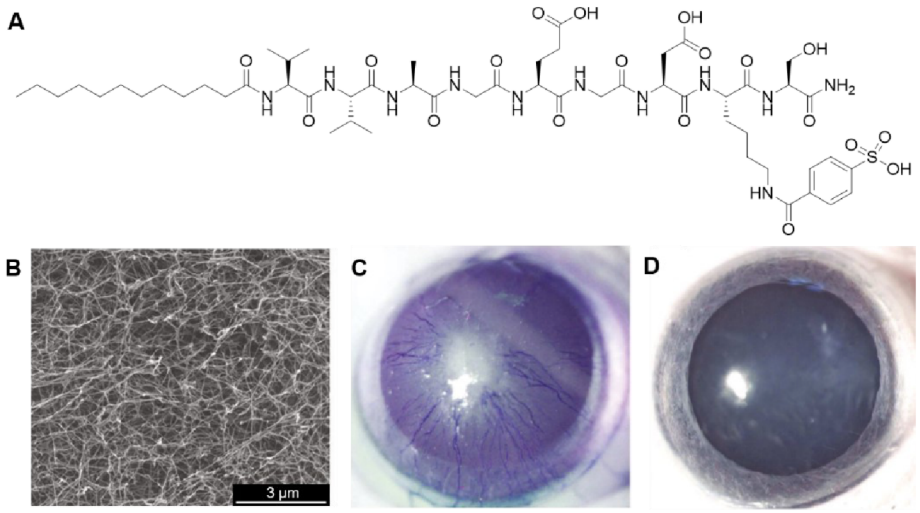

Figure 7: Structure (A) of a heparin mimicking peptide amphiphile and scanning electron microscopy (SEM) image of fibers formed by self-assembly of the compound (B). Vascularization in the cornea (C) after injection of the hydrogel in combination with growth factors and lack of vascularization at absence of the peptide hydrogel but with growth factors (D).[71] Reprinted with permission from "Heparin Mimetic Peptide Nanofibers Promote Angiogenesis" by R. Mammadov, B. Mammadov, S. Toksoz, B. Aydin, R. Yagci, A. B. Tekinay, M.O. Guler, *Biomacromolecules* **2011** *12* (10), 3508-3519. Copyright (2011) American Chemical Society.

1.1.1.4 Stimulus-responsive Peptide Assembly

Integration of a stimulus-responsive unit into the peptide can provide spatio-temporal control over assembly, which can broaden the application of peptide assembly derived materials. Inducing self-assembly in response to a trigger could be for instance used for localized drug release and hydrogelation as well as *in vivo* molecular imaging and sensing.[72],[73] In order to gain control over assembly processes, various enzymatic approaches have been used to trigger the assembly of short aromatic peptides (Figure 8). Thermolysin and lipase have been used for catalyzing reversed hydrolysis of peptides to induce self-assembly.[74],[75],[76] Here, the enzymes catalyzed amide bond formation between amino acids yielding in self-assembling peptide sequences. Using a different enzyme named subtilisin, methyl-ester hydrolysis on the *C*-terminus of pro-assembling peptides could lead to structure formation by uncaging the polar carboxylic acid group.[77] Phosphatase, an enzyme which catalyzes the dephosphorylation of hydroxy-functionalized amino acids such as serine, tyrosine and threonine could also lead to self-assembly into fibrillar structures. In one study, the self-assembly of Fmoc-FY was blocked by phosphorylation of the hydroxyl functionality of tyrosine (Y), which led to electrostatic repulsion of negatively charged phosphate groups. Upon treatment with the enzyme alkaline phosphatase, the self-assembling sequence was released, leading to formation of a fibrillar hydrogel. During incubation with E. coli bacteria in inosine supplemented media, which induced overexpression of the enzyme in the periplasmic space of E. coli cells, the transformation from the pro-assembling into the assembling sequence was demonstrated and showed antimicrobial activity.[78]

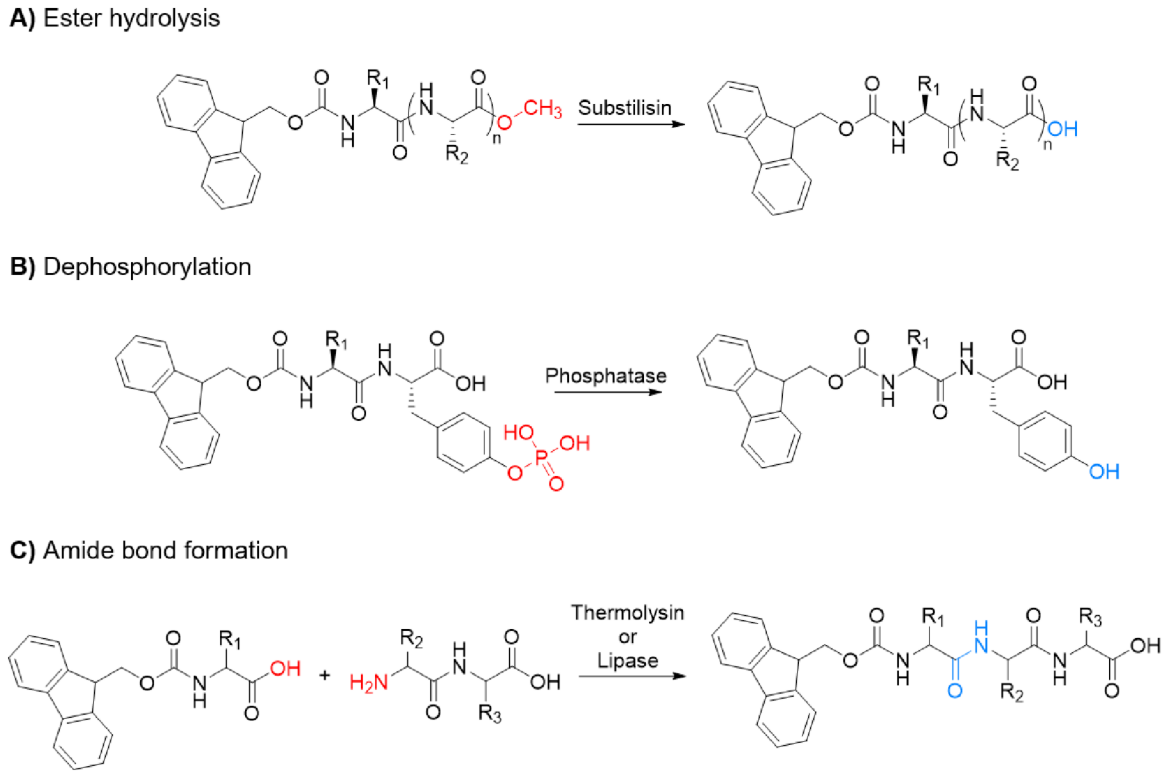

Figure 8: Selected enzymatically induced reactions leading to peptide self-assembly: A) Subtilisin catalyzed methylester hydrolysis[74], B) phosphatase catalyzed dephosphorylation[78], C) thermolysin/lipase catalyzed amide bond formation.[74],[76]

Besides enzymatic control, self-assembly of short aromatic peptides can also be influenced by pH. Fmoc-FF has been reported to form hydrogels containing paired fibrils at the pH range between 9.5 and 10.2, while decreasing the pH to 6.2 leads to thickening of the fibers into ribbons. Further decrease in pH values to less than 5.2 leads to aggregation and precipitation of the peptides. At a pH higher than 10.2 a clear solution is observed.[79]

To further expand the great applicability of peptide assembly and introduce other triggers for assembly, non-natural amino acids have been incorporated into peptides. Besides enhancing the stability against proteases, they also offer new possibilities for stimulus-responsiveness and creation of smart biomaterials with unique properties. Non-standard amino acids include side chain modifications which are not incorporated into the twenty-one natural amino acids, but also β- and γ-amino acids, which contain one or two carbon atoms more between the amino- and carboxyl groups respectively to the natural occurring α-amino acids and display better metabolic stability as well as higher flexibility. Furthermore, α,β-dehydro amino acids such as dehydrophenylalanine have been utilized for building up more protease stable peptide assemblies, displaying more conformal rigidity due the double bond in the peptide backbone.[80], [81]

Utilizing non-natural amino acids for peptide synthesis offers the possibility for incorporating chemical functionalities which are not present in nature, therefore assembly of these peptides can be bioorthogonal and controlled by applying external stimuli or they can be

made to respond to the natural environment in living systems. Introducing azobenzene residues gives photo-responsive peptides and hence can provide light induced architectural changes in the self-assembled materials. Based on the irradiation induced change between the *cis*- and *trans*-conformation of azobenzene, the physical properties such as thermal stability and mechanical strength of peptide-based hydrogels could be modulated as isomerization disrupts π-π-stacking interactions.[81]

Using dynamic covalent chemistry, the generation of defined quaternary structures was achieved upon assembly of hydrazide and aldehyde functionalized peptides. Here, complementary oligopeptide sequences were assembled into zipper-like structures, macrocycles and other shapes utilizing the dynamic covalent formation of hydrazones. The assemblies displayed enhanced antimicrobial activity against Gram positive bacteria *S. aureus* in comparison to the monomeric peptide sequences.[82] Another technique for assembly of peptides using non-covalent interactions is metal binding. Utilizing natural amino acids such as histidine, cysteine, tryptophan or glutamic acid for metal coordination can lead to assembly into distinct architectures. However, artificial ligands offer advantages over naturally occurring amino acids, as they possess higher binding strength. [83] Synthetic ligands which have been used for peptide assembly are pyridine, bipyridine, terpyridine, nitrilotriacetic acid and iminodiacetate to name a few.[84],[85],[86],[87],[88] Each of these functional groups have been reported to bind to multiple transition metal ions such as iron, zinc, copper, platinum, ruthenium, cobalt and nickel and have been used to assemble peptides into distinct structures.[83]

In summary, peptide assembly not only offers many advantages for application as biomaterials, but also a wide range of peptides and building blocks to choose from in order to fine-tune and design a material which is tailored specifically for its desired purpose (Figure 9).

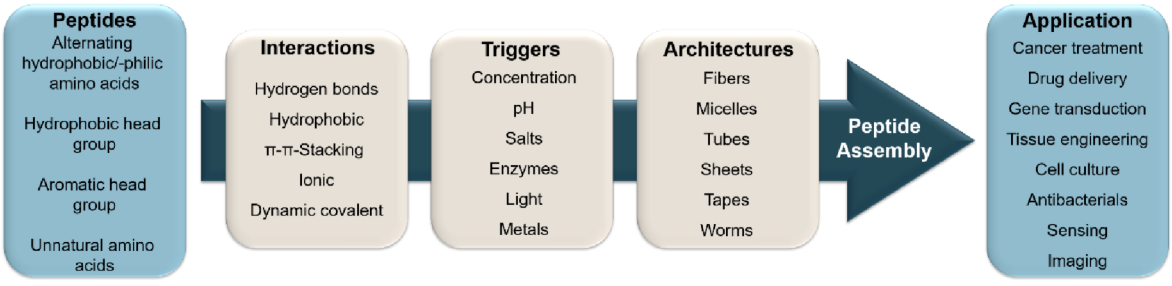

Figure 9: Overview over classes of assembling peptides and interactions the self-assembly processes are based on, as well as triggers that can induce self-assembly into various architectures and their applications.

Degradability of peptide-derived biomaterials is a very important factor which needs to be considered for many applications especially *in vivo*. As described before, self-assembled peptides are more stable towards degradation than their monomers, therefore controlled

disassembly of the material by a biocompatible trigger would be a key advantage for accomplishing efficient decomposition of the material and clearance of the peptides, which will be described in the next chapter.

1.1.4 Disassembly of Peptides

Depending on the application of the self-assembled peptide architectures, controlled rearrangement into different structures or disassembly into either smaller parts or into the peptidic monomers is highly desirable, for example to promote biodegradability of peptide-based materials in tissue engineering or for drug release.[72],[89] Various enzymatic, chemical and physical triggers have been exploited to induce peptide disassembly by degradation, chemical modification or change of conformational or physical properties of peptides, which will be described below. For biomedical use, it is especially important to develop a disassembly strategy which can be applied in the biological milieu using biocompatible and bioorthogonal triggers.

Enzymatic switches for induced peptide assembly and disassembly have received huge interest due to their natural abundance in living systems and the mild conditions required for these reactions.[90],[91],[72],[92] Cell-type specific treatment, 3D cell culture and tissue regeneration have been reported as potential applications for these systems.[74] As enzymatically controlled assembly and disassembly is conducted under mild conditions, easy attachment and detachment of cells from surfaces could potentially be provided by responsive peptide materials. Furthermore, the responsiveness of such materials to enzymes could enable the cells to create more space for spreading, proliferation and migration by degradation of the biomaterials which would also be beneficial for tissue regeneration.[33],[90],[93] The controlled disassembly of peptide architectures could protect cells from damage, which might occur upon assembly inside the cells if they produce the enzyme that is needed for this task. At the same time, cells that do not contain the enzyme, for example cancer cells, would not be protected and therefore suffer from the formation of peptide nanostructures, which could be used for cancer treatment.[92]

Many strategies using enzymes for controlling peptide assembly revolve around changes in peptide solubility in the aqueous milieu upon creation or cleavage of chemical bonds. Phosphorylation of hydroxyl groups in the side chains of serine and threonine enhances the solubility of peptides and can therefore lead to disassembly of peptide nanostructures.[72] This strategy has been used for amphiphiles containing a hydrophobic alkyl tail as well as short aromatic peptide amphiphiles. The extracellular cancer biomarker protein kinase A has been used for phosphorylation leading to peptide disassembly, which could be reversed upon treatment with the enzyme alkaline phosphatase to yield self-assembled nanostructures (Figure 10A).[72] The nanofilaments were able to encapsulate the drug

doxorubicin and release it in the presence of protein kinase A secreting cancer cells, which showed that this system is a promising candidate for sensing cancer cells and responding by drug release.

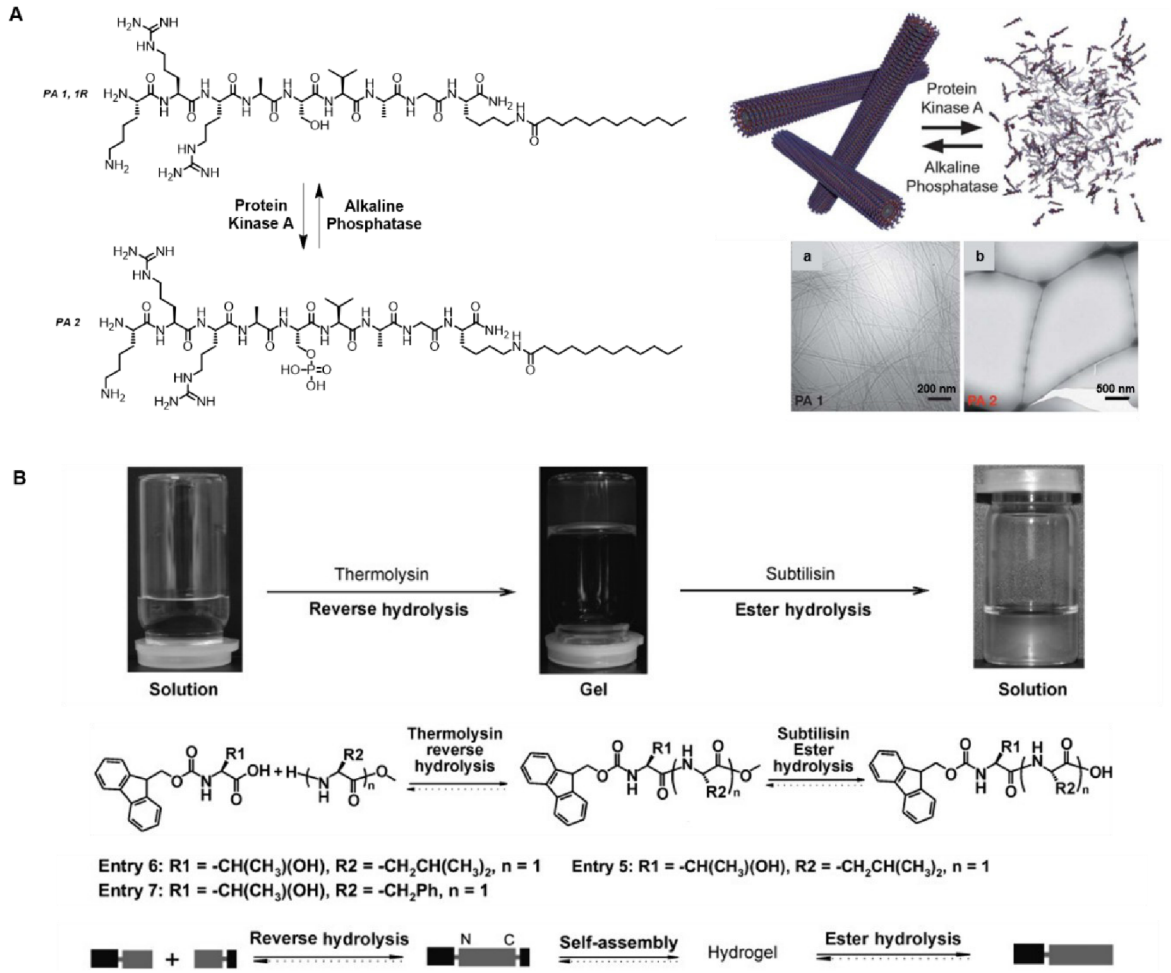

Figure 10: A) Chemical structures and TEM images of enzymatically controlled assembly and disassembly of peptide amphiphiles by phosphorylation and dephosphorylation of serine.[72] Republished with permission of Royal Society of Chemistry, from "Switching of self-assembly in a peptide nanostructure with a specific enzyme", M. J. Webber, C.J. Newcomb, R. Bittonc , S. I. Stupp, *Soft Matter*, **2011**,7, 9665-9672, permission conveyed through Copyright Clearance Center, Inc. B) Assembly and disassembly of short aromatic peptides induced by enzymatic reverse hydrolysis and ester hydrolysis respectively.[74] The figure was reprinted from a publication by Das et al.[74] with permission of John Wiley & Sons – Copyright 2008 Wiley-VCH Verlag GmbH & Co. KGaA).

Another system utilizing enzymatically controlled assembly and disassembly of peptides was reported. Here, thermolysin catalyzed the reverse hydrolysis of the peptide Fmoc-Thr-Leu-OMe, which led to nanofiber formation. Ester hydrolysis using the enzyme subtilisin led to disassembly (Figure 10B).[74] In a similar approach, carboxylesterase was used to hydrolyze the *C*-terminal ester of a short aromatic peptide to induce peptide disassembly.[92] Matrix metalloproteinases (MMP) have also been used for degradation of self-assembling peptides. Gelatinase/type IV collagenase (MMP-2) was shown to cleave the amino acid sequence $(RADA)_3PVGLIG(RADA)_3$ between glycine and leucine leading to disassembly of the peptides. While the peptide was completely cleaved by MMP-2 within 24 h in solution, hydrogels resulting from self-assembled peptides were only digested on their surface, as

the enzyme was not able to penetrate the gel due to its high molecular weight and small pore sizes of the gel.[94] This shows that the use of enzymatic cleavage suffers from efficiency when used for degradation of bulk materials. Another disadvantage of enzymatic approaches is the requirement of expression of the specific enzyme by the cell and therefore limited application for different systems. Therefore, chemical approaches using small molecules, which are able to diffuse into self-assembled peptide materials, or physical stimuli to trigger disassembly might offer certain advantages.

UV-cleavable nitrobenzyl residues have been used for controlled disassembly of peptide architectures. This strategy is based on the manipulation of the balance between hydrophobic and hydrophilic moieties in the peptide chain. Attachment of an alkyl chain on the *N*-terminus of a PEGylated peptide using the UV-sensitive linker led to fiber formation due to generation of an amphiphilic peptide sequence. However, upon irradiation the hydrophobic chain was cleaved and the peptide fibers disassembled subsequently.[95] In a different approach, a near-UV light cleavable Nvoc (4,5-dimethoxy-2-nitrobenzyloxycarbonyl) side chain modified lysine was used to create a balance between hydrophobic and hydrophilic residues in the peptide side chains of Aβ16 (KLVFFAE), leading to formation of β-sheets and subsequently self-assembly into fibrillar structures. Upon removal of the photocage the positive charge of the lysine side chain amino group was restored, destabilizing the β-sheet structures and leading to disassembly of the fragment of amyloid β.[89]

Although the light-triggered disassembly of peptides has been proven for various peptide sequences, photodamage of cells which can occur upon irradiation with UV light, as well as the low penetration depth display limitations of this method for biomedicinal applications.[96] Furthermore, this strategy does not offer reversibility of peptide disassembly, which might be interesting in various fields. In order to provide reversibility, pH triggered assembly/disassembly processes were investigated. As described above self-assembly is dictated by an interplay between hydrophilic and hydrophobic chemical groups, therefore changing the pH can have a significant effect on peptide assembly.[97] The hydrophilicity of peptides can significantly increase upon protonation or deprotonation of the *N*- and *C*-terminus as well as certain amino acid side chains such as the amine in lysine and carboxylic acid functionalized aspartic and glutamic acid. A C_3-symmetric amphiphilic peptide with the sequence FEMEM was shown to build up supramolecular nanorods at acidic pH values, while no nanostructures were observed at neutral pH due to electrostatic repulsion between deprotonated carboxylate groups in the glutamic acid side chains.[97] Furthermore, peptide disassembly was achieved upon oxidation of the methionine side chain to methionine sulfoxide, which has a dipolar character and therefore also significantly increases the hydrophilicity of the peptide. The reversibility of methionine oxidation was

shown using the enzyme methionine sulfoxide reductase. Another chemical strategy to disassemble methionine functionalized peptide amphiphile based nanostructures was reported using CNBr mediated hydrolysis. Here, the reaction between cyanogen bromide and methionine leads to cleavage at the *C*-terminus of Met, detaching the N-terminal bound alkyl chain which is responsible for the assembly into peptide fibers.[98]

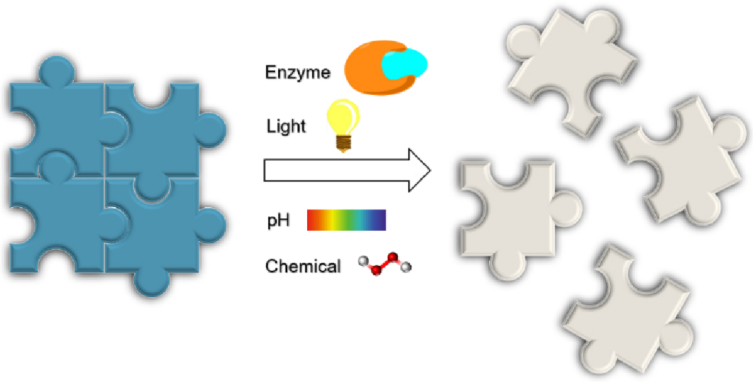

Figure 11: Schematical depiction of controlled peptide disassembly and utilized biological, chemical and physical triggers.

In summary, different approaches have been taken to disassemble peptide architectures into their monomeric components utilizing physical, chemical and enzymatic triggers. While some suffer from poor biocompatibility, other techniques can be performed in the presence of living systems.

The reversibility of peptide disassembly is given only for some stimuli and therefore ultimately the choice which system is used is highly dependent on the application. Besides using natural amino acids for induced assembly and disassembly such as pH dependent protonation processes, unnatural functional groups and their stimulus-responsivity can expand the toolbox for controlling peptide-peptide interactions.

As described before, degradation of peptide-based materials is of key importance when utilized for applications *in vivo*. Therefore, the next chapter will focus on the state of art of intracellular peptide assembly.

1.1.5 Peptide Assembly in Living Systems

Assembly of peptides into defined nanostructures inside living systems bears promising potential for studying intracellular processes, imaging and for targeted treatment in cancer and antibacterial therapy as well as for tissue engineering.[99],[12] However, many obstacles must be overcome in order to achieve this challenging task. As self-assembly of most peptides happens spontaneously in aqueous conditions and therefore might prevent cellular uptake, architecture formation should preferentially be delayed till the monomeric peptides are uptaken by cells to achieve intracellular assembly.[100] Furthermore, sufficient cellular uptake needs to be guaranteed in order to reach the critical aggregation concentrations

inside cells, leading to formation of peptide assemblies. Ideally, the assembly processes should be controlled by a trigger that is specific to the targeted location or the peptides should preferentially accumulate in this area to protect healthy cells and tissue.[99],[101] As an example, the formation of fibrillar structures by a pyrene-labeled phenylalanine-phenylalanine peptide inside mitochondria led to disruption of the organelle membrane and hence apoptosis of HeLa cells as well as other cancer cell lines (Figure 12A).[102] Self-assembly of the peptide was observed after reaching the critical aggregation concentration upon accumulation inside mitochondria which could be achieved by functionalization of the peptide with a triphenylphosphonium (TPP) ligand, which is known to target this organelle. Variation of the peptide sequence by substitution of the phenylalanine-phenylalanine with glycine-glycine significantly diminished the cytotoxicity, as the new peptide did not form fibers but micelles. These spherical nanostructures did not rupture the mitochondrial membrane, which shows the importance of the architecture that is formed by peptide assembly.

Although this study nicely represents intracellular assembly, it is lacking control over the assembly processes as it is solely based on accumulation of peptides and does not specifically target cancer cells. Other systems which utilize a trigger that is specific to certain cell types would provide advantages concerning controlled assembly in comparison to a system which relies only on high peptide concentrations. Stimulus controlled structure formation of peptides is mainly investigated in literature using enzymatic triggers and is known as enzyme-instructed self-assembly (EISA), which can be divided into pericellular, intracellular and subcellular EISA.[99] Alkaline phosphatase (ALP) was investigated in many studies for enzymatically induced peptide self-assembly for cancer therapy and molecular imaging.[99] A phosphorous ester on the side chain of tyrosine provides hydrophilicity to the precursor peptide preventing the self-assembly into nanofibers and formation of a hydrogel. Upon enzymatically catalyzed hydrolysis of the tyrosine phosphate, the hydrogelator is released (Figure 12B). The fluorescence intensity of the NBD-labeled (4-nitro-2,1,3-benzoxadiazole) peptide increased upon self-assembly revealing the intracellular structure formation at the endoplasmatic reticulum (ER), as the phosphatase is known to be localized at the cytoplasmic face of the ER.[103]

Another enzyme which was used for controlled intracellular hydrogelation of peptides is matrix metalloproteinase-7 (MMP-7). The enzyme is shown to be secreted by HeLa cells as well as other cancer cell lines and induces cleavage of peptides, while targeting the sequence Pro-Leu-Gly-Leu and cleaving the amide bond between glycine and leucine outside cells. The palmitoyl-modified peptide sequence underwent self-assembly upon enzymatically induced hydrolytic removal of the cationic peptide sequence leucine-alanine-arginine-lysine from the *C*-terminus (Figure 12B). Intracellular self-assembly led to a

significantly enhanced cytotoxic effect towards cancer cells in comparison to healthy cells, as they secrete higher concentrations of MMP-7.[104] Besides MMP and ALP, also other enzymes such as esterase, enterokinase, caspase-3/7 and furin have been used for enzymatically induced peptide self-assembly.[105],[106],[107],[108]

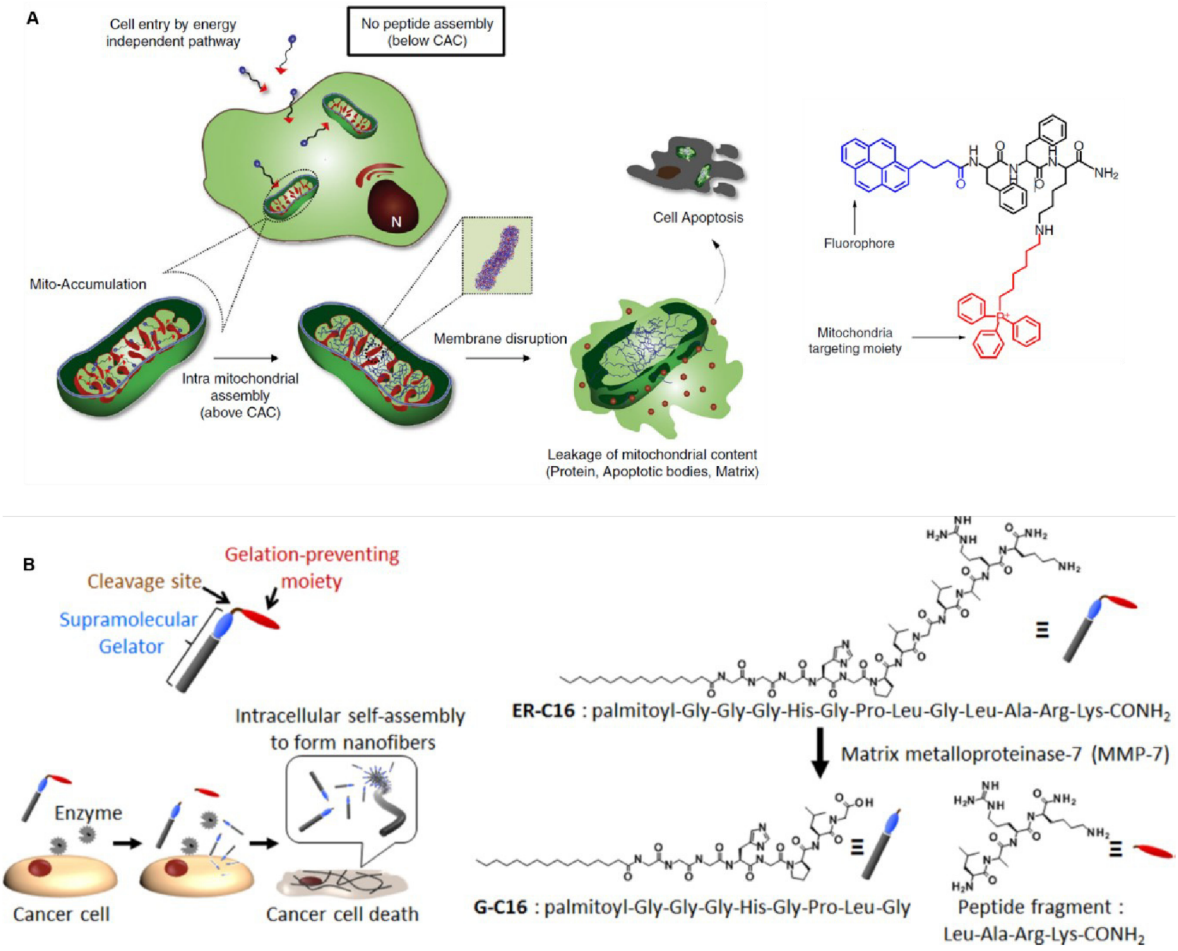

Figure 12: A) Accumulation inside mitochondria induces peptide self-assembly and subsequently leads to mitochondrial membrane disruption and apoptosis.[102] Reprinted from "Mitochondria localization induced self-assembly of peptide amphiphiles for cellular dysfunction" by Jeena et al. [102] (https://www.nature.com/articles/s41467-017-00047-z#rightslink) with minor changes. The copyright (2017) belongs to the authors, the article was published by Springer Nature. This is an open access article under the CC BY license (https://creativecommons.org/licenses/by/4.0/). B) MMP-7 induced enzymatical cleavage of peptides leads to peptide self-assembly and cell death.[104] Reprinted with permission from "Cancer Cell Death Induced by the Intracellular Self-Assembly of an Enzyme-Responsive Supramolecular Gelator", A. Tanaka, Y. Fukuoka, Y. Morimoto, T. Honjo, D. Koda, M. Goto, T.Maruyama, *Journal of the American Chemical Society* **2015** *137* (2), 770-775). Copyright 2015 American Chemical Society.

Although many studies have used enzymatic stimuli to induce peptide assembly inside cells, this strategy is generally not applicable to all cell types as the availability of the required enzyme is limited to certain cell lines and cell compartments. Therefore, using a physical or chemical stimulus instead of a biological trigger might offer a wider range of application. While many stimuli such as pH changes, ionic strength, metal ions, irradiation and chemical reactions have been reported to induce peptide assembly,[12],[97],[109],[83],[110],[111],[112],[113] intracellular structure formation has not been investigated much for these triggers. While the applicability of some of these triggers inside cells might be challenging for example due

to limited biocompatibility or the limited control over ionic strength and pH in living systems, chemical triggers are interesting candidates, especially when utilizing intracellularly available compounds.[12] A glutathione (GSH) induced removal of a PEG chain was reported to lead to a transition of micelles into peptide fibers and subsequent drug release based on the high glutathione concentrations inside cancer cells. Peptide fibers were shown to have a significant impact on the surface morphology of cancer cells and enhanced their viscosity and rigidity which is related to lower cell viability. The micelles accumulated at tumor sites in mice and formation of peptide nanofibers was observed, which in synergy with doxorubicin led to a significant decrease in tumor volumes.[13]

As described in this chapter intracellular peptide assembly frequently has a detrimental effect on cell viability. Although mechanisms of cell death are complex, some research groups have published postulations on the origin of peptide assembly induced cellular dysfunction. Disruption of actin filaments in cells which were treated with self-assembling peptide sequences has been reported, which showed the interference of intracellular assembly with actin filaments and hence potentially leads to cell death.[114] The same study reported an increase of the apoptosis signaling molecules active caspase3 and active PARP (poly(ADP-ribose])polymerase) upon treatment with self-assembling peptides. Another research group also reported changes in the cytoskeleton and furthermore postulated mitochondrial dysfunction, as a result of self-assembly of TPP functionalized peptides. This claim was supported by the release of cytochrome C into the cytosol which activates intrinsic apoptosis. Incubation of cells with necroptosis inhibitor (Nec-1) partially rescued cells, which indicates that necroptosis also plays a role in peptide assembly induced cell death.[115] Mitochondrial damage was also observed using another TPP labeled self-assembling peptide. The research group reported an interaction of peptide fibrils with the mitochondrial membrane, which resulted in membrane disruption. Furthermore, they observed enhanced production of reactive oxygen species (ROS) induced by self-assembly. An imbalance of ROS can lead to damage of DNA and proteins, as well as membrane disruption and ultimately a decrease in cell viability.[102]

The described examples for intracellular peptide assembly show the applicability of this concept for treatment of cancer by taking advantage of biological or chemical triggers offered by the cancer cell. While enzymatic triggers have been studied heavily in the past two decades, chemical triggers are not exploited frequently, although inducing peptide assembly by chemical stimuli would offer a significant increase in applicability of peptide nanoarchitecture formation *in vivo*. Therefore, the next chapter will give an insight into chemical functions and reactions based on boronic acids that can aid intracellular peptide assembly and formation of peptide-based biomaterials.

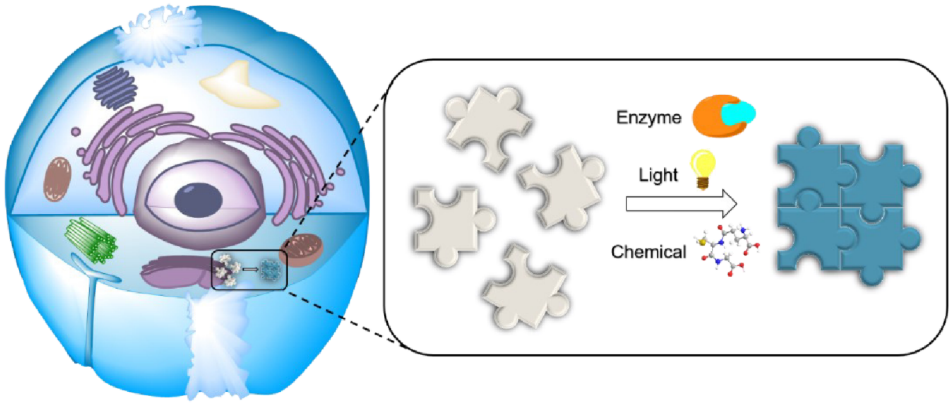

Figure 13: Overview of a selection of triggers which have been used for intracellular peptide assembly.

1.2 Stimulus-Responsiveness of Boronic Acids

1.2.1 General Introduction to Boronic Acids

Synthetic chemistry offers the possibility of introducing new building blocks into peptides which can be utilized for bioorthogonal assembly. Expanding the naturally occurring variation of intermolecular interactions can provide tunability of material properties and control over assembly processes. A prominent example for bioorthogonal and reversible reactions is the dynamic covalent formation of boronate esters.

Boron is known to be crucial for plant growth as it plays an important role in cell wall synthesis and cell division, yet the trace element is not considered essential for human health.[116],[117],[118] However, boron has been reported to have many beneficial effects in humans such as influencing the metabolism of bones, improving the half-life of estrogen and vitamin D, reduction of inflammatory biomarkers and improving joint health as well as wound healing.[119],[118],[120] Boron intake is provided by a plant-rich diet, as plant roots are able to absorb water-soluble boron derivatives such as boric acid from soil and store the trace element in their roots, stalks, cell walls and shoots. Here, the transport of boron is based on its ability to complex *cis*-diols.[117],[119]

Similarly to boric acid, boronic acid is able to form complexes with *cis*-diols and other related compounds. Boronic acids are organoborane compounds derived from boric acid, where one of the hydroxyl group is replaced by an aryl or alkyl substituent. Their reactivity is based on a vacant p-orbital which is centered at the boron atom with a trigonal planar geometry and allows the interactions of boronic acids as mild Lewis acids with nucleophiles. The reversible reaction with a basic nucleophile adds a negative charge and leads to formation of a tetrahedral geometry of the boronate.[121] Coordination of one nucleophile, two vicinal nucleophiles as well as tridentate ligands have been reported.[122] A wide range of oxygen- and nitrogen-based nucleophiles form covalent bonds with boronic acids, hence these

interactions were exploited for various applications such as drug delivery, carbohydrate sensors, purification of glycoproteins and for therapeutic use.[123],[124],[125] Due to the reversibility of many boronate esters, it is crucial to choose a suitable ligand for the boronic acid based on the requirements of the targeted application. Boronate esters have been found to be cleaved upon changing the pH and addition of competitive ligands.[126],[127]

Besides the often reversible boronic acid complex formation, boronic acids can also be irreversibly oxidized by reactive oxygen species (ROS) such as hydrogen peroxide (H_2O_2). The oxidative cleavage of boronic acids has been used in the development of pro-drugs, H_2O_2 sensing and reversible protein modifications.[128],[129],[130]

Furthermore, boronic acids act as catalysts in various reactions such as the Friedel-Crafts reactions and can be used for fluoride sensing.[131],[132],[133],[134],[135] They are also crucial educts for the Suzuki-Miyaura cross-coupling and can react in other organic reactions such as a tandem Nazarov cyclization/Diels–Alder reaction and the Petasis reaction.[136],[137],[138]

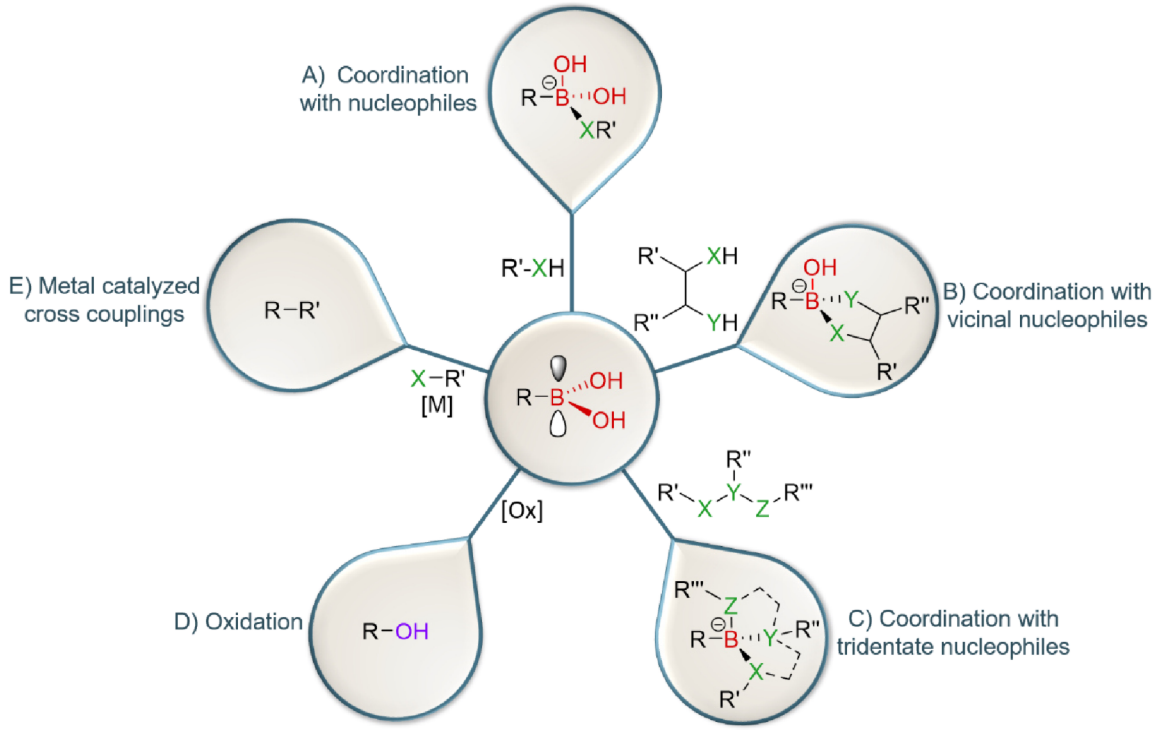

Figure 14: Chemical reactivity of boronic acids. X, Y, Z= oxygen or nitrogen. The figure was recreated and modified based on António et al.[122] published by The Royal Society of Chemistry.

The versatile chemistry of boronic acids makes them highly attractive for utilization in responsive biomaterials, which will be discussed in the next chapters.

1.2.2 Dynamic Covalent Interactions of Phenylboronic Acids

Boronic acids are known to act as Lewis acids towards nucleophilic compounds containing heteroatoms such as oxygen, nitrogen, phosphorous and sulfur.[139] These interactions can be reversible or irreversible depending on the ligand chosen for phenylboronic acid (PBA)

binding and therefore lay a great foundation for fine-tuning the binding strength and stimulus-responsivity of materials for many types of applications, ranging from sensors to drug delivery.[140]

Especially, boronate ester formation with 1,2- and 1,3- vicinal diols has been used in many studies for various intentions such as hydrogel formation, drug delivery, sensing of glucose and other carbohydrates, molecular recognition, protein purification and macromolecular assembly to name a few.[141],[123],[142],[143],[125],[144] Condensation of boronic acids with diols leads to formation of dynamic covalently bound compounds, which can be hydrolyzed upon changing the pH. The optimal binding conditions and binding affinity depend on both substrates, where electron-deficient boronic acids (BA) contribute to stronger binding, whereas weaker binding is observed for bulky boronic acids. Electron-rich, non-bulky ligands enhance the binding affinity.[145] Furthermore, the binding affinity highly depends on the pH and buffer concentration as well as buffer type.[146]

Saccharides typically show weak binding with binding affinities in the low molar range. At pH 7.4 the binding affinity for glucose towards phenylboronic acid was reported to be 4.6 M^{-1}, while the binding of fructose was 3.5 times higher (160 M^{-1}). However, for both molecules the binding affinity increases slightly upon complexation at higher pH values.[145] Nevertheless, boronic acids have been successfully applied as sensors for saccharides, while the main focus was set on glucose sensing, as it offers the possibility for glucose-induced insulin release for treatment of diabetes.[147],[148],[149]

The binding equilibria of phenylboronic acid to 1,2- and 1,3-diols is presented in Figure 15. Condensation can yield trigonal and tetrahedral boronate esters, while the tetrahedral and charged derivative is more stable, the trigonal form is hydrolyzed easier. Therefore, the binding constant K_{tetra} is higher than K_{trig}.[150] Condensation products of boronic acids with 1,2-diols have been reported to be more stable than six-membered cyclic boronate ester that are the products of condensation with 1,3-diols.[139]

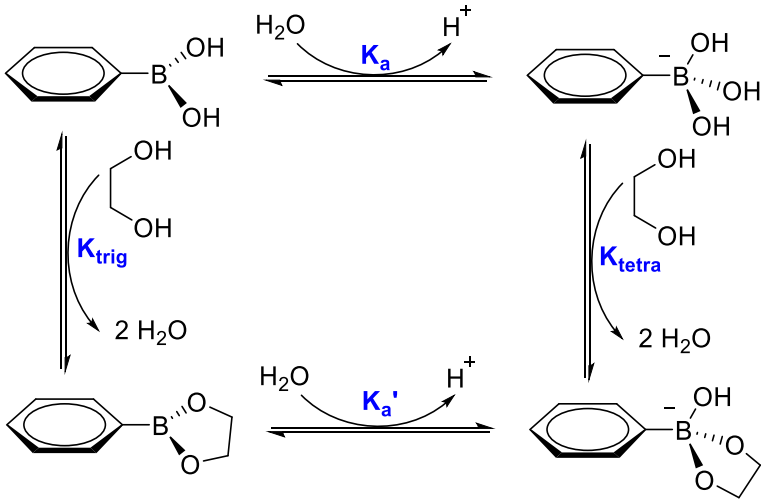

Figure 15: Reaction of boronic acids with diols yielding in boronate esters.[146] Adapted from "A detailed examination of boronic acid–diol complexation", G. Springsteen, B. Wang, Tetrahedron, Vol. 58, 5291-5300, Copyright 2002, with permission from Elsevier.

Catechol derivatives are frequently used in molecular assembly with boronic acids due to their facile synthetic accessibility and enhanced binding affinity to PBA in comparison to saccharides. The binding affinity of catechol to phenylboronic acid at pH 7.4 was determined to be 830 M^{-1} and was found to be pH-responsive.[145] The ability of these compounds to dynamically response to stimuli by self-organizing, rearranging and self-healing makes them excellent candidates within the array of dynamic covalent interactions for various applications. The dynamic covalent binding that can be reversed upon acidification was exploited for molecular recognition, hydrogel formation, encapsulation, drug delivery and release.[143],[144],[151],[123] Bortezomib (BTZ) is a boronic acid functionalized dipeptide which has been approved for treatment of multiple myeloma and mantle cell lymphoma treatment due to its ability to inhibit cancer cell proteasomes by binding to threonine, which is located in the active sites of some proteases for example serine protease.[123],[152] Due to its unfavorable pharmacokinetic properties, delivery inside tumor cells was investigated by complexation of the boronic acid residue to catechol functionalized polyethylene glycol (PEG) polymers. Targeted delivery into cancer cells was achieved by biotinylation of the polymer. While the complex was stable at physiological pH of 7.4, the acidic environment of pH 5.5, which can be found inside tumor cells, caused the release of the drug (Figure 16). This led to enhanced cytotoxicity towards breast cancer cells than non-cancer cells *in vitro*.[123]

Another strategy for delivering drug molecules to the tumor site was reported utilizing the assembly of hydrophobic boronic acid modified deoxycholic acid with hydrophilic dopamine functionalized polymers. The neurotransmitter dopamine contains a catechol moiety that can interact with phenylboronic acids, which has been exploited for numerous

applications.[153],[154],[155],[25] Here, coincubation of the polymer and the boronic acid derivative at pH 7.4 leads to formation of micelles, which are able to encapsulate the hydrophobic drug doxorubicin (Dox). The micelles were shown to be stable at conditions mimicking the bloodstream, but successfully released the drug after accumulation in tumor tissue and acidic hydrolysis of the boronate ester complexes in the endo- and lysosomes of cancer cells (Figure 16).[151]

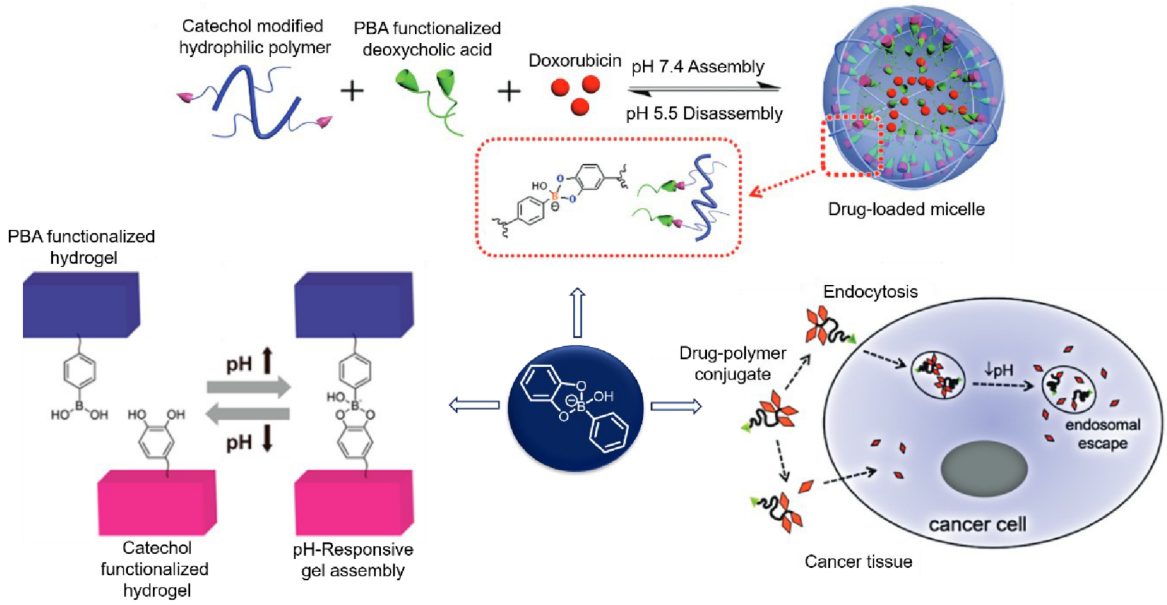

Figure 16: Selected applications utilizing the reversible formation of boronate esters by interactions of boronic acids with catechol such as drug delivery by encapsulation or conjugation and hydrogel formation.[151],[144],[123] Republished with permission of Royal Society of Chemistry, from "Facile dynamic one-step modular assembly based on boronic acid-diol for construction of a micellar drug delivery system"[151], Z. Zhao, Y. Zhang, C. Tian, T. Yin, C. Zhang, *Biomater. Sci.*, **2018**, *6*, 2605-2618, permission conveyed through Copyright Clearance Center, Inc. Reprinted with permission from "pH- and Sugar-Responsive Gel Assemblies Based on Boronate–Catechol Interactions"[144] by M. Nakahata, S. Mori, Y. Takashima, A. Hashidzume, H. Yamaguchi, A. Harada, *ACS Macro Letters* **2014** *3* (4), 337-340. Copyright (2014) American Chemical Society. Republished with permission of the American Chemical Society, from "Catechol Polymers for pH-Responsive, Targeted Drug Delivery to Cancer Cells"[123] by J. Su, F.Chen, V. L. Cryns, P. B. Messersmith, Journal of the American Chemical Society **2011** *133* (31), 11850-11853 (https://pubs.acs.org/doi/full/10.1021/ja203077x). Further permissions related to the material excerpted should be directed to the ACS

The affinity of boronic acid to catechol was also shown by the synthesis of two polymers which contained either 4-vinylboronic acid or 4-vinylcatechol residues (Figure 16). Both acrylamide and *N,N'*-methylenebis(acrylamide) copolymers formed hydrogels by themselves. Upon coincubation in buffer at pH 10.0 the gels co-assembled by formation of boronate-catechol esters. The gels were disconnected upon decreasing the pH to 4.0 due to hydrolysis of the dynamic covalent bond. Furthermore, the gels showed responsiveness towards monosaccharides.[144]

Significantly enhanced binding affinities towards boronic acids in comparison to catechol were achieved by incorporation of nitrogen atoms into the binding ligand. Salicylhydroxamic acid derivatives (SHA) have been shown to bind phenylboronic acids in highly pH-

dependent fashion. Optimal binding is achieved at pH 7.4 with a binding affinity of 17800 M^{-1}, while hydrolysis of these dynamic covalent complexes is achieved at pH 5.0 and lower due to the low binding affinity of only 4 M^{-1} (at pH 4.5) under these conditions. The hydroxamic acid residue and the hydroxyl group each provide an oxygen atom that can bind to the boronic acid, but the hydroxamic acid also contains a nitrogen atom capable of coordination as well. Thus, two possible configurations can be formed between the complexation partners (Figure 17). The six-membered ring containing one B-O and one B-N bond is formed preferentially to the five-membered boronate ester with two B-O bonds.[145],[156]

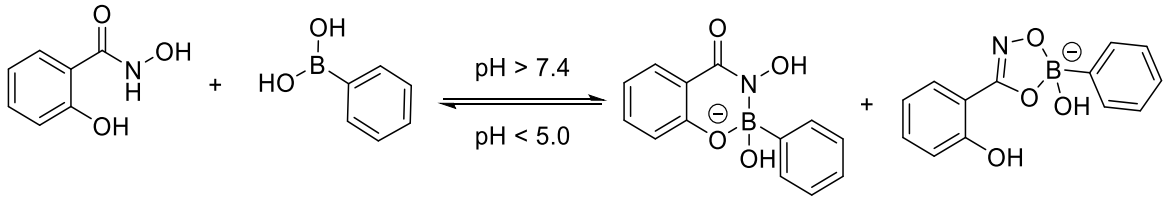

Figure 17: pH responsive interaction of phenylboronic acid with salicylhydroxamate.

The enhanced binding affinity of SHA towards PBA prevents formation of competitive complexes with biologically relevant nucleophiles like glucose, the amino acids cysteine and serine as well as other components present in cell media such as proteins and small-molecule co-factors.[157] Another benefit of this dynamic covalent interaction are its high reaction kinetics at physiological pH with a rate constant of $(7.01\pm2.04)\times10^{6}$ $M^{-2}s^{-1}$.[157] The bioorthogonality of PBA-SHA complexation has been utilized for various applications such as delivery of proteins and enzymes into cells and creation of pH-responsive biomaterials like hydrogels.[158],[159],[160],[161] Its first reported use was for chromatographic purification, where sepharose gel was functionalized with salicylhydroxamate to retain boronic acid modified enzymes, which could be collected upon decreasing the pH.[162]

Boronic acid decorated proteins and enzymes have been successfully uptaken by cells upon utilization of salicylhydroxamate equipped delivery moieties. Construction of dendrimer-enzyme hybrids using SHA functionalized poly(amidoamine) (PAMAM) dendrimers and boronic acid derivatives of trypsin, papain and DNase I led to cellular uptake of the enzymes. The bulky dendrimer shell was able to block the enzymatic activity, which could be restored quantitively upon acidic hydrolytic cleavage inside lysosomes.[158] In this study, cellular uptake was facilitated by the positively charged PAMAM dendrimers, however also other approaches for uptake of BA-enzymes have been published. SHA-modified somatostatin allowed for cancer cell specific cellular uptake of PBA-modified cytochrome C (Cyt C) and human serum albumin (HSA). Somatostatin is a naturally occurring cyclic peptide and is known for providing uptake into cancer cells that express somatostatin receptors.[163] The boronic acid modification did not hinder the enzymatic

activity of Cyt C, therefore a cytotoxic effect towards A549 cancer cells was observed.[160] In another study, SHA-functionalized polyethylenglycol (PEG) was used to decorate the surface of the same proteins.[159] Nanogels, which were formed using boronic acid labelled proteins and salicylhydroxamate modified PEG-methylacrylate polymers were also used to promote delivery inside cells. Here, four proteins with different sizes and surface charges RNase I, green fluorescent protein (GFP), bovine serum albumin (BSA) and β-galactosidase were modified with cleavable phenylboronic acid functionalities. Improved cellular uptake and release of active enzymes were shown in HeLa cancer cells by co-assembly of the enzymes and the polymer shell.[164] The presented examples show the versatility of SHA for functionalization of different types of molecules such as polymers, peptides and dendrimers which can be utilized for inducing cell uptake.

Formation of native protein hydrogels by cross-linking boronic acid modified cytochrome C was reported by Seidler et al.[161] Either two- or four-arm salicylhydroxamate functionalized PEG polymers were used for creation of pH-responsive and self-healing hydrogel networks with possible application as locally administered apoptosis-promoting materials. PEG was chosen as the cross-linker due to its ability to retain water and the high flexibility to respond to dynamic changes in the gel. Variation of chain length and number of salicylhydroxamate-functionalized PEG arms allowed the tuning of gel stiffness. Acidification to pH 5.0 led to disintegration of the gel by breaking the PBA-SHA bond and hence induced the release of the enzyme into solution.

Other boronic acid-salicylhydroxamate based gel forming systems were reported by the group of Kiser.[165],[150] The pH responsive co-assembly of two polymers which were functionalized with either PBA or SHA was investigated for a potential application in prevention of male-to-female transmission of HIV-1.[150] Poly(hydroxypropylacrylamide) (pHPMAm) was used due to its biocompatibility and good water solubility and contained 5 mol% side chain substitution of either PBA or SHA. The tunable viscoelasticity of the gel was shown upon changes of pH, where an acidic pH led to low viscosity suitable for application in the vaginal environment. Upon neutralization of the pH, which would occur upon subjection to seminal plasma, an increase of PBA-SHA cross-links would yield in domination of elastic behaviors of the gel. Reduction in gel mesh size at neutral pH could slow down the Brownian motion of HIV-1 by acting as a barrier, which showed that this hydrogel is a promising candidate for reducing the heterosexual transmission of HIV.

As demonstrated, the pH-responsive reversible binding of phenylboronic acids to salicylhydroxamate has been utilized for applications in biomedicine like drug delivery and formation of responsive biomaterials where its potential has received increased attention.

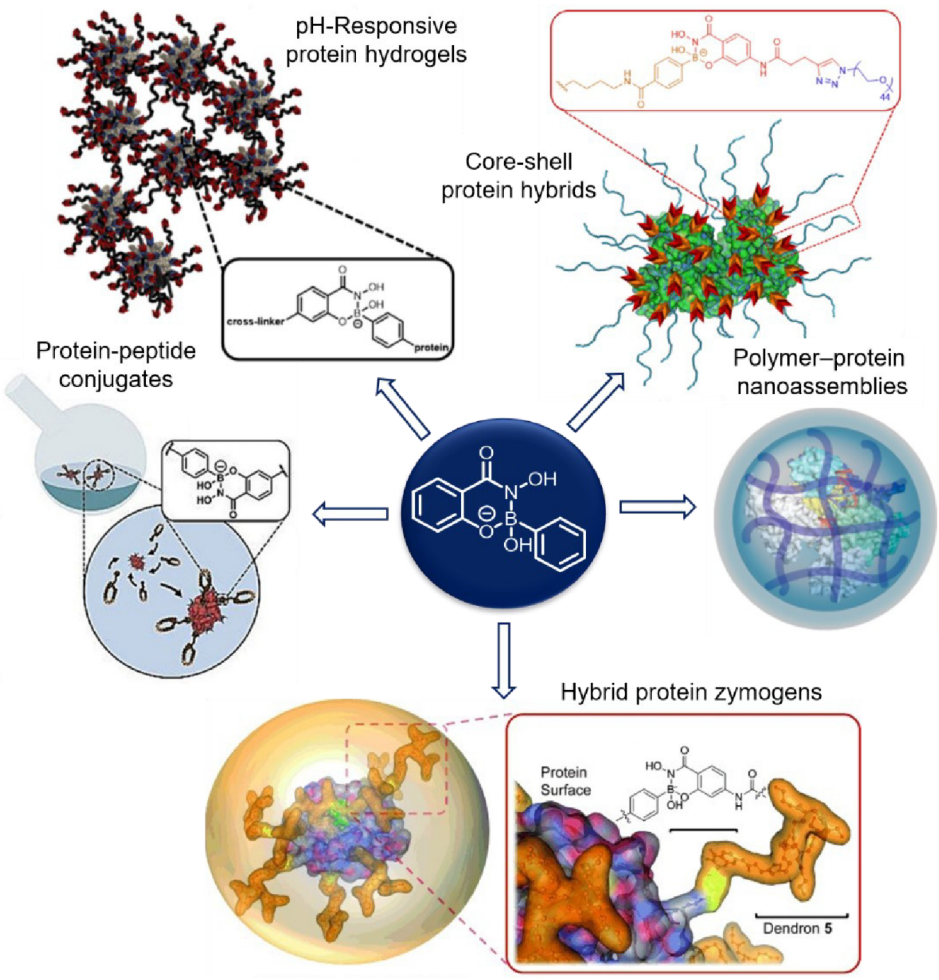

Figure 18: Applications of the interaction between boronic acids and salicylhydroxamic acid for creation of core shell systems and hydrogels.[159],[161],[160],[158],[164] A part of the figure was reprinted from "pH responsive supramolecular core-shell protein hybrids" by Seidler et al.[159] with the permission of the Taylor & Francis Group (http://www.tandfonline.com). A part of the figure was reprinted from "Native protein hydrogels by dynamic boronic acid chemistry" by Seidler et al.[161] with permission of Elsevier. This is an open access article under the CC BY license (https://creativecommons.org/licenses/by/4.0/). A part of the figure was reprinted from a publication by Seidler et al.[160] with permission of John Wiley & Sons – Copyright 2018 Wiley-VCH Verlag GmbH & Co. KGaA. A part of the figure was adapted from a publication by Ng et al.[158], reprinted with permission of John Wiley & Sons – Copyright 2014 Wiley-VCH Verlag GmbH & Co. KGaA).Reprinted with permission from "Reversible Click Chemistry for Ultrafast and Quantitative Formation of Protein–Polymer Nanoassembly and Intracellular Protein Delivery" by B. Liu, M. Ianosi-Irimie, S. Thayumanavan, *ACS Nano* **2019** *13* (8), 9408-9420. Copyright (2019) American Chemical Society."

In recent years, the molecular design concerning boronic acids was expanded towards other ligands, which partially lead to formation of more stable or even irreversible complexes, as they can further broaden the utility of PBAs for biological applications and their use inside living systems.[140] Addition of an aldehyde or ketone group in *ortho*-position to the boronic acid not only enables ligation with new molecular components, but also provides the possibility for multi-component reactions which partially exhibit significantly enhanced hydrolytic stability.[166]

A still reversible, yet selective and fast labeling strategy was applied by the reaction of 2-formyl phenylboronic acid with *N*-terminal cysteines. It has been reported that initial imine formation and activation of the imine by the boronic acid upon formation of a B-N bond leads

to a nucleophilic attack of the thiol on the imine, forming the thiazolidine product. Unlike conventional formation of thiazolidines by cysteine and aldehydes that require acidic conditions, the boronic acid assisted reaction can occur at neutral pH and offers higher rate constants in the order of 10^3 $M^{-1}s^{-1}$. Thiazolidino boronate structures were shown to hydrolyze upon acidification, but are stable at neutral pH and the formation is not disturbed by potential inhibitors such as fructose, glutathione, serine and lysine. The utilization of this labeling technique was shown by modification of small peptides and a model protein.[167]

In order to label proteins in an irreversible fashion, the “click” reaction between *ortho*-acetylboronic acid and thiosemicarbazide-nopoldiol was used. These two bifunctional compounds were found to form a conjugate under physiological conditions without being disturbed by potential biocompetitors such as glucose, fructose and catechol as well as pyruvoyl and glyoxyly electrophiles. The non-toxic educts quickly reacted with each other upon formation of a boronate ester as well as a thiosemicarbazone residue. The biorthogonality of this reaction was demonstrated by labeling HEK293T cells after the boronic acid compounds were installed on the cell surface.[168] Pinanediol derivatives themselves, for example nopoldiol, form one of the most hydrolytically stable boronate esters with binding affinities of 10^5-10^6 M^{-1}. Here, the rigidity of pinanediol hinders hydrolysis, while at the same time coplanar preorganization of the hydroxyl groups leads to practically no loss in entropy during ester formation compared to the unbound diol.[169],[170]

As presented in this chapter, boronic acids engage in interactions with many nucleophiles which can be utilized for various applications. An overview of selected boronic acid complexes is shown in Figure 19.

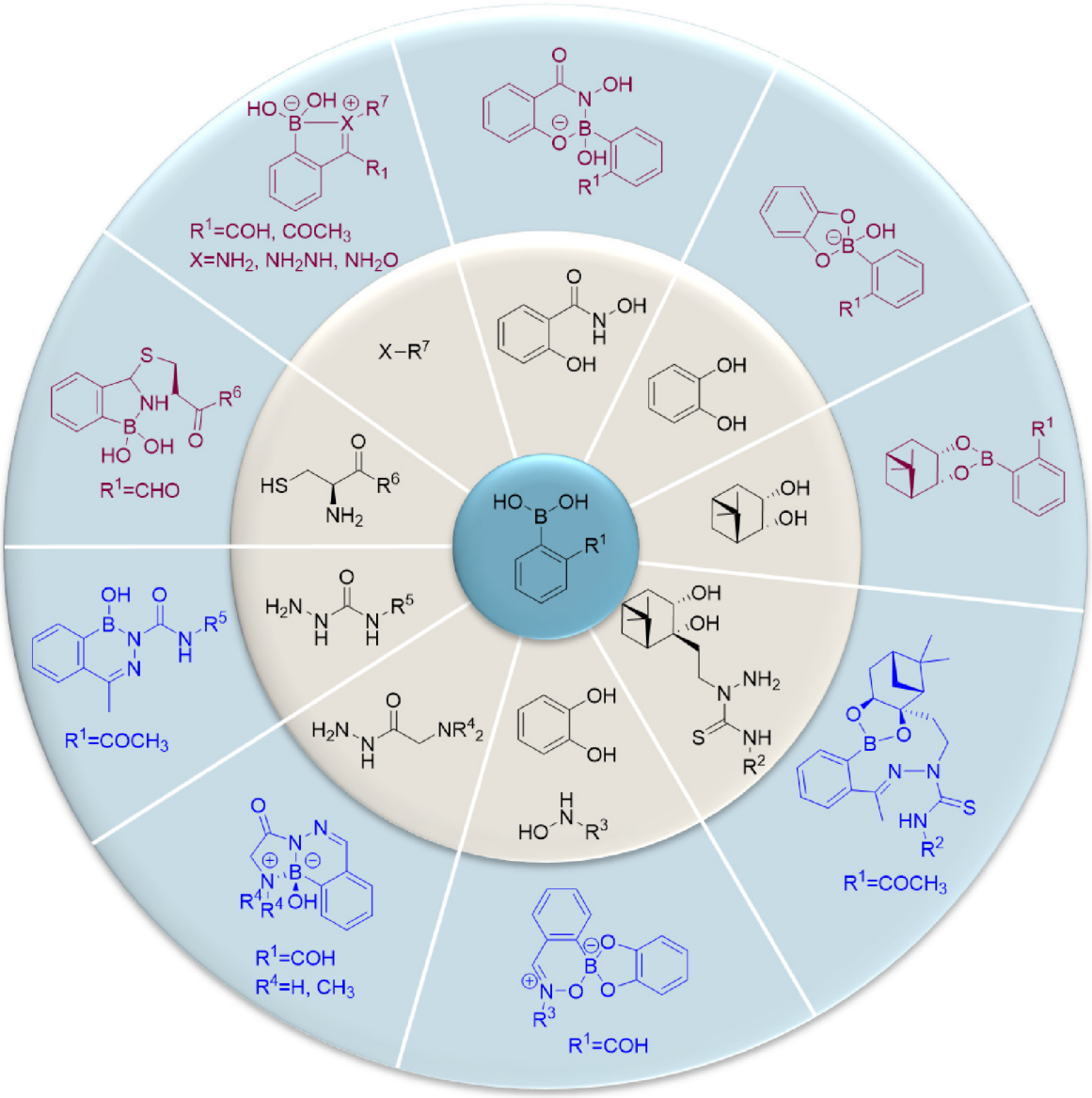

Figure 19: Overview over reversible (purple) and irreversible (blue) interactions of boronic acids with various compounds.[140],[166]

1.2.3 Oxidation of Phenylboronic Acids

As discussed in the previous chapter, boronic acids can act as Lewis acids towards oxygen containing nucleophiles. This reactivity is also exploited in the irreversible oxidation of phenylboronic acids to the corresponding phenol derivative.[171] The reaction has been reported to occur with various reactive oxygen species (ROS) while the research focus is mainly on the oxidation using hydrogen peroxide, as it is one of the most stable ROS and shows high reactivity towards PBA.[172],[173]

The first step of the reaction is the coordination of a hydroperoxide anion to boron leading to the formation of a negatively charged tetrahedral boronate which has been described before in chapter 1.2.2. A nucleophilic rearrangement results in the insertion of an oxygen

atom in the C-B bond, which marks the oxidation step. Slightly basic aqueous conditions lead to hydrolysis of the borate ester and release of boric acid. Depending on the substitution and reactivity of the phenol derivative, the newly generated phenolate can further undergo a cascade reaction, which through an 1,6-elimination reaction results in the release of *para*-quinone methide that will be hydrolyzed into 4-(hydroxymethyl)phenol in aqueous media (Figure 20).[171] The elimination reaction has been reported to occur with boronic acid derivatives which are substituted with hydroxymethyl based linkers such as ethers, esters, carbonates and carbamates. The oxidation leads to release of alcohols when using ether-based linkers, while esters result in the corresponding carboxylic acid. Due to the instability of carbamic acids and monosubstituted carbonate esters, the elimination reaction will be followed by release of CO_2 for carbamates and carbonates, which thermodynamically drives the reaction and generates the respective amine or alcohol derivative.[174]

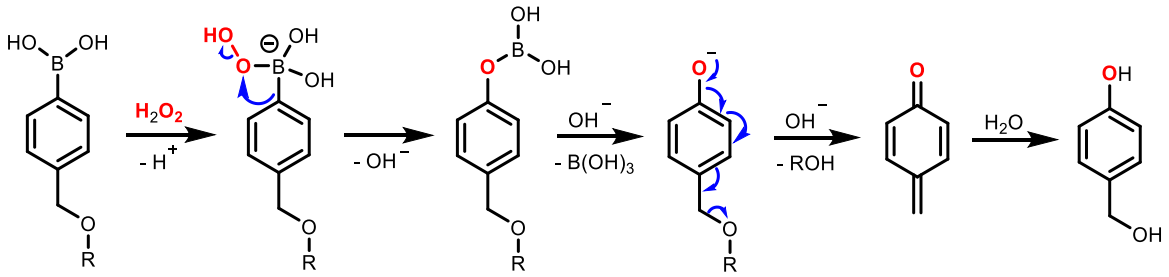

Figure 20: Reaction mechanism of hydrogen peroxide induced oxidation of phenylboronic acids.[171] Recreated with permission from “The Chemistry of Boronic Acids in Nanomaterials for Drug Delivery” by A.Stubelius, S. Lee, A. Almutairi, *Accounts of Chemical Research* **2019** *52* (11), 3108-3119. Copyright (2019) American Chemical Society."

As the oxidation of boronic acids occurs at physiological temperature and pH values in aqueous media, the reaction is a promising candidate for performing chemical reactions inside living systems. Further important factors are that the side products boric acid and 4-(hydroxymethyl)phenol are considered non-toxic and the reaction can be triggered by physiological concentrations of hydrogen peroxide.[128],[175]

Even though the production of ROS is required for cellular defense mechanisms and signaling, elevated concentrations can be detrimental for cells.[176] Oxidative stress related diseases, which are characterized by an imbalance of oxidizing and reducing agents in the biological environment, are accompanied with higher amounts of reactive oxygen species than healthy organisms. Diseases such as cancer, Alzheimer’s disease, cardiovascular disorders and amyotrophic lateral sclerosis (ALS) are medical conditions which are related to high oxidative stress.[177],[129] Cancer cells have been reported to produce elevated ROS concentrations in comparison to healthy cells as these reagents are involved in many processes such as metastasis, proliferation, angiogenesis and apoptosis.[178],[179],[128] For this reason, the oxidative cleavage of boronic acids is an attractive tool for therapeutic and

diagnostic applications in cancer research and medicine.[176] Due to the variation of functional groups which can be modified by cleavable boronic acids and the aforementioned abundance of H_2O_2 in living systems, this strategy has been used and described in multiple research articles. Besides the sensing of reactive oxygen species, the oxidation reaction has also been exploited for drug release systems as well as pro-drug synthesis. Here, boronic acids have been used as protecting groups for small drug molecules but also for temporarily masking the activity of enzymes.[129],[176],[180],[130]

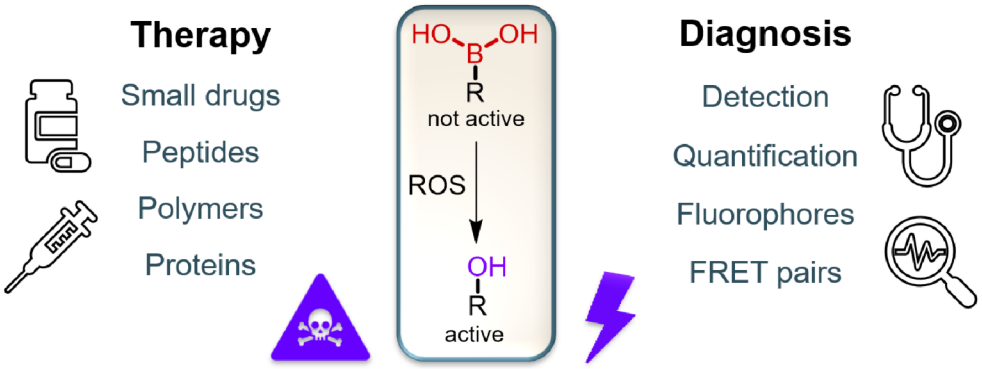

Figure 21: The use of boronic acid oxidation as therapeutic and diagnostic tools.

Cancer tissue is known to contain elevated concentrations of ROS such as H_2O_2, hydroxyl radicals and superoxide anions in comparison to healthy tissue, therefore utilizing the selective cleavage of boronic acids inside cancer tissue might lead to increased efficiency of drugs or drug release and prevent side effects.[176],[128] Additionally, boronic acids showed increased selectivity towards cancer cells due to interaction with the glycocalyx, the polysaccharide coated cancer cell surface.[180] Masking of hydroxyl groups in drug molecules by boronic acids can lead to inhibition of their activity, which can successfully be restored by oxidative cleavage of the protecting group. Lei Wang et al. reported that treatment with boronic acid protected SN-38, which is a camptothecin derivative, could inhibit the growth of multiple cancer cell lines and showed anti-tumor activity in a xenograft model (Figure 22).[180] Furthermore, the group of Kim was able to create a theranostic tool by incorporation of a coumarin derivative into a boronic acid prodrug of SN-38. Upon reacting with intracellular hydrogen peroxide, the active drug and the fluorophore were released, which led to increased fluorescence inside lysosomes. The self-reporting drug inhibited tumor growth in a mouse model of metastatic lung cancer.[128] Derivatives of 4-hydroxytamoxifen as well as nitrogen mustard were also used for ROS-activated release of active drugs in cancer cells.[181],[182] Kuang et al. synthesized two boronic acid modified nitrogen mustard derivatives. In contrast to the systems described before, the drug molecule was bound to the boronic acid by an ammonium group and not by oxygen-based linkers or direct substitution of a hydroxyl group by $B(OH)_2$. Upon treatment with hydrogen peroxide, nitrogen mustard was released leading to interstrand cross-linking of DNA

(deoxyribonucleic acid), which is known to be the reason for the cytotoxicity of the drug. The group successfully reported cell growth inhibition of various cancer cell lines, while healthy lymphocytes showed no apoptosis. These experiments showed that the toxic effect of nitrogen mustard was inhibited by the boronic acid masking group and released selectively upon oxidation by high concentrations of ROS inside cancer cells.

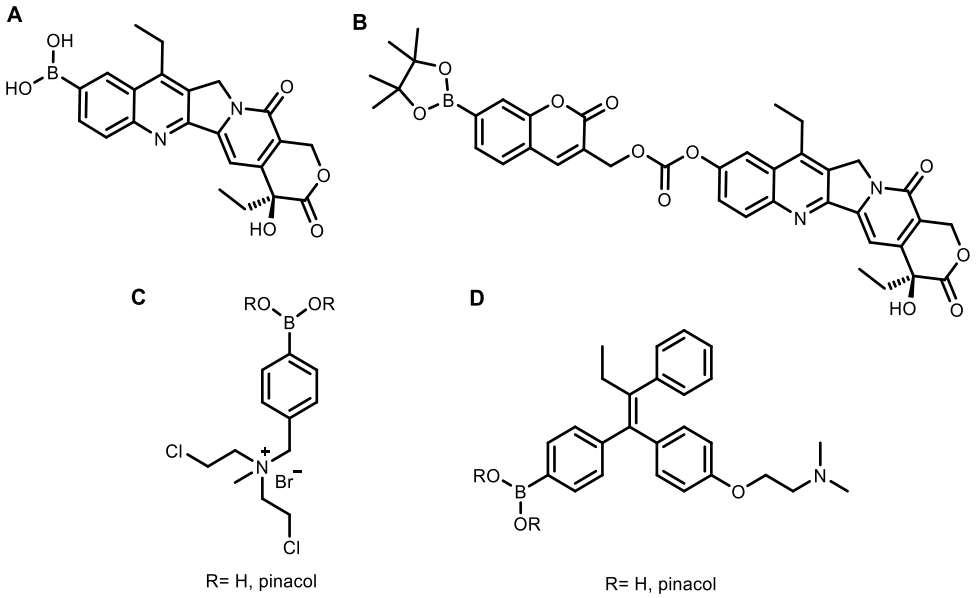

Figure 22: Boronic acid prodrugs of SN-38 (A)[180], camptothecin (B)[128], nitrogen mustard (C)[182] and tamoxifen (D)[181].

Oxidative removal of boronic acid groups also found application in the field of reversible protein modification. Qiaobing Xu and coworkers reported the functionalization of RNase A (ribonuclease A) lysine residues with carbamate bound boronic acids, which decreased the activity of the enzyme to 5% (Figure 23). Upon oxidative removal of the PBA protecting groups, the enzymatic activity was successfully restored to 95%. The cytotoxic effectivity of the protein, which is based in the cleavage of RNA, was rehabilitated inside various tumor cell lines by oxidation with endogenous H_2O_2 inducing the traceless release of the enzyme.[130]

In a similar approach Hoang et al. showed the caging of the lysine residue Lys40, which is a key component for the ribonucleolytic activity of angiogenin (ANG), with boronic acid.[183] ANG was reported to be a promising candidate for the treatment of amyotrophic lateral sclerosis (ALS), which is correlated to a high concentration of ROS. However, strong side effects such as tumor growth are expected during long-term treatment with ANG, which is why a protecting group, that can selectively be cleaved of in the area of interest, would be beneficial. The research group replaced the lysine residue with a cysteine for site-selective modification with a phenylboronic acid derivative by a radical-initiated thiol-ene reaction. Upon cleavage of the protecting group with hydrogen peroxide the enzymatic activity of ANG was restored and it also regained its ability to induce cell proliferation. Furthermore,

boronic acid modified ANG protected astrocytes from ROS-related damage which made it a promising candidate as a prodrug for ALS patients. The side products of the reaction did not show toxicity towards astrocytes.

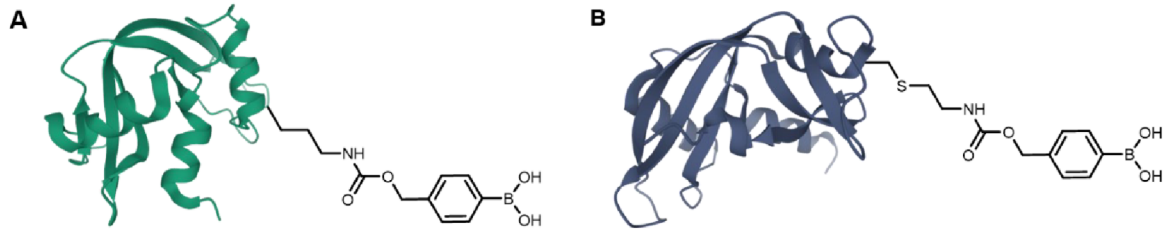

Figure 23: Structure of boronic acid modified RNase A (A)[130] and angiogenin (B)[183]. Protein structures were adapted from the RCSB protein data bank: RNase A was found under "1KF5" and angiogenin under "1ANG".

Another way for therapeutic use of boronic acids are polymer particles loaded with drugs, which can be released on demand upon oxidative cleavage at the place of interest. Almutairi and coworkers developed polyester based nanoparticles which were able to release loaded cargo based on removal of boronic acid groups and subsequent particle degradation at biologically relevant concentrations.[176] Another approach for hydrogen peroxide induced cargo release was published by the group of Fréchet, which used boronic acid modified dextran to release chicken egg albumin in $CD8^+$ T-cells (Figure 24).[184]

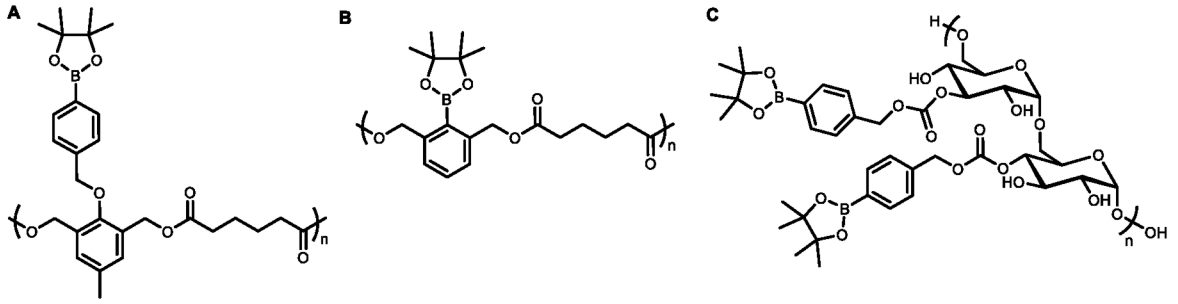

Figure 24: Boronic acid functionalized polymers by Almutairi et al. (A and B)[176] and Fréchet et al. (C).[184]

Besides potential therapeutic use of the oxidative cleavage of boronic acids, the reaction has also been utilized in many sensing systems to detect hydrogen peroxide *in vitro* and *in vivo*. Due to the similarities in size and shape of many ROS and hydrogen peroxide selective detection is challenging. Therefore, using its chemical reactivity is the preferred method for selective sensing of hydrogen peroxide.[129] In recent years many boronic acid based fluorescent sensors for H_2O_2 detection have been developed, which often utilize phenylboronic acids to prevent fluorescence.[185],[186],[187] Upon oxidative removal of the protecting group, the ability of the sensor molecule to emit light upon irradiation is uncaged and can be detected (Figure 25).

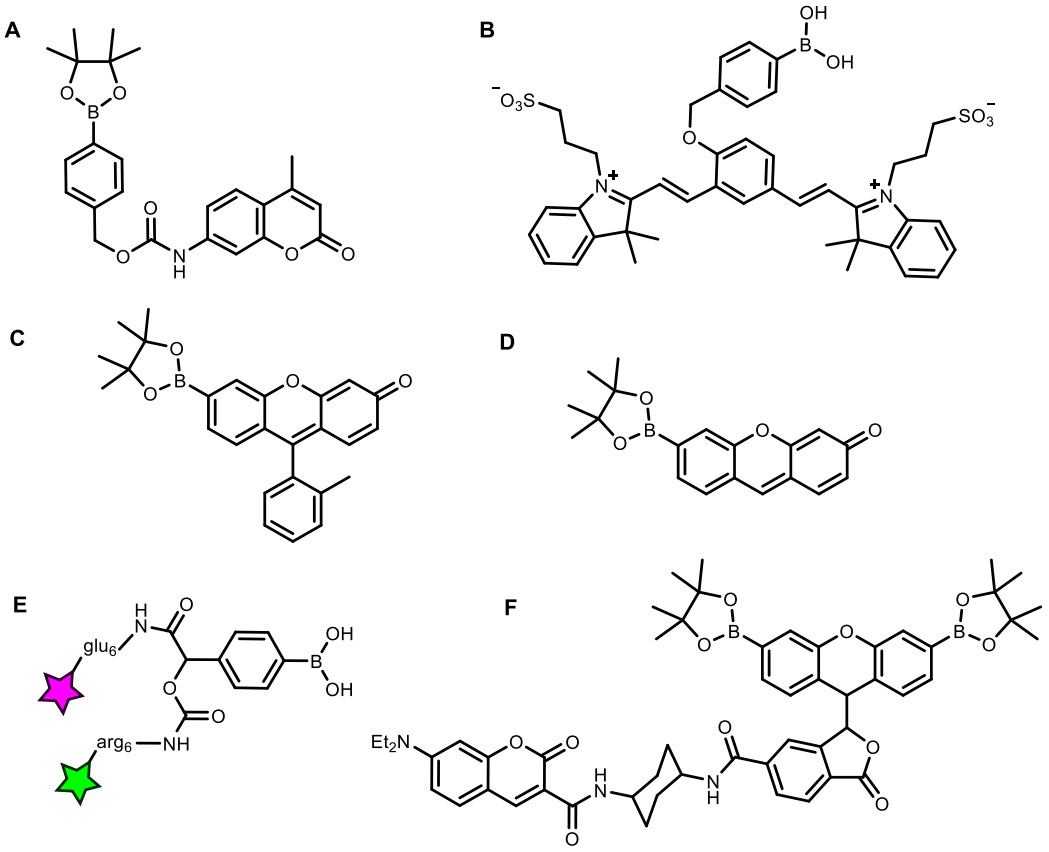

Figure 25: Boronic acid modified fluorescent probes A[185], B[186], C and D[187] that are activated upon oxidative removal of PBA and FRET systems E[175] and F[188] utilizing the same reactivity of boronic acids.

Other systems involve the unleashing of FRET upon treatment with hydrogen peroxide.[188],[189],[190] Utilizing activatable cell-penetrating peptides Tsien et al. demonstrated peptide cleavage upon treatment with endogenous hydrogen peroxide. The hairpin peptide consisted of a cell-penetrating residue with the sequence D-Arg_9 and the inhibitory sequence D-Glu_9, which were linked by 4-boronic mandelic acid and the peptide was labelled with a FRET pair. Oxidation of the boronic acid linker and the subsequent 1,6-elimination led to cleavage of the peptide into the anionic and cationic parts. Dissociation of the FRET pair led to change in fluorescence and cellular uptake, which could be monitored in an *in vivo* mouse model of lung inflammation.[175]

Oxidation of boronic acids by other reactive oxygen species has not been investigated as thoroughly as for hydrogen peroxide. However, some groups compared the reactivity of their systems with different ROS. Lei Wang et al. showed that the release of SN-38 has been decreased dramatically upon switching from H_2O_2 to hypochlorite (OCl^-), hydroxyl- and *tert*-butoxy radicals as well as *tert*-butylhydroperoxide. The latter ROS showed a release of 8% of the drug while hydrogen peroxide led to 100% drug release.[180] Kim et al. reported the selectivity of their prodrug towards hydrogen peroxide, as it was not cleaved by other biologically relevant ROS such as TBHP (*tert*-butyl hydrogen peroxide), hydroxyl

radicals ($OH^{\cdot}$), *tert*-butoxy radicals ($^{\cdot}O^{t}Bu$) super oxide (O_2^{-}), and hypochlorite anions (OCl^{-}).[128] Boronic acid modified nitrogen mustard derivatives showed slight reactivity towards TBHP and hypochlorite, while they were barely affected by other ROS excluding hydrogen peroxide.[182] The same applied for boronic acid modified RNase A, which besides hydrogen peroxide was also cleaved by TBHP and OCl^{-}.[130]

Unlike other ROS excluding hydrogen peroxide, peroxynitrite was reported to show high reactivity towards boronic acids. In a study using boronic acid modified peroxy-caged luciferin, Bonini and co-workers reported the efficient transformation of the bioluminescent sensor into its phenol derivative and subsequently into luciferin under physiological conditions induced by peroxynitrite triggered boronic acid oxidation.[191]

Furthermore, Xiao et al. reported the aerobic oxidative hydroxylation of phenylboronic acid using photocatalytic methods. Here, a transition metal catalyst $[Ru(bpy)_3Cl_2]\cdot 6H_2O$ and triethylamine were used for the generation of superoxide radical anions out of ambient oxygen molecules upon irradiation with visible light, which subsequently oxidized the boronic acid to the respective phenol derivative.[192] In a similar approach Scaiano's group reported the metal-free hydroxylation of boronic acids using methylene blue as the photocatalyst.[193]

Summarizing, the oxidative removal of boronic acid groups has been utilized in various ways for potential applications in treatment and diagnosis of diseases with elevated oxidative stress. While some ROS also show reactivity towards boronic acids, hydrogen peroxide is the most well studied biologically relevant oxidizer for such applications which shows its attractiveness in this field.

2 Motivation

Inspired by how nature uses polypeptides and proteins to execute numerous tasks in catalysis, replication, molecular recognition and energy storage, peptide derived materials have become highly attractive for many applications in nanobiotechnology and biomedicine in recent years.[14] Besides their diverse functions and tuneable properties, their outstanding biocompatibility and biodegradability are of high advantage in these fields which offer the possibility to use them in living systems.[194]

The broad diversity of amino acids provided by nature as well as easy synthetic availability of peptides by well-established solid-phase peptide synthesis facilitate the modulation of the characteristics of peptide materials on demand. Precise positioning of each amino acid within the primary peptide sequence can provide the control over inter- and intramolecular interactions of the peptides by choosing amino acids with the appropriate side chain functionality. Supramolecular interactions between peptides can lead to assembly into various nanostructures which is of high interest for various applications, as the dynamics and reversibility of supramolecular binding provides responsiveness of the materials to their environment.[195] In detail, supramolecular peptide assemblies have been investigated for the use in tissue engineering[33], drug delivery and controlled drug release[196],[197], sensing[198] and as antimicrobial materials[199]. While the twenty-one naturally encoded amino acids offer a wide variety of hydrophobic, hydrophilic, charged and aromatic residues[194], this diversity of functional groups can further be expanded by numerous unnatural amino acids and chemical modification, which can add new functions and characteristics to the peptides.

To further tune the properties of the peptide assemblies and form them on demand on the place of interest, precise control over assembly processes is necessary. Using bioorthogonal chemical tools, peptides can be designed to assemble upon treatment with biologically relevant stimuli in a controlled fashion. As many applications inside living systems require degradation and clearance of the biomaterial after serving its purpose, controlled disassembly of the material should also be granted.[40],[200] By taking advantage of reversible dynamic covalent chemistry as well as selective chemical modifications by reagents present in biological systems, the controlled disassembly of peptide-based materials can be achieved. This could promote the biological degradation of assembled peptide materials, which are generally more stable than their monomeric form.[12]

This thesis will present the controlled assembly of peptides induced by chemical reactions in both reversible and irreversible fashion, where strategies offering the possibility for controlled disassembly are also explored. For application as biomaterials or in living

systems, triggers must be used which are capable of inducing the peptide assembly in a bioorthogonal fashion in the targeted area. In order to be suitable for this task the stimulus needs to already be present inside the biological system or has to be applied without causing any negative effects such as toxicity. Furthermore, peptide assembly preferably should be induced only at the targeted site, therefore the stimuli should preferentially be only present at this location or at a higher concentration. The pro-assembling sequences need to be in their monomeric form and stable in absence of the trigger, however once the stimulus is applied, the peptides should be reactive enough to facilitate assembly before clearance or degradation of the peptides occurs. Good candidates for triggering peptide assembly which fulfill these criteria are enzymes, irradiation with light, changes in pH or biologically relevant reactive molecules. Some of these stimuli have been utilized within this thesis to control the assembly and disassembly of peptides.

The first presented peptide assembly is based on a kinked depsipeptide which is not able to self-assemble till it is linearized by an *O,N*-acyl shift. In previous reports, depsi-bonds have been introduced into peptides in order to optimize the synthesis of difficult sequences, however their utility for inhibiting structure formation in biological applications is low.[201] Since depsipeptides are only stable at pH values lower than 2, they cannot be applied *in vivo* as this pH is far below physiological values and exceeding this value would lead to an *O,N*-acyl shift and formation of peptide assemblies in an uncontrolled manner. To solve this problem, in this project the depsipeptide was secured using a carbamate bound protecting group preventing the *O,N*-acyl shift. Upon carbamate hydrolysis in phosphate buffered saline at pH 7.4 the peptide is uncaged, which leads to an intramolecular shift forming an amide bond while sacrificing the ester. This intramolecular rearrangement causes the generation of a linear peptide with the capability of self-assembling into fibrillar nanostructures guided by supramolecular interactions at physiological conditions. The controlled disassembly of peptides is achieved by oxidative transformation of methionine into methionine sulfoxide, as the significant change in polarity from the unpolar thioether in the side chain of methionine into the dipolar sulfoxide leads to repulsion of peptide molecules as well as higher water solubility and therefore deconstruction of the peptide fibers. Utilizing hydrogen peroxide which is present in biological systems for the controlled disassembly of peptide nanostructures showed the potential for application of these peptide assemblies as biodegradable materials.

For application in living systems, a similar approach for the controlled assembly of peptides is presented in the second project. Peptide assembly inside cells has been studied in recent years to develop new strategies for cancer treatment. Furthermore, studying intracellular self-assembly of peptides might give insights into self-assembly in nature such as formation of cell membranes or the cytoskeleton and might also help to understand the processes of

protein aggregation which are responsible for medical conditions such as Alzheimer's disease.[12]

Within this project uncaging of the depsipeptide is achieved by oxidative removal of a phenylboronic acid protecting group inside living cells, after previously being delivered into the cell by a dynamic covalently bound cell-penetrating peptide. Here, the cell-penetrating peptide TAT (transactivator of transcription)[202] is bound to the depsipeptides utilizing pH-responsive interactions between boronic acids and salicylhydroxamic acid. After cellular uptake, hydrolysis of the TAT-depsipeptide complex and oxidation of the PBA protecting group, the subsequent rearrangement of the peptide amphiphiles leads to intracellular fiber formation via π-π stacking interactions. Building-up dense peptide fiber networks showed severe effects on the morphology and faith of cancer cells. Combination of boronic acid chemistry with peptide assembly was shown to fulfill all requirements needed for delivery and controlled assembly of peptides inside living cells.

To increase the specificity of peptide-peptide interactions and receive fully reversible assemblies, dynamic covalent interactions between non-natural amino acids have been investigated in the third study. In collaboration with Marco Hebel et al. multivalent boronate ester formation between peptide chains offered the possibility to tune the binding properties of peptides mimicking the specificity of DNA binding to form double strands. Acidic hydrolysis of dynamic covalent boronic acid-catechol esters offers control over the assembly processes in a bioorthogonal fashion leading to disassembly of the peptide conjugates. As peptide assembly is induced at physiological pH of 7.4 and disassembly occurs at slightly acidic pH values which are found in acidic cellular compartments, this project represents a valuable approach for precise bioorthogonal peptide assemblies with possible applications in pH-responsive conjugation of macromolecules and as prototypes towards developing synthetic DNA mimics.

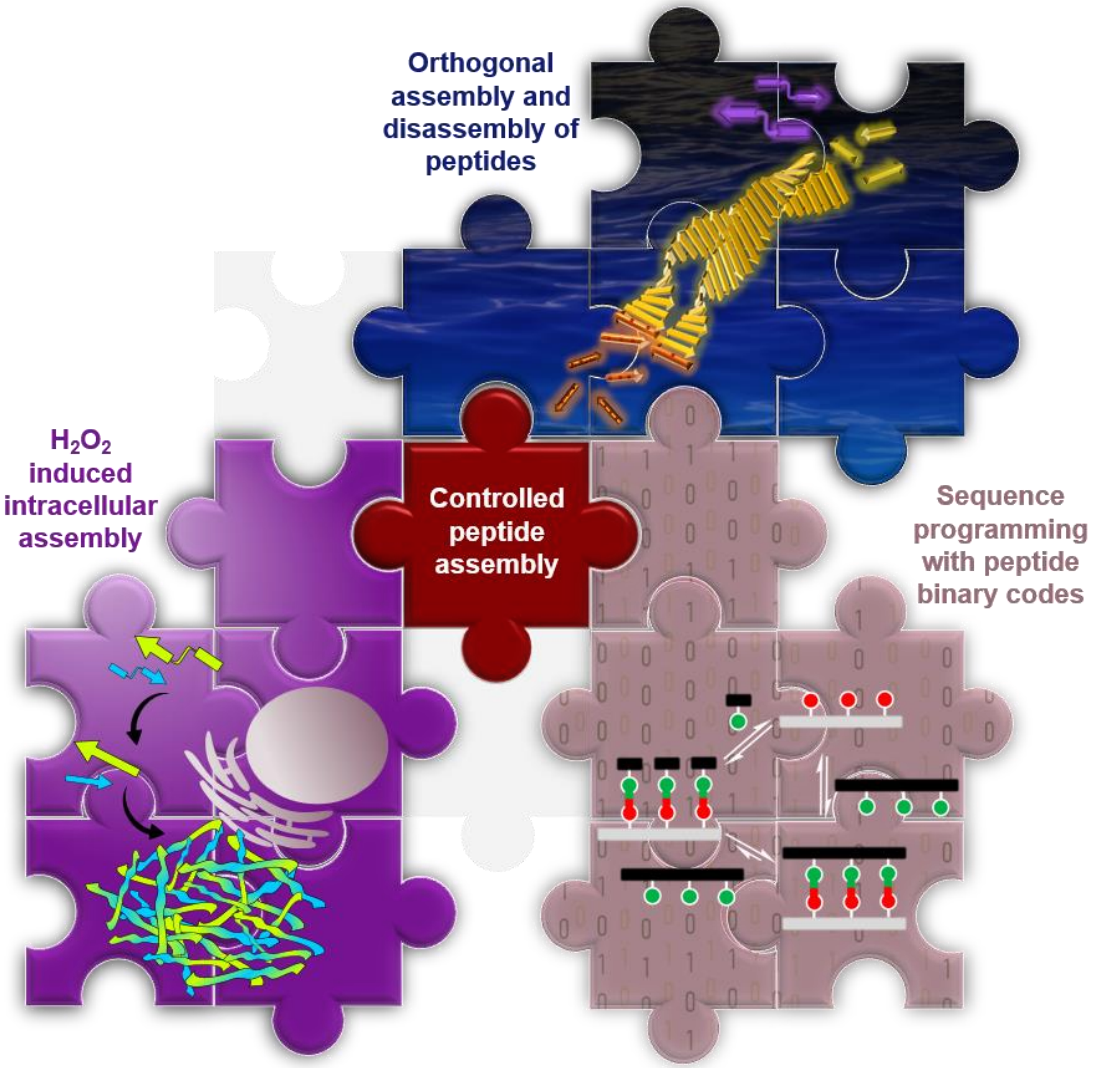

Figure 26: Schematic overview of the three projects on controlled peptide assembly utilizing different types of bioorthogonal stimuli and peptide-peptide interactions. A part of the figure was adapted from a publication by Pieszka et al.[203] (https://pubs.acs.org/doi/abs/10.1021/jacs.0c05261), Copyright 2019 American Chemical Society, licensed under CC BY 4.0, https://creativecommons.org/licenses/by/4.0. A part of the figure was recreated based on a publication from Hebel et al.[204] (https://pubs.acs.org/doi/abs/10.1021/jacs.9b03107), Copyright 2019 American Chemical Society, licensed under CC BY 4.0, https://creativecommons.org/licenses/by/4.0. A part of the figure was adapted from a publication by Pieszka et al. with permission of John Wiley & Sons, Inc. – Copyright 2019.[205]

The results of the afore described projects have been published in three publications and are presented in the next chapters.

3 Results

3.1 Orthogonally Stimulated Assembly/Disassembly of Depsipeptides by Rational Chemical Design

Stimulus-responsive peptide assembly and disassembly is a promising approach for formation of novel biomaterials with distinct features such as biocompatibility and biodegradability. While many systems have been reported for creating peptide-based materials based on their supramolecular assembly, only limited cases for the controlled formation of peptide nanostructures such as peptide fibers have been published, mainly focusing on enzymatic approaches.[12] Inducing peptide assembly upon treatment with a stimulus offers the high advantage of spatio-temporal control over structure formation which can provide new ways for application of these systems such as self-assembly *in vivo*. However, not only the formation of the nanomaterials, but also their fate inside biological systems needs to be considered. As it is well known, that peptide assemblies such as amyloid β fibers can have detrimental effects such as Alzheimer's disease and exhibit toxicity, controlling the disassembly of the peptide fibers has a high level of importance.[206] Only a limited number of triggers for disassembly of peptides have been investigated as described in 1.1.4 and their use is very constricted for applications as biomaterials, as they need to meet a wide range of requirements such as bioorthogonality and not being toxic. Triggers, which are already available in the biological milieu are among the best candidates for controlled assembly and disassembly of peptide fibers in living organisms, as they are already produced by cells and therefore are not toxic towards them. As mentioned before, the majority of reports on controlled assembly and disassembly focus on enzymatically catalyzed reactions. Even though various enzymes have been shown to be able to cause formation or destruction of chemical bonds yielding in either assembly into or disassembly of peptide nanostructures, their applicability is limited by the cellular expression of the respective biocatalyst. Therefore, more universal strategies to induce assembly processes utilizing ubiquitous stimuli are desired to expand the area of application.

A chemical approach for controlling peptide assembly involves depsipeptides. Here, introducing an ester bond into the primary sequence of the peptide leads to the formation of a kink, which prevents the assembly of the molecules. The kink which is created by coupling an amino acid to the side chain hydroxyl group of serine – leading to the formation of an ester bond and therefore the so-called depsipeptide – can be linearized by an *O,N*-acyl shift.[60] This shift is realized by an intramolecular nucleophilic attack by serine's amino

group towards the ester bond at pH > 2. The self-assembly is unlocked by the pH induced linearization of the peptide sequence. Unfortunately, this approach for inducing peptide assembly has its limitations to certain applications, as the depsipeptides are only stable at pH < 2. Treatment of cells, which are cultured at neutral pH values, with depsipeptides would lead to immediate transformation of the peptide and subsequent self-assembly, which might prevent cellular uptake. On the other hand, attempting to prevent the premature formation of peptide assemblies by treatment with acidic peptide solutions might be harmful to living organisms.[207]

In order to face these difficulties, in this work the controlled assembly of KIKISQINM into peptide fibers was shown by using the depsipeptide approach combined with a phenylboronic acid caging group, which was bound to the *N*-terminus of serine by a hydrolytically sensitive carbamate bond. Introducing a kink into the primary structure of KIKISQINM at the position between isoleucine and serine has been shown previously to prevent the self-assembly, however in this study the peptide quickly underwent rearrangement into the linear sequence when the pH was increased to a value higher than 2.[60] Within this thesis, securing the amine with a protecting group was anticipated to improve the stability of the depsipeptides at higher pH values, as besides the *O,N*-acyl shift, the required hydrolysis of the carbamate adds another gate to be passed in order to form peptide fibers.[201],[208]

To facilitate controlled disassembly of KIKISQINM peptide fibers, methionine was introduced into the peptide sequence. Hydrogen peroxide induced oxidation of the thioether in the side chain led to disassembly of nanostructures based on the switch from unpolar methionine to polar methionine sulfoxide. As the balance between hydrophobic and hydrophilic residues in amphiphilic peptides is important for fiber formation, its manipulation can lead to disassembly of the nanostructures.

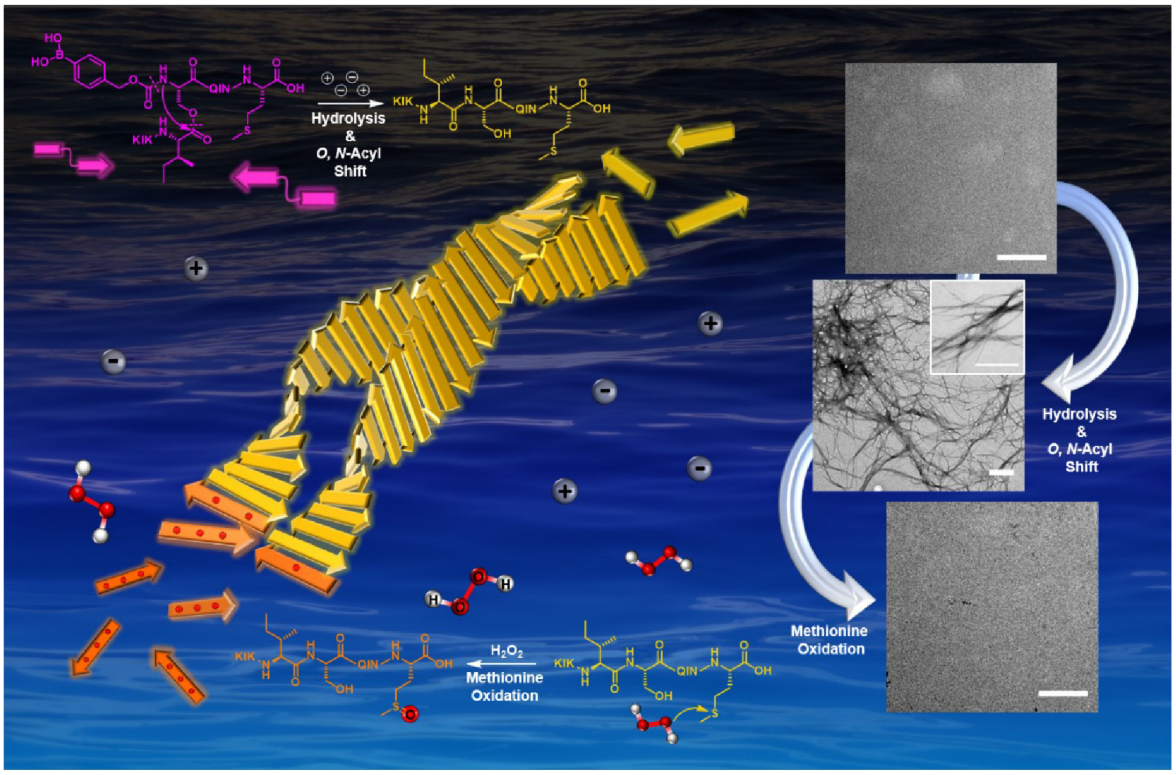

Figure 27: The assembly of KIKISQINM is controlled by the hydrolysis of the boronic acid based protecting group, which induces an *O,N*-acyl shift. Furthermore, the peptide fibers are disassembled upon oxidation of methionine to methionine sulfoxide by hydrogen peroxide. The assembly and disassembly of peptide fibers are shown by TEM, scale bars 500 nm. The figure was adapted from a publication by Pieszka et al. with permission of John Wiley & Sons, Inc. – Copyright 2019.[205]

The boronic acid caged depsipeptide depsi(KIKI)PBA-SQINM was synthesized using the standard Fmoc strategy of microwave-assisted solid phase peptide synthesis. After coupling of Fmoc-serine, which unconventionally was not protected in its side chain due to the need of a free hydroxyl group for creating the ester bond, the boronic acid modification was introduced into the molecule by carbamate bond formation on the *N*-terminus. Subsequent amino acid coupling reactions were performed without microwave assistance to preserve the heat labile carbamate bond. The kink in the peptide primary sequence was formed between serine and isoleucine by carbodiimide assisted ester bond formation.

The hydrolysis of the carbamate bond of depsi(KIKI)PBA-SQINM as well as the subsequent *O,N*-acyl shift leading to the linear fiber forming peptide sequence KIKISQINM were shown by a high-performance liquid chromatography (HPLC) based study. Formation of the intermediate depsi(KIKI)SQINM was already observed after 30 min, which shows the sensitivity of the carbamate towards hydrolysis, possibly originating from the electron-withdrawing properties of the boronic acid residue.[121] The removal of the caging group and the acyl rearrangement to form the linear peptide were completed after 24 h in phosphate buffered saline (PBS), after which the addition of hydrogen peroxide led to full conversion into the oxidized disassembling sequence depsi(KIKI)PBA-SQIN(M=O) in 8 h. The hydrolysis as well as the oxidation were not only shown by the shift in retention time in

HPLC, but also by matrix-assisted laser desorption/ionization mass spectrometry-time of flight (MALDI-ToF).

To proof the hydrolysis induced fiber formation, as well as the disassembly of the peptide fibers upon oxidation, the Proteostat Aggregation assay, as well as transmission electron microscopy (TEM) measurements were performed. Proteostat is known to bind to peptide fibers along their axis, which leads to appearance of a fluorescence signal, while the non-bound Proteostat is not fluorescent.[209] Addition of Proteostat to the depsipeptide did not show fluorescence, which indicates that no fiber formation has occurred. This was further proven by transmission electron microscopy. Meanwhile, after hydrolysis and a successful *O,N*-acyl shift, the assay showed a high fluorescence signal, which shows the interaction between β-sheet containing peptide fibers and the dye. TEM measurements clearly showed formation of dense fiber networks already one hour after starting the reaction. Upon addition of hydrogen peroxide, the peptide fibers were destroyed, which is indicated by the loss of the fluorescence signal as well as disappearance of all fibrillar networks observed by TEM imaging. As formation and disassembly of peptide fibers involves changes in molecular packing,[210] the peptide secondary structure was investigated using Fourier-Transform infrared spectroscopy (FT-IR) as well as circular dichroism spectroscopy (CD). CD showed the change of the peptide secondary structure upon hydrolysis and rearrangement from primarily random structures to primarily β-sheets. Oxidation of methionine led to partial destruction of the β-sheets, which was shown by CD. FT-IR measurements confirmed these findings by showing a decreased β-sheet content in the amide I band.

In conclusion, this study has shown the controlled assembly of peptides into nanostructures as well as the controlled disassembly of these peptide fibers, which aims to lay the foundation for application as stimulus-responsive biomaterials. Addition of the phenylboronic acid protecting group onto the depsipeptide prevented the *O,N*-acyl shift and subsequent peptide fiber formation in water. The ability of forming peptide nanostructures was uncaged by hydrolysis of the carbamate bound protecting group in PBS and led to fibrillation within an hour. Oxidation of methionine by hydrogen peroxide to methionine sulfoxide successfully led to decomposition of the structures, which is attributed to the dipolar character of the sulfoxide.[97]

As natural triggers for both assembly and disassembly have been utilized, it is imaginable that the knowledge gained through this study, may open the pathway for many applications in biotechnology as well as the induced formation of such structures inside living systems.

3.2 Controlled Supramolecular Assembly inside Living Cells by Sequential Multi-staged Chemical Reactions

As described in the previous chapter 3.1, gaining control over peptide fiber formation using natural stimuli offers new opportunities for building up nanostructures inside living systems, which could help us to understand biological processes and their dynamics as well as being utilized for detection and treatment of pathological conditions.

The first obstacle, which has to be overcome to achieve the challenging task of intracellular peptide assembly is cellular uptake of the peptides, which can be facilitated by using peptides that intrinsically are able to interact with the cell membrane or by modification of the peptides with membrane-permeable entities. Another issue which has to be solved is, that since peptide assembly is a spontaneous process which occurs at ambient temperature in aqueous solution such as cell culture medium, fibers can form before the peptides enter the cell. To solve this problem, peptides can be incubated at concentrations which are lower than concentrations required for fiber formation and be accumulated inside the cells by targeting specific organelles. Alternatively, pro-assembling sequences can be synthesized which are transformed into the self-assembling sequence inside cells upon interaction with a stimulus. However, triggering self-assembly by transformation of the peptides needs to fulfill all criteria of biocompatibility such as being non-toxic and being able to occur at physiological conditions.

Fiber formation inside living cells has been reported by a small amount of research groups using various techniques to induce peptide assembly. Such approaches include the assembly which is based solely on accumulation of peptides inside specific organelles for example mitochondria[102] and nucleoli[211], but also enzymatic reactions where functional groups which are preventing the assembly are removed or parts of the peptides are cleaved off, releasing the fiber forming sequence.[99] While these approaches are already promising candidates for building up nanoarchitectures inside cells, they also suffer from drawbacks such as the need for expression of the respective enzyme by the used cell line and fiber formation outside cells.

To overcome these issues, I designed new peptide sequences which co-assemble into peptide fibers upon treatment with hydrogen peroxide, an oxidant that is known to be overly produced by certain cancer cell lines.[212] To accomplish intracellular fiber formation, pro-assembling peptides had to be stable at the absence of hydrogen peroxide until they are being uptaken by cells and then undergo a transformation leading to peptide assembly. Cellular uptake had to be granted by using a membrane-permeable residue, which may not disturb peptide assembly. Furthermore, the peptides should offer the possibility for

intracellular detection for example by being fluorescent and the intracellular H_2O_2 concentration had to be sufficient for inducing peptide assembly. To address these requirements for formation of intracellular assemblies, two peptides were designed.

One of the peptides contains a Fmoc group, which is widely known for inducing peptide fiber formation of many short peptide sequences, while the other is equipped with a coumarin derivative, providing a facile way for imaging by fluorescence microscopy.[50] Additionally, the peptides are specifically transported into cancer cells by using a cell-penetrating peptide named TAT, which is dynamic covalently bound to the precursors of the fiber forming sequences and can be cleaved upon the change in pH in acidic cellular compartments.[160] In this work, I show that the intracellular formation of peptide fiber architectures cannot only be induced by using the natural abundant trigger hydrogen peroxide, but also has a detrimental effect on cancer cells.

Like in the previously described project, the depsipeptide strategy was used to prevent formation of peptide fibers. Furthermore, a boronic acid protecting group was attached to the *N*-terminus of serine, which has shown to be significantly more stable towards hydrolysis than in the case of KIKISQINM. Therefore, it was possible to use hydrogen peroxide as the trigger for deprotection, followed by the *O,N*-acyl shift and the subsequent peptide assembly, instead of using hydrolysis. To my knowledge this is the first example for incorporation of a depsi-bond into short aromatic peptide sequences.

As described in chapter 1.2.3, H_2O_2 is known to oxidize boronic acids, which induces a cascade reaction releasing a free amine from the carbamate. I designed the short aromatic peptide sequences Fmoc-ISA and Coumarin343-ISA for the co-assembly inside cancer cells, as comparable fmoc-containing sequences have been reported to efficiently form peptide fibers and coumarin 343 provides fluorescence.[213] Isoleucine and alanine were introduced into the sequence as it has been reported that hydrophobic residues in the primary peptide sequence further facilitate fiber formation.[14] The boronic acid did not only serve as a protecting group for the depsipeptide, but also as a chemical anchor for salicylhydroxamate functionalized TAT. The formation of the dynamic covalent bond between SHA and PBA at a pH value of 7.4 facilitates the cellular uptake of the depsi-sequences, which are released into the cytosol by acidic hydrolysis of the complex.

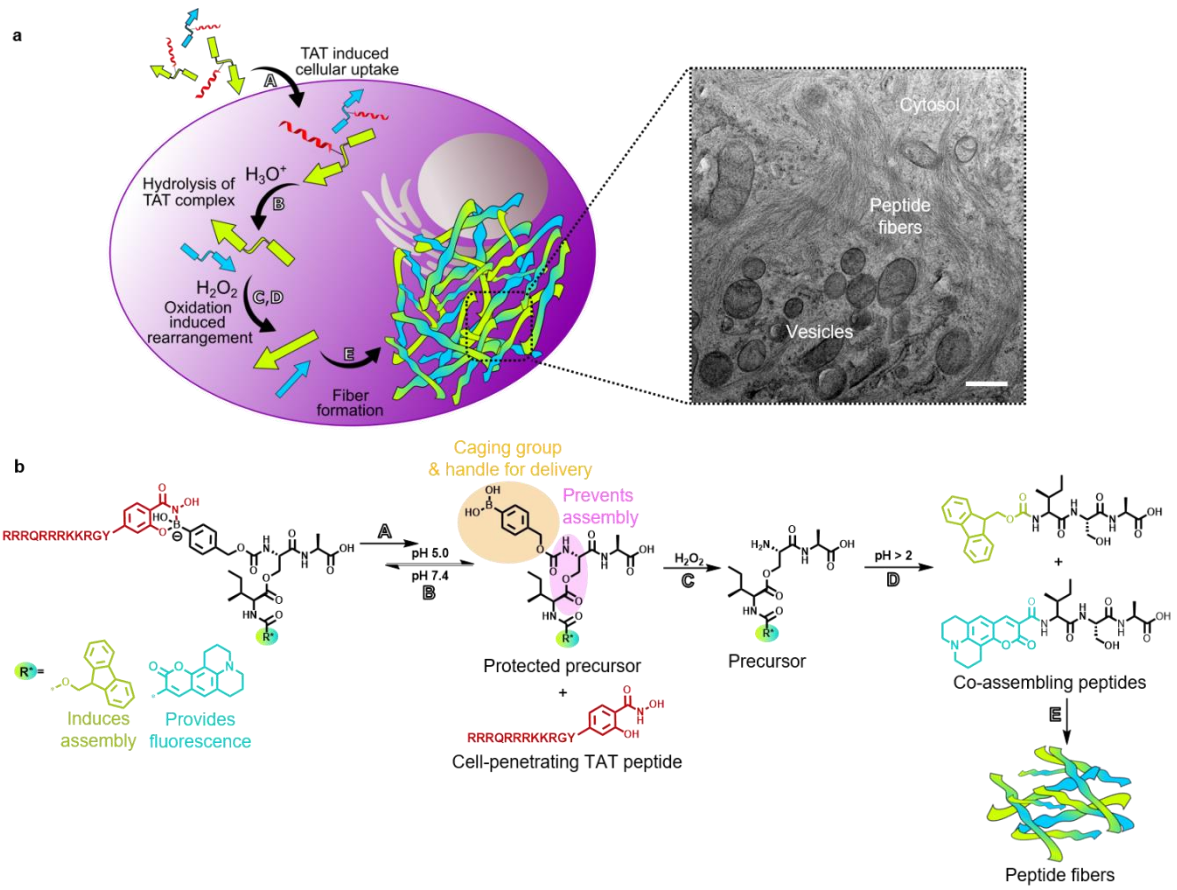

Figure 28: Intracellular co-assembly of peptides into fibrillar structures. a) Depsipeptides (kinked arrows) are uptaken by the help of dynamic covalently bound TAT (A). These complexes are hydrolyzed due to the decrease in pH in cellular compartments (B), which is followed by the oxidation induced rearrangement of the peptides (C, D). The rearranged peptides form peptide fibers inside cancer cells (E) which are imaged by TEM (scale bar 500 nm). b) Chemical reactions, which lead to cell uptake and the release of the precursor peptides into the cytosol, as well as the oxidation induced *O,N*-acyl shift, which leads to fiber formation. The figure was reprinted from a publication by Pieszka et al.[203] (https://pubs.acs.org/doi/abs/10.1021/jacs.0c05261), Copyright 2019 American Chemical Society, licensed under CC BY 4.0, https://creativecommons.org/licenses/by/4.0.

The fmoc and coumarin 343 functionalized depsipeptides were synthesized by SPPS and the ester bond as well as the boronic acid caging group were introduced into the sequence as described before in chapter 3.1. The hydrolytic stability of the depsipeptides in buffer solution as well as the H_2O_2 induced boronic acid cleavage and *O,N*-acyl shift were shown by HPLC. Both sequences were stable in ammonium bicarbonate buffer at pH 7.4, while addition of the oxidizing reagent led to complete transformation of the PBA depsipeptides into the respective linear peptides in 24 h for C343-ISA and 48 h for Fmoc-ISA.

TEM micrographs of the depsipeptides did not show formation of nanoarchitectures, while linearization was revealed to induce self-assembly. Fmoc-ISA was shown to form peptide fiber networks, while Coumarin343-ISA on its own formed amorphous aggregates. Coincubation of the peptides at an optimized ratio of 5:1 of Fmoc-ISA to C343-ISA showed formation of both - fibers and aggregates. To prove the incorporation of the fluorescent coumarin peptide into Fmoc-ISA fibers, fluorescence microscopy was used. Proteostat staining revealed the formation of peptide fibers, which overlaid with the coumarin 343

channel showed that C343-ISA indeed co-assembled with Fmoc-ISA to build up fibrillar networks. These findings were further supported by circular dichroism measurements, which showed changes in molar ellipticity upon coincubation of the peptides.

Formation of fibers by fmoc-peptides is linked to the secondary structure that is developed during the assembly processes.[214] Therefore FT-IR measurements were performed to determine the secondary structure of Fmoc-ISA in water. The results showed that different secondary structures are formed under these conditions, which was supported by results from solid state NMR, where formation of multiple secondary structures was revealed.

To achieve cellular uptake, a salicylhydroxamate functionalized TAT peptide was needed. The novel TAT derivative was synthesized by standard SPPS conditions and functionalized with 4-pentynoic acid, after which a copper(I)-catalyzed alkyne-azide cycloaddition was performed using protected 4-azido salicylhydroxamate. This novel molecule was synthesized in five steps starting from 4-amino salicylic acid. MALDI spectrometry showed that both depsipeptides were successfully bound to SHA-TAT by incubation with the cell-penetrating peptide in buffer at pH 7.4 and fluorescence quenching experiments revealed a dissociation constant of 2.67 µM for the dynamic covalent complex of depsi(C343-I)pba-SA and SHA-TAT, which is in accordance with previous reports.[215]

Adenocarcinomic human alveolar basal epithelial A549 cells were incubated with the depsipeptides and imaged by confocal laser scanning microscopy, which showed the successful cellular uptake by endocytosis, when the depsipeptides were preincubated with SHA-TAT. Without the delivery vehicle, no internalization was observed. Dissociation of the dynamic covalent complexes inside cells was shown by disappearance of a FRET (Förster resonance energy transfer) signal 4 h after coincubation of cells with the depsipeptides and fluorescently labelled SHA-TAT. Cells were imaged by fluorescence microscopy and by TEM, which clearly showed formation of fibrillar networks inside cancer cells. Depsipeptide-TAT complex treated cells were lysed and analysis of the cell lysate by TEM and fluorescence microscopy further proved peptide fiber formation. A cell viability assay showed that the viability of A549 cells was significantly decreased upon peptide fiber formation, as only 14% of the cells were still metabolically active after 6 h. Performance of the Annexin-V/propidium iodide assay showed that cells died via apoptosis.

In conclusion, this study yielded two novel peptide sequences, which were able to self- and co-assemble inside and outside cancer cells. As a result of the chemical design, cellular uptake and co-assembly of the peptides was controlled by natural triggers that are abundant inside cancer cells - pH and H_2O_2. Combining two properties of phenylboronic acid chemistry, on the one hand its ability to form dynamic covalent complexes, and on the other hand its oxidation induced immolation, a facile way was found to create peptide nanostructures on demand inside living systems. This work might not only be relevant in

cancer research but might also open new ways for investigating the dynamics of intracellular assembly processes.

3.3 Sequence Programming with Dynamic Boronic Acid / Catechol Binary Codes

While chapter 3.2 described the use of boronic acids to prevent assembly of peptides, the ability of boronic acids to spontaneously form dynamic covalent complexes at neutral pH can also be utilized to initiate interactions between peptides and lead to molecular ordering in a precise and programmed fashion mimicking DNA.

Only four nucleic bases are needed for building up DNA, which is the origin of all life. The highly specific binding of adenine to thymine and guanine to cytosine via hydrogen bonding leads to formation of a double helix, which stores and processes genetic information that is read by sequence-selective duplex formation and copied using it as a template.[216] The structure and function of DNA is defined by the preprogrammed monomer sequence and its ability to form DNA double strands with a complementary DNA sequence. To mimic the duplex formation of DNA while improving its properties, in one approach the backbone of DNA, which suffers from enzymatic degradation, has been replaced by a peptide backbone creating peptide nucleic acids (PNA), while maintaining the same base pairs. They showed enhanced binding affinity and higher stability towards proteases und nucleases.[217] While such biochemical approaches are well established, synthetic approaches are not developed as far. However, inspired by DNA-duplex formation some studies using hydrogen bonding, salt bridges and metal coordination have been reported to mimic the pairing of DNA.[218] Establishing synthetic DNA mimics contains numerous challenges, as many requirements have to be met in order to achieve successful binding. While easy synthetic accessibility is needed to guarantee sufficient sequence length, the monomeric units should also be small enough to avoid sterical hindrance. Furthermore, binding should be selective and sufficiently strong at physiological conditions but at the same time of dynamic nature in order to provide the option for error correction in the assemblies.

In this work, in collaboration with M. Sc. Marco Hebel, boronic acid chemistry was used to program the assembly of peptides by dynamic covalent interactions, which can be controlled by a change of pH. The binding partner used for L-boronophenylalanine was the catechol side chain residue of L-3,4-dihydroxyphenylalanine (L-DOPA). The boronic acid-catechol binding pair was chosen as a promising candidate for duplex formation, as it meets all requirements for such systems mentioned above. The size of the unnatural amino acids L-borophenylalanine and L-DOPA are similar to natural amino acids, therefore sterical hindrance was not expected to occur when appropriate spacers are incorporated into the peptide sequence. Additionally, the required amino acids can either be purchased or easily synthesized and solid-phase peptide synthesis is a well-established technique which

facilitates simple synthetic accessibility of the oligopeptides. Furthermore, sufficient binding affinity of the PBA-catechol interaction for biological applications as well as its reversibility have been demonstrated in previous reports.[123],[219]

Within this work, multiple peptide sequences were synthesized to evaluate the effect of the amino acid primary sequence concerning both the amino acids chosen as well as their position and the length of the peptide. Addition of spacer amino acids in the form of lysine between the boronic acid and catechol residues provided water solubility and facilitated the binding event. In this way, three oligopeptides functionalized with PBA $(AX)_1$, $(AX)_2$, $(AX)_3$ (A=L-borophenylalanine, X= L-lysine) and their catechol counterparts $(BX)_1$, $(BX)_2$, $(BX)_3$ (B=L-DOPA, X= L-lysine) were synthesized to elucidate the influence of multivalency on binding affinity.

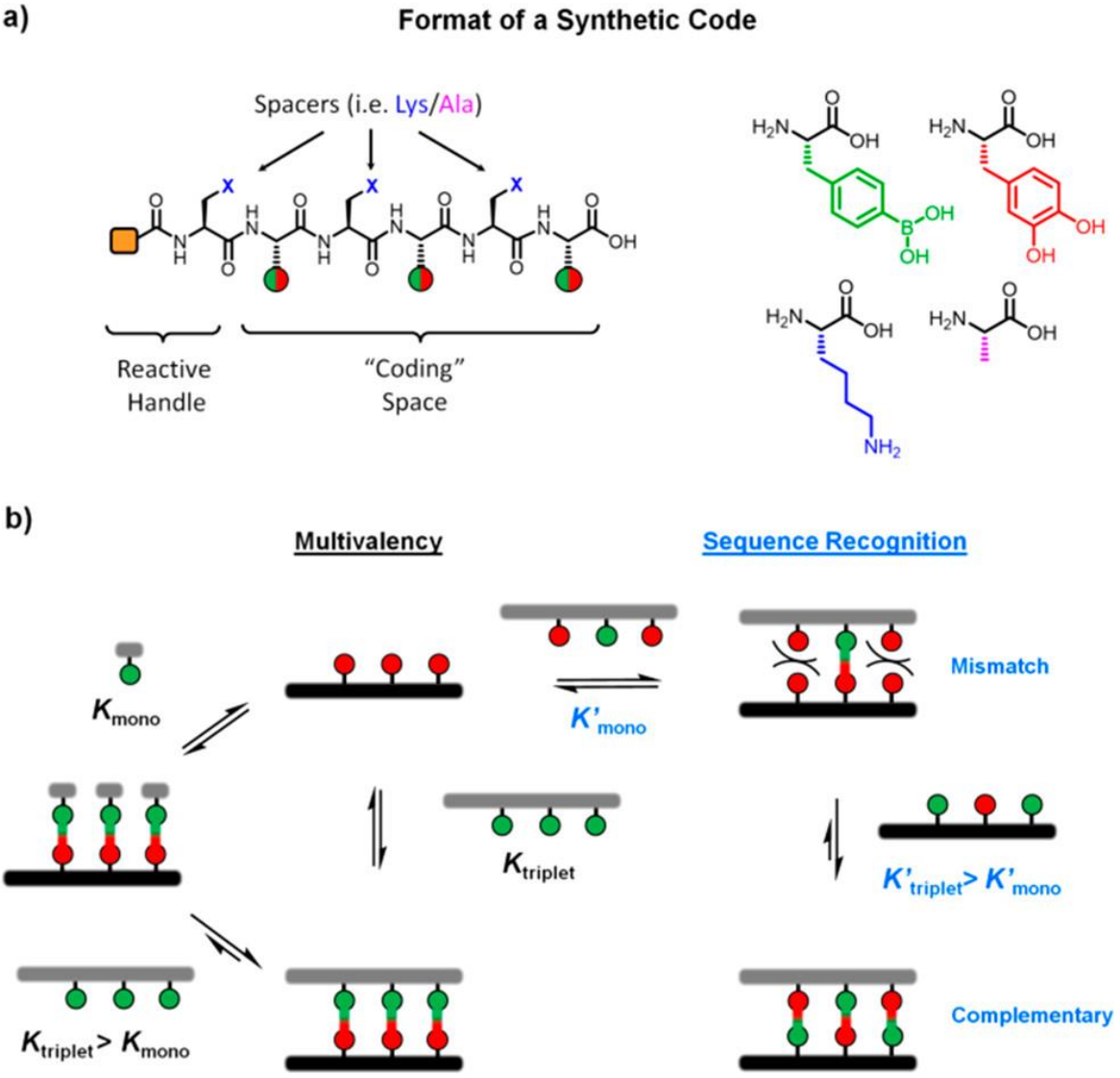

Figure 29: a) Chemical structure of the synthetic binary codes. b) Thermodynamic processes of peptide assembly demonstrating the effects of multivalency, complementarity and mismatching. The figure was reprinted from a publication by Hebel et al.[204] (https://pubs.acs.org/doi/abs/10.1021/jacs.9b03107), Copyright 2019 American Chemical Society, licensed under CC BY 4.0, https://creativecommons.org/licenses/by/4.0.

Measurements of fluorescence microscale thermophoresis between fluorescein labeled boronic acid peptides and their complementary counterparts showed that the binding affinity increased almost 10-fold from 1300 M^{-1} for single binding to divalent binding (12500 M^{-1}) and to 81400 M^{-1} for the trivalent binding event. In comparison to DNA binding, the trivalent boronic acid-catechol peptides exhibited similar affinity to each other as eight base pair long DNA strands with 50% guanine-cytosine content, which shows the superiority of the PBA-catechol binding.[220],[221] The trivalent peptide assembly was further characterized by MALDI-ToF, Fourier-transform infrared spectroscopy (FT-IR) and multidimensional proton nuclear magnetic resonance spectroscopy (^{1}H-NMR), which confirmed the binding event at pH 7.4. No peptide assemblies were observed at pH 5.0 in mass spectrometry, which verified the pH dependency of the dynamic covalent interactions. The assemblies were additionally characterized by circular dichroism spectroscopy (CD) and density-functional theory calculations (DFT). CD spectroscopy revealed a strong negative molar ellipticity at 210 nm at pH 7.4, which is assigned to the n-π* transition of a carbonyl group.[222] DFT calculations (density-functional theory) confirmed hydrogen bond formation between the carbonyl group of lysine and hydroxyl groups of the tetrahedral boronate ester.

Various sequences containing the boronic acid residues A, catechol amino acids B and both complementary parts as well as errors, which are not complementary, were synthesized to show sequence specific binding. While binding of ABA to BAB was slower than the trivalent binding between $(AX)_3$ and $(BX)_3$, the affinity was similar (79 400 M^{-1}). A possible reason for decreasing binding velocity is the time correction of errors in binding might take. Mismatch peptide pairs such as $(AX)_3$ and BYBB (Y=L-alanine) did not show binding.

Based on the higher binding affinity between trivalent peptide strands, the dynamics of displacement were studied by titration with the trivalent DyLight650-$(BX)_3$ analog of trivalent fluorescein labelled $(AX)_3$, which was saturated with monovalent $(BX)_1$. Förster resonance energy transfer measurements (FRET) showed at least 50% replacement of the monovalent catechol peptide by the trivalent one, demonstrating the superior binding due to multivalency.

Finally, the applicability of the binary codes in molecular recognition was shown by functionalization of polyethylenglycol and cytochrome C with complementary peptides. MALDI-ToF measurements of the dynamic covalently bound macromolecular assembly demonstrated the compatibility of the assembling peptide sequences for building up macromolecular conjugates.

In conclusion this study presented the use of dynamic covalent interactions of boronic acids with catechol in the context of peptide assembly. The design of complementary peptide sequences represents a first step towards synthetic DNA analogs with enhanced backbone stability and improved binding affinity.[217] As these peptides can easily be modified with

functional groups such as amines, thiols and maleimides as shown in the publication, they provide many possibilities for further functionalization and optimization. Furthermore, they offer a synthetic platform for the assembly of macromolecules in a bioorthogonal and pH responsive manner.

4 Conclusion

Within this thesis boronic acid modified peptides were utilized for controlled assembly and disassembly by exploiting reversible and irreversible PBA chemistry, as well as other bioorthogonal reactions such as oxidation and pH dependent hydrolysis. As peptide-derived materials are gaining more popularity in biomedicine, modulating their characteristics and properties by introducing dynamics into and control over these compounds will further expand their range of applications.

In the first study the orthogonal assembly and disassembly of peptides was presented which demonstrated the importance of peptide geometry as well as electrostatic properties for peptide-peptide interactions and therefore self-assembly. The hydrolytically induced linearization of depsi(KIKI)pbaSQINM led to formation of β-sheets and subsequent assembly into peptide fibers. These fibers were successfully disassembled upon oxidation of methionine by hydrogen peroxide into the respective sulfoxide. This study showed for the first time, that a boronic acid based protecting group can prevent the *O,N*-acyl shift in depsipeptides and release the assembling sequence upon hydrolysis of the carbamate linker at high salt concentrations in PBS. Within the same study, the first disassembly of KIKISQINM derived peptide fibers was shown by using the naturally occurring oxidative reagent H_2O_2, which is an important step towards biodegradable peptide materials that can be applied within living systems. To enhance the scope of application of controlled fiber assembly and disassembly, future experiments might focus on testing the reversibility of fiber disassembly. Here, reducing methionine sulfoxide back to methionine might possibly lead to reconstruction of peptide fiber networks in a controlled fashion. This might alter the properties of the peptide material and open new ways for tuning its characteristics. The enzyme methionine reductase might be a promising candidate for biochemically controlled formation of peptide fibers.[97]

The bioorthogonal formation of peptide fibers inside cancer cells was presented in the follow-up study. Here, intracellularly produced hydrogen peroxide induced peptide co-assembly into fluorescent fibers, which led to a significant decrease in cell viability of A549 cells. The responsiveness of the system towards increased oxidative stress makes it a promising candidate for application in tumor therapy as well as other diseases related to increased production of reactive oxygen species. In this project, dynamic covalent interactions of boronic acids have been used to ensure cellular uptake by reversible complexation with salicylhydroxamate modified TAT. To further enhance the applicability of the boronic acid depsipeptides for therapeutic application in cancer treatment, the cell-penetrating peptide might be exchanged for a cancer targeting moiety in future studies.[160]

Furthermore, the short peptide offers many possibilities for chemical modifications such as incorporation of drug molecules, which could add to its therapeutic value. Following the path of the firstly presented project, modification of the peptide primary sequence with amino acids containing functional groups that lead to a significant change in polarity upon a chemical reaction might be a first step towards intracellular, controlled disassembly of peptide fibers. While the oxidative induced fiber formation of boronic acid caged depsipeptides and the oxidative disassembly of methionine functionalized peptides are not orthogonal, bioorthogonal chemistry offers a wide toolbox for compatible reactions, which could be explored.

A completely reversible peptide assembly by boronate ester formation between PBA and catechol functionalized peptides was demonstrated in the last study. Here, the binding affinity of boronic acid towards catechol was significantly increased by exploiting the multivalency effect and selective binding was achieved using complementary peptide sequences. In the future, this system might be upgraded towards mimicking DNA by addition of orthogonal supramolecular and dynamic covalent interactions, which could help to fine-tune the binding affinity and stabilize this system. These requirements would need to be met in order to apply this assembly technique inside living systems like cells. Due to the dynamic nature of boronate ester formation one might also envision to incorporate drug molecules such as bortezomib into the peptide assemblies, which could be selectively released inside the acidic environment of tumor tissue. Furthermore, the peptide binary codes were able to reversibly conjugate macromolecules in the form of proteins and polymers, which expands their applicability for drug delivery and synthesis of pH responsive biomaterials.

In summary this thesis demonstrated diverse methods for controlling the assembly and disassembly of peptides by different biologically available stimuli such as changes in pH and hydrogen peroxide. The use of irreversible as well as reversible assembly techniques highlights the broad applicability of boronic acid chemistry in creation of dynamic and responsive peptide-based nanomaterials. As both, the acidic pH as well as increased oxidative stress are involved in cancer and other severe diseases, the use of the herein presented compounds might expand the utilization of peptides in the treatment of these medical conditions.

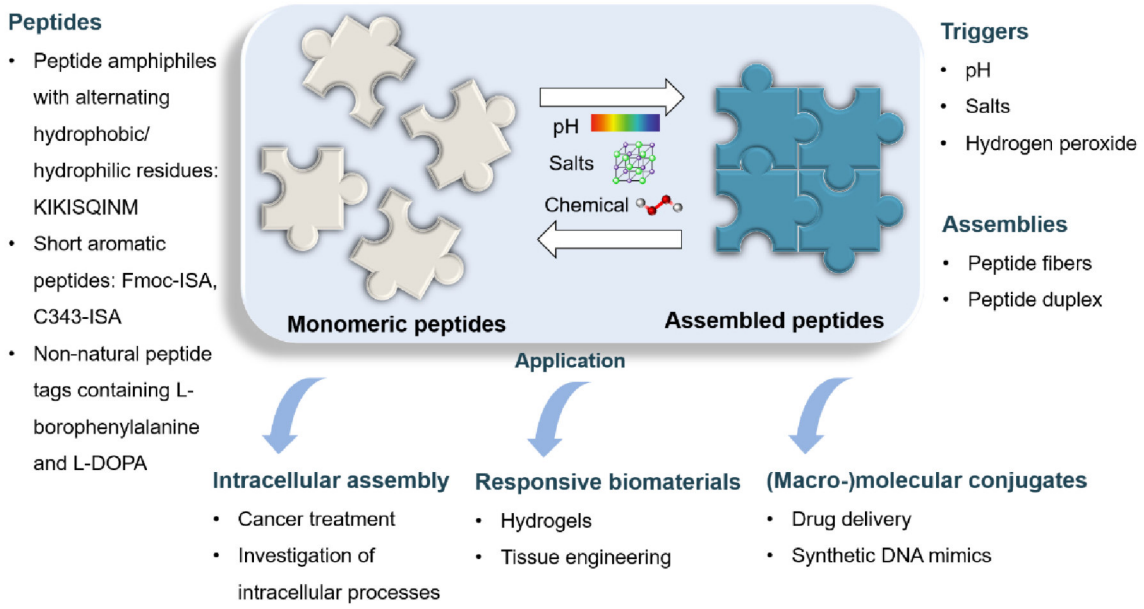

Figure 30: Summary of the presented projects and their potential applications.

5 References

[1] N. Seewald, H.-D. Jakubke, *Peptides: Chemistry and Biology*, Wiley-VCH Verlag GmbH & Co. KGaA, **2009**, 1-4.

[2] H. C. Greenwood, S. R. Bloom, K. G. Murphy, *Rev. Diabet. Stud.* **2011**, *8*, 355-368.

[3] F. Naider, J. Anglister, *Curr. Opin. Struct. Biol.* **2009**, *19*, 473-482.

[4] S. Shi, P. K. Nguyen, H. J. Cabral, R. Diez-Barroso, P. J. Derry, S. M. Kanahara, V. A. Kumar, *Bioact. Mater.* **2016**, *1*, 109-121.

[5] J. Thundimadathil, *J. Amino Acids* **2012**, *2012*, 967347.

[6] N. Schall, N. Page, C. Macri, O. Chaloin, J.-P. Briand, S. Muller, *J. Autoimmun.* **2012**, *39*, 143-153.

[7] C. M. O'Connor, J. U. Adams, J. Fairman, *Cambridge, MA: NPG Education* **2010**, *1*, 54.

[8] T. Fan, X. Yu, B. Shen, L. Sun, *J.Nanomater.* **2017**, *2017*, 4562474.

[9] V. Mäde, S. Els-Heindl, A. G. Beck-Sickinger, *Beilstein J. Org. Chem.* **2014**, *10*, 1197-1212.

[10] S. L. Pedersen, A. P. Tofteng, L. Malik, K. J. Jensen, *Chem. Soc. Rev.* **2012**, *41*, 1826-1844.

[11] G. Litwack, in *Human Biochemistry* (Ed.: G. Litwack), Academic Press, Boston, **2018**, pp. 319-336.

[12] J. Gao, J. Zhan, Z. Yang, *Adv. Mater.* **2020**, *32*, 1805798.

[13] W.-W. Guo, Z.-T. Zhang, Q. Wei, Y. Zhou, M.-T. Lin, J.-J. Chen, T.-T. Wang, N.-N. Guo, X.-C. Zhong, Y.-Y. Lu, Q.-Y. Yang, M. Han, J. Gao, *Biomacromolecules* **2020**, *21*, 444-453.

[14] S. Fleming, R. V. Ulijn, *Chem. Soc. Rev.* **2014**, *43*, 8150-8177.

[15] J. Steed, D. Turner, K. Wallace, *Core Concepts in Supramolecular Chemistry and Nanotechnology,* Jon Wiley & Sons, Ltd, **2007**.

[16] P. J. Cragg, *Supramolecular chemistry: from biological inspiration to biomedical applications*, Springer Science & Business Media, **2010**.

[17] J. Wang, K. Liu, R. Xing, X. Yan, *Chem. Soc. Rev.* **2016**, *45*, 5589-5604.

[18] T. Rehm, C. Schmuck, *Chem. Commun.* **2008**, 801-813.

[19] M. Albrecht, *Naturwissenschaften* **2007**, *94*, 951-966.

[20] C. Mortimer, U. Müller, *Chemie: Das Basiswissen der Chemie, 9., überarbeitete Auflage,* Georg Thieme Verlag: Stuttgart, **2007**.

[21] Z. Song, X. Chen, X. You, K. Huang, A. Dhinakar, Z. Gu, J. Wu, *Biomater. Sci.* **2017**, *5*, 2369-2380.

[22] F. Rico, A. Rigato, L. Picas, S. Scheuring, *J. Nanobiotechnology* **2013**, *11*, S3.

[23] K. Sato, M. P. Hendricks, L. C. Palmer, S. I. Stupp, *Chem. Soc. Rev.* **2018**, *47*, 7539-7551.

[24] L. Adler-Abramovich, E. Gazit, *Chem. Soc. Rev.* **2014**, *43*, 6881-6893.

[25] S. Sieste, T. Mack, C. V. Synatschke, C. Schilling, C. Meyer zu Reckendorf, L. Pendi, S. Harvey, F. S. Ruggeri, T. P. J. Knowles, C. Meier, D. Y. W. Ng, T. Weil, B. Knöll, *Advanc. Healthc. Mater.* **2018**, *7*, 1701485.

[26] J. J. Panda, V. S. Chauhan, *Polym. Chem.* **2014**, *5*, 4418-4436.

[27] J. Li, Y. Gao, Y. Kuang, J. Shi, X. Du, J. Zhou, H. Wang, Z. Yang, B. Xu, *J. Am. Chem. Soc.* **2013**, *135*, 9907-9914.

[28] X. Yan, Q. He, K. Wang, L. Duan, Y. Cui, J. Li, *Angew. Chem. Int. Ed.* **2007**, *46*, 2431-2434.

[29] T. Fan, X. Yu, B. Shen, L. Sun, *J. Nanomater.* **2017**, *2017*, 4562474.

[30] M. Genji, Y. Yano, M. Hoshino, K. Matsuzaki, *Chem. Pharm. Bull.* **2017**, *65*, 668-673.

[31] N. Kol, L. Adler-Abramovich, D. Barlam, R. Z. Shneck, E. Gazit, I. Rousso, *Nano Lett.* **2005**, *5*, 1343-1346.

[32] A. Mahler, M. Reches, M. Rechter, S. Cohen, E. Gazit, *Adv. Mater.* **2006**, *18*, 1365-1370.

[33] M. Zhou, A. M. Smith, A. K. Das, N. W. Hodson, R. F. Collins, R. V. Ulijn, J. E. Gough, *Biomaterials* **2009**, *30*, 2523-2530.

[34] V. Castelletto, G. Cheng, B. W. Greenland, I. W. Hamley, P. J. F. Harris, *Langmuir* **2011**, *27*, 2980-2988.

[35] R. Vegners, I. Shestakova, I. Kalvinsh, R. M. Ezzell, P. A. Janmey, *J. Pept. Sci.* **1995**, *1*, 371-378.

[36] C. Tang, R. V. Ulijn, A. Saiani, *Langmuir* **2011**, *27*, 14438-14449.

[37] M. Ma, Y. Kuang, Y. Gao, Y. Zhang, P. Gao, B. Xu, *J. Am. Chem. Soc.* **2010**, *132*, 2719-2728.

[38] A. Rajbhandary, W. W. Brennessel, B. L. Nilsson, *Crys. Growth Des.* **2018**, *18*, 623-632.

[39] Z. Yang, L. Wang, J. Wang, P. Gao, B. Xu, *J. Mater. Chem.* **2010**, *20*, 2128-2132.

[40] G. Fichman, E. Gazit, *Acta Biomater.* **2014**, *10*, 1671-1682.

[41] R. Ischakov, L. Adler-Abramovich, L. Buzhansky, T. Shekhter, E. Gazit, *Biorg. Med. Chem.* **2013**, *21*, 3517-3522.

[42] Z. Huang, S. Guan, Y. Wang, G. Shi, L. Cao, Y. Gao, Z. Dong, J. Xu, Q. Luo, J. Liu, *J. Mater. Chem. B* **2013**, *1*, 2297-2304.

[43] Z. Yang, G. Liang, M. Ma, Y. Gao, B. Xu, *J. Mater. Chem.* **2007**, *17*, 850-854.

[44] V. Jayawarna, S. M. Richardson, A. R. Hirst, N. W. Hodson, A. Saiani, J. E. Gough, R. V. Ulijn, *Acta Biomater.* **2009**, *5*, 934-943.

[45] Y. Kuang, Y. Gao, B. Xu, *Chem. Commun.* **2011**, *47*, 12625-12627.

[46] Y. Zhang, Z. Yang, F. Yuan, H. Gu, P. Gao, B. Xu, *J. Am. Chem. Soc.* **2004**, *126*, 15028-15029.

[47] C. Ou, J. Zhang, X. Zhang, Z. Yang, M. Chen, *Chem. Commun.* **2013**, *49*, 1853-1855.

[48] Y. Huang, Z. Qiu, Y. Xu, J. Shi, H. Lin, Y. Zhang, *Org. Biomol. Chem.* **2011**, *9*, 2149-2155.

[49] S. Rode, M. Hayn, A. Röcker, S. Sieste, M. Lamla, D. Markx, C. Meier, F. Kirchhoff, P. Walther, M. Fändrich, T. Weil, J. Münch, *Bioconjugate Chem.* **2017**, *28*, 1260-1270.

[50] K. Tao, A. Levin, L. Adler-Abramovich, E. Gazit, *Chem. Soc. Rev.* **2016**, *45*, 3935-3953.

[51] R. N. Rambaran, L. C. Serpell, *Prion* **2008**, *2*, 112-117.

[52] D. J. Selkoe, J. Hardy, *EMBO Mol. Med.***2016**, *8*, 595-608.

[53] R. Langer, D. A. Tirrell, *Nature* **2004**, *428*, 487-492.

[54] U. Shimanovich, I. Efimov, T. O. Mason, P. Flagmeier, A. K. Buell, A. Gedanken, S. Linse, K. S. Åkerfeldt, C. M. Dobson, D. A. Weitz, T. P. J. Knowles, *ACS Nano* **2015**, *9*, 43-51.

[55] C. Meier, I. Lifincev, M. E. Welland, *Biomacromolecules* **2015**, *16*, 558-563.

[56] R. S. Jacob, D. Ghosh, P. K. Singh, S. K. Basu, N. N. Jha, S. Das, P. K. Sukul, S. Patil, S. Sathaye, A. Kumar, A. Chowdhury, S. Malik, S. Sen, S. K. Maji, *Biomaterials* **2015**, *54*, 97-105.

[57] M. S. Ekiz, G. Cinar, M. A. Khalily, M. O. Guler, *Nanotechnology* **2016**, *27*, 402002.

[58] S. Cavalli, F. Albericio, A. Kros, *Chem. Soc. Rev.* **2010**, *39*, 241-263.

[59] M. Yolamanova, C. Meier, A. K. Shaytan, V. Vas, C. W. Bertoncini, F. Arnold, O. Zirafi, S. M. Usmani, J. A. Müller, D. Sauter, C. Goffinet, D. Palesch, P. Walther, N. R. Roan, H. Geiger, O. Lunov, T. Simmet, J. Bohne, H. Schrezenmeier, K. Schwarz, L. Ständker, W.-G. Forssmann, X. Salvatella, P. G. Khalatur, A. R. Khokhlov, T. P. J. Knowles, T. Weil, F. Kirchhoff, J. Münch, *Nature Nanotechnol.* **2013**, *8*, 130.

[60] J. Gačanin, J. Hedrich, S. Sieste, G. Glaßer, I. Lieberwirth, C. Schilling, S. Fischer, H. Barth, B. Knöll, C. V. Synatschke, T. Weil, *Adv. Mater.* **2019**, *31*, 1805044.

[61] H. Chang, C. Li, R. Huang, R. Su, W. Qi, Z. He, *J. Mater. Chem. B* **2019**, *7*, 2899-2910.

[62] H. Green, G. Ochbaum, A. Gitelman-Povimonsky, R. Bitton, H. Rapaport, *RSC Advances* **2018**, *8*, 10072-10080.

[63] C. Schilling, T. Mack, S. Lickfett, S. Sieste, F. S. Ruggeri, T. Sneideris, A. Dutta, T. Bereau, R. Naraghi, D. Sinske, T. P. J. Knowles, C. V. Synatschke, T. Weil, B. Knöll, *Adv. Funct. Mater.* **2019**, *29*, 1809112.

[64] I. W. Hamley, *Chem. Commun.* **2015**, *51*, 8574-8583.

[65] J. A. Hutchinson, S. Burholt, I. W. Hamley, *J. Pept. Sci.* **2017**, *23*, 82-94.

[66] M. P. Hendricks, K. Sato, L. C. Palmer, S. I. Stupp, *Acc. Chem. Res.* **2017**, *50*, 2440-2448.

[67] T.-Y. Cheng, M.-H. Chen, W.-H. Chang, M.-Y. Huang, T.-W. Wang, *Biomaterials* **2013**, *34*, 2005-2016.

[68] E. L. Bakota, Y. Wang, F. R. Danesh, J. D. Hartgerink, *Biomacromolecules* **2011**, *12*, 1651-1657.

[69] S. M. Albelda, C. A. Buck, *FASEB J.* **1990**, *4*, 2868-2880.

[70] G. Tansik, E. Kilic, M. Beter, B. Demiralp, G. Kiziltas Sendur, N. Can, H. Ozkan, E. Ergul, M. O. Guler, A. B. Tekinay, *Biomater. Sci.* **2016**, *4*, 1328-1339.

[71] R. Mammadov, B. Mammadov, S. Toksoz, B. Aydin, R. Yagci, A. B. Tekinay, M. O. Guler, *Biomacromolecules* **2011**, *12*, 3508-3519.

[72] M. J. Webber, C. J. Newcomb, R. Bitton, S. I. Stupp, *Soft Matter* **2011**, *7*, 9665-9672.

[73] D. B. Rasale, A. K. Das, *Int. J. Mol. Sci.* **2015**, *16*, 10797-10820.

[74] A. K. Das, R. Collins, R. V. Ulijn, *Small* **2008**, *4*, 279-287.

[75] S. Toledano, R. J. Williams, V. Jayawarna, R. V. Ulijn, *J. Am. Chem. Soc.* **2006**, *128*, 1070-1071.

[76] L. Chronopoulou, S. Lorenzoni, G. Masci, M. Dentini, A. R. Togna, G. Togna, F. Bordi, C. Palocci, *Soft Matter* **2010**, *6*, 2525-2532.

[77] H. Xu, A. K. Das, M. Horie, M. S. Shaik, A. M. Smith, Y. Luo, X. Lu, R. Collins, S. Y. Liem, A. Song, P. L. A. Popelier, M. L. Turner, P. Xiao, I. A. Kinloch, R. V. Ulijn, *Nanoscale* **2010**, *2*, 960-966.

[78] M. Hughes, S. Debnath, C. W. Knapp, R. V. Ulijn, *Biomater. Sci.* **2013**, *1*, 1138-1142.

[79] C. Tang, A. M. Smith, R. F. Collins, R. V. Ulijn, A. Saiani, *Langmuir* **2009**, *25*, 9447-9453.

[80] S. Parween, A. Misra, S. Ramakumar, V. S. Chauhan, *J. Mater. Chem. B* **2014**, *2*, 3096-3106.

[81] F. Clerici, E. Erba, M. L. Gelmi, S. Pellegrino, *Tetrahedron Lett.* **2016**, *57*, 5540-5550.

[82] J. F. Reuther, J. L. Dees, I. V. Kolesnichenko, E. T. Hernandez, D. V. Ukraintsev, R. Guduru, M. Whiteley, E. V. Anslyn, *Nat. Chem.* **2017**, *10*, 45-50.

[83] R. Zou, Q. Wang, J. Wu, J. Wu, C. Schmuck, H. Tian, *Chem. Soc. Rev.* **2015**, *44*, 5200-5219.

[84] B. P. Gilmartin, K. Ohr, R. L. McLaughlin, R. Koerner, M. E. Williams, *J. Am. Chem. Soc.* **2005**, *127*, 9546-9555.

[85] D. E. Przybyla, C. M. Rubert Pérez, J. Gleaton, V. Nandwana, J. Chmielewski, *J. Am. Chem. Soc.* **2013**, *135*, 3418-3422.

[86] M. B. Coppock, J. R. Miller, M. E. Williams, *Inorg. Chem.* **2011**, *50*, 949-955.

[87] M. M. Pires, J. Chmielewski, *J. Am. Chem. Soc.* **2009**, *131*, 2706-2712.

[88] M. M. Pires, D. E. Przybyla, C. M. Rubert Pérez, J. Chmielewski, *J. Am. Chem. Soc.* **2011**, *133*, 14469-14471.

[89] T. J. Measey, F. Gai, *Langmuir* **2012**, *28*, 12588-12592.

[90] D. W. P. M. Löwik, E. H. P. Leunissen, M. van den Heuvel, M. B. Hansen, J. C. M. van Hest, *Chem. Soc. Rev.* **2010**, *39*, 3394-3412.

[91] Z. Yang, G. Liang, B. Xu, *Soft Matter* **2007**, *3*, 515-520.

[92] Z. Feng, H. Wang, R. Zhou, J. Li, B. Xu, *J. Am. Chem. Soc.* **2017**, *139*, 3950-3953.

[93] K. M. Galler, L. Aulisa, K. R. Regan, R. N. D'Souza, J. D. Hartgerink, *J. Am. Chem. Soc.* **2010**, *132*, 3217-3223.

[94] Y. Chau, Y. Luo, A. C. Y. Cheung, Y. Nagai, S. Zhang, J. B. Kobler, S. M. Zeitels, R. Langer, *Biomaterials* **2008**, *29*, 1713-1719.

[95] J. T. Meijer, M. J. A. G. Henckens, I. J. Minten, D. W. P. M. Löwik, J. C. M. van Hest, *Soft Matter* **2007**, *3*, 1135-1137.

[96] S. Wu, H.-J. Butt, *Phys. Chem. Chem. Phys.* **2017**, *19*, 23585-23596.

[97] D. Spitzer, L. L. Rodrigues, D. Straßburger, M. Mezger, P. Besenius, *Angew. Chem. Int. Ed.* **2017**, *56*, 15461-15465.

[98] D. W. P. M. Löwik, J. T. Meijer, I. J. Minten, H. van Kalkeren, L. Heckenmüller, I. Schulten, K. Sliepen, P. Smittenaar, J. C. M. van Hest, *J. Pept. Sci.* **2008**, *14*, 127-133.

[99] B. J. Kim, B. Xu, *Bioconjug. Chem.* **2020**, *31*, 492-500.

[100] D. Xu, D. S. K. Samways, H. Dong, *Bioact. Mater.* **2017**, *2*, 260-268.

[101] F.-H. Liu, Y. Cong, G.-B. Qi, L. Ji, Z.-Y. Qiao, H. Wang, *Nano Lett.* **2018**, *18*, 6577-6584.

[102] M. T. Jeena, L. Palanikumar, E. M. Go, I. Kim, M. G. Kang, S. Lee, S. Park, H. Choi, C. Kim, S.-M. Jin, S. C. Bae, H. W. Rhee, E. Lee, S. K. Kwak, J.-H. Ryu, *Nat. Commun.* **2017**, *8*, 26.

[103] Y. Gao, J. Shi, D. Yuan, B. Xu, *Nat. Commun.* **2012**, *3*, 1033.

[104] A. Tanaka, Y. Fukuoka, Y. Morimoto, T. Honjo, D. Koda, M. Goto, T. Maruyama, *J. Am. Chem. Soc.* **2015**, *137*, 770-775.

[105] J. Zhou, X. Du, J. Li, N. Yamagata, B. Xu, *J. Am. Chem. Soc.* **2015**, *137*, 10040-10043.

[106] H. He, J. Wang, H. Wang, N. Zhou, D. Yang, D. R. Green, B. Xu, *J. Am. Chem. Soc.* **2018**, *140*, 1215-1218.

[107] M. Palner, B. Shen, J. Jeon, J. Lin, F. T. Chin, J. Rao, *J. Nucl. Med.* **2015**, *56*, 1415-1421.

[108] Y. Yuan, J. Zhang, X. Qi, S. Li, G. Liu, S. Siddhanta, I. Barman, X. Song, M. T. McMahon, J. W. M. Bulte, *Nat. Mater.* **2019**, *18*, 1376-1383.

[109] A. Ghosh, M. Haverick, K. Stump, X. Yang, M. F. Tweedle, J. E. Goldberger, *J. Am. Chem. Soc.* **2012**, *134*, 3647-3650.

[110] H. Ma, J. Fei, Q. Li, J. Li, *Small* **2015**, *11*, 1787-1791.

[111] L. A. Haines, K. Rajagopal, B. Ozbas, D. A. Salick, D. J. Pochan, J. P. Schneider, *J. Am. Chem. Soc.* **2005**, *127*, 17025-17029.

[112] C. J. Bowerman, B. L. Nilsson, *J. Am. Chem. Soc.* **2010**, *132*, 9526-9527.

[113] X. Miao, W. Cao, W. Zheng, J. Wang, X. Zhang, J. Gao, C. Yang, D. Kong, H. Xu, L. Wang, Z. Yang, *Angew. Chem. Int. Ed.* **2013**, *52*, 7781-7785.

[114] J. Li, D. Bullara, X. Du, H. He, S. Sofou, I. G. Kevrekidis, I. R. Epstein, B. Xu, *ACS Nano* **2018**, *12*, 3804-3815.

[115] H. Wang, Z. Feng, Y. Wang, R. Zhou, Z. Yang, B. Xu, *J. Am. Chem. Soc.* **2016**, *138*, 16046-16055.

[116] W. Ahmad, A. Niaz, S. Kanwal, M. Khalid, *J. Agric. Res.* **2009**, *47*.

[117] V. M. Dembitsky, R. Smoum, A. A. Al-Quntar, H. A. Ali, I. Pergament, M. Srebnik, *Plant Sci.* **2002**, *163*, 931-942.

[118] J. Prejac, A. A. Skalny, A. R. Grabeklis, S. Uzun, N. Mimica, B. Momčilović, *J. Trace Elem. Med. Biol.* **2018**, *45*, 50-56.

[119] L. Pizzorno, *Integr Med (Encinitas)* **2015**, *14*, 35-48.

[120] C. T. Price, J. R. Langford, F. A. Liporace, *Open Orthop. J* **2012**, *6*, 143-149.

[121] D. G. Hall, *Boronic Acids*, Wiley-VCH GmbH & Co. KGaA, **2011**, 1-133.

[122] J. P. M. António, R. Russo, C. P. Carvalho, P. M. S. D. Cal, P. M. P. Gois, *Chem. Soc. Rev.* **2019**, *48*, 3513-3536.

[123] J. Su, F. Chen, V. L. Cryns, P. B. Messersmith, *J. Am. Chem. Soc.* **2011**, *133*, 11850-11853.

[124] X. Sun, W. Zhai, J. S. Fossey, T. D. James, *Chem. Commun.* **2016**, *52*, 3456-3469.

[125] X. Wang, N. Xia, L. Liu, *Int. J.Mol. Sci.* **2013**, *14*, 20890-20912.

[126] W. L. A. Brooks, C. C. Deng, B. S. Sumerlin, *ACS Omega* **2018**, *3*, 17863-17870.

[127] E. V. Lampard, A. C. Sedgwick, T. Sombuttan, G. T. Williams, B. Wannalerse, A. T. A. Jenkins, S. D. Bull, T. D. James, *ChemistryOpen* **2018**, *7*, 266-268.

[128] E.-J. Kim, S. Bhuniya, H. Lee, H. M. Kim, C. Cheong, S. Maiti, K. S. Hong, J. S. Kim, *J. Am. Chem. Soc.* **2014**, *136*, 13888-13894.

[129] Z. Guo, I. Shin, J. Yoon, *Chem. Commun.* **2012**, *48*, 5956-5967.

[130] M. Wang, S. Sun, C. I. Neufeld, B. Perez-Ramirez, Q. Xu, *Angew. Chem. Int. Ed.***2014**, *53*, 13444-13448.

[131] H. Zheng, M. Lejkowski, D. G. Hall, *Chem. Sci.* **2011**, *2*, 1305-1310.

[132] H. Zheng, S. Ghanbari, S. Nakamura, D. G. Hall, *Angew. Chem. Int. Ed.* **2012**, *51*, 6187-6190.

[133] X. Mo, J. Yakiwchuk, J. Dansereau, J. A. McCubbin, D. G. Hall, *J. Am. Chem. Soc.* **2015**, *137*, 9694-9703.

[134] J. A. McCubbin, H. Hosseini, O. V. Krokhin, *J. Org. Chem.* **2010**, *75*, 959-962.

[135] Z. Xu, S. K. Kim, S. J. Han, C. Lee, G. Kociok-Kohn, T. D. James, J. Yoon, *Eur. J. Org. Chem.* **2009**, *2009*, 3058-3065.

[136] N. Miyaura, A. Suzuki, *Chem. Rev.* **1995**, *95*, 2457-2483.

[137] H. Zheng, M. Lejkowski, D. G. Hall, *Tetrahedron Lett.* **2013**, *54*, 91-94.

[138] T. Koolmeister, M. Södergren, M. Scobie, *Tetrahedron Lett.* **2002**, *43*, 5965-5968.

[139] R. Nishiyabu, Y. Kubo, T. D. James, J. S. Fossey, *Chem. Commun.* **2011**, *47*, 1124-1150.

[140] B. Akgun, D. G. Hall, *Angew. Chem. Int. Ed.* **2018**, *57*, 13028-13044.

[141] J. Lee, J. H. Ko, K. M. Mansfield, P. C. Nauka, E. Bat, H. D. Maynard, *Macromol. Biosci.* **2018**, *18*, e1700372.

[142] G. Vancoillie, R. Hoogenboom, *Sensors* **2016**, *16*, 1736.

[143] D. Li, Y. Chen, Z. Liu, *Chem. Soc. Rev.* **2015**, *44*, 8097-8123.

[144] M. Nakahata, S. Mori, Y. Takashima, A. Hashidzume, H. Yamaguchi, A. Harada, *ACS Macro Lett.* **2014**, *3*, 337-340.

[145] M. Arzt, C. Seidler, D. Y. W. Ng, T. Weil, *Chem. Asian J.* **2014**, *9*, 1994-2003.

[146] G. Springsteen, B. Wang, *Tetrahedron* **2002**, *58*, 5291-5300.

[147] T. Elshaarani, H. Yu, L. Wang, A. Zain ul, R. S. Ullah, M. Haroon, R. U. Khan, S. Fahad, A. Khan, A. Nazir, M. Usman, K.-u.-R. Naveed, *J. Mater. Chem. B* **2018**, *6*, 3831-3854.

[148] H. Gaballa, P. Theato, *Biomacromolecules* **2019**, *20*, 871-881.

[149] L. Zhao, Q. Huang, Y. Liu, Q. Wang, L. Wang, S. Xiao, F. Bi, J. Ding, *Materials* **2017**, *10*, 170.

[150] J. I. Jay, S. Shukair, K. Langheinrich, M. C. Hanson, G. C. Cianci, T. J. Johnson, M. R. Clark, T. J. Hope, P. F. Kiser, *Adv. Funct. Mater.* **2009**, *19*, 2969-2977.

[151] Z. Zhao, Y. Zhang, C. Tian, T. Yin, C. Zhang, *Biomater. Sci.* **2018**, *6*, 2605-2618.

[152] M. Groll, C. R. Berkers, H. L. Ploegh, H. Ovaa, *Structure* **2006**, *14*, 451-456.

[153] S. Basu, P. S. Dasgupta, *J. Neuroimmunol.* **2000**, *102*, 113-124.

[154] H.-Y. Liu, Z. Qiao, X.-X. Mao, J.-C. Zha, J. Yin, *Langmuir* **2019**, *35*, 11850-11858.

[155] W. Scarano, H. Lu, M. H. Stenzel, *Chem. Commun.* **2014**, *50*, 6390-6393.

[156] M. L. Stolowitz, C. Ahlem, K. A. Hughes, R. J. Kaiser, E. A. Kesicki, G. Li, K. P. Lund, S. M. Torkelson, J. P. Wiley, *Bioconjug. Chem.* **2001**, *12*, 229-239.

[157] S. B. Y. Shin, R. D. Almeida, G. Gerona-Navarro, C. Bracken, S. R. Jaffrey, *Chem. Biol.* **2010**, *17*, 1171-1176.

[158] D. Y. W. Ng, M. Arzt, Y. Wu, S. L. Kuan, M. Lamla, T. Weil, *Angew. Chem. Int. Ed.* **2014**, *53*, 324-328.

[159] C. Seidler, D. Y. W. Ng, Y. Wu, T. Weil, *Supramol. Chem.* **2016**, *28*, 742-746.

[160] C. Seidler, M. M. Zegota, M. Raabe, S. L. Kuan, D. Y. W. Ng, T. Weil, *Chem. Asian J.* **2018**, *13*, 3474-3479.

[161] C. Seidler, D. Y. W. Ng, T. Weil, *Tetrahedron* **2017**, *73*, 4979-4987.

[162] J. P. Wiley, K. A. Hughes, R. J. Kaiser, E. A. Kesicki, K. P. Lund, M. L. Stolowitz, *Bioconjug. Chem.* **2001**, *12*, 240-250.

[163] S. E. Katz, D. D. Klisovic, M. S. O'Dorisio, R. Lynch, M. Lubow, *Arch. Ophthalmol.* **2002**, *120*, 1540-1543.

[164] B. Liu, M. Ianosi-Irimie, S. Thayumanavan, *ACS Nano* **2019**, *13*, 9408-9420.

[165] M. C. Roberts, M. C. Hanson, A. P. Massey, E. A. Karren, P. F. Kiser, *Adv. Mater.* **2007**, *19*, 2503-2507.

[166] B. M. Chapin, P. Metola, V. M. Lynch, J. F. Stanton, T. D. James, E. V. Anslyn, *J. Org. Chem.* **2016**, *81*, 8319-8330.

[167] A. Bandyopadhyay, S. Cambray, J. Gao, *Chem. Sci.* **2016**, *7*, 4589-4593.

[168] B. Akgun, C. Li, Y. Hao, G. Lambkin, R. Derda, D. G. Hall, *J. Am. Chem. Soc.* **2017**, *139*, 14285-14291.

[169] B. Akgun, D. G. Hall, *Angew. Chem. Int. Ed.* **2016**, *55*, 3909-3913.

[170] D. G. Hall, *Boronic Acids*, Wiley-VCH Verlag GmbH & Co. KGaA, **2011**, 1-133.

[171] A. Stubelius, S. Lee, A. Almutairi, *Acc. Chem. Res.* **2019**, *52*, 3108-3119.

[172] D. R. Gough, T. G. Cotter, *Cell Death Dis.* **2011**, *2*, e213.

[173] V. S. Lin, B. C. Dickinson, C. J. Chang, *Methods Enzymol., Vol. 526*, Elsevier, **2013**, 19-43.

[174] J. L. M. Jourden, K. B. Daniel, S. M. Cohen, *Chem. Commun.* **2011**, *47*, 7968-7970.

[175] R. Weinstain, E. N. Savariar, C. N. Felsen, R. Y. Tsien, *J. Am. Chem. Soc.* **2014**, *136*, 874-877.

[176] C. de Gracia Lux, S. Joshi-Barr, T. Nguyen, E. Mahmoud, E. Schopf, N. Fomina, A. Almutairi, *J. Am. Chem. Soc.* **2012**, *134*, 15758-15764.

[177] S. C. Barber, R. J. Mead, P. J. Shaw, *Biochim. Biophys. Acta Mol. Basis Dis.* **2006**, *1762*, 1051-1067.

[178] M. Kita, J. Yamamoto, T. Morisaki, C. Komiya, T. Inokuma, L. Miyamoto, K. Tsuchiya, A. Shigenaga, A. Otaka, *Tetrahedron Lett.* **2015**, *56*, 4228-4231.

[179] M. López-Lázaro, *Cancer Lett.* **2007**, *252*, 1-8.

[180] L. Wang, S. Xie, L. Ma, Y. Chen, W. Lu, *Eur. J. Med. Chem.* **2016**, *116*, 84-89.

[181] Q. Jiang, Q. Zhong, Q. Zhang, S. Zheng, G. Wang, *ACS Med. Chem. Lett.* **2012**, *3*, 392-396.

[182] Y. Kuang, K. Balakrishnan, V. Gandhi, X. Peng, *J. Am. Chem. Soc.* **2011**, *133*, 19278-19281.

[183] T. T. Hoang, T. P. Smith, R. T. Raines, *Angew. Chem. Int. Ed.* **2017**, *56*, 2619-2622.

[184] K. E. Broaders, S. Grandhe, J. M. J. Fréchet, *J. Am. Chem. Soc.* **2011**, *133*, 756-758.

[185] L.-C. Lo, C.-Y. Chu, *Chem. Commun.* **2003**, 2728-2729.

[186] N. Karton-Lifshin, E. Segal, L. Omer, M. Portnoy, R. Satchi-Fainaro, D. Shabat, *J. Am. Chem. Soc.* **2011**, *133*, 10960-10965.

[187] E. W. Miller, O. Tulyathan, E. Y. Isacoff, C. J. Chang, *Nat. Chem. Biol.* **2007**, *3*, 263-267.

[188] A. E. Albers, V. S. Okreglak, C. J. Chang, *J. Am. Chem. Soc.* **2006**, *128*, 9640-9641.

[189] F. He, F. Feng, S. Wang, Y. Li, D. Zhu, *J. Mater. Chem.* **2007**, *17*, 3702-3707.

[190] F. He, Y. Tang, M. Yu, S. Wang, Y. Li, D. Zhu, *Adv. Funct. Mater.* **2006**, *16*, 91-94.

[191] N. A. Sieracki, B. N. Gantner, M. Mao, J. H. Horner, R. D. Ye, A. B. Malik, M. E. Newcomb, M. G. Bonini, *Free Radic. Biol. Med.* **2013**, *61*, 40-50.

[192] Y.-Q. Zou, J.-R. Chen, X.-P. Liu, L.-Q. Lu, R. L. Davis, K. A. Jørgensen, W.-J. Xiao, *Angew. Chem. Int. Ed.* **2012**, *51*, 784-788.

[193] S. P. Pitre, C. D. McTiernan, H. Ismaili, J. C. Scaiano, *J. Am. Chem. Soc.* **2013**, *135*, 13286-13289.

[194] T. Fan, X. Yu, B. Shen, L. Sun, *J. Nanomater.* **2017**, *2017*, 4562474.

[195] M. J. Webber, E. A. Appel, E. W. Meijer, R. Langer, *Nat. Mater.* **2016**, *15*, 13-26.

[196] Y. Gao, Y. Kuang, Z.-F. Guo, Z. Guo, I. J. Krauss, B. Xu, *J. Am. Chem. Soc.* **2009**, *131*, 13576-13577.

[197] J. Nanda, A. Banerjee, *Soft Matter* **2012**, *8*, 3380–3386.

[198] Z. Yang, B. Xu, *Chem. Commun.* **2004**, 2424-2425.

[199] S. Debnath, A. Shome, D. Das, P. K. Das, *J. Phys. Chem. B* **2010**, *114*, 4407-4415.

[200] S. Eskandari, T. Guerin, I. Toth, R. J. Stephenson, *Adv. Drug Deliv. Rev.* **2017**, *110-111*, 169-187.

[201] Y. Sohma, T. Yoshiya, A. Taniguchi, T. Kimura, Y. Hayashi, Y. Kiso, *Biopolymers* **2007**, *88*, 253-262.

[202] H. D. Herce, A. E. Garcia, *PNAS* **2007**, *104*, 20805.

[203] M. Pieszka, S. Han, C. Volkmann, R. Graf, I. Lieberwirth, K. Landfester, D. Y. W. Ng, T. Weil, *J. Am. Chem. Soc.* **2020**, *142*, 15780-15789.

[204] M. Hebel, A. Riegger, M. M. Zegota, G. Kizilsavas, J. Gačanin, M. Pieszka, T. Lückerath, J. A. S. Coelho, M. Wagner, P. M. P. Gois, D. Y. W. Ng, T. Weil, *J. Am. Chem. Soc.* **2019**, *141*, 14026-14031.

[205] M. Pieszka, A. M. Sobota, J. Gačanin, T. Weil, D. Y. W. Ng, *ChemBioChem* **2019**, *20*, 1376-1381.

[206] R. N. Rambaran, L. C. Serpell, *Prion* **2008**, *2*, 112-117.

[207] R. W. Putnam, in *Cell Physiology Source Book (Fourth Edition)* (Ed.: N. Sperelakis), Academic Press, San Diego, **2012**, 303-321.

[208] A. Taniguchi, Y. Sohma, M. Kimura, T. Okada, K. Ikeda, Y. Hayashi, T. Kimura, S. Hirota, K. Matsuzaki, Y. Kiso, *J. Am. Chem. Soc.* **2006**, *128*, 696-697.

[209] S. Navarro, S. Ventura, *Biotechnol. J.* **2014**, *9*, 1259-1266.

[210] K. Tao, A. Levin, L. Adler-Abramovich, E. Gazit, *Chem. Soc. Rev.* **2016**, *45*, 3935-3953.

[211] H. Wang, Z. Feng, W. Tan, B. Xu, *Bioconjug. Chem.* **2019**, *30*, 2528-2532.

[212] H. Hagen, P. Marzenell, E. Jentzsch, F. Wenz, M. R. Veldwijk, A. Mokhir, *J. Med. Chem.* **2012**, *55*, 924-934.

[213] X. Liu, J. M. Cole, K. S. Low, *J. Phys. Chem. C* **2013**, *117*, 14723-14730.

[214] R. Xing, C. Yuan, S. Li, J. Song, J. Li, X. Yan, *Angew. Chem. Int. Ed.* **2018**, *57*, 1537-1542.

[215] M. M. Zegota, T. Wang, C. Seidler, D. Y. W. Ng, S. L. Kuan, T. Weil, *Bioconjug. Chem* **2018**, *29*, 2665-2670.

[216] I. Hirao, M. Kimoto, R. Yamashige, *Acc. Chem. Res.* **2012**, *45*, 2055-2065.

[217] A. Gupta, A. Mishra, N. Puri, *J. Biotechnol.* **2017**, *259*, 148-159.

[218] J. A. Swain, G. Iadevaia, C. A. Hunter, *J. Am. Chem. Soc.* **2018**, *140*, 11526-11536.

[219] Y. Li, W. Xiao, K. Xiao, L. Berti, J. Luo, H. P. Tseng, G. Fung, K. S. Lam, *Angew. Chem. Inter. Ed.* **2012**, *51*, 2864-2869.

[220] W. A. Kibbe, *Nucleic Acids Res.* **2007**, *35*, W43-W46.

[221] T. Ratilainen, A. Holmén, E. Tuite, G. Haaima, L. Christensen, P. E. Nielsen, B. Nordén, *Biochemistry* **1998**, *37*, 12331-12342.

[222] B. Ranjbar, P. Gill, *Chem. Biol. Drug Des.* **2009**, *74*, 101-120.

6 List of Abbreviations

AFM	Atomic force microscopy	GSH	Glutathione
Ala, A	L-Alanine	His, H	L-Histidine
ALP	Alkaline phosphatase	HIV	Human immunodeficiency virus
ALS	Amyotrophic lateral sclerosis	HPLC	High performance liquid chromatography
ANG	Angiogenin	HSA	Human serum albumin
Arg, R	L-Arginine	Ile, I	L-Isoleucine
Asn, N	L-Asparagine	L-DOPA	L-3,4-Dihydroxyphenylalanine
Asp, D	L-Aspartic acid	Lys, K	L-Lysine
Aβ	Amyloid-β	Maldi-ToF	Matrix-assisted laser desorption/ionization mass spectrometry-time of flight
BA	Boronic acid	Met, M	L-Methionine
Bpy	Bipyridine	MMP	Matrix metalloproteinase
BSA	Bovine serum albumin	mRNA	Messenger ribonucleic acid
BTZ	Bortezomib	NBD	4-Nitro-2,1,3-benzoxadiazole
C343	Coumarin 343	NMR	Nuclear magnetic resonance
CD	Circular dichroism	Nvoc	4,5-Dimethoxy-2-nitrobenzyloxycarbonyl
Cyt C	Cytochrome C	PAMAM	Poly(amidoamine)
DFT	Density functional theory	PBA	Phenylboronic acid
DNA	Deoxyribonucleic acid	PBS	Phosphate buffered saline
Dox	Doxorubicin	PEG	Polyethylene glycol
EISA	Enzyme-instructed self-assembly	Phe, F	L-Phenylalanine
ER	Endoplasmatic reticulum	pHPMAm	Poly(hydroxypropylacrylamide)
Fmoc	Fluorenylmethyloxycarbonyl	PNA	Peptide nucleic acid
FRET	Förster resonance energy transfer	Pro, P	L-Proline
FT-IR	Fourier-transform infrared	RNA	Ribonucleic acid
GFP	Green fluorescent protein	RNase A	Ribonuclease A
Gln, Q	L-Glutamine	ROS	Reactive oxygen species
Glu, E	L-Glutamic acid	Ser, S	L-Serine

SPPS	Solid-phase peptide synthesis	Trp, W	L-Tryptophane
SEM	Scanning electron microscopy	Tyr, Y	L-Tyrosine
SHA	Salicylhydroxamic acid	Val, V	L-Valine
SST	Somatostatin	TEM	Transmission electron microscopy
TAT	Trans-activator of transcription	Thr, T	L-Threonine
tBu	*tert*-Butyl	TPP	Triphenylphosphine

7 List of Figures

8 Publications

8.1 Orthogonally Stimulated Assembly/Disassembly of Depsipeptides by Rational Chemical Design

Michaela Pieszka[+], Adriana Maria Sobota, Jasmina Gačanin, Tanja Weil,[‡] and David Ng[‡]
[+]first author, [‡]corresponding author
Published in *ChemBioChem* **2019**, *20*, 1376-1381.
Date of Publication: 28 January 2019

Abstract

Controlling the assembly and disassembly of cross-b-sheet-forming peptides is one of the predominant challenges for this class of supramolecular material. As they constitute a continuously propagating material, every atomic change can be exploited to bring about distinct responses at the architectural level. We report herein that, by using rational chemical design, serine and methionine can both be used as orthogonal chemical triggers to signal assembly/disassembly through their corresponding stimuli. Serine is used to construct an ester-bond oligopeptide that can undergo *O,N*-acyl rearrangement, whereas methionine is sensitive to oxidation by H_2O_2. Using the example peptide sequence, KIKISQINM, we demonstrate that assembly and disassembly can be independently controlled on demand.

Contributions

Michaela Pieszka: Planning and execution of all experiments including peptide design, synthesis and characterization as well as scientific evaluation of results. Preparing all figures and writing parts of the manuscript.

Adriana M. Sobota: Repetition and optimization of the synthesis of boronic acid depsipeptide (compound 5), which was used in some experiments.

Jasmina Gačanin: Prepared and provided Depsi(KIKI)SQINM and KIKISQINM (compounds 6 and 7 respectively) as references for the HPLC study, these peptides were designed and developed by her in one of her previous publications. Was involved in scientific discussions.

Tanja Weil: Acquiring funding for the project and its management, discussion and interpretation of the results, writing and revision of the manuscript.

David Y. W. Ng: Management of the project, discussion and interpretation of the results, writing and revision of the manuscript.

ChemPubSoc Europe

DOI: 10.1002/cbic.201800781

CHEMBIOCHEM Communications

VIP *Very Important Paper*

Orthogonally Stimulated Assembly/Disassembly of Depsipeptides by Rational Chemical Design

Michaela Pieszka,[a, b] Adriana Maria Sobota,[a] Jasmina Gačanin,[a, b] Tanja Weil,*[a, b] and David Y. W. Ng*[a]

Controlling the assembly and disassembly of cross-β-sheet-forming peptides is one of the predominant challenges for this class of supramolecular material. As they constitute a continuously propagating material, every atomic change can be exploited to bring about distinct responses at the architectural level. We report herein that, by using rational chemical design, serine and methionine can both be used as orthogonal chemical triggers to signal assembly/disassembly through their corresponding stimuli. Serine is used to construct an ester-bond oligopeptide that can undergo O,N-acyl rearrangement, whereas methionine is sensitive to oxidation by H_2O_2. Using the example peptide sequence, KIKISQINM, we demonstrate that assembly and disassembly can be independently controlled on demand.

The molecular ordering of small molecules formed by regular and precise intermolecular forces represents one of the leading principles of supramolecular material synthesis.[1] Programmed through molecular design, these interactions involve a selection of hydrogen bonds, π-stacks, and van der Waals as well as electrostatic forces in which self-association of the molecules is often a thermodynamic minimum.[1] As it is coupled with the release of solvent molecules, the assembly is also driven entropically and, thus, derives its innate sensitivity towards both temperature and the concentration of the monomers.[2] As these various parameters can all affect self-assembly, it can often be a challenge to exert direct control over the kinetics and responsiveness of superstructure formation.

Among different self-assembling systems, the cross-β-sheet arrangement of many peptides, which forms so-called amyloid structures, has emerged a major class of nanomaterials with several unique features. Amyloid structures are often associated with severe neurodegenerative disorders such as Alzheimer's disease.[3] The propagation of the disease stems from several known oligopeptide sequences that exhibit a very strong tendency to form cross-β-sheets that subsequently assemble into hierarchical fibrillary networks.[4] Although the accumulation of these fibrils into larger aggregates can be detrimental to neurons, they have been exploited as excellent molecular support in both nano- and bulk materials, especially when targeted to biomedical applications.[3,5]

Nonetheless, the processability as well as temporal control over the self-assembly and disassembly of amyloid-like peptides are prominent limitations to their use in vivo. Hence, significant efforts have been directed towards the design of oligopeptides to allow a higher level of control of β-sheet formation.[6] Hydrophilic amino acids within the sequence, such as lysine or glutamic acid, can be leveraged to promote or inhibit intermolecular interactions depending on their protonation state.[7] On the other hand, depsipeptides, in which a serine residue within the peptide sequence is connected through an ester bond instead, have shown exceptional promise for amyloid fibril formation by an external pH stimulus.[8]

Depsipeptides were originally developed to alleviate solubility issues with ultra-long peptides by providing a kink in the otherwise linear structure.[9] This kink, caused by the ester-linked serine residue, would undergo an five-membered O,N-acyl shift due to the higher nucleophilicity of the free amine upon deprotection to furnish the designated peptide. Hence, we envisioned that, depending on the mechanism to release the free amine, the O,N-acyl shift could be controlled covalently on demand.

Likewise, the disassembly of amyloids is a concern for the development of biomaterials, especially for use in vivo.[10] The degradation of these systems is essential for their extrusion once their designated purpose has been achieved. However, the disassembly of typical amyloids under physiological conditions is highly unfavourable due to their thermodynamic stability; they are widely known to be heat and proteolytically resistant.[11]

To overcome this, we demonstrate that orthogonal chemical triggers can be rationally designed and incorporated within an oligopeptide such that the assembly/disassembly can be controlled independently by external stimuli (Figure 1). We introduced a depsipeptide sequence containing a boronic acid–carbamate bond to cage the amine of the serine. The self-assembling sequence of the oligopeptide contains a methionine resi-

[a] M. Pieszka, A. M. Sobota, J. Gačanin, Prof. Dr. T. Weil, Dr. D. Y. W. Ng
Synthesis of Macromolecules
Max Planck Institute for Polymer Research
Ackermannweg 10, 55128 Mainz (Germany)
E-mail: weil@mpip-mainz.mpg.de
david.ng@mpip-mainz.mpg.de

[b] M. Pieszka, J. Gačanin, Prof. Dr. T. Weil
Institute of Inorganic Chemistry I, Ulm University
Albert-Einstein-Allee-11, 89081 Ulm (Germany)

Supporting information and the ORCID identification numbers for the authors of this article can be found under https://doi.org/10.1002/cbic.201800781.

This article is part of the young researchers' issue ChemBioTalents. To view the complete issue, visit http://chembiochem.org/chembiotalents

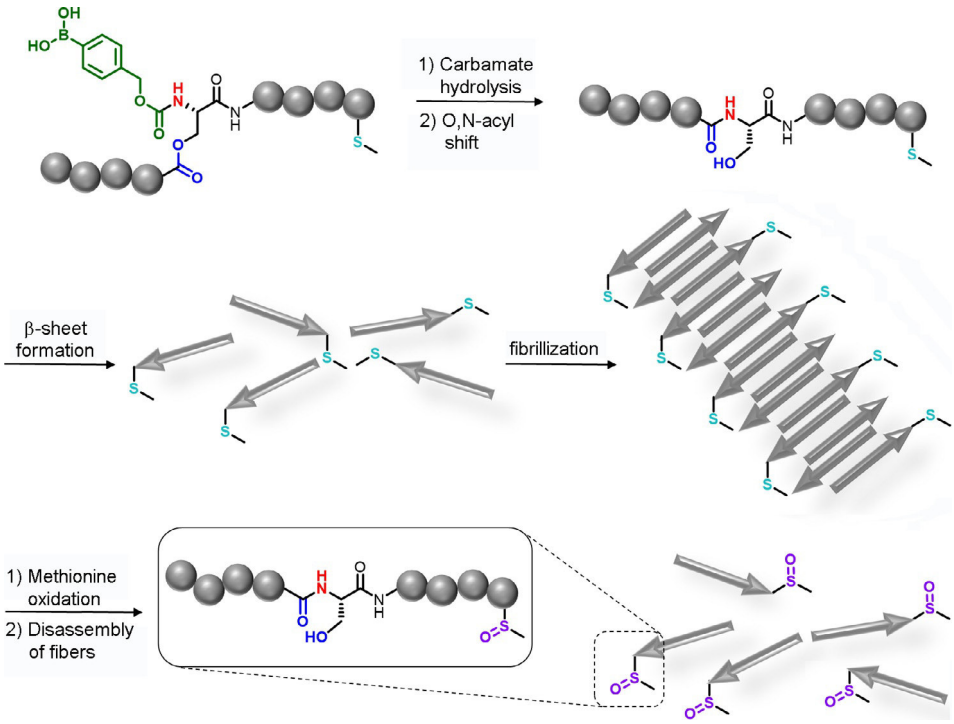

Figure 1. Chemical design and structure of a depsi-oligopeptide controlled by a boronic acid carbamate bond. The carbamate and methionine provide the two orthogonal stimuli.

due in which the thioether motif directly imparts sensitivity to local oxidative conditions. In particular, an oxidative stimulus is attractive as it is well known that cancerous tissues contain a much higher concentration of hydrogen peroxide and various reactive oxygen species.[12] By integrating both aspects, amyloid self-assembly is directly controlled by the cleavage of the carbamate bond, whereas the disassembly is dictated by the oxidation of the methionine at the C terminus. In addition, the effects of these triggers produce distinct morphological changes that can be visualized by transmission electron microscopy (TEM). In establishing this concept, we anticipate that the methodology will provide enormous synergy with existing amyloid-based technology ranging from hydrogels[13] to drug delivery[14] and viral gene transduction.[5b]

David Ng studied chemistry at the National University of Singapore (B.Sc., first-class hons) followed by a doctorate with Prof. Dr. Tanja Weil jointly funded by the Max Planck Institute for Polymer Research and Ulm University (Dr. rer. nat., summa cum laude). After graduating in 2014, he began his career as a junior group leader at Ulm University and accepted his current position in 2016. He leads the group for synthetic life-like nanosystems focusing on using organic and polymer chemistry to instil synthetic functions into the architectures of peptides, proteins and DNA.

The synthesis of the oligopeptide takes place in the solid phase on Wang resin preloaded with the first amino acid, methionine (**1**). Standard microwave-assisted peptide synthesis was used to construct the peptide in sequence with asparagine, isoleucine and glutamine by using double coupling steps. Following this, 9-fluorenylmethyloxycarbamate (Fmoc)-Ser-OH (Scheme 1) was coupled in a single step—in order to prevent side reactions with the free hydroxy group—to form **2**. The Fmoc group was removed, then a boronic acid-carbamate caging group was installed by using 4-nitrophenyl(4-(4,4,5,5-tetramethyl-1,3,2-dioxaborolan-2-yl)benzyl)carbonate with *N*,*N*-diisopropylethylamine in DMF at room temperature overnight. The depsi-ester bond from the serine was constructed by treating **3** with Fmoc-Ile-OH, diisopropylcarbodiimide (DIC) and 4-dimethylaminopyridine (DMAP) to afford **4**. The coupling of the next three residues—lysine, isoleucine and lysine—was conducted at room temperature as the carbamate bond is heat sensitive. Cleavage of the peptide, together with complete deprotection with 95% trifluoroacetic acid (TFA), 2.5% TIPS and 2.5% water afforded the target caged-oligopeptide **5**.

The responsiveness of oligopeptide **5** towards the assembly trigger rests upon the boronic acid–carbamate caging group. Benzylic carbamate bonds are sensitive to hydrolytic conditions, and their stability can be tuned over a wide range, depending on the aromatic substituents.[15] Boronic acid was chosen both as an electron-withdrawing group and as a potential reactive chemical function. Hence, the experiment was designed to monitor the mechanism of bond cleavage by kinetic profiling using analytical HPLC (Figure 2 A and Figure S5

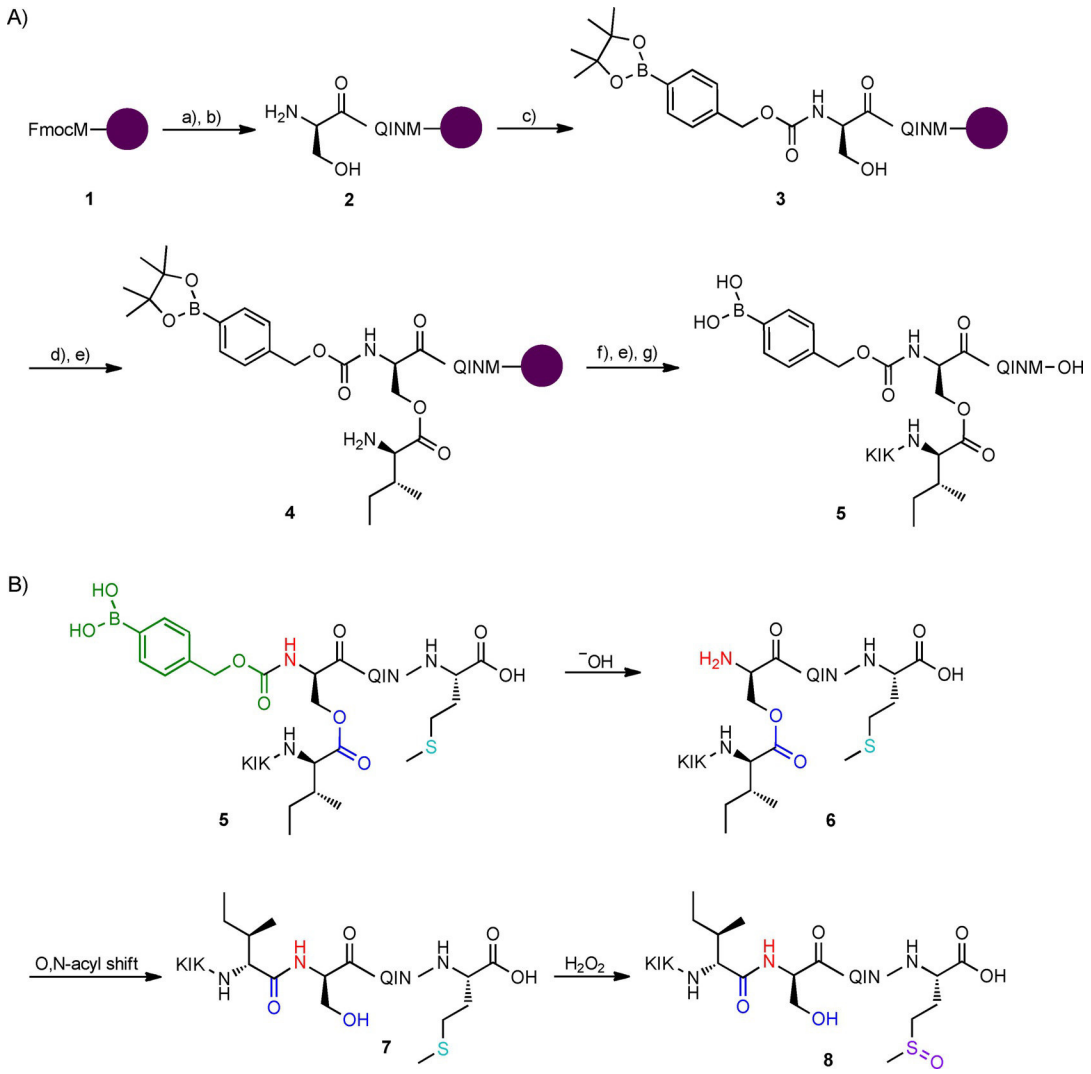

Scheme 1. A) Microwave assisted solid-phase peptide synthesis of the target boronic acid caged depsipeptide **5**. a) Piperidine/DMF, 75 °C, 2 and 5 min; b) Fmoc-Asn(Trt)-OH/Fmoc-Ile-OH/Fmoc-Gln(Trt)-OH/Fmoc-Ser-OH, PyBOP, DIPEA, 75 °C, 2×10 min for Asn Ile, and Gln, 10 min for Ser; c) 4-nitrophenyl (4-(4,4,5,5-tetramethyl-1,3,2-dioxaborolan-2-yl)benzyl) carbonate, DIPEA, RT, overnight; d) Fmoc-Ile-OH, DIC, DMAP, RT, 2 h and overnight; e) piperidine, RT, 2×10 min; f) Fmoc-Ile/Fmoc-Lys(Boc)-OH, PyBOP, DIPEA, RT, 2×60 min; g) TFA, TIPS, water, RT, 2 h. B) Mechanism of stimulus-responsive O,N-acyl rearrangement of **5** and subsequent oxidation of methionine.

in the Supporting Information). We found that the carbamate bond can be cleaved selectively in the presence of kosmotropic agents such as phosphate salts, but is stable in pure water. A retention time of 11.0 min was observed for the caged peptide **5**. Gradual hydrolysis of the carbamate bond is observed over time, with the intermediate free depsipeptide **6** being formed at 10.3 min. It is important to note that **6** can be observed to undergo rapid O,N-acyl shift to form the linear peptide **7** at 10.2 min. After 24 h, full conversion to the linear peptide form was attained, although its formation and spontaneous self-assembly had already begun after 1 h (Figure S5). In order to confirm the peak assignments, oligopeptides **6** and **7** were synthesised separately and analysed as controls in the HPLC (Figure S5).

In a similar fashion, disassembly through the oxidation of methionine by applying H_2O_2 was monitored (Figures 2B and S6). The final and linear forms of **7** were treated with 100 mM H_2O_2. Oxidation of the thioether into a sulfoxide was apparent from the HPLC within 5 min (Figure 2B). A significant shift in the retention time towards higher polarity from 10.2 to 9.4 min was observed; this is in agreement with the formation of the more polar sulfoxide functional group. The conversion was about 85% within 1 h and was shown to be complete within 8 h.

Although the HPLC studies show definitive changes in the oligopeptide structure in response to both orthogonal stimuli, a molecular-level characterization would reinforce these observations. To this end, we used MALDI-TOF-MS to elucidate the peak identities (Figures 2C–E and S7). The loss of the carbamate caging motif from oligopeptide **5** (*m/z*: 1234.68 $[M-H_2O+H]^+$) could be correlated to the linear peptide **7** (*m/z*: 1074.45 $[M+H]^+$, 1096.43 $[M+Na]^+$). As the molecular weights of **6** and **7** are identical, characterization by MALDI-TOF MS is not possible. However, the transient presence of a

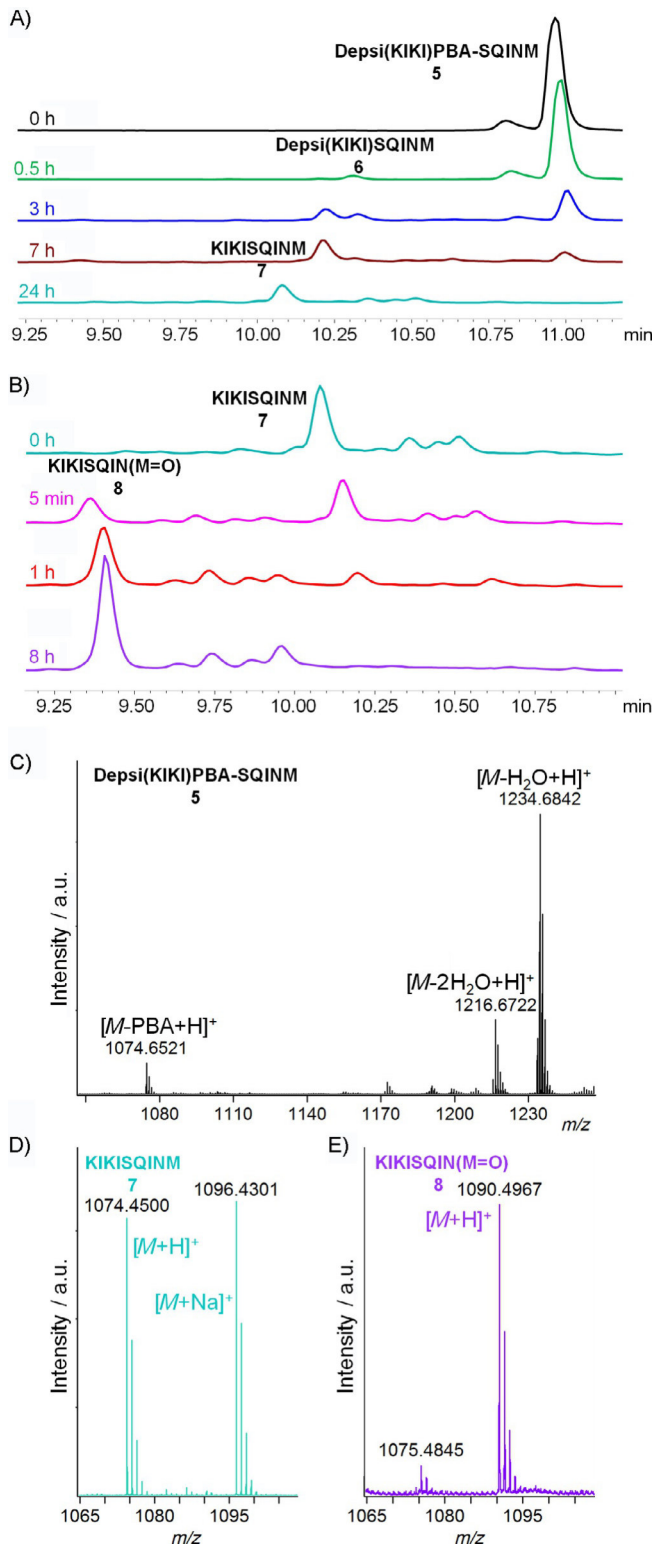

Figure 2. Kinetic profiling of A) hydrolysis of boronic acid-carbamate **5** with subsequent O,N-acyl rearrangement into **7** and B) oxidation of **7** by H_2O_2. MALDI-TOF-MS of C) Depsipeptide **5**, D) linearized peptide **7** and E) Oxidation of **7** into **8** by H_2O_2.

peak at $t_R = 10.3$ min correlates to the well-reported rapid O,N-acyl shift of depsipeptide **6**.[9] In a complementary fashion, oxidation of oligopeptide **7** by H_2O_2 was confirmed by the addition of oxygen to form the sulfoxide **8** (*m/z*: 1090.50 $[M+H]^+$).

Upon the investigation of the molecular mechanisms, the self-assembling behaviour of caged depsipeptide **5** as a response towards both stimuli was elucidated. As the fundamental linear peptide sequence is known to form strong β-sheet supramolecular nanostructures, the rearrangement reaction could be characterized by Proteostat staining. The fluorogenic stain produced a large increase in fluorescence intensity upon triggering with phosphate salts, thus implying the responsive formation of β-sheet structures (Figures 3A and S8). In contrast, a control experiment containing the caged depsipeptide **5** in pure water did not show fluorescence upon staining. Subsequently, upon adding H_2O_2 to **7** as the disassembly stimulus, the fluorescence diminished, thus implying the destruction of the cross-β-sheet structures.

These results were further supported by performing FTIR and comparing these values to the known literature vibrational frequencies of the β-sheet peptidic assemblies.[16] Self-assembled peptide **7** showed distinct absorbances at 1635 and 1667 cm^{-1}, which correspond to β-sheet structures and other secondary structures, respectively (Figures 3B and S9). Although the IR spectrum upon oxidation looks relatively similar it is important to note that the relative content of other non-β-sheet structures is more significant. The higher absorbance at 1667 cm^{-1} implies that β-sheet interactions are less dominant after the oxidation reaction. Hence, we speculate that the corresponding increase in other competing secondary structures is detrimental to self-assembly and interferes in the stability of the fibrillar structure. To support the results from IR, circular dichroism spectra of **5**, **7** and **8** were recorded (Figure S10). The spectrum of depsi(KIKI)PBA-SQINM **5** showed expected unordered structures, whereas KIKISQINM **7** was proven to form β-sheets. Upon oxidation of **7** to **8**, the spectrum changed considerably, with a reduction in β-sheet content and a corresponding increase in unordered structures (Figure S10, Table S1).[17]

To visualize our spectroscopic analysis, we performed transmission electron microscopy (TEM) of both the stimulated assembly of the depsipeptide and disassembly of the nanostructure (Figure 3C). Caged depsipeptide **5** was observed to spontaneously self-assemble into fibrillar nanostructures after hydrolysis of the carbamate bond in phosphate-buffered saline and subsequent rearrangement (Figure 3C). These nanofibres show the well-observed characteristic features of amyloid-like peptides that are known to build from continuous β-sheet interactions. The length of the fibres varies between around 100 nm and several micrometres. The diameter of the fibres is 9.44 ± 1.59 nm, yet in some fibres the thickness can be observed to change periodically; this indicates twisting of the fibre strand along its axis. As can be seen in Figure S12, the twist is left-handed. Separated fibres as well as dense fibre networks can be observed. Some fibres are organised into multi-stranded assemblies, which appear a lot darker and thicker in TEM image than solitary fibres.[18] In agreement to other reports, a time-lapse study demonstrated that these nanofibres formed rapidly (1 h), with no observable increase in fibre densi-

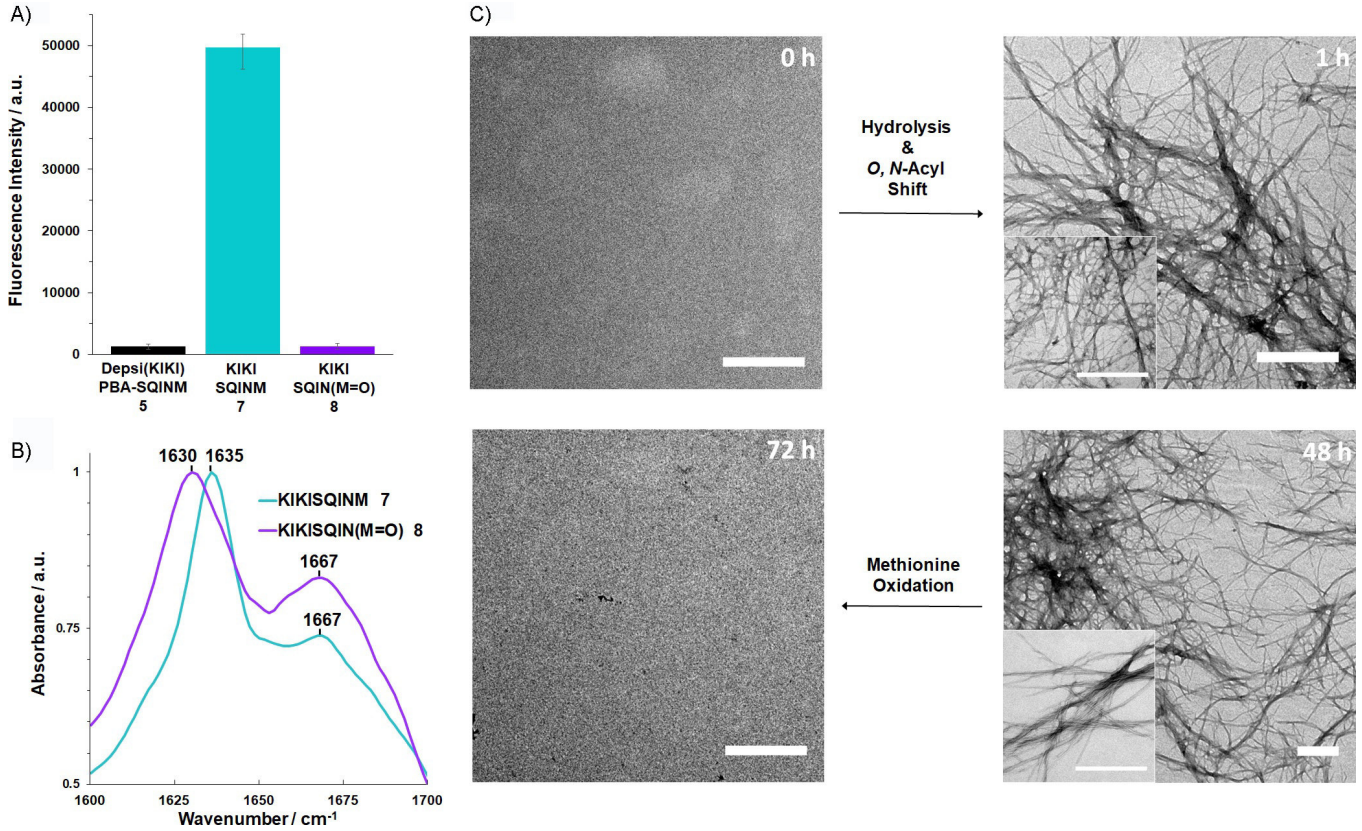

Figure 3. A) Proteostat assay of depsipeptide **5**, hydrolysis of peptide **5** into **7** and oxidized peptide **8**. Data are represented as mean ± SEM, $n = 4$. B) FTIR spectra of peptide **7** and oxidized peptide **8**. C) TEM images of the O,N-acyl shift–triggered fibrillization (top) within 1 h. Complete disassembly of nanofibres by H_2O_2 oxidation (bottom) over 24 h. Times are represented as cumulative intervals. Scale bars: 500 nm.

ty for the next 8 h (Figures S11, S13 and S14).[6a, 8a] Subsequent oxidation with 100 mM H_2O_2 successfully led to disassembly (Figure 3C).

The assembly of the peptides into β-sheets and further into nanofibres is based on an interplay of hydrogen bonds that are formed between the amide groups in the peptide backbone and hydrophobic interactions between the nonpolar amino acid side chains of isoleucine and methionine.[19] Additional stabilization of the structure is provided by hydrogen bonds formed by the side chains of glutamine and asparagine.[20] As shown by FTIR (Figure 3B), parallel β-sheets are formed; this is in accordance with Wang et al. who reported that peptides with strongly hydrophobic side chains form parallel rather than antiparallel β-sheets.[19c]

Oxidation of the nonpolar thioether in the methionine side chain to the corresponding sulfoxide significantly enhances the polarity of the side chain.[21] The dipolar character of sulfoxides is suspected to cause electrostatic repulsion between the methionine sulfoxide residues in the peptide side chains, and this leads to disassembly of the fibres.

In summary, we have presented a synthetic methodology that facilitates direct and independent control over the self-assembly of amyloid-like oligopeptides. Serine and methionine are necessary components of the design to implement the chemical triggers. Serine provides a unique handle to control the overall conformation of the peptidic backbone through the depsi-ester bond, whereas methionine is sensitive to oxidation. Although the concentration of H_2O_2 applied within this study still exceeds those in cancer environments, enzymatic triggers such as glucose oxidase could be combined—for example, in a hydrogel—to elevate local H_2O_2 production as a response to glucose. Chemically, different caging groups that introduce other stimuli such as enzymes, light and pH could be tailored to fit a designated application. By providing this facile platform, we envision that control over self-assembly could be further extended beyond the peptide sequence.

Acknowledgements

The authors gratefully acknowledge funding support from the Horizon 2020 project "AD GUT" (no. 686271) and from the Volkswagen Foundation Project 89943.

Conflict of Interest

The authors declare no conflict of interest.

Keywords: amyloid peptides · nanostructures · rearrangement · self-assembly · stimulus-responsive assembly

[1] D. B. Amabilino, D. K. Smith, J. W. Steed, *Chem. Soc. Rev.* **2017**, *46*, 2404 – 2420.
[2] M. J. Webber, E. A. Appel, E. W. Meijer, R. Langer, *Nat. Mater.* **2016**, *15*, 13.
[3] G. Wei, Z. Su, N. P. Reynolds, P. Arosio, I. W. Hamley, E. Gazit, R. Mezzenga, *Chem. Soc. Rev.* **2017**, *46*, 4661 – 4708.
[4] I. W. Hamley, *Chem. Rev.* **2012**, *112*, 5147 – 5192.
[5] a) D. Straßburger, N. Stergiou, M. Urschbach, H. Yurugi, D. Spitzer, D. Schollmeyer, E. Schmitt, P. Besenius, *ChemBioChem* **2018**, *19*, 912 – 916; b) M. Yolamanova, C. Meier, A. K. Shaytan, V. Vas, C. W. Bertoncini, F. Arnold, O. Zirafi, S. M. Usmani, J. A. Müller, D. Sauter, C. Goffinet, D. Palesch, P. Walther, N. R. Roan, H. Geiger, O. Lunov, T. Simmet, J. Bohne, H. Schrezenmeier, K. Schwarz, L. Ständker, W.-G. Forssmann, X. Salvatella, P. G. Khalatur, A. R. Khokhlov, T. P. J. Knowles, T. Weil, F. Kirchhoff, J. Münch, *Nat. Nanotechnol.* **2013**, *8*, 130.
[6] a) Y. Liu, Y. Yang, C. Wang, X. Zhao, *Nanoscale* **2013**, *5*, 6413 – 6421; b) S. J. Sigg, V. Postupalenko, J. T. Duskey, C. G. Palivan, W. Meier, *Biomacromolecules* **2016**, *17*, 935 – 945; c) E. Lump, L. M. Castellano, C. Meier, J. Seeliger, N. Erwin, B. Sperlich, C. M. Stürzel, S. Usmani, R. M. Hammond, J. von Einem, G. Gerold, F. Kreppel, K. Bravo-Rodriguez, T. Pietschmann, V. M. Holmes, D. Palesch, O. Zirafi, D. Weissman, A. Sowislok, B. Wettig, C. Heid, F. Kirchhoff, T. Weil, F.-G. Klärner, T. Schrader, G. Bitan, E. Sanchez-Garcia, R. Winter, J. Shorter, J. Münch, *eLife* **2015**, *4*, e05397.
[7] P. Ahlers, H. Frisch, R. Holm, D. Spitzer, M. Barz, P. Besenius, *Macromol. Biosci.* **2017**, *17*, 1700111.
[8] a) J. Gačanin, J. Hedrich, S. Sieste, G. Glaßer, I. Lieberwirth, C. Schilling, S. Fischer, H. Barth, B. Knöll, C. V. Synatschke, T. Weil, *Adv. Mater.* **2019**, *31*, 1805044; b) A. Taniguchi, Y. Sohma, Y. Hirayama, H. Mukai, T. Kimura, Y. Hayashi, K. Matsuzaki, Y. Kiso, *ChemBioChem* **2009**, *10*, 710 – 715.
[9] I. Coin, R. Dölling, E. Krause, M. Bienert, M. Beyermann, C. D. Sferdean, L. A. Carpino, *J. Org. Chem.* **2006**, *71*, 6171 – 6177.
[10] L. Sun, C. Zheng, T. J. Webster, *Int. J. Nanomed.* **2016**, *12*, 73 – 86.
[11] A. Dehsorkhi, V. Castelletto, I. W. Hamley, *J. Pept. Sci.* **2014**, *20*, 453 – 467.
[12] C. Lennicke, J. Rahn, R. Lichtenfels, L. A. Wessjohann, B. J. C. C. Seliger, *Cell Commun. Signal.* **2015**, *13*, 39.
[13] S. Das, K. Zhou, D. Ghosh, N. N. Jha, P. K. Singh, R. S. Jacob, C. C. Bernard, D. I. Finkelstein, J. S. Forsythe, S. K. Maji, *NPG Asia Mater.* **2016**, *8*, e304.
[14] N. Habibi, N. Kamaly, A. Memic, H. Shafiee, *Nano Today* **2016**, *11*, 41 – 60.
[15] A. K. Ghosh, M. Brindisi, *J. Med. Chem.* **2015**, *58*, 2895 – 2940.
[16] G. Zandomeneghi, M. R. H. Krebs, M. G. McCammon, M. Fändrich, *Protein Sci.* **2004**, *13*, 3314 – 3321.
[17] a) Y. Liu, L. Zhang, W. Wei, *Int. J. Nanomed.* **2017**, *12*, 659 – 670; b) R. Xing, C. Yuan, S. Li, J. Song, J. Li, X. Yan, *Angew. Chem. Int. Ed.* **2018**, *57*, 1537 – 1542; *Angew. Chem.* **2018**, *130*, 1553 – 1558.
[18] K. Pagel, S. C. Wagner, K. Samedov, H. von Berlepsch, C. Böttcher, B. Koksch, *J. Am. Chem. Soc.* **2006**, *128*, 2196 – 2197.
[19] a) K. Liu, R. Xing, C. Chen, G. Shen, L. Yan, Q. Zou, G. Ma, H. Möhwald, X. Yan, *Angew. Chem. Int. Ed.* **2015**, *54*, 500 – 505; *Angew. Chem.* **2015**, *127*, 510 – 515; b) N. R. Lee, C. J. Bowerman, B. L. Nilsson, *Biomacromolecules* **2013**, *14*, 3267 – 3277; c) J. Wang, K. Liu, R. Xing, X. Yan, *Chem. Soc. Rev.* **2016**, *45*, 5589 – 5604; d) C. Yuan, S. Li, Q. Zou, Y. Ren, X. Yan, *Phys. Chem. Chem. Phys.* **2017**, *19*, 23614 – 23631.
[20] S. Sieste, T. Mack, C. V. Synatschke, C. Schilling, C. Meyer zu Reckendorf, L. Pendi, S. Harvey, F. S. Ruggeri, T. P. J. Knowles, C. Meier, D. Y. W. Ng, T. Weil, B. Knöll, *Adv. Healthcare Mater.* **2018**, *7*, 1701485.
[21] D. Spitzer, L. L. Rodrigues, D. Straßburger, M. Mezger, P. Besenius, *Angew. Chem. Int. Ed.* **2017**, *56*, 15461 – 15465; *Angew. Chem.* **2017**, *129*, 15664 – 15669.

Manuscript received: December 10, 2018
Accepted manuscript online: January 28, 2019
Version of record online: April 12, 2019

CHEMBIOCHEM

Supporting Information

Orthogonally Stimulated Assembly/Disassembly of Depsipeptides by Rational Chemical Design

Michaela Pieszka,[a, b] Adriana Maria Sobota,[a] Jasmina Gačanin,[a, b] Tanja Weil,*[a, b] and David Y. W. Ng*[a]

cbic_201800781_sm_miscellaneous_information.pdf

Table of Contents

1. Materials and Instruments

1.1 Materials

All solvents and reagents were bought from commercial sources (Sigma Aldrich, GL Biochem, Carl Roth, Fisher Scientific, Acros Organics, Merck Novabiochem) and used without any further purification. All reagents used for peptide synthesis were used in Peptide Synthesis grade. HPLC was performed using HPLC grade acetonitrile. Water for HPLC and reactions was obtained from a Millipore purification system. Thin-layer chromatography (TLC) was performed on Macherey-Nagel Alugram Sil G/UV_{254} plates and visualized under UV light at 254 nm. Column chromatography was carried out using Macherey-Nagel silica gel 0.04 – 0.063 mm.

1.2 Instruments

1.2.1 Nuclear Magnetic Resonance Spectroscopy (NMR)

NMR spectra were recorded on a Bruker Avance II 300 MHz and Avance III 700 MHz NMR spectrometer. The solvent signal was used as a reference (deuterated chloroform δ = 7.26 ppm for ^{1}H, 77.16 ppm for ^{13}C). The data was processed in MestReNova.

1.2.2 Microwave Peptide Synthesizer

Peptide Synthesis was performed in a Liberty Blue Automated Microwave Peptide Synthesizer by CEM.

1.2.3 High-Performance Liquid Chromatography (HPLC)

Purification of the peptides was done on a preparative HPLC setup by Shimadzu. An Agilent ZORBAX Eclipse XDB-C18 HPLC column (9.4 x 250 mm, 5 µm) was used for the purification at a flowrate of 4 mL/min. Analytical HPLC measurements were performed on a semi-

preparative HPLC by Shimadzu using an Atlantis T3 column (4.6 x 100 mm, 5 µm) with a flowrate of 1 mL/min. Acetonitrile and MilliQ water, each acidified to 0.1% TFA were used as solvents. Absorbance was measured at 190, 214 and 254 nm. Spectra were processed with the software LabSolutions.

1.2.4 Liquid Chromatography - Mass Spectrometry (LC-MS)

HPLC-ESI-MS was measured on the device LC-MS 2020 by Shimadzu using a Kinetex 2.6 µm EVO C18 100 Å LC 50 x 2.1 mm column. The solvents were MilliQ water + 0.1% formic acid and acetonitrile. Samples were prepared in methanol. The solvent gradient started at 5% ACN content, which was increased to 95% within 12 min. The data was processed with LabSolutions.

1.2.5 Matrix-Assisted Laser Desorption/Ionization - Time of Flight Mass Spectrometry (MALDI-TOF)

MALDI-TOF spectra were measured on a rapifleX MALDI-TOF/TOF from Bruker and MALDI Synapt G2-SI from Waters. Samples were prepared by mixing with a saturated α-cyano-4-hydroxycinnamic acid (CHCA) solution in water/ACN 1/1 + 0.1% TFA. The data was processed in mMass.

1.2.6 Fluorescence Spectroscopy

Fluorescence intensity was measured using a SPARK 20M microplate reader by the company Tecan Group Ltd. A Greiner 384 flat black wellplate was used and the data was processed with Excel.

1.2.7 Fourier-Transform Infrared Spectroscopy (FTIR)

FTIR spectra were measured using a Bruker TENSOR II spectrometer equipped with a PLATINUM ATR single reflection diamond ATR accessory. The data was processed using Excel.

1.2.8 Circular Dichroism Spectroscopy (CD)

CD was measured on a JASCO J-1500 spectrometer in a 1 mm High Precision Cell by HellmaAnalytics. The data was processed in the softwares Spectra Analysis and CD Multivariate SSE by JASCO.

1.2.9 Transmission Electron Microscopy (TEM)

TEM pictures were taken on a JEOL 1400 transmission electron microscope. Formvar/carbon-film coated copper grids (300 mesh) were purchased from Plano GmbH. The pictures were processed in ImageJ.

2. Synthesis

2.1 Synthesis of 4-Nitrophenyl (4-(4,4,5,5-tetramethyl-1,3,2-dioxaborolan-2-yl)benzyl) carbonate

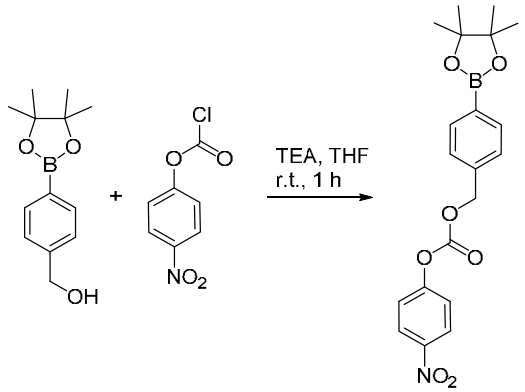

4-Hydroxymethylphenylboronic acid pinacol ester (3.00 g, 12.81 mmol) was dissolved in 30 mL dry THF under argon atmosphere. After triethylamine (3.6 ml, 25.97 mmol) was added to the reaction flask, the flask was cooled in an ice bath. 4-Nitrophenyl chloroformate (2.84 g, 14.10 mmol) was added in portions and the reaction mixture was stirred for one hour at room temperature, then the solvent was removed *in vacuo*. The mixture was suspended in ethylacetate and washed with 1 M HCl_{aq}, saturated sodium bicarbonate solution and brine. Ethylacetate was removed *in vacuo* and the reaction mixture was purified by silica chromatography (1:4 ethylacetate:*n*-hexane). After drying *in vacuo* 5.11 g (8.97 mmol, 70% yield) of 4-nitrophenyl (4-(4,4,5,5-tetramethyl-1,3,2-dioxaborolan-2-yl)benzyl) carbonate was received as a white crystalline powder.[1]

^{1}H NMR (300 MHz, $CDCl_3$) δ [ppm] = 8.27 (d, J = 9.1 Hz, 2H), 7.85 (d, J = 7.6 Hz, 2H), 7.41 (m, 4H), 5.31 (s, 2H), 1.35 (s, 12H).

^{13}C NMR (176 MHz, $CDCl_3$) δ [ppm] = 155.67, 152.57, 145.57, 137.20, 135.34, 127.77, 125.45, 121.92, 84.14, 70.95, 25.01.

2.2 Peptide Synthesis

2.2.1 Depsi(KIKI)PBA-SQINM

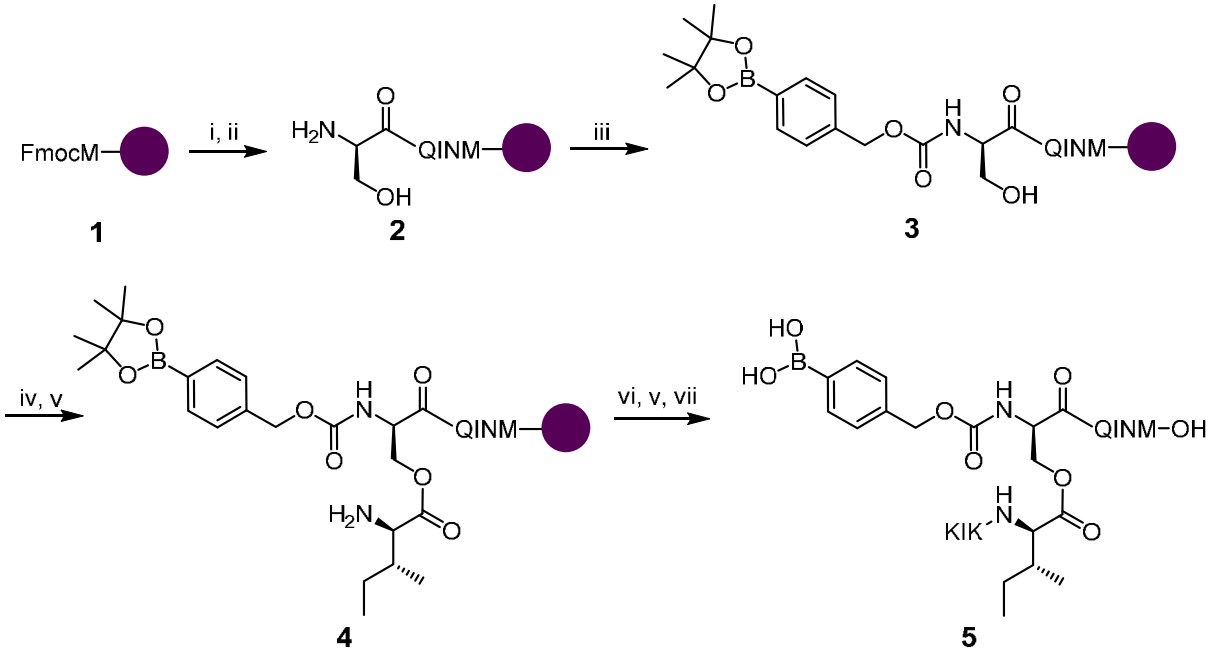

Peptide synthesis was performed according to the solid phase peptide synthesis Fmoc strategy by Merrifield. The peptide was synthesized from the *C* to the *N*-terminus in a microwave peptide synthesizer. After Fmoc-Methionine Wang resin **1** (147 mg, 0.1 mmol) was swollen in DMF for one hour at room temperature, the Fmoc protecting group was removed by two deprotection steps with 20% piperidine in DMF (3 mL) at 75 °C for 2 and 5 min (i). Fmoc-Asn(Trt)-OH, Fmoc-Ile-OH and Fmoc-Gln(Trt)-OH (5 eq in 2.5 mL DMF) were double coupled consecutively for 10 min at 75 °C (ii). PyBOP (5 eq in 1 mL DMF) and DIPEA (10 eq in 0.5 mL DMF) were added in every coupling step. Each coupling was followed by two deprotection steps (2 and 5 min) and three washes with DMF. Fmoc-Ser-OH was also coupled for 10 min (ii), but not double coupled to prevent side reactions on its unprotected hydroxyl group. After the deprotection of the *N*-terminal protecting group of serine (i), 0.025 mmol of the resin were modified on the *N*-terminus with 4-nitrophenyl (4-(4,4,5,5-tetramethyl-1,3,2-dioxaborolan-2-yl)benzyl) carbonate (99.79 mg, 0.25 mmol) in DMF and DIPEA (87 µL, 0.5 mmol) overnight at room temperature (iii). After the resin was thoroughly washed with DMF and DCM, the depsi ester bond was formed by a reaction of the serine side chain hydroxyl group with Fmoc-Ile-OH

(88.35 mg, 0.25 mmol) using DIC (39 µL, 0.25 mmol) and 4-DMAP (3.05 mg, 0.025 mmol) in 1 mL DMF for two hours at room temperature (iv). The reagents were removed and the same amount of Fmoc-Ile-OH, DIC, 4-DMAP and DMF was added to the resin, which was stirred overnight afterwards. After washing the resin with DMF and DCM, Fmoc-Lys(Boc)-OH, Fmoc-Ile-OH and Fmoc-Lys(Boc)-OH were double coupled, while every coupling step was performed for 60 min at room temperature (vi). In between the couplings, double Fmoc deprotection was performed at room temperature for 10 min each (v). After final Fmoc-deprotection (2x10 min, room temperature) the resin was washed with DMF and stirred in a cleavage cocktail containing trifluoroacetic acid/triisopropylsilane/water 95/2.5/2.5% (2 mL) for 2 h to cleave the peptide from the resin (vii). This also removed the side chain protecting groups and the pinacol protecting group of the PBA modification. The crude peptide was precipitated in 20 mL of cold diethylether, centrifuged (4 °C, 3800 rpm, 10 min), dissolved in ACN/water and purified by HPLC. The gradient started with 5% ACN, which was kept constant for 1 min, then the ACN content was increased linearly to 100% within 15 min. The retention time of the product was 13.25 min. After lyophilization Depsi(KIKI)PBA-SQINM **5** was received as a white powder.

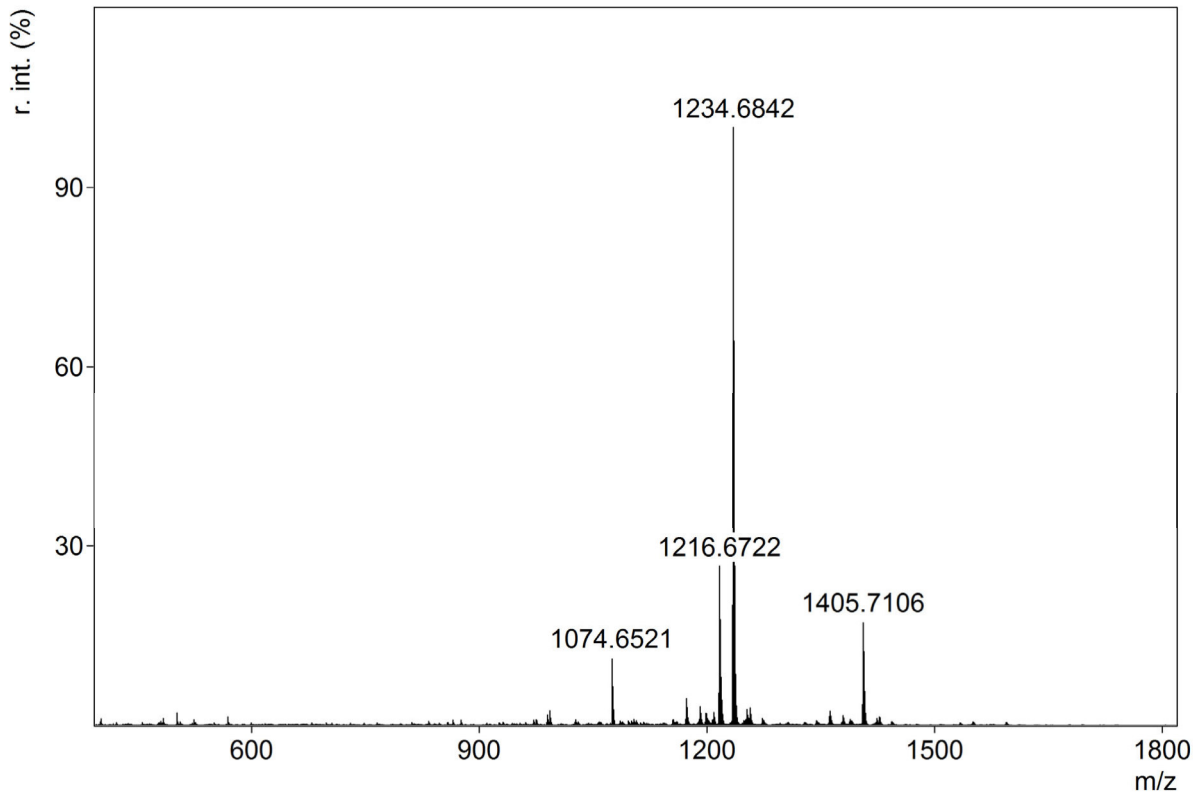

Figure S1: MALDI-TOF MS of Depsi(KIKI)PBA-SQINM **5** using α-cyano-4-hydroxycinnamic acid as matrix. m/z calculated: $[M+H]^+$ = 1251.67 g/mol, found: $[M\text{-}PBA]^+$ = 1074.6521 g/mol, $[M\text{-}OH\text{-}H_2O]^+$ = 1216.6722 g/mol, $[M\text{-}OH]^+$ = 1234.6842 g/mol, $[M+K+TFA]^+$ = 1405.7106 g/mol. Note: Due to the instability of the carbamate bond, some PBA is cleaved during the measurement.

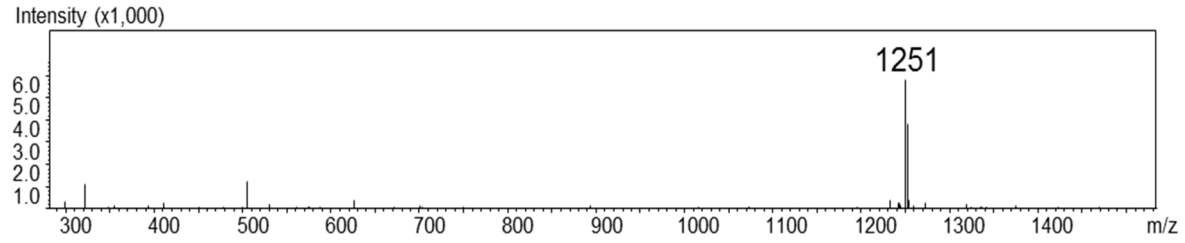

Figure S2: LCMS-ESI spectrum of the Depsi(KIKI)PBA-SQINM **5** calculated, $[M-H]^-$ = 1250.67 g/mol, found: [M-H] = 1251 g/mol.

2.2.2 Depsi(KIKI)SQINM 6

Depsi(KIKI)SQINM **6** was synthesized following the protocol of Gačanin *et al.* [2]

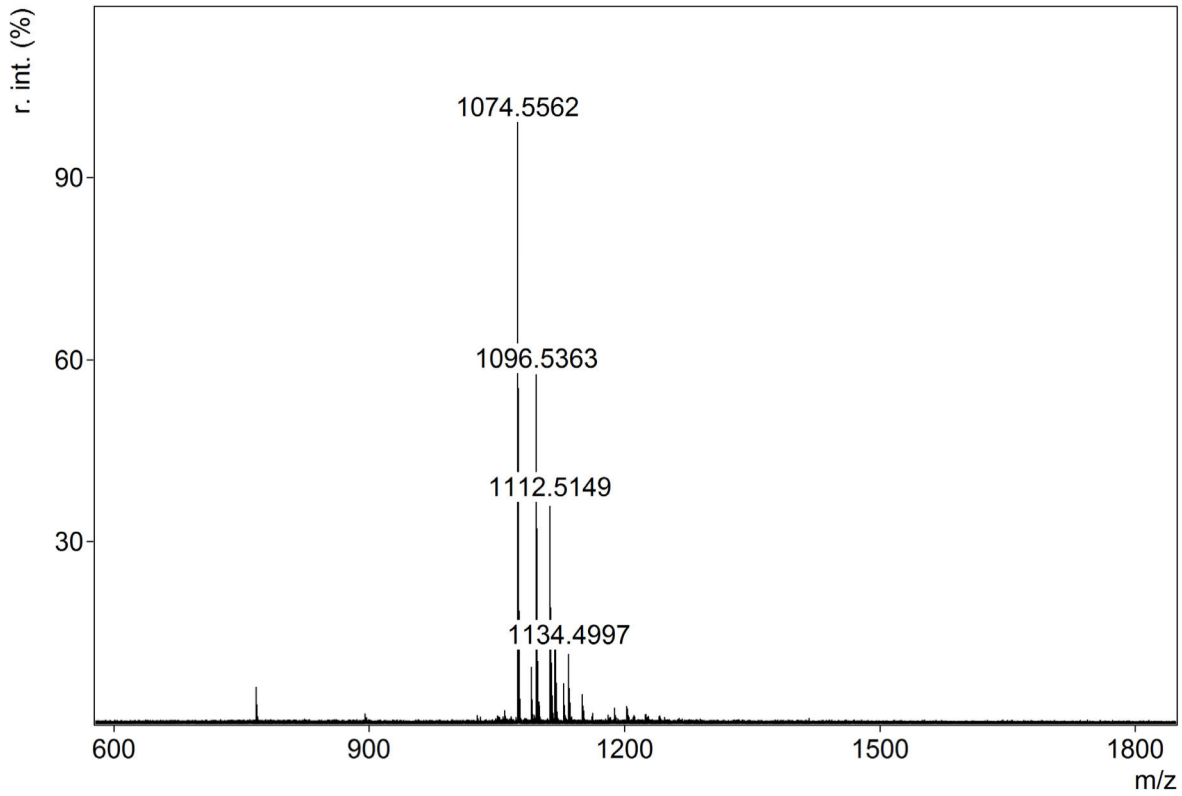

Figure S3: MALDI-TOF MS of Depsi(KIKI)SQINM **6** using α-cyano-4-hydroxycinnamic acid as matrix. m/z calculated: $[M+H]^+$ = 1074.35 g/mol, found: $[M+H]^+$ = 1074.5562 g/mol, $[M+Na]^+$ = 1096.5363 g/mol, $[M+K]^+$ = 1112.5149 g/mol, $[M+Na+K-H]^+$ = 1134.4997 g/mol.

2.2.3 KIKISQINM 7

KIKISQINM **7** was synthesized following the protocol of Gačanin *et al.*[2]

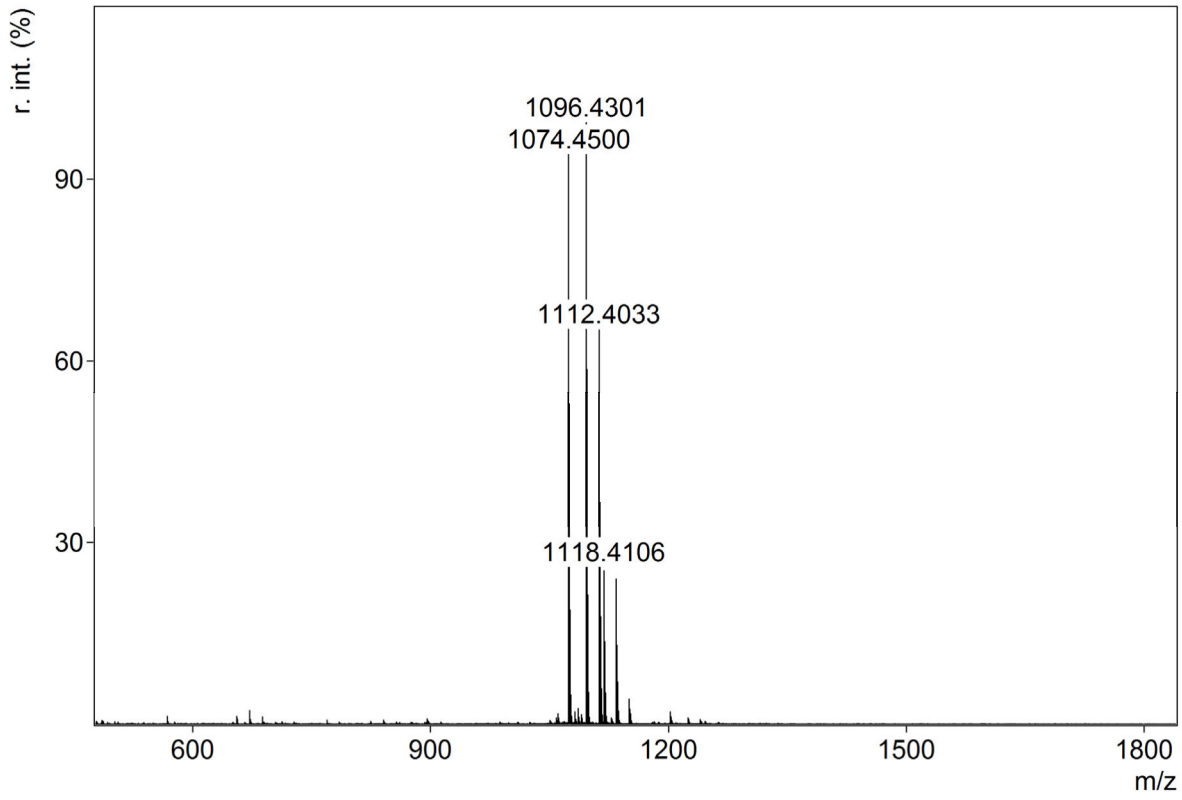

Figure S4: MALDI-TOF MS of KIKISQINM **7** using α-cyano-4-hydroxycinnamic acid as matrix. m/z calculated: $[M+H]^+$ = 1074.35 g/mol, found: $[M+H]^+$ = 1074.4500 g/mol, $[M+Na]^+$ = 1096.4301 g/mol, $[M+K]^+$ = 1112.4033 g/mol, $[M+2Na-H]^+$ = 1118.4106 g/mol.

3. Characterization

3.1 HPLC Study

Depsi(KIKI)PBA-SQINM **5** (0.2 mg) was dissolved in 400 µL tetrahydrofuran and diluted to 0.1 mg·ml^{-1} with 1.6 mL PBS (Dulbecco's phosphate buffered saline). HPLC spectra were measured by injection of 50 µL of the reaction solution at certain time points using an analytical column (see 1.2.3) with a flowrate of 1 mL/min (Figure S5). The gradient started at 5% ACN, which was kept constant for 1 min, then the acetonitrile content was increased linearly to 100% ACN within 15 min. After 24 h incubation time the hydrolysis and *O, N* - acyl shift were completed, therefore 35% H_2O_2 solution was added to receive a concentration of 100 mM. HPLC spectra were taken until completion of the oxidation reaction (Figure 6).

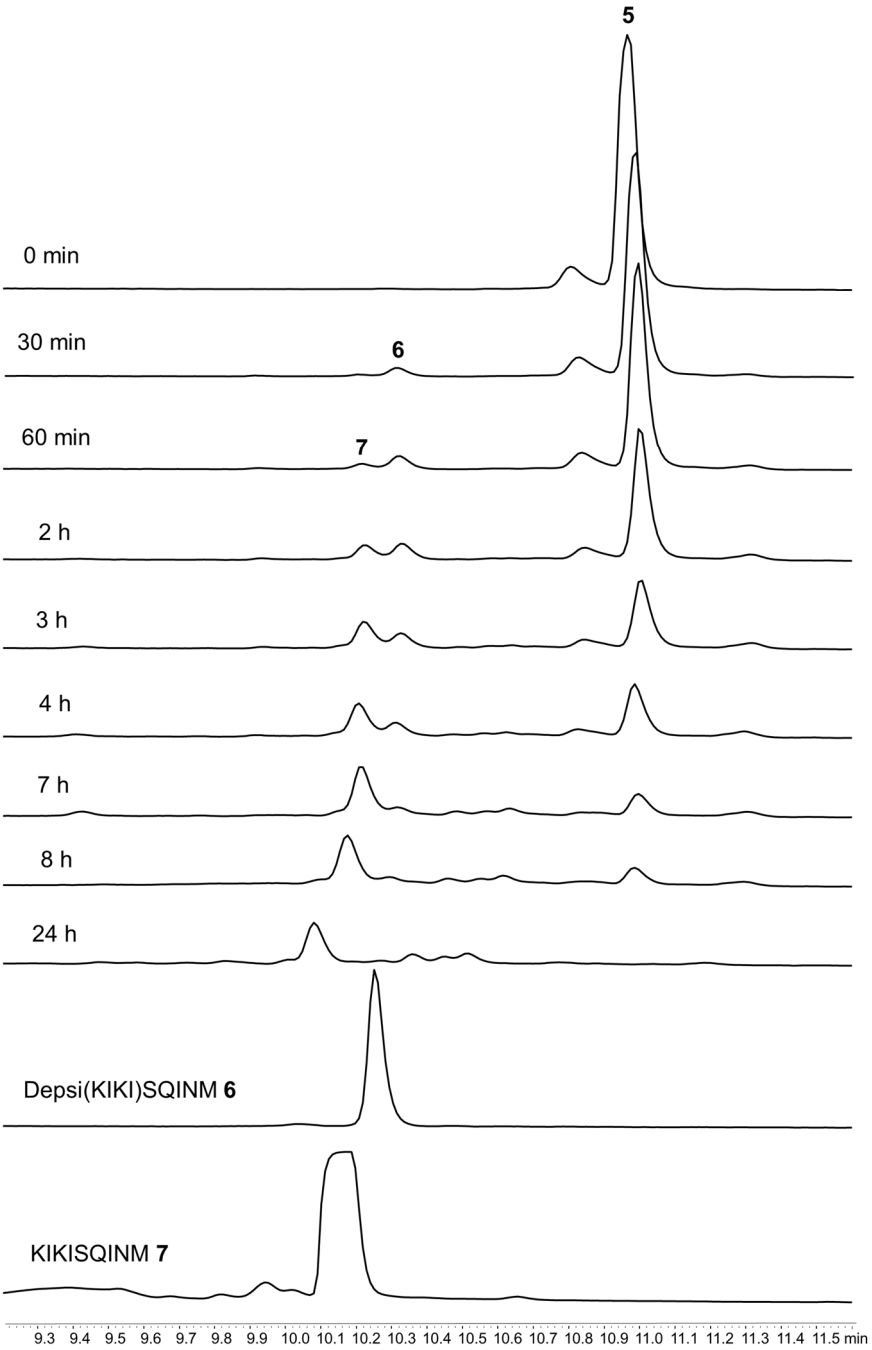

Figure S5: HPLC spectra at 190 nm taken after certain time points to observe the carbamate hydrolysis and *O, N*-acyl shift. The peak at 11 min is the educt Depsi(KIKI)PBA-SQINM **5**. After 30 min the peak of Depsi(KIKI)SQINM **6** is observed at 10.3 min. KIKISQINM **7** is observed after 10.2 min. Note: the retention time of KIKISQINM and its depsi form shifts slightly upon increasing its concentration.

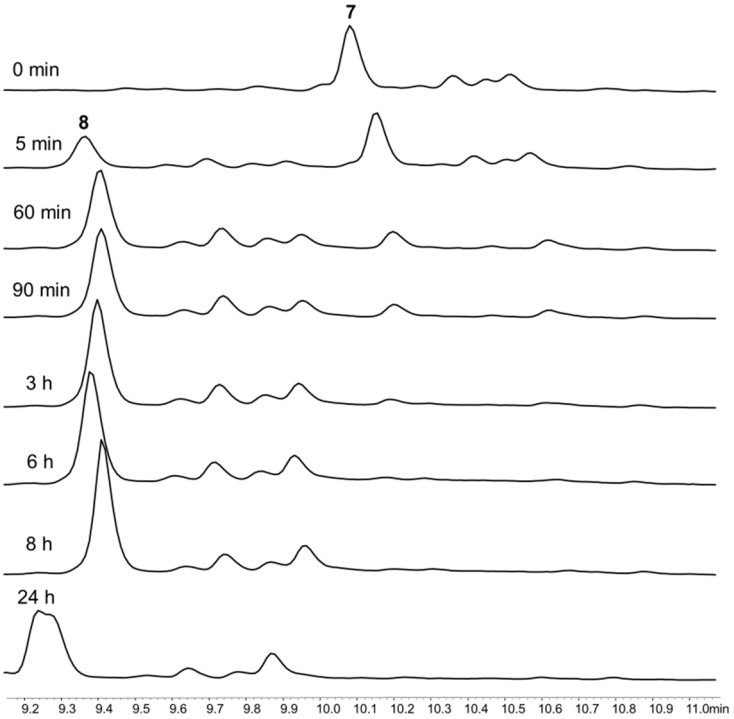

Figure 6: HPLC spectra at 190 nm taken after certain time points to observe methionine oxidation in KIKISQINM (retention time 10.15 min) to KIKISQIN(M=O) **8** (9.40 min).

3.2 MALDI-TOF

MALDI spectra of the educt Depsi(KIKI)PBA-SQINM **5**, KIKISQINM **7** and KIKISQIN(M=O) **8**, resulting from the HPLC study (3.1) were recorded to prove methionine oxidation.

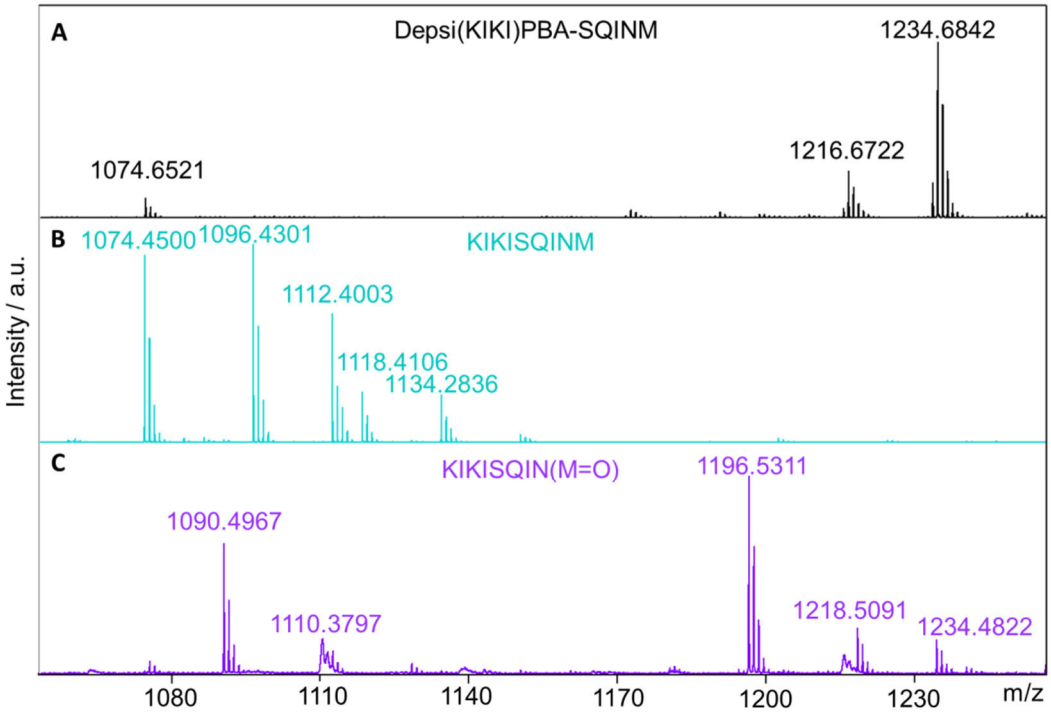

Figure S7: MALDI-TOF MS of Depsi(KIKI)PBA-SQINM **5**, KIKISQINM **7** and KIKISQIN(M=O) **8** using α-cyano-4-hydroxycinnamic acid as matrix. A: Depsi(KIKI)PBA-SQINM m/z calculated: $[M+H]^+$ = 1251.67 g/mol, found: $[M-PBA]^+$ = 1074.6521 g/mol, $[M-OH-H_2O]^+$ = 1216.6722 g/mol, $[M-OH]^+$ = 1234.6842 g/mol, Note: Due to the instability of the carbamate bond, some PBA is cleaved during the measurement. B: KIKISQINM m/z calculated: $[M+H]^+$ = 1074.63 g/mol, found: $[M+H]^+$ = 1074.4500 g/mol, $[M+Na]^+$ = 1096.4301 g/mol, $[M+K]^+$ = 1112.4003 g/mol, $[M+2Na-H]^+$ = 1118.4106 g/mol, $[M+Na+K-H]^+$ = 1134.2836 g/mol. C: KIKISQIN(M=O) m/z calculated: $[M+H]^+$ = 1089.62 g/mol, found: $[M+H]^+$ = 1090.4967 g/mol, $[M+Na+2ACN]^+$ = 1196.5311 g/mol, $[M+2Na+2ACN-H]^+$ = 1218.5091 g/mol, $[M-Na+K+2ACN-H]^+$ = 1234.4822 g/mol.

3.3 Peptide Fibrillation

Peptide fibers were formed by dissolving the peptide in DMSO at a concentration of 10 mg/ml and diluting with Dulbecco's phosphate buffered saline (PBS) to receive a final concentration of 1 mg/ml (0.8 mM). The peptides were incubated at room temperature for 24 h in an orbital shaker. In order to destroy the fibers by oxidation of methionine to methionine sulfoxide, hydrogen peroxide was added as a 35% solution to receive a concentration of 100 mM of H_2O_2 and incubated for further 24 h.

3.4 Proteostat Assay

The Proteostat Protein Aggregation Assay Kit was purchased from *Enzo Life Sciences, Inc*. 0.13 µL of the Proteostat stock solution was diluted with 24.62 µL MilliQ water and 0.25 µL assay buffer. 1 µL of this solution was added to 9 µL peptide solution (see 3.3) in a Greiner 384 flat black wellplate. The solutions were incubated in the dark for 15 min while shaking at 510 rpm. The fluorescence intensity was measured with an excitation and emission bandwidth of 20 nm and an emission wavelength of 600 nm after excitation with light at 550 nm. The experiment was done four times. Control measurements were done by incubating Proteostat solution in MilliQ water, PBS and PBS with 100 mM H_2O_2.

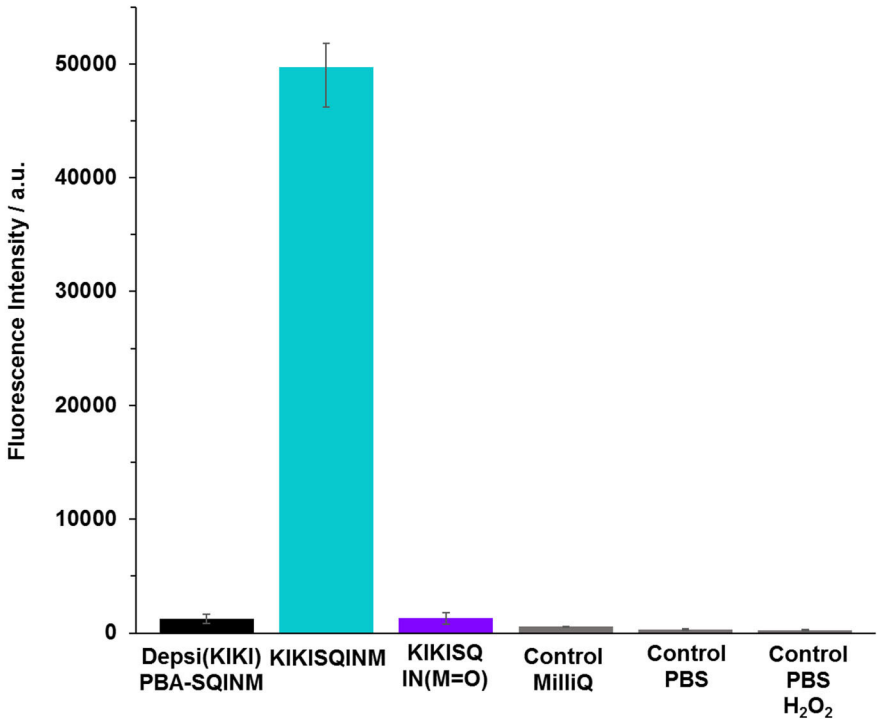

Figure S8: Fluorescence intensity spectra of peptides incubated with Proteostat, measured at 600 nm after irradiation with 550 nm. Depsi(KIKI)PBA-SQINM **5** was incubated in water/DMSO 9:1 for 48 h. KIKISQINM was fibrillized by dissolving Depsi(KIKI)PBA-SQINM **5** in PBS:DMSO 9:1 and incubating for 48 h. KIKISQIN(M=O) **8** was formed by adding 100 mM hydrogen peroxide to KIKISQINM **7** fiber solution and further incubation for 24 h.

3.5 Fourier-Transform Infrared Spectroscopy

100 µL of peptide solution (see 3.3) were lyophilized. FT-IR spectra of the lyophilized peptides were measured at wavenumbers from 400 to 4000 cm^{-1}.

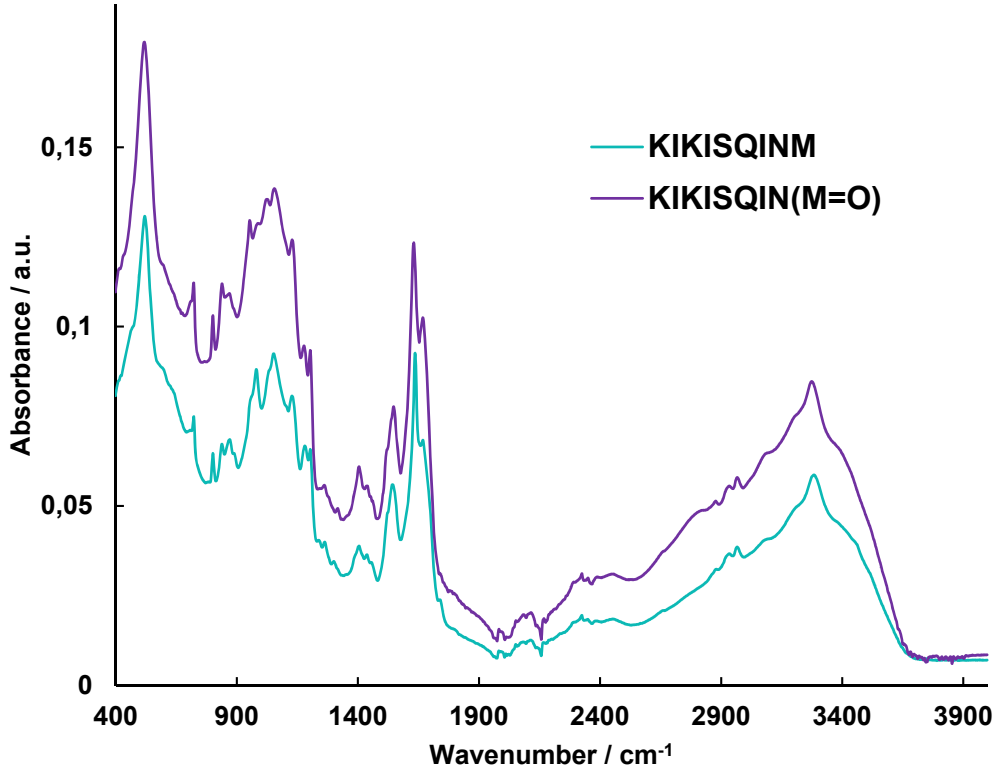

Figure S9: FT-IR spectra of KIKISQINM **7** and the oxidized derivative KIKISQIN(M=O) **8**.

3.6 Circular Dichroism

After KIKISQINM **7** was dissolved in 40 µL MilliQ water (1 mg/mL), the pH was adjusted to 7 with a 1 M NaOH solution. After 2 h incubation time at room temperature the sample was divided in two and 35% hydrogen peroxide solution was added to one sample to achieve a 100 mM concentration of H_2O_2. After incubation overnight both samples were further diluted with 240 µL MilliQ water and circular dichroism was measured at room temperature from 260 to 190 nm with a bandwith of 1 nm. The data pitch was set to 0.2 nm, while the scanning speed was 5 nm/min. Each sample was measured three times and the data accumulated. For comparison Depsi(KIKI)PBA-SQINM **5** was dissolved in MilliQ water and CD spectra were measured at the same concentration and the same settings as **7** and **8**.

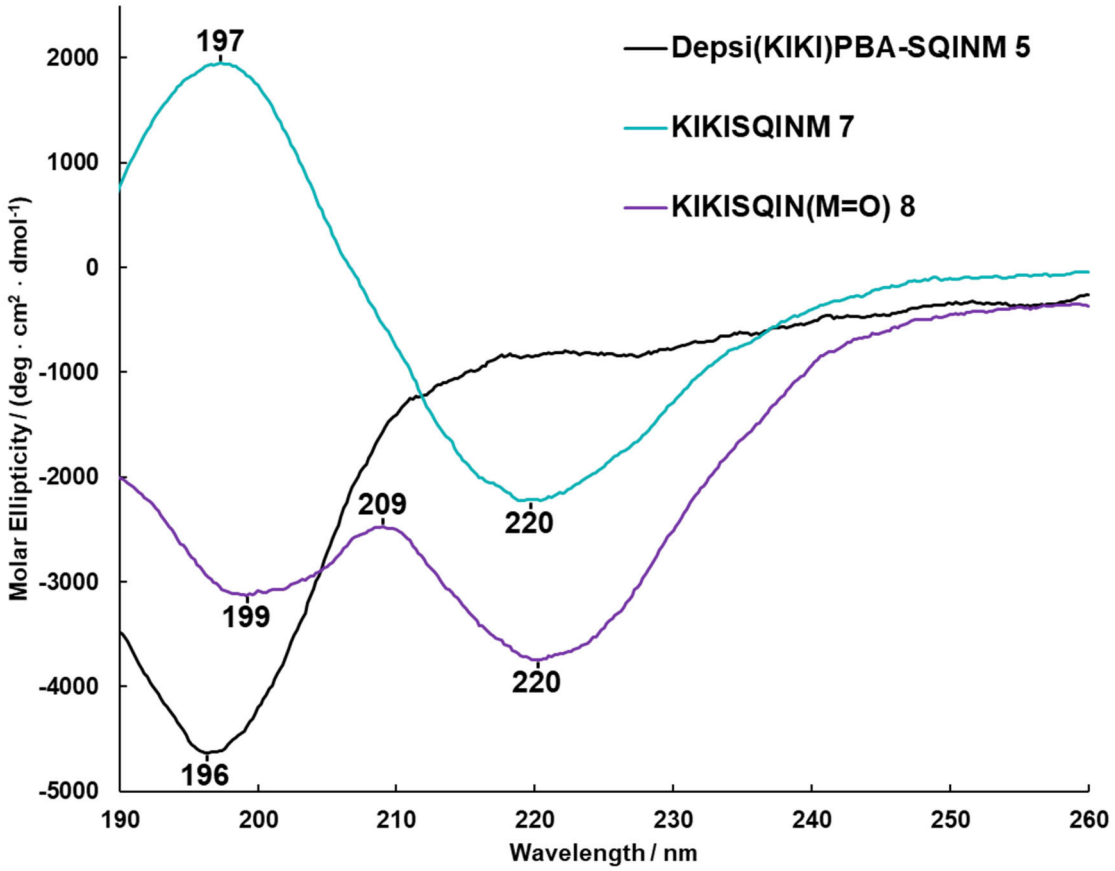

Figure S10: CD spectra of Depsi(KIKI)PBA-SQINM **5**, KIKISQINM **7** and the oxidized derivative KIKISQIN(M=O) **8**.

The spectra were used to calculate the content of each secondary structure with the software CD Multivariate SSE by JASCO.

Table S1: Content of secondary structures calculated based on CD.

	Helix	Sheet	Turn	Unordered
Depsi(KIKI)PBA-SQINM **5**	0.0%	38.1%	13.6%	50.0%
KIKISQINM **7**	4.7%	42.6%	13.4%	39.3%
KIKISQIN(M=O) **8**	2.7%	36.9%	15.1%	45.2%

3.7 Transmission Electron Microscopy

4 µL of peptide fiber solution (see 3.3) were pipetted onto freshly etched Formvar coated copper grids and incubated for 5 min. The solutions were removed with filter paper and the grids were stained with 4% uranyl acetate solution for 2.5 min. After washing with MilliQ water three times the grids were left to dry before they were measured.

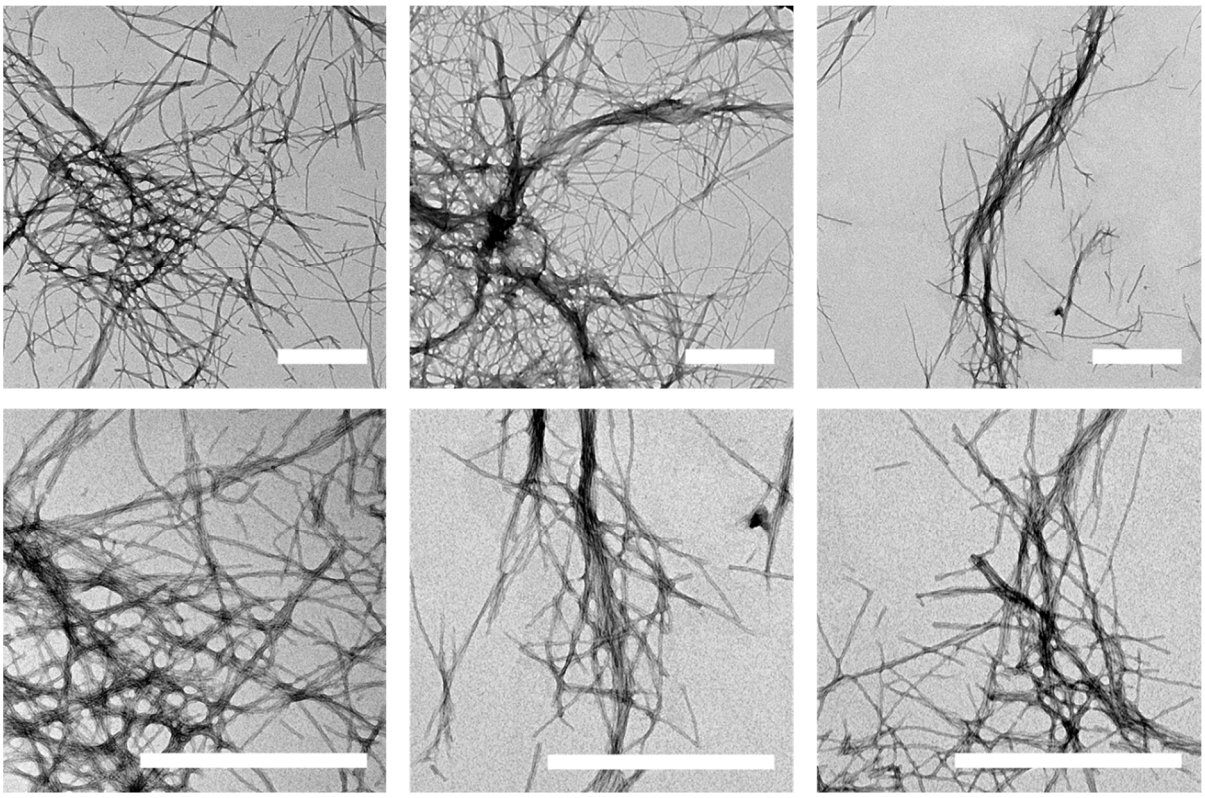

Figure S11: TEM after hydrolysis and *O, N*-acyl shift of Depsi(KIKI)PBA-SQINM **5** to KIKISQINM **7** in PBS after 48 h incubation. Scale bar = 500 nm.

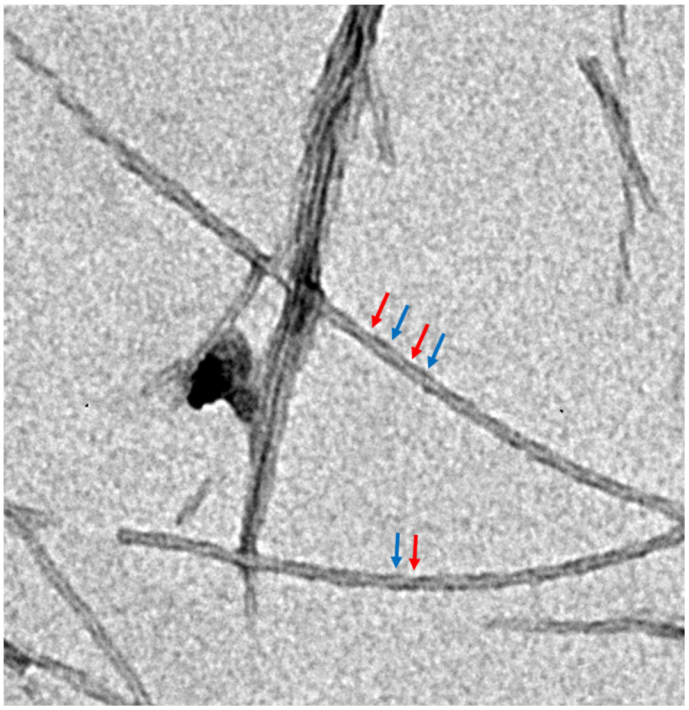

Figure S12: TEM of left-handed twisted peptide fibers formed by KIKISQINM. The red arrow indicates the thinner part of the peptide fiber with a diameter of 9 nm, the blue arrow shows the thicker one with a diameter of 11 nm.

In order to determine how long it takes till fibers are formed and how the fibers change upon time, TEM grids were prepared as described above at certain time points after adding PBS (45 µL) to the peptide stock solution in DMSO (50 µg in 5 µL).

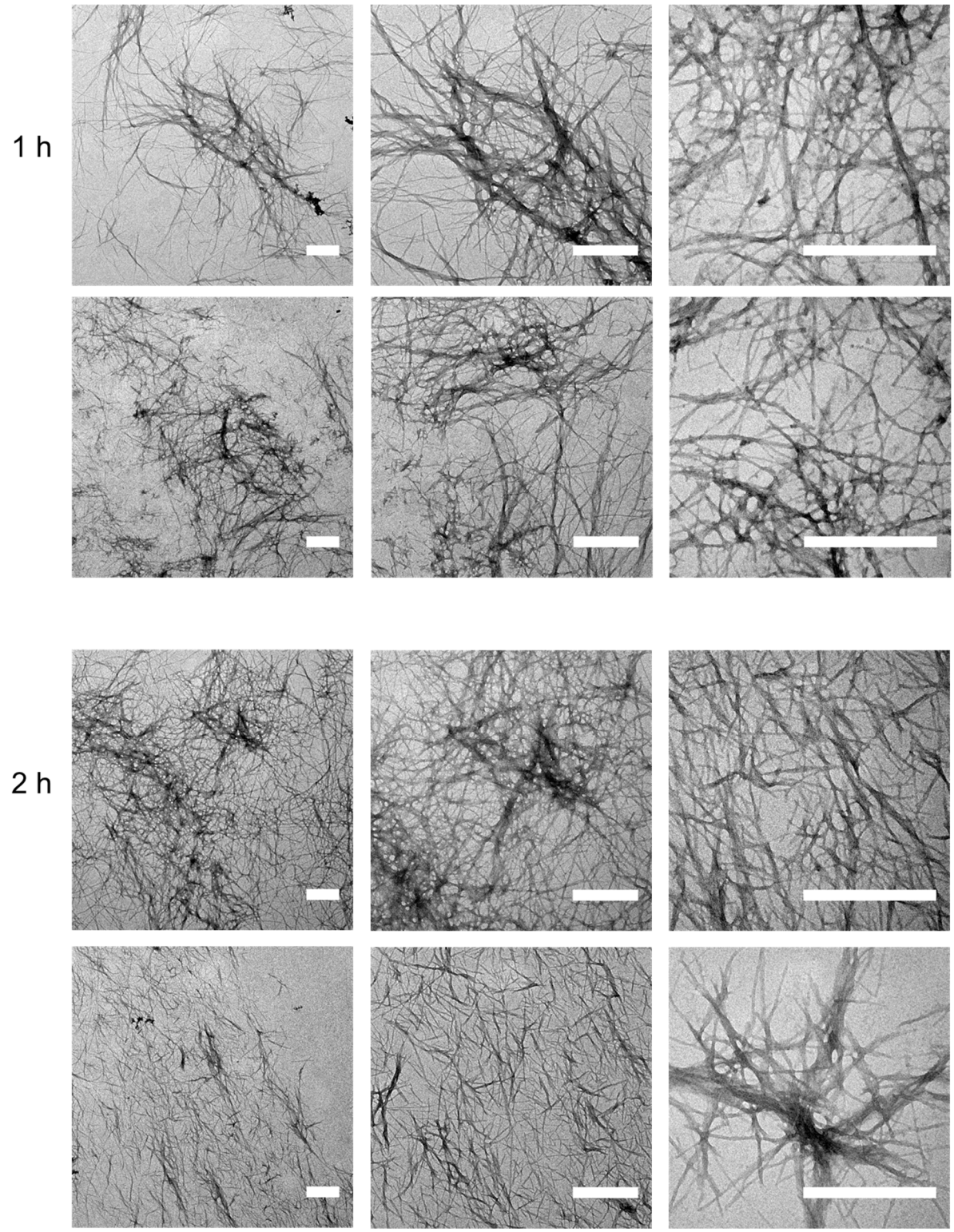

Figure S13: TEM after hydrolysis and *O, N*-acyl shift of Depsi(KIKI)PBA-SQINM **5** to KIKISQINM **7** in PBS after one and two hours. Scale bar = 500 nm.

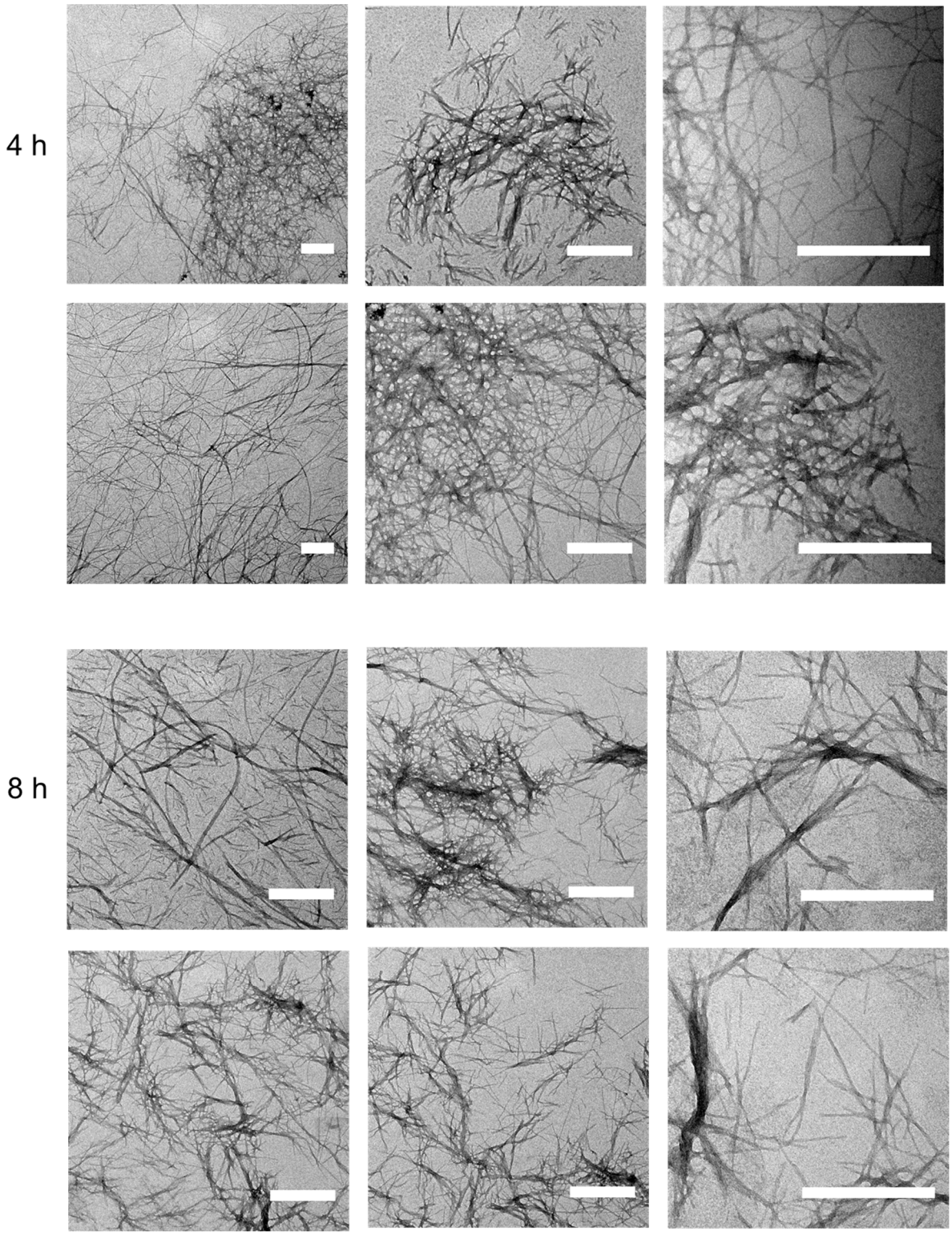

Figure S14: TEM after hydrolysis and *O, N*-acyl shift of Depsi(KIKI)PBA-SQINM **5** to KIKISQINM **7** in PBS after four and eight hours. Scale bar = 500 nm.

4. Literature

[1] J. Li, Y. Li, Q. He, Y. Li, H. Li, L. Liu, *Org. Biomol. Chem.* **2014**, *12*, 5435–5441.

[2] J. Gačanin, J. Hedrich, S. Sieste, G. Glaßer, I. Lieberwirth, C. Schilling, S. Fischer, H. Barth, B. Knöll, C. V. Synatschke, T. Weil, *Adv. Mater.* **2018**, 1805044.

8.2 Controlled Supramolecular Assembly inside Living Cells by Sequential Multi-staged Chemical Reactions

M. Pieszka[+], S. Han, C. Volkmann, R. Graf, I. Lieberwirth, K. Landfester, D. Y. W. Ng[‡], T. Weil[‡]

[+]first author, [‡]corresponding author

Published in *Journal of the American Chemical Society* **2020**, *142* (37), 15780–15789.

Date of Publication: 19 August 2020

Abstract

Synthetic assembly within living cells represents an innovative way to explore purely chemical tools that can direct and control cellular behavior. We use a simple and modular platform that is broadly accessible and yet incorporates highly intricate molecular recognition, immolative, and rearrangement chemistry. Short bimodular peptide sequences undergo a programmed sequence of events that can be tailored within the living intracellular environment. Each sequential stage of the pathways beginning with the cellular uptake, intracellular transport, and localization imposes distinct structural changes that result in the assembly of fibrillar architectures inside cells. The observation of apoptosis, which is characterized by the binding of Annexin V, demonstrates that programmed cell death can be promoted by the peptide assembly. Higher complexity of the assemblies was also achieved by coassembly of two different sequences, resulting in intrinsically fluorescent architectures. As such, we demonstrate that the *in situ* construction of architectures within cells will broaden the community's perspective toward how structure formation can impact a living system.

Contributions

Michaela Pieszka: Project and peptide design, synthesis and characterization as well as scientific evaluation of results. Planning and execution of all experiments (excluding binding affinity experiment) and performance of the respective measurements (excluding solid state NMR, TEM inside cells and confocal imaging). Preparing all figures and writing parts of the manuscript.

Shen Han: TEM measurements of cells and interpretation of the results for characterization of intracellular fiber formation as well as preparing the stitched images. TEM measurement of cell lysate of cells without PMA treatment.

Christiane Volkmann: Determination of the binding affinity between the depsipeptide and SHA-TAT including the measurements and data analysis.

Robert Graf: Solid state NMR measurements, as well as data analysis and interpretation.

Ingo Lieberwirth: Was involved in discussions concerning TEM measurements of cells and interpretation of the results for characterization of intracellular fiber formation.

Katharina Landfester: Was involved in discussions and interpretation of the results for characterization of intracellular fiber formation and prove-read the manuscript.

David Y. W. Ng: Management of the project, discussion and interpretation of all results, writing and revision of the manuscript. Performed confocal microscopy imaging and interpreted the results.

Tanja Weil: Acquiring funding for the project and its management, discussion and interpretation of all results, writing and revision of the manuscript.

JACS
JOURNAL OF THE AMERICAN CHEMICAL SOCIETY

pubs.acs.org/JACS

Article

Controlled Supramolecular Assembly Inside Living Cells by Sequential Multistaged Chemical Reactions

Michaela Pieszka, Shen Han, Christiane Volkmann, Robert Graf, Ingo Lieberwirth, Katharina Landfester, David Y. W. Ng,* and Tanja Weil*

Cite This: *J. Am. Chem. Soc.* 2020, 142, 15780−15789

Read Online

ACCESS | Metrics & More | Article Recommendations | Supporting Information

ABSTRACT: Synthetic assembly within living cells represents an innovative way to explore purely chemical tools that can direct and control cellular behavior. We use a simple and modular platform that is broadly accessible and yet incorporates highly intricate molecular recognition, immolative, and rearrangement chemistry. Short bimodular peptide sequences undergo a programmed sequence of events that can be tailored within the living intracellular environment. Each sequential stage of the pathways beginning with the cellular uptake, intracellular transport, and localization imposes distinct structural changes that result in the assembly of fibrillar architectures inside cells. The observation of apoptosis, which is characterized by the binding of Annexin V, demonstrates that programmed cell death can be promoted by the peptide assembly. Higher complexity of the assemblies was also achieved by coassembly of two different sequences, resulting in intrinsically fluorescent architectures. As such, we demonstrate that the in situ construction of architectures within cells will broaden the community's perspective toward how structure formation can impact a living system.

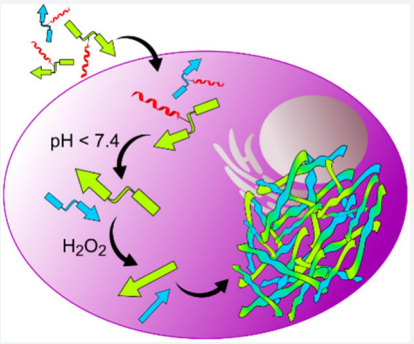

INTRODUCTION

Supramolecular interactions govern core aspects of cellular life where they are omnipresent in every biological pathway. On the molecular level, noncovalent forces guide structure formation and biomolecular interactions, which can be seen within the DNA double helix, the secondary to quaternary structures of proteins, and the dipoles of lipids. Systematically, the individual assemblies propagate into interconnecting systems to perform DNA replication/transcription, protein folding/receptor interactions, and shuttling molecules in and out of cells.[1] The resulting dynamics between these biological processes would thus define the fundamental elements of life (i.e., proliferation, homeostasis, metabolism).

As a whole, it is critical to realize that many of these assemblies elicit their function at the nanometer level, while their separate constituents are seemingly nonfunctional (i.e., nucleotides/DNA, fatty acids/vesicles, rRNA/ribosome).[1] Therefore, instead of using intrinsically bioactive components like proteins or DNA, the impact of nanoscience toward biology can also be realized through structure formation. Application wise, there has been growing interest in methods to enrich and accumulate drug molecules within cells to circumvent efflux-based drug resistance.[2,3] As the rate of efflux of molecules is directly dependent on size,[4,5] significant efforts have been made to direct drug/imaging molecules to form aggregates within cells[6,7] and with promising in vivo results.[8,9]

Nonetheless, the bioactivity of these systems often originates from known small molecule interactions such as from a chemotherapeutic agent or singlet oxygen production by metal complexes.[10,11] In contrast, specific biological responses, like programmed cell death, driven purely by the formed self-assembled nanostructures are less known. We envisioned that the assembly of nonfunctional constituents into functional architectures directly in a living cell would not only be a significant milestone in nanobiotechnology but also provide a platform to integrate synthetic chemistry with living processes.

Herein, we report the construction of two peptide sequences designed to undergo a multistage transformation that results in the assembly of fibrillar architectures inside cancer cells (Figure 1). The first stage, comprising the cellular entry process, is gated by a pH-dependent boronic acid−salicylhydroxamate complexation.[12] This chemistry links a transporter "TAT" sequence (trans-activator of transcription), derived from the human immunodeficiency virus (HIV),[13] together with a pro-assembling sequence (henceforth referred as depsipeptide). As such, upon successful endocytosis, acidification within the intracellular vesicles releases the pro-assembling sequence. Here, the second and third stage are incorporated into the pro-assembling sequence with the second stage guarded by an

Received: May 13, 2020
Published: August 19, 2020

https://dx.doi.org/10.1021/jacs.0c05261
J. Am. Chem. Soc. 2020, 142, 15780−15789

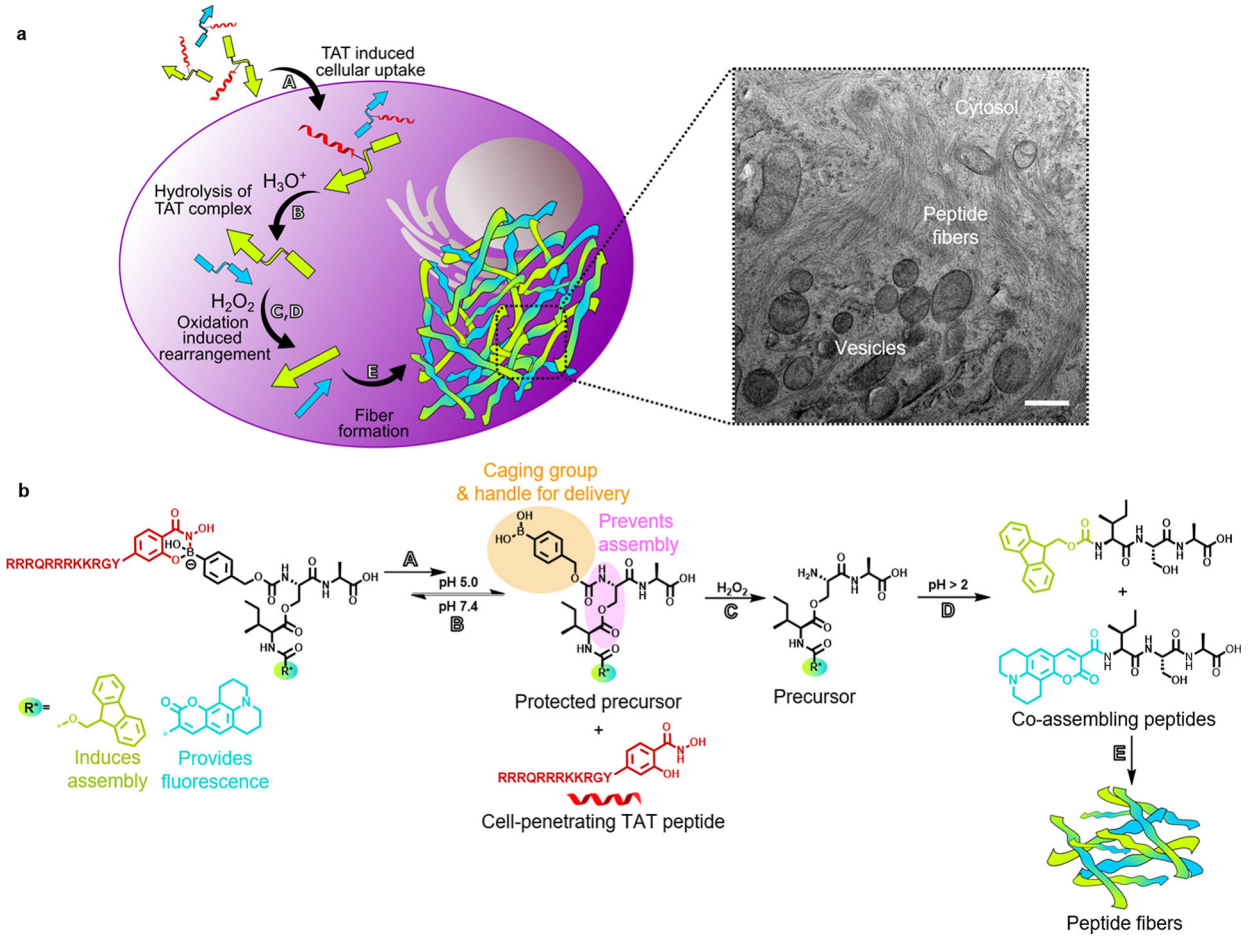

Figure 1. Intracellular coassembly of peptides. (a) Depsipeptides (kinked arrows) are uptaken by cells due to dynamic covalently bound salicylhydroxamate-TAT (SHA-TAT, red coil, step A). After hydrolysis of the complex in an acidic environment (step B), the boronic acid headgroup of the depsipeptides is cleaved by intracellular hydrogen peroxide (step C). Subsequent *O,N*-acyl shift forms the linear coassembling peptides (step D). Linear peptides (straight arrows) form fibrillar networks inside A549 cells (step E), which are visible by transmission electron microscopy (TEM, scale bar 500 nm). (b) Chemical reactions that lead to cellular uptake, peptide linearization, and peptide coassembly of Fmoc (green) and coumarin 343 (blue) functionalized ISA.

immolative boronic acid cage sensitive toward elevated or endogenous H_2O_2 within cancer cells.[14−16] Upon the immolation of the cage, the third stage is triggered by the *O,N*-acyl rearrangement of the depsipeptide that generates the linear isoleucine-serine-alanine (ISA) self-assembling motif.[17,18] Production of ISA promotes the final stage of self-assembly into fibrillar architectures and in the process triggers apoptosis.

In essence, the design comprises three modular components: (1) the pro-assembling depsi unit and its pH-reversible functionalization with TAT, (2) the peroxide-triggered cleavage of the boronic acid masking group, and the (3) pH-controlled *O,N*-acyl rearrangement to generate the self-assembling peptide sequence. In this way, intracellular transport, release, and supramolecular assembly into peptide fibrils is individually and sequentially programmed inside different cellular compartments by consecutive chemical reactions (Figure 1).

In addition, we demonstrate coassembly as a strategy to increase the level of functionality by imparting fluorescence into the fibrillar structures to allow imaging.[19,20] Coassembly, i.e., assembly of more than a single component, is prevalent in Nature, and important examples include the assembly of α-/β-tubulin in microtubules,[21] cholesterol/phospholipids in membranes,[22] or the Arp2/3 complex in actins.[23] While Nature uses highly specific proteins to transport and program these assemblies, synthetic methods are advantageous as they can be bioorthogonal and also be specifically tailored. By incorporating sophisticated chemical designs into a simple bimodular peptide sequence, we demonstrate that synthetic architectures can be formed directly within living systems using natural triggers.

RESULTS AND DISCUSSION

Solid-phase peptide synthesis using fluorenylmethoxycarbonyl (Fmoc) chemistry was conducted with alanine-preloaded Wang resin (Scheme 1). Fmoc-serine was added as the second amino acid using (benzotriazol-1-yloxy)tripyrrolidinophosphonium hexafluorophosphate (PyBOP) and *N,N*-diisopropylethylamine (DIPEA).[24] Importantly, Fmoc-serine was used without a protecting group on the hydroxyl group in order to create an ester bond with isoleucine later in the synthesis. After Fmoc deprotection of serine, modification of the N-terminus using 4-(nitrophenyl)phenylboronic acid pinacol ester was performed. Fmoc-isoleucine was coupled on the amino acid side chain of serine using *N,N′*-diisopropylcarbodiimide (DIC) and 4-(dimethylamino)pyridine (DMAP), forming the ester and therefore the so-called depsipeptide.[17] The peptide was removed from the solid support, and the boronic acid was deprotected simultaneously using a cleavage cocktail based on trifluoroacetic acid (TFA). After purification by high-perform-

https://dx.doi.org/10.1021/jacs.0c05261
J. Am. Chem. Soc. 2020, 142, 15780−15789

Scheme 1. Synthesis of Depsipeptides Depsi(Fmoc-I)pba-SA 1a and Depsi(C343-I)pba-SA 1b by Solid-Phase Peptide Synthesis[a]

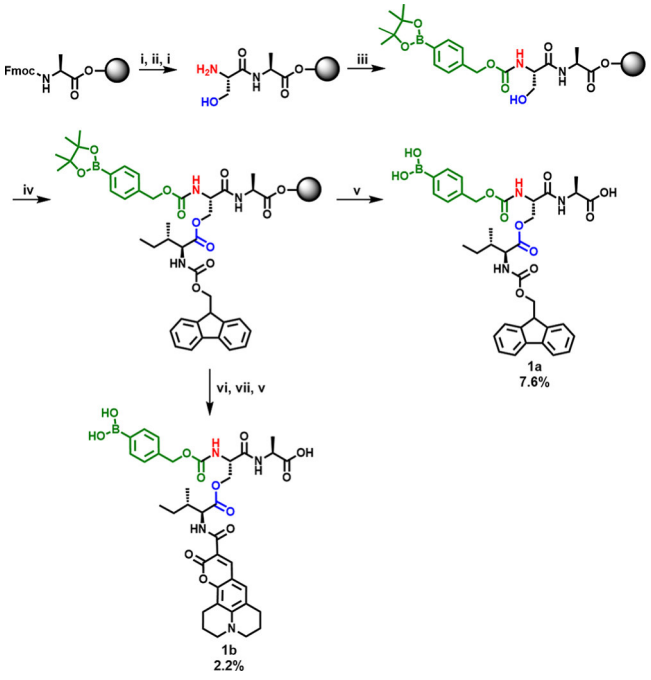

[a](i) Piperidine, (ii) Fmoc-Serine, PyBOP, DIPEA, (iii) 4-(nitrophenyl)phenylboronic acid pinacol ester, DIPEA, (iv) Fmoc-isoleucine, DIC, DMAP, (v) TFA, triisopropylsilane, H_2O, (vi) piperidine, (vii) coumarin 343, PyBOP, DIPEA.

ance liquid chromatography (HPLC), the pure peptide **1a** was characterized by electrospray ionization mass spectrometry (ESI-MS, Figure S6). In order to synthesize the fluorescent Depsi(C343-I)pba-SA (Depsi(coumarin 343-isoleucine)-phenylboronic acid-serine-alanine), the Fmoc group was removed using piperidine and the peptide was modified with coumarin 343 using PyBOP/DIPEA for activation before cleavage of the peptide from the solid support. The identity of the product **1b** was confirmed after HPLC purification by ESI-MS (Figure S9), which also showed that the peptide was isolated in high purity.

In order to prove the hydrogen peroxide-induced removal of the PBA protecting group and the subsequent *O,N*-acyl shift in solution outside cells, Depsi(Fmoc-I)pba-SA **1a** was incubated in NH_4HCO_3 buffer pH 7.4 with and without hydrogen peroxide (Figure 2a–c, Figure S15). The peptide (R_T = 15.6 min) was stable in the absence of H_2O_2 and led to only 3% conversion into Fmoc-ISA **3a** (R_T = 14.6 min) within 45 h due to slow hydrolysis of the carbamate bond. In contrast, addition of hydrogen peroxide led to a yield of 94% Fmoc-ISA **3a** in the same time. The intermediate Depsi(Fmoc-I)-SA **2a** could also be observed by the appearance of a peak at 14.0 min, which started to decrease after 8 h, while the product peak of **3a** increased. The same study was performed using Depsi(C343-I)pba-SA **1b**, and the results showed that both the removal of the phenylboronic acid by H_2O_2 as well as the *O,N*-acyl shift were successful for the coumarin derivative of the peptide (Figures 2e and S16). After 4 h, Depsi(C343-I)pba-SA **1b** (R_T = 6.9 min) was no longer present, while the peaks for Depsi(C343-I)-SA **2b** (R_T = 5.0 min) and the linear peptide C343-ISA **3b** (R_T = 6.2 min) increased. After 24 h only **3b** was found in the sample. Incubation of Depsi(C343-I)pba-SA **1b** in NH_4HCO_3 buffer without H_2O_2 led to formation of only 3% of the linear peptide **3b**, which proves the stability of the peptide under these conditions (Figure 2 d).

TEM measurements of Depsi(Fmoc-I)pba-SA **1a** in phosphate buffer pH 7.4 after 24 h incubation with and without hydrogen peroxide showed the oxidation-triggered self-assembly of the peptide due to formation of the linear fibrillating sequence Fmoc-ISA **3a**, while the corresponding boronic acid-modified depsipeptide **1a** did not form peptide fibers (Figure 2f and 2g). In order to determine the critical fibrillation concentration of Fmoc-ISA **3a**, which is important for intracellular fiber formation, Fmoc-ISA was incubated at different concentrations ranging from 2 mM to 15 μM for 24 h in phosphate-buffered saline (PBS). In TEM measurements, the lowest detectable concentration of peptide fibers was 62.5 μM (Figure S26).

The fluorescent peptide Depsi(C343-I)pba-SA **1b** was synthesized in order to enable live cell imaging of the peptide fibers by coassembly of both intracellularly rearranged peptides. While incubation of Depsi(C343-I)pba-SA **1b** in phosphate buffer did not lead to fiber formation, addition of H_2O_2 led to the appearance of amorphous aggregates in TEM (Figure 2h and 2i). Coincubation of both PBA depsipeptides upon hydrogen peroxide treatment at a ratio of 5:1 of **1a:1b** led to a mixture of fibers and some aggregates (Figure 2j). Preliminary confirmation of coassembly was accomplished by fluorescence microscopy, demonstrating the colocalization of the coumarin 343 signal with Proteostat, which detects cross-β-sheet-containing peptide fibers (Figure 2k).[19,20,24,25]

Next, we elucidated the secondary structure of Fmoc-ISA as it is the primary driving force for fiber formation. To address this question, we performed Fourier transform infrared spectroscopy measurements (Figure S29). The results indicated formation of β-sheets due to the appearance of a maximum at 1634 cm^{-1}. Another maximum at 1688 cm^{-1} is usually assigned to antiparallel β-sheets in proteins but recently has been reported to derive from the carbamate bond of the Fmoc group. A shoulder which appeared at 1653 cm^{-1} in the FT-IR spectrum might be assigned to either α-helices or disordered structures.[26−29] ^{13}C (^1H) CP-MAS NMR spectra (cross-polarization-magic angle spinning nuclear magnetic resonance) confirmed formation of three different competing structures by showing two sharp peaks and one broad peak for the Fmoc carbonyl as well as several overlapping peaks for the C═O groups of the amino acids (Figure S30).

For additional proof of coassembly of both peptides, circular dichroism spectroscopy was used to visualize changes in the secondary structure (Figure 2l). The CD spectrum of Fmoc-ISA **3a** in water showed a maximum at 218 nm, which can be attributed to a $n \rightarrow \pi^*$ transition, and a shoulder peak at ~209 nm was observed in the CD spectrum as well as a minimum at 190 nm.[30] Notably, a strong positive Cotton effect was observed with a maximum at 267 nm, which corresponds to the $\pi \rightarrow \pi^*$ transition of the Fmoc groups in the self-assembled peptide fibers.[18] In contrast, the CD spectrum of C343-ISA **3b** revealed a maximum at 195 nm and a minimum at 215 nm with opposite ellipticity compared to **3a**. In proteins these signals are attributed to β-sheets and correspond to $\pi \rightarrow \pi^*$ and $n \rightarrow \pi^*$ transitions, respectively.[31] For coassembly, the study was accomplished using two different sample preparation methods: (1) the individual peptides (**3a** and **3b**) were first mixed before triggering the coassembly in H_2O, and (2) the separate peptide

https://dx.doi.org/10.1021/jacs.0c05261
J. Am. Chem. Soc. 2020, 142, 15780−15789

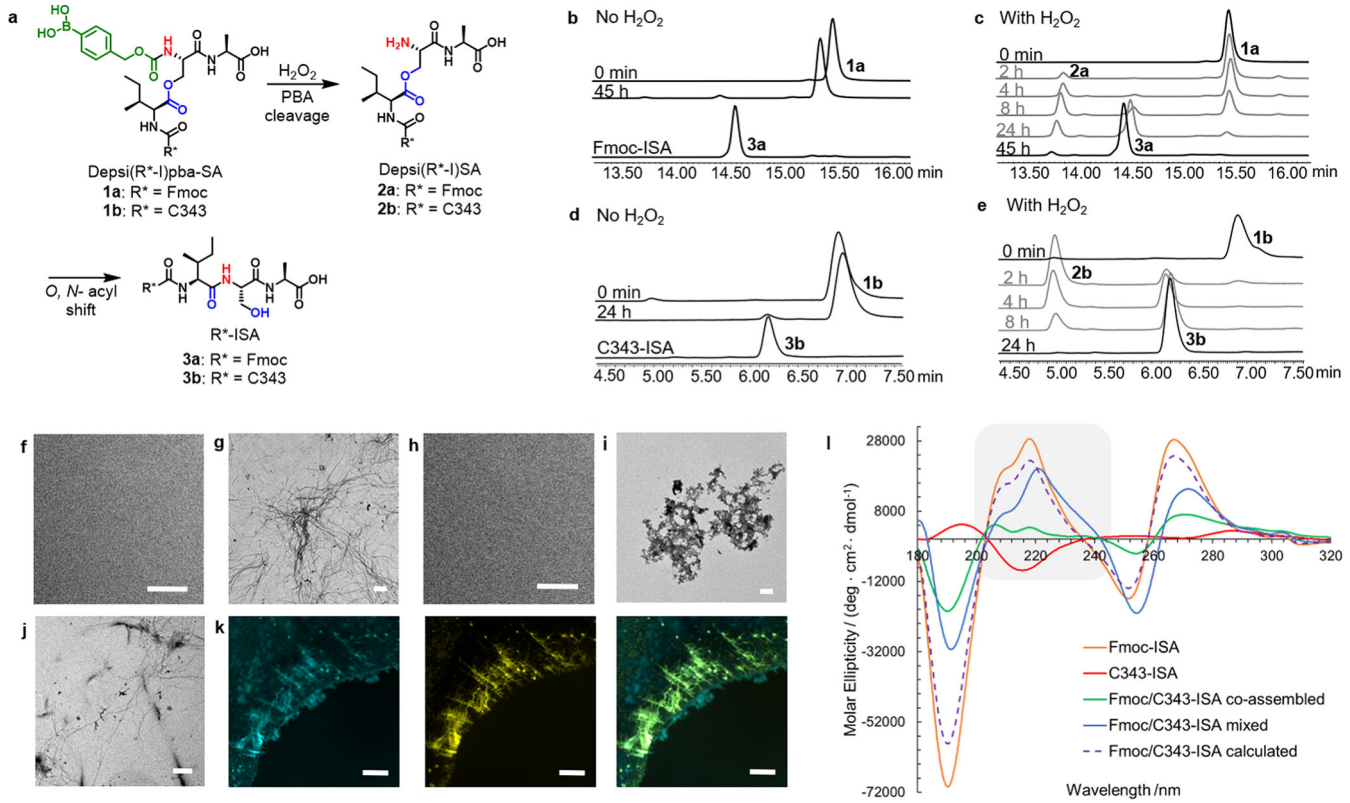

Figure 2. Hydrogen peroxide induced peptide fiber formation. (a) Phenylboronic acid removal of Depsi(R*-I)pba-SA peptides **1a** and **1b** and subsequent O,N-acyl shift to give R*-ISA **3a** and **3b** (R* = Fmoc or coumarin 343). (b) HPLC spectra at different time points showing the stability of Depsi(Fmoc-I)pba-SA **1a** (15.6 min) in NH_4HCO_3 buffer and reference spectrum of Fmoc-ISA **3a** (14.6 min). (c) H_2O_2 (2 mM) induced removal of the boronic acid to give Depsi(Fmoc-I)SA **2a** (14.0 min) and linearization of the peptide to Fmoc-ISA **3a** (14.6 min). (d) Stability of Depsi(C343-I)pba-SA **1b** (6.9 min) in buffer, and HPLC spectrum of C343-ISA **3b** (6.2 min). (e) H_2O_2 (1 mM) induced PBA removal and O,N-acyl shift of Depsi(C343-I)pba-SA **1b** (6.9 min) to first give Depsi(C343-I)SA **2b** (5.0 min) and finally C343-ISA **3b** (6.2 min). TEM images of (f) Depsi(Fmoc-I)pba-SA **1a**, (g) Fmoc-ISA **3a**, (h) Depsi(C343-I)pba-SA **1b**, (i) C343-ISA **3b**, (j) coincubation of Fmoc-ISA **3a** and C343-ISA **3b** 5:1. Scale bars 500 nm. (k) Fluorescence microscope images of Fmoc-ISA:C343-ISA **3a**:**3b** 5:1. (Left) Coumarin 343 channel (cyan). (Middle) Proteostat stained peptide fibers (yellow). (Right) Merged Proteostat and coumarin 343 channel showing the overlay of the fluorescent dyes (green). Scale bars 20 μm. (l) Circular dichroism spectra of Fmoc-ISA (orange), C434-ISA (red), and their differently prepared assemblies in H_2O (coassembled, green; mixed, blue). Fmoc/C343-ISA (calculated, dashed purple line) is the sum of the separately recorded spectra of Fmoc-ISA and C343-ISA at a ratio of 5:1 to match the experimental conditions. Region of interest is highlighted in gray.

assemblies are preformed in H_2O, and the resultant nanostructures are combined. Mixing of the preformed nanostructures leads to the appearance of an additional shoulder peak at ~235 nm and an overall decrease in signal intensities. This effect is larger than expected from the spectral sum of a 5:1 mixture of **3a**:**3b**, which represents the hypothetical spectrum in the absence of interactions between **3a** and **3b**. Hence, the results indicate interactions at the nanostructure level, causing a decrease in chirality of the assemblies. Upon coincubation of both peptides to induce coassembly, the intensities of the maxima and minima are further decreased significantly, which also includes signals attributed to electronic transitions of the Fmoc groups. This is especially visible in the change of peak proportions at 218 and at 206 nm where the latter was previously observed as a shoulder at ~209 nm. We conclude that upon coassembly of **3a** and **3b**, the overall structural chirality of the peptide assemblies is decreased, leading to a comparable CD spectrum of **3a** due to the 5-fold excess but with distinct differences in ellipticity.[32−34]

In order to provide cellular uptake of depsipeptides **1a**/**b**, a salicylhydroxamate-functionalized TAT peptide **12** was needed. TAT, which has the amino acid sequence YGRKKRRQRRR, was synthesized by standard SPPS methods and was modified with 4-pentynoic acid on its N-terminus to give molecule **11** (Figure S11). After a copper-catalyzed azide−alkyne cycloaddition (CuAAC) with trityl (Trt)- and (2-methoxyethoxy)-methoxy (MEM)-protected 4-azido salicylhydroxamate **10**, which was synthesized in seven synthetic steps (Figure S1), the peptide was cleaved from the solid support and purified by HPLC. After isolation of the pure peptide SHA-TAT **12**, it was characterized by MALDI-TOF mass spectrometry (matrix-assisted laser desorption/ionization-time-of-flight, Figure S13).

Attachment of the transporter peptide TAT was accomplished by boronic acid/salicyl hydroxamate chemistry. Formation of the dynamic covalent bond between the boronic acid-functionalized depsipeptides **1a** and **1b** and SHA-TAT **12** in phosphate buffer pH 7.4 was proven by MALDI-TOF measurements for both Fmoc- and C343-modified peptides **1a** and **1b**. Both products were formed by condensation of PBA and SHA, and multiple cation adducts were observed in the spectra (Figure 3a and 3b). Fluorescence quenching experiments with Depsi(C343-I)pba-SA **1b** and SHA-TAT **12** gave an K_D of 2.67 μM, which was expected due to previously reported results for SHA-PBA complexes (Figure 3c).[35] Reversibility of the complexation was accomplished at pH 5, which results in the recovery of fluorescence (Figure S31). The binding and release

https://dx.doi.org/10.1021/jacs.0c05261
J. Am. Chem. Soc. 2020, 142, 15780−15789

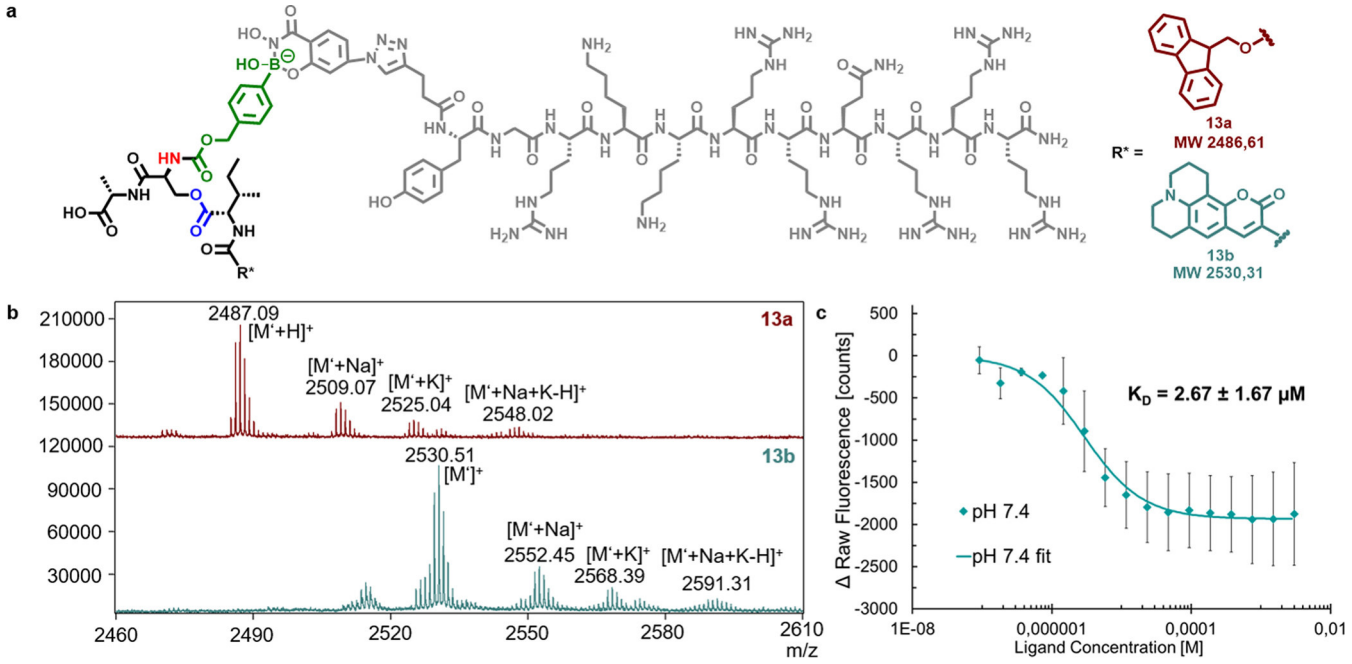

Figure 3. Complexes of SHA-TAT **12** and the boronic acid depsipeptides **1a** and **1b**. (a) Chemical structure of dynamic covalently bound SHA-TAT and boronic acid-modified depsipeptide conjugates **13a** and **13b**. (b) MALDI spectra showing the successful formation of complexes of SHA-TAT **12** with Depsi(Fmoc-I)pba-SA **1a** (top) and Depsi(C343-I)pba-SA **1b** (bottom). [M'] corresponds to the molecular weight after loss of OH^-. [M'] = [M−OH^-]. (c) Determination of the K_D of the SHA-TAT complex with Depsi(C343-I)pba-SA (**13b**) by fluorescence quenching.

were confirmed by previous reports by our group to transport proteins into cells.[36,37]

Alongside the acidification-induced release of the pro-assembling sequence **1a/b** from the TAT complexes **13a/b** inside endosomes, the H_2O_2 stimulus is required for assembly. The average concentration of H_2O_2 within A549 cells was assayed using the Intracellular Hydrogen Peroxide Assay Kit from Sigma-Aldrich and found to be 1.64 ± 0.16 μM (Figure S 57). Stimulation of H_2O_2 production can be performed with 100 nM of phorbol-12-myristat-13-acetate (PMA),[38] affording a 49% increase to 2.45 ± 0.37 μM. Using these conditions, the TAT-complexed depsipeptides **13a/b** were incubated with A549 cells, and successful cellular uptake was shown by confocal microscopy (Figure 4a). The concentration of the depsipeptides was adjusted to 150 μM in total to meet the requirements of the critical fibrillation concentration. The depsipeptides were used at a ratio of 5:1 (**13a:13b**) in order to receive a sufficient fluorescence signal by coumarin 343 inside cells while maintaining an excess of the Fmoc peptides to direct fiber formation. Incubation of cells with only the depsipeptides **1a** and **1b** did not show internalization of the peptides, which proves the necessity of SHA-TAT **12** for cellular uptake (Figure 4a, top row). The increase in fluorescence intensity of coumarin 343 in the presence of PMA suggests local accumulation of fluorescent **3b** upon fiber formation, indicating that the coassembly was more pronounced at higher concentrations of H_2O_2, although as shown in Figures S47 and S48, peptide fiber formation also occurs without PMA. Significant cell deformation and nuclear condensation imply that cell viability is significantly affected (Figures S38, S39, and S41). Incubation of the peptide samples with the cells for 2 h showed less cellular uptake, while extending it to 6 h led to more internalization of the peptides (Figure S34). Peptide-treated cells were also examined under higher magnification, where fibrillar structures inside the cell were visible in the coumarin 343 channel (Figure S35). A striking observation was the inefficient staining of the nucleus in cells where the postulated assembly has occurred. This phenomenon has already been described in the literature, where formation of peptide fibers inside cells prevented the staining of nuclei as nuclear stains were trapped inside fibrillar networks.[39]

We subsequently explored the mechanisms involved in each step of intracellular transport using time-lapsed Förster resonance energy transfer (FRET) and colocalization studies. TAT was labeled with 5-FAM (compound **14**) serving as the FRET acceptor for coumarin 343 (Figure S14). Using this FRET-labeled variant of **13a/b**, named **15a/b**, we performed confocal microscopy at 1 and 4 h time points (Figure 4 c). At 1 h, uptake of **15a/b** can be visualized as punctuated spots characteristic of vesicle-based intracellular transport. A significant proportion of these vesicles exhibits FRET signals (red), suggesting that most of the uptaken **15a/b** has not undergone dissociation. Nonetheless, a first indication of release into the cytosol was observed for a small proportion of these vesicles. At 4 h, among cells that are still intact, assembly has been accomplished in large areas of the cells. In these regions, FRET signals are absent, suggesting that **15a/b** has been mostly dissociated into **1a/b** and TAT **14** followed by the peroxide-driven cascade. However, remaining amounts of undissociated **15a/b** could be observed to proceed further along the TAT transportation pathway into the nuclear region. Here, the complex remains bound as the pH within the nucleus is no longer acidic.[40] The transport pathway through TAT-promoted endocytosis was confirmed using early/late endosome studies with CellLight, which saw major colocalization (Figure S37).

In addition, endosomal escape could also be visualized as diffused coumarin 343 signals in the cytosol. Furthermore, nuclear transport of undissociated peptides **13a/b**, demonstrated by SYTO RNASelect Green, was found to be localized inside the nucleolus, most likely due to the electrostatic

https://dx.doi.org/10.1021/jacs.0c05261
J. Am. Chem. Soc. 2020, 142, 15780−15789

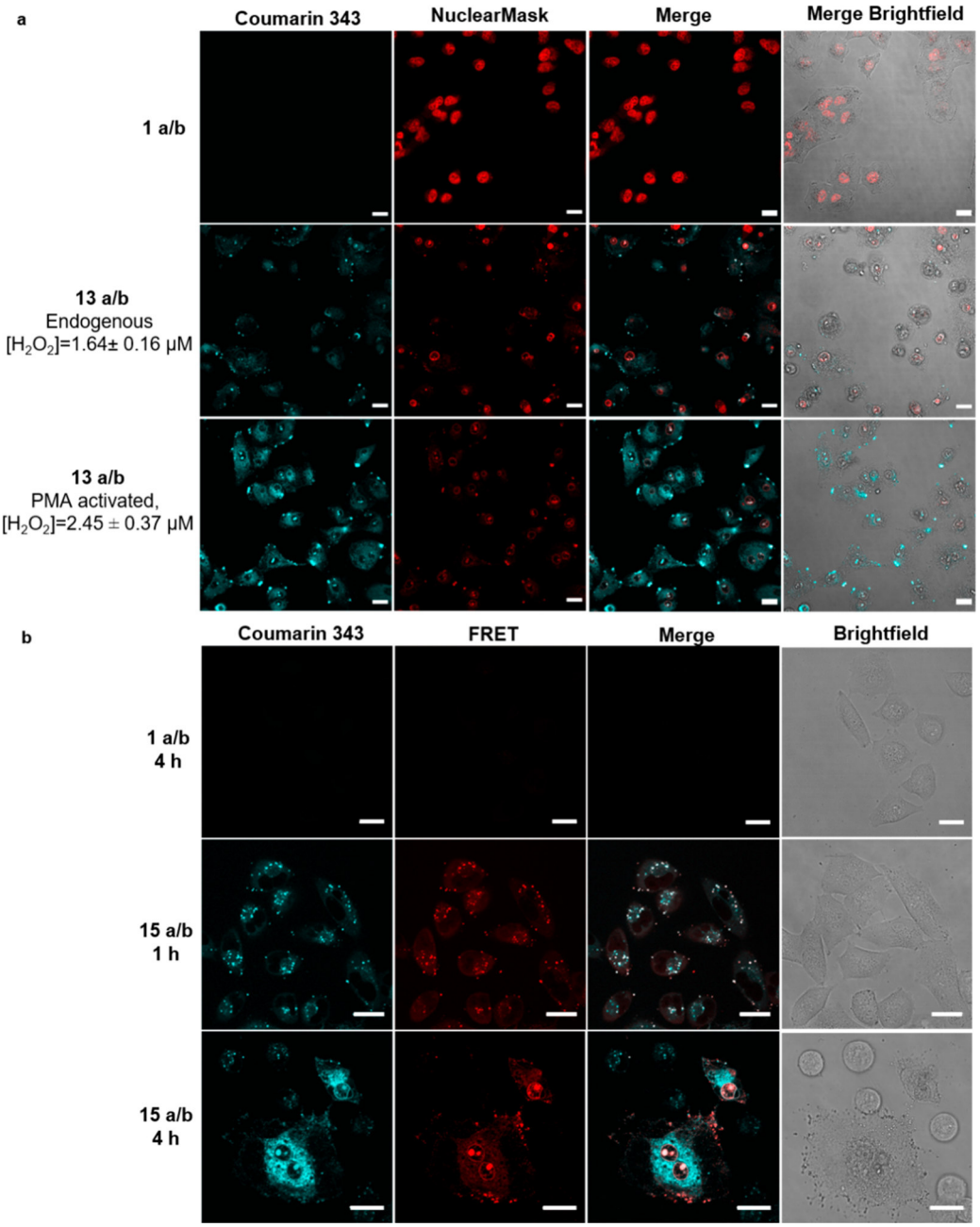

Figure 4. Cellular uptake and intracellular coassembly of peptides. (a) Confocal laser scanning micrographs of A549 cells treated for 4 h with only the depsipeptide mixture of **1a** and **1b** (top row) and treated with addition of SHA-TAT **12** to induce cellular uptake without (middle row) and with PMA (bottom row). Scale bars 20 μm. (b) Förster resonance energy transfer studies on A549 cells with **15a**/**b** using coumarin343 (donor, cyan) and 5-FAM (acceptor, red) as FRET pairs. Scale bars 20 μm, λ_{ex} = 405 nm.

attraction between TAT and DNA/RNA or perhaps hydrophobic interactions with the depsipeptides (Figure S40).[41] A previous report showed that self-assembling peptides might interact with RNA located inside the nucleoli.[42] In order to ascertain that the H_2O_2-driven assembly is specific toward the cytosol, we monitored the fiber formation using TEM at pH 5.0, 6.0, and 7.4 (Figures S23 and S25). At both acidic pH values, corresponding to the early and late endosomes as well as lysosomes, H_2O_2 does not possess enough oxidative strength to initiate the reaction cascade for assembly. This pH-dependent activity of H_2O_2 was reported in the literature.[43] As such, the acidic conditions within the endosomes specifically trigger the dissociation of **13a**/**b**, while the cytosolic environment provides the condition for the oxidative cascade to initiate fiber formation. To demonstrate the molecular rearrangement of the depsipeptides inside cells, we analyzed cell lysates by HPLC and showed the H_2O_2-induced conversion of **1b** to **3b** (Figure S49).

The biological response of the cells to the intracellular assembly was subsequently investigated by Annexin-V/propidium iodide assay (Figure 5a). Annexin-V is a protein that binds to phosphatidylserine, which is located on the external leaflet of the membrane structures exclusively during apoptosis.[44] The assay was conducted after 2 and 4 h on A549 cells treated with **13a**/**b**.

https://dx.doi.org/10.1021/jacs.0c05261
J. Am. Chem. Soc. 2020, 142, 15780−15789

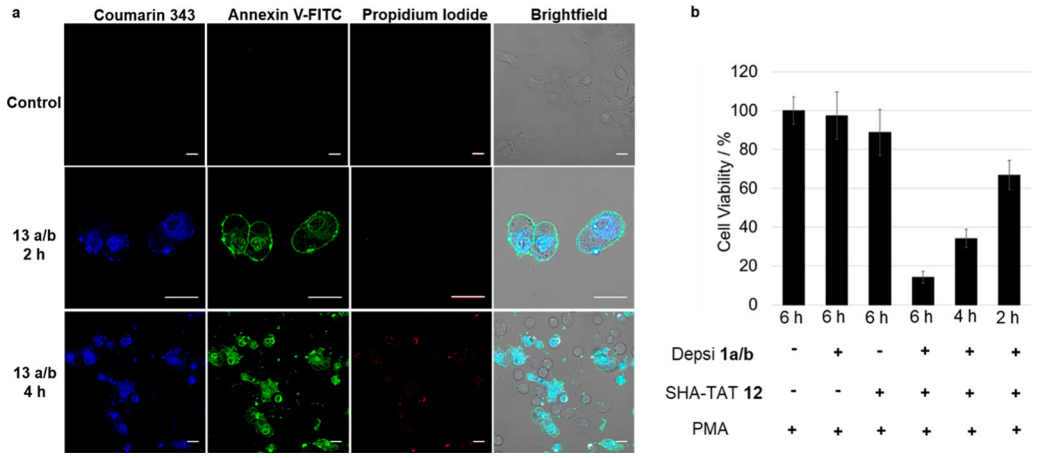

Figure 5. (a) Apoptosis assay using Annexin V-FITC/propidium iodide on **13a/b** and PMA-treated A549 cells over 2 and 4 h. Binding of Annexin V (green) toward the cell membrane was observed prominently at 2 h, demonstrating cells undergoing apoptosis due to inversion of the phosphatidylserine motifs. Membrane collapse at 4 h was detected with the entry of propidium iodide (red) into the nucleus. Scale bars 20 μm. (b) Cell viability of depsipeptides **1a** and **1b** and/or TAT **12**-treated A549 cells determined by CellTiter-Glo Luminescent Cell Viability Assay. Cells were treated for different incubation times from 2 to 6 h with only the depsipeptides **1a** and **1b**, only SHA-TAT **12**, or both to create **13a** and **13b** at a concentration of 150 μM. Significant cytotoxic effect was observed for A549 cells treated with the depsipeptide−TAT complexes **13a** and **13b**. All samples were coincubated with 100 nM PMA.

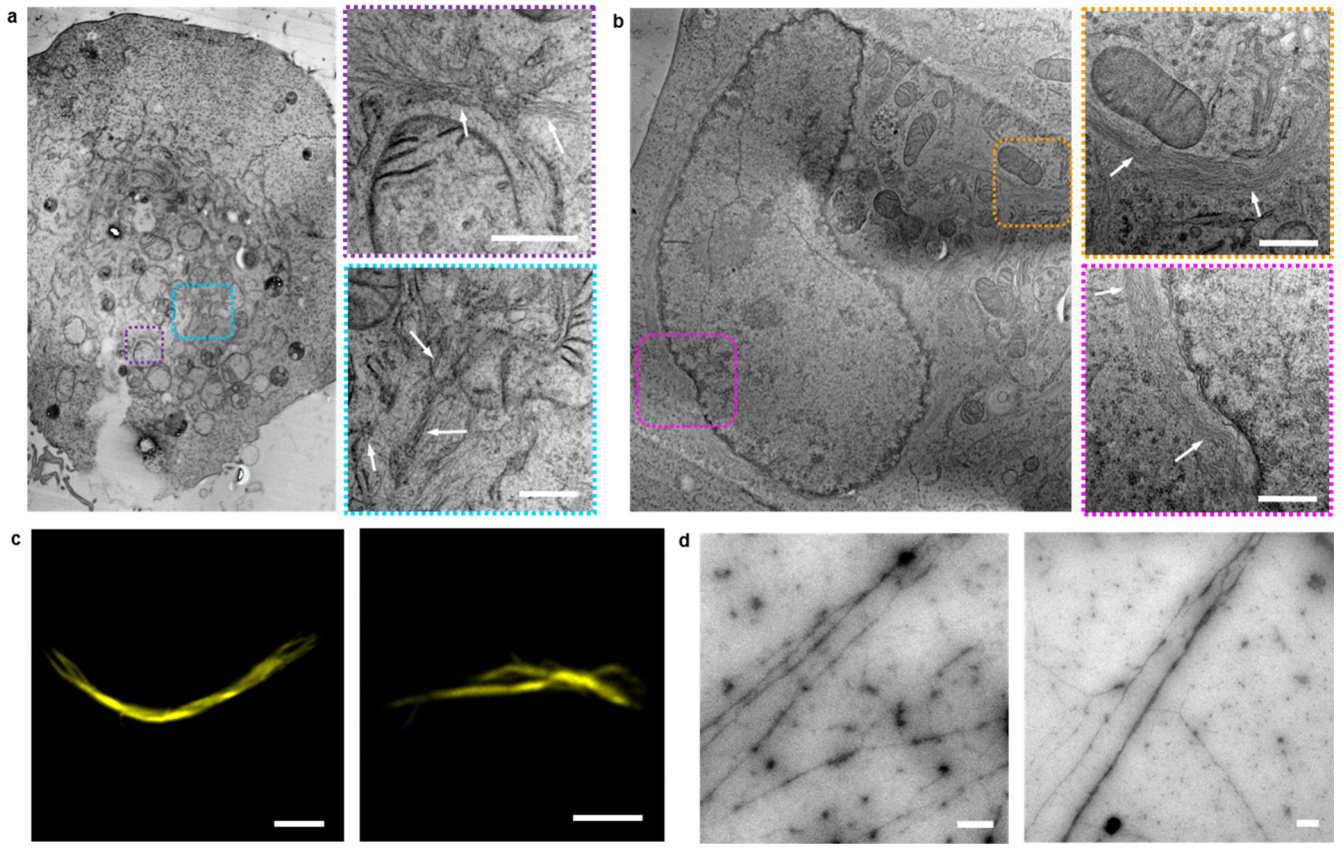

Figure 6. Intracellular peptide fiber formation. (a and b) TEM micrographs of peptide fibers inside A549 cells (marked with dashed lines) after coassembly of intracellularly generated Fmoc-ISA **3a** and C343-ISA **3b** and images of a cell, which were received after stitching TEM images together. Scale bars 500 nm. (c) Fluorescence microscopy images of Proteostat-stained peptide fibers after formation inside cells and extraction from the cells by lysis. Scale bars 5 μm. (d) TEM micrographs of peptide fibers, which were received after lysis of depsipeptide TAT complex 1**3a**- and **13b**-treated A549 cells. Scale bars 500 nm.

At 2 h, Annexin-V was found to bind prominently to the cell membranes, indicating that affected cells are undergoing apoptosis. At this time frame, the integrity of the cell membrane still remains intact as propidium iodide failed to enter the cells. In contrast, at 4 h, propidium iodide signals were observed in the nuclear region due to its affinity toward DNA.[44] This observation represented the membrane permeabilization process associated with late-stage apoptosis. Analysis of

https://dx.doi.org/10.1021/jacs.0c05261
J. Am. Chem. Soc. 2020, 142, 15780−15789

cytotoxicity was accomplished using CellTiter-Glo luminescent cell viability assay, which is based on quantification of adenosine triphosphate (ATP) and therefore actively metabolizing cells.[45] No significant toxic effects were observed after incubation of **1a/b** at a concentration of 150 μM for 6 h with A549 cells (Figure 5b). However, upon complexing with TAT to form **13a/b**, a significant impact toward cell viability was observed. Only 14% of cells was viable after 6 h, while incubation for 4 or 2 h led to a viability of 34% and 66%, respectively. As the A549 cancer cells do produce intrinsic H_2O_2, transformation of **1a/b** into **3a/b** still occurs in cells which are not treated with PMA, and therefore, the cell viability without PMA was 40% after 4 h (Figure S56), which is similar to the cell viability with addition of PMA. As the increase of hydrogen peroxide concentration by PMA stimulation (49%) does not cause a significant difference in cell viability, we conclude that nonstimulated cells already offer enough H_2O_2 to generate sufficient peptide fibers leading to effective apoptosis. In addition, as known from β-amyloid structures, we believe that shorter fibers/protofibrils can already contribute to the apoptotic effects.[46]

Lastly, to visualize the intracellular fiber formation directly, **13a/b**-treated cells were fixed by high-pressure freezing, and subsequently, freeze substitution was performed using acetone. After infiltration with epoxy resin and its polymerization, sample blocks were sectioned into slices. The slices of the cells were examined in TEM (Figure 6a and 6b). Formation of many dense peptide fiber networks was clearly visible inside the cells. Peptide fibrils were distributed inside the cell and were also observed to form next to the nucleus and mitochondria. To further show the formation of fibers, cells were lysed after treatment with the sample and the cell lysate was analyzed by TEM and fluorescence microscopy (Figure 6c and 6d).

Fibers were observed in TEM, which further proved the successful assembly of **3a/b** inside cells. Furthermore, Proteostat staining of the cell lysate clearly showed formation of amyloid, cross-ß-sheet structures to which Proteostat is known to bind, and coumarin 343 fluorescent fibers could also be observed in the lysate (Figures S45 and S46). Due to the resolution in the fluorescence microscope, only very thick fibers could be found in the cell lysate. Cell lysates of cells which were not treated with PMA but only with the complexes **13a/b** also contained fibers, which shows that enhancing the intracellular H_2O_2 concentration with PMA is not necessary to induce peptide assembly, as cells naturally already produce hydrogen peroxide (Figures S47 and S48).[33] TEM images of cells as well as cell lysate of A549 cells, which were not treated with the depsipeptide-TAT complexes **13a** and **13b**, did not show fibrillar structures, which demonstrates that fibers derived from the coassembly of the intracellularly rearranged peptides Fmoc-ISA **3a** and C343-ISA **3b** (Figures S44, S54, and S55).

CONCLUSIONS

In summary, we designed a peptide sequence that provides synthetic components for controlling cellular entry, intracellular dissociation, and supramolecular assembly. The reactivity of each synthetic component within the peptide sequence is dictated by the intracellular localization where its immediate environment defines its chemistry and subsequent transport pathway. Consecutive reactions are initiated in a controlled fashion to afford coassembling sequences that form fibrillar structures within the cytosol. Formation of these superstructures was imaged by fluorescence and electron microscopy and led to programmed cell death accompanied by nuclear fragmentation, actin disruption, and membrane collapse. Furthermore, coassembly features the potential of the nanosystem to dynamically customize functions and/or components to tune additional biological behavior. Collectively, the platform provides a broad accessibility and expands the domain of nanotechnology to directly impact living systems through structure formation.

ASSOCIATED CONTENT

Supporting Information

The Supporting Information is available free of charge at https://pubs.acs.org/doi/10.1021/jacs.0c05261.

Materials and methods as well as extensive supplementary figures and data (PDF)

AUTHOR INFORMATION

Corresponding Authors

David Y. W. Ng − *Max Planck Institute for Polymer Research, 55128 Mainz, Germany;* orcid.org/0000-0002-0302-0678; Email: david.ng@mpip-mainz.mpg.de

Tanja Weil − *Max Planck Institute for Polymer Research, 55128 Mainz, Germany; Institute of Inorganic Chemistry I, Ulm University, 89081 Ulm, Germany;* orcid.org/0000-0002-5906-7205; Email: weil@mpip-mainz.mpg.de

Authors

Michaela Pieszka − *Max Planck Institute for Polymer Research, 55128 Mainz, Germany; Institute of Inorganic Chemistry I, Ulm University, 89081 Ulm, Germany*

Shen Han − *Max Planck Institute for Polymer Research, 55128 Mainz, Germany*

Christiane Volkmann − *Max Planck Institute for Polymer Research, 55128 Mainz, Germany*

Robert Graf − *Max Planck Institute for Polymer Research, 55128 Mainz, Germany;* orcid.org/0000-0003-2302-0760

Ingo Lieberwirth − *Max Planck Institute for Polymer Research, 55128 Mainz, Germany;* orcid.org/0000-0003-1323-524X

Katharina Landfester − *Max Planck Institute for Polymer Research, 55128 Mainz, Germany;* orcid.org/0000-0001-9591-4638

Complete contact information is available at: https://pubs.acs.org/10.1021/jacs.0c05261

Notes

The authors declare no competing financial interest.

ACKNOWLEDGMENTS

This project received funding from the Max Planck-Bristol Centre for Minimal Biology and the Volkswagen Foundation under project number 89943. We thank Dr. Anke Kaltbeitzel for help with planning of the experiment, Christoph Sieber for sample preparation for TEM of cells, Dr. Gönül Kizilsavas for assigning NMR peaks, Jutta Schnee for measuring MALDI spectra, and Jessica Wagner for measuring an APCI spectrum. We thank the reviewers for their efforts in stimulating additional experiments that improved the quality of the manuscript. Open Access funding provided by the Max Planck Society.

REFERENCES

(1) Cragg, P. J. *Supramolecular Chemistry*; Springer Science+Business Media B.V.: Dordrecht, Heidelberg, London, New York, 2010.

(2) Eckford, P. D. W.; Sharom, F. J. ABC Efflux Pump-Based Resistance to Chemotherapy Drugs. *Chem. Rev.* **2009**, *109* (7), 2989−3011.
(3) Nikaido, H. Prevention of drug access to bacterial targets: permeability barriers and active efflux. *Science* **1994**, *264* (5157), 382.
(4) Brownlee, W. J.; Seib, F. P. Impact of the hypoxic phenotype on the uptake and efflux of nanoparticles by human breast cancer cells. *Sci. Rep.* **2018**, *8* (1), 12318.
(5) Shen, Z.; Wu, J.; Yu, Y.; Liu, S.; Jiang, W.; Nurmamat, H.; Wu, B. Comparison of cytotoxicity and membrane efflux pump inhibition in HepG2 cells induced by single-walled carbon nanotubes with different length and functional groups. *Sci. Rep.* **2019**, *9* (1), 7557.
(6) Ng, D. Y. W.; Vill, R.; Wu, Y.; Koynov, K.; Tokura, Y.; Liu, W.; Sihler, S.; Kreyes, A.; Ritz, S.; Barth, H.; Ziener, U.; Weil, T. Directing intracellular supramolecular assembly with N-heteroaromatic quaterthiophene analogues. *Nat. Commun.* **2017**, *8* (1), 1850.
(7) Qiao, S.-L.; Ma, Y.; Wang, Y.; Lin, Y.-X.; An, H.-W.; Li, L.-L.; Wang, H. General Approach of Stimuli-Induced Aggregation for Monitoring Tumor Therapy. *ACS Nano* **2017**, *11* (7), 7301−7311.
(8) Nakamura, H.; Lee, A. A.; Afshar, A. S.; Watanabe, S.; Rho, E.; Razavi, S.; Suarez, A.; Lin, Y.-C.; Tanigawa, M.; Huang, B.; DeRose, R.; Bobb, D.; Hong, W.; Gabelli, S. B.; Goutsias, J.; Inoue, T. Intracellular production of hydrogels and synthetic RNA granules by multivalent molecular interactions. *Nat. Mater.* **2018**, *17* (1), 79−89.
(9) Ye, D.; Shuhendler, A. J.; Cui, L.; Tong, L.; Tee, S. S.; Tikhomirov, G.; Felsher, D. W.; Rao, J. Bioorthogonal cyclization-mediated in situ self-assembly of small-molecule probes for imaging caspase activity in vivo. *Nat. Chem.* **2014**, *6* (6), 519−526.
(10) Blunden, B. M.; Stenzel, M. H. Incorporating ruthenium into advanced drug delivery carriers − an innovative generation of chemotherapeutics. *J. Chem. Technol. Biotechnol.* **2015**, *90* (7), 1177−1195.
(11) Cheng, Z.; Cheng, Y.; Chen, Q.; Li, M.; Wang, J.; Liu, H.; Li, M.; Ning, Y.; Yu, Z.; Wang, Y.; Wang, H. Self-assembly of pentapeptides into morphology-adaptable nanomedicines for enhanced combinatorial chemo-photodynamic therapy. *Nano Today* **2020**, *33*, 100878.
(12) Shin, S. B. Y.; Almeida, R. D.; Gerona-Navarro, G.; Bracken, C.; Jaffrey, S. R. Assembling ligands in situ using bioorthogonal boronate ester synthesis. *Chem. Biol.* **2010**, *17* (11), 1171−1176.
(13) Herce, H. D.; Garcia, A. E. Molecular dynamics simulations suggest a mechanism for translocation of the HIV-1 TAT peptide across lipid membranes. *Proc. Natl. Acad. Sci. U. S. A.* **2007**, *104* (52), 20805−20810.
(14) Hagen, H.; Marzenell, P.; Jentzsch, E.; Wenz, F.; Veldwijk, M. R.; Mokhir, A. Aminoferrocene-based prodrugs activated by reactive oxygen species. *J. Med. Chem.* **2012**, *55* (2), 924−934.
(15) Jourden, J. L. M.; Daniel, K. B.; Cohen, S. M. Investigation of self-immolative linkers in the design of hydrogen peroxide activated metalloprotein inhibitors. *Chem. Commun.* **2011**, *47* (28), 7968−7970.
(16) Weinstain, R.; Savariar, E. N.; Felsen, C. N.; Tsien, R. Y. In Vivo Targeting of Hydrogen Peroxide by Activatable Cell-Penetrating Peptides. *J. Am. Chem. Soc.* **2014**, *136* (3), 874−877.
(17) Coin, I.; Dölling, R.; Krause, E.; Bienert, M.; Beyermann, M.; Sferdean, C. D.; Carpino, L. A. Depsipeptide Methodology for Solid-Phase Peptide Synthesis: Circumventing Side Reactions and Development of an Automated Technique via Depsidipeptide Units. *J. Org. Chem.* **2006**, *71* (16), 6171−6177.
(18) Tao, K.; Levin, A.; Adler-Abramovich, L.; Gazit, E. Fmoc-modified amino acids and short peptides: simple bio-inspired building blocks for the fabrication of functional materials. *Chem. Soc. Rev.* **2016**, *45* (14), 3935−3953.
(19) Liu, X.; Cole, J. M.; Low, K. S. Molecular origins of dye aggregation and complex formation effects in coumarin 343. *J. Phys. Chem. C* **2013**, *117* (28), 14723−14730.
(20) Rode, S.; Hayn, M.; Röcker, A.; Sieste, S.; Lamla, M.; Markx, D.; Meier, C.; Kirchhoff, F.; Walther, P.; Fändrich, M.; Weil, T.; Münch, J. Generation and characterization of virus-enhancing peptide nanofibrils functionalized with fluorescent labels. *Bioconjugate Chem.* **2017**, *28* (4), 1260−1270.
(21) Lewis, S. A.; Tian, G.; Cowan, N. J. The α- and β-tubulin folding pathways. *Trends Cell Biol.* **1997**, *7* (12), 479−484.
(22) Ohvo-Rekilä, H.; Ramstedt, B.; Leppimäki, P.; Slotte, J. P. Cholesterol interactions with phospholipids in membranes. *Prog. Lipid Res.* **2002**, *41* (1), 66−97.
(23) Goley, E. D.; Welch, M. D. The ARP2/3 complex: an actin nucleator comes of age. *Nat. Rev. Mol. Cell Biol.* **2006**, *7* (10), 713−726.
(24) Coste, J.; Le-Nguyen, D.; Castro, B. PyBOP®: A new peptide coupling reagent devoid of toxic by-product. *Tetrahedron Lett.* **1990**, *31* (2), 205−208.
(25) Navarro, S.; Ventura, S. Fluorescent dye proteostat to detect and discriminate intracellular amyloid-like aggregates in escherichia coli. *Biotechnol. J.* **2014**, *9* (10), 1259−1266.
(26) Fleming, S.; Frederix, P. W. J. M.; Ramos Sasselli, I.; Hunt, N. T.; Ulijn, R. V.; Tuttle, T. Assessing the Utility of Infrared Spectroscopy as a Structural Diagnostic Tool for β-Sheets in Self-Assembling Aromatic Peptide Amphiphiles. *Langmuir* **2013**, *29* (30), 9510−9515.
(27) Jackson, M.; Mantsch, H. H. The use and misuse of FTIR spectroscopy in the determination of protein structure. *Crit. Rev. Biochem. Mol. Biol.* **1995**, *30* (2), 95−120.
(28) Micsonai, A.; Wien, F.; Kernya, L.; Lee, Y.-H.; Goto, Y.; Réfrégiers, M.; Kardos, J. Accurate secondary structure prediction and fold recognition for circular dichroism spectroscopy. *Proc. Natl. Acad. Sci. U. S. A.* **2015**, *112* (24), E3095−E3103.
(29) Wei, G.; Su, Z.; Reynolds, N. P.; Arosio, P.; Hamley, I. W.; Gazit, E.; Mezzenga, R. Self-assembling peptide and protein amyloids: from structure to tailored function in nanotechnology. *Chem. Soc. Rev.* **2017**, *46* (15), 4661−4708.
(30) Argudo, P. G.; Contreras-Montoya, R.; Álvarez de Cienfuegos, L.; Cuerva, J. M.; Cano, M.; Alba-Molina, D.; Martín-Romero, M. T.; Camacho, L.; Giner-Casares, J. J. Unravelling the 2D self-assembly of Fmoc-dipeptides at fluid interfaces. *Soft Matter* **2018**, *14* (46), 9343−9350.
(31) Jiang, J.; Abramavicius, D.; Bulheller, B. M.; Hirst, J. D.; Mukamel, S. Ultraviolet spectroscopy of protein backbone transitions in aqueous solution: combined QM and MM simulations. *J. Phys. Chem. B* **2010**, *114* (24), 8270−8277.
(32) Horgan, C. C.; Rodriguez, A. L.; Li, R.; Bruggeman, K. F.; Stupka, N.; Raynes, J. K.; Day, L.; White, J. W.; Williams, R. J.; Nisbet, D. R. Characterisation of minimalist co-assembled fluorenylmethyloxycarbonyl self-assembling peptide systems for presentation of multiple bioactive peptides. *Acta Biomater.* **2016**, *38*, 11−22.
(33) Mu, X.; Eckes, K. M.; Nguyen, M. M.; Suggs, L. J.; Ren, P. Experimental and Computational Studies Reveal an Alternative Supramolecular Structure for Fmoc-Dipeptide Self-Assembly. *Biomacromolecules* **2012**, *13* (11), 3562−3571.
(34) Smith, D. K. Lost in translation? Chirality effects in the self-assembly of nanostructured gel-phase materials. *Chem. Soc. Rev.* **2009**, *38* (3), 684−694.
(35) Zegota, M. M.; Wang, T.; Seidler, C.; Wah Ng, D. Y.; Kuan, S. L.; Weil, T. Tag and Modify" protein conjugation with dynamic covalent chemistry. *Bioconjugate Chem.* **2018**, *29* (8), 2665−2670.
(36) Seidler, C.; Ng, D. Y. W.; Wu, Y.; Weil, T. pH responsive supramolecular core-shell protein hybrids. *Supramol. Chem.* **2016**, *28* (9−10), 742−746.
(37) Seidler, C.; Zegota, M. M.; Raabe, M.; Kuan, S. L.; Ng, D. Y. W.; Weil, T. Dynamic core−shell bioconjugates for targeted protein delivery and release. *Chem. - Asian J.* **2018**, *13* (22), 3474−3479.
(38) Kuwabara, W. M. T.; Zhang, L.; Schuiki, I.; Curi, R.; Volchuk, A.; Alba-Loureiro, T. C. NADPH oxidase-dependent production of reactive oxygen species induces endoplasmatic reticulum stress in neutrophil-like HL60 cells. *PLoS One* **2015**, *10* (2), e0116410.
(39) Zhou, J.; Du, X.; Yamagata, N.; Xu, B. Enzyme-instructed self-assembly of small D-peptides as a multiple-step process for selectively killing cancer cells. *J. Am. Chem. Soc.* **2016**, *138* (11), 3813−3823.
(40) Llopis, J.; McCaffery, J. M.; Miyawaki, A.; Farquhar, M. G.; Tsien, R. Y. Measurement of cytosolic, mitochondrial, and Golgi pH in single living cells with green fluorescent proteins. *Proc. Natl. Acad. Sci. U. S. A.* **1998**, *95* (12), 6803−6808.

https://dx.doi.org/10.1021/jacs.0c05261
J. Am. Chem. Soc. 2020, 142, 15780−15789

(41) Audas, T. E.; Jacob, M. D.; Lee, S. Immobilization of Proteins in the Nucleolus by Ribosomal Intergenic Spacer Noncoding RNA. *Mol. Cell* **2012**, *45* (2), 147−157.
(42) Wang, H.; Feng, Z.; Tan, W.; Xu, B. Assemblies of D-peptides for targeting cell nucleolus. *Bioconjugate Chem.* **2019**, *30* (10), 2528−2532.
(43) Bruice, T. C.; Zipplies, M. F.; Lee, W. A. The pH dependence of the mechanism of reaction of hydrogen peroxide with a nonaggregating, non-mu-oxo dimer-forming iron (III) porphyrin in water. *Proc. Natl. Acad. Sci. U. S. A.* **1986**, *83* (13), 4646.
(44) Demchenko, A. P. Beyond annexin V: fluorescence response of cellular membranes to apoptosis. *Cytotechnology* **2013**, *65* (2), 157−172.
(45) Hannah, R.; Beck, M.; Moravec, R.; Riss, T. CellTiter-Glo luminescent cell viability assay: A sensitive and rapid method for determining cell viability. *Promega Cell Notes* **2001**, *2*, 11−13.
(46) Jan, A.; Adolfsson, O.; Allaman, I.; Buccarello, A.-L.; Magistretti, P. J.; Pfeifer, A.; Muhs, A.; Lashuel, H. A. Aβ42 Neurotoxicity Is Mediated by Ongoing Nucleated Polymerization Process Rather than by Discrete Aβ42 Species. *J. Biol. Chem.* **2011**, *286* (10), 8585−8596.

https://dx.doi.org/10.1021/jacs.0c05261
J. Am. Chem. Soc. 2020, 142, 15780−15789

Supporting Information

Controlled Supramolecular Assembly inside Living Cells by Sequential Multi-staged Chemical Reactions

Michaela Pieszka[1,2], Shen Han[1], Christiane Volkmann[1], Robert Graf[1], Ingo Lieberwirth[1], Katharina Landfester[1], David Y. W. Ng[1*] and Tanja Weil[1,2*]

[1] *Max Planck Institute for Polymer Research, Ackermannweg 10, 55128 Mainz, Germany*

[2] *Institute of Inorganic Chemistry, Ulm University, Albert-Einstein-Allee 11, 89081 Ulm, Germany*

E-mail: david.ng@mpip-mainz.mpg.de, weil@mpip-mainz.mpg.de

Table of Contents

1. Materials and Instruments

1.1 Materials

Reagents and solvents were purchased from commercial sources and were used without any further purification. Peptide Synthesis grade reagents were used for synthesizing the peptides. HPLC was performed using acetonitrile in HPLC grade and water for HPLC and reactions was obtained from a Millipore purification system. Thin-layer chromatography (TLC) was performed on Macherey-Nagel Alugram Sil G/UV_{254} plates and substances were visualized under UV light at 254 nm. Column chromatography was carried out using Macherey-Nagel silica gel 0.04–0.063 mm.

1.2 Instruments

1.2.1 Nuclear Magnetic Resonance Spectroscopy (NMR)

NMR spectra of dissolved compounds were recorded on a Bruker Avance II 300 MHz spectrometer. The solvent signal was used as a reference (deuterated chloroform $CDCl_3$ δ = 7.26 ppm for ^{1}H, 77.16 ppm for ^{13}C, deuterated DCM CD_2Cl_2 5.32 ppm for ^{1}H and 53.84 ppm for ^{13}C and for DMSO-d_6 2.50 ppm and 39.52 ppm respectively). The data were processed in MestReNova.

1.2.2 Microwave Peptide Synthesizer

Peptides were synthesized in a Liberty Blue Automated Microwave Peptide Synthesizer by CEM Corporation.

1.2.3 High-Performance Liquid Chromatography (HPLC)

Peptides were purified by preparative HPLC using a setup by Shimadzu. For purification either a ZORBAX Eclipse XDB-C18 HPLC column (9.4 × 250 mm, 5 µm) was used at a flowrate of 4 mL/min or an Atlantis T3 Prep OBD™ 5 µm, 19 × 150 mm column was used with a flowrate of 10 mL/min or a Phenomenex Gemini 5 µm NX-C18 110 Å 150 × 30 mm was used at a flowrate of 25 mL/min.

For analytical measurements an Atlantis T3 column (4.6 × 100 mm, 5 µm) was used at a flowrate of 1 mL/min, with the exception of analysis of cell lysates where a ZORBAX Eclipse, XDB-C18, 80Å, 5 µm, 4.6 × 250 mm column was used at a flowrate of 1mL/min. All measurements and purification steps were done using gradients of acetonitrile and MilliQ water, each acidified with 0.1% TFA. Absorbance was recorded at 190, 214, 254 and 433 nm wavelength. The software LabSolutions by Shimadzu and Powerpoint were used to process all HPLC spectra.

1.2.4 Liquid Chromatography - Mass Spectrometry (LC-MS)

Compounds were analyzed by HPLC-ESI-MS on a LC-MS 2020 by Shimadzu using a Kinetex 2.6 µm EVO C18 100 Å LC 50 × 2.1 mm column. MilliQ water, acidified with 0.1% formic acid and acetonitrile were used as solvents for all measurements. The solvent gradient started with 5% ACN and 95% water, while the ACN content was linearly increased to 95% in 12 min. Data were processed in LabSolutions and Powerpoint.

1.2.5 Matrix-Assisted Laser Desorption/Ionisation - Time of Flight Mass Spectrometry (MALDI-TOF)

All MALDI-TOF spectra were recorded on either a rapifleX MALDI-TOF/TOF from Bruker or MALDI Synapt G2-SI from Waters. Samples were mixed with a saturated solution of the matrix

α-cyano-4-hydroxycinnamic acid (CHCA) in water/ACN 1/1 + 0.1% TFA. Data processing was performed in mMass.

1.2.6 APCI-MS

APCI (atmospheric pressure chemical ionisation) mass spectra were measured on an Advion expression-L Compact Mass Spectrometer (CMS) by Advion Inc. with an atmospheric solid analysis probe (ASAP).

1.2.7 Fluorescence and Absorbance Spectroscopy

A SPARK 20M microplate reader by the company Tecan Group Ltd. was used to record fluorescence and absorbance intensity. Samples were measured in a Greiner 384 flat black well plate and data processing was done using Excel.

Binding affinity of PBA to SHA was determined by fluorescence quenching. Measurements were performed using a Monolith NT.115 instrument and data was analyzed with MO.Affinity Analysis software by NanoTemper Technologies GmbH.

1.2.8 Luminescence Intensity

Luminescence intensity was measured in a white half area 96-well plate on a Promega GloMax®-Multi Detection System using the settings for the CellTiter-Glo Luminescent Cell Viability Assay. Data were processed in Excel.

1.2.9 Fourier-Transform Infrared Spectroscopy (FTIR)

FTIR spectra were measured on a Bruker TENSOR II spectrometer equipped with a PLATINUM ATR single reflection diamond ATR accessory. Data were processed in Excel.

1.2.10 Circular Dichroism Spectroscopy (CD)

CD spectra were recorded on a JASCO J-1500 spectrometer in a 1 mm High Precision Cell by HellmaAnalytics. Data were processed in Spectra Analysis by JASCO and Excel.

1.2.11 Solid-State NMR

CP-MAS ^{13}C (^{1}H) spectra were recorded on a Bruker Avance III 700 MHz spectrometer using a 2.5-mm $^{1}H/X$ double-resonance CP/MAS probe. Measurements were performed at MAS speeds of 25 kHz and CP/MAS measurements were done with a contact time of 3 ms and 100-kHz radio frequency nutation frequency swept-frequency two-pulse phase modulation high-power composite pulse decoupling. The CH_3 group of L-alanine with the 1.3 ppm and 20.5 ppm peak for ^{1}H and ^{13}C, respectively, were used as a secondary standard to reference the chemical shifts to tetramethylsilane.

1.2.12 Transmission Electron Microscopy (TEM)

TEM pictures of peptide solutions were taken on a JEOL 1400 transmission electron microscope at a voltage of 120 kV. Samples were prepared on Formvar/carbon-film coated copper grids (300 mesh) by Plano GmbH. In order to prepare the TEM grids, 4 µL of peptide solution were put on freshly etched (30 s at 20% oxygen content) Formvar coated copper grids. After 5 min the solution was removed using a filter paper and grids were stained with uranyl acetate 4% for 2.5 min. The grids were washed three times with MilliQ water and dried before measuring. TEM images were processed in ImageJ.

For TEM measurements of cells, sections were carefully placed onto 300-mesh carbon coated copper grid for standard bright-field imaging in a FEI Tecnai F20 200 kV transmission electron microscope. Bright-field TEM micrographs were obtained with a Gatan US1000 2k CCD camera.

1.2.13 Cell Culture

A549 cells were cultured at 37 °C and 5% CO_2 in Dulbecco's Modified Eagle's Medium (DMEM, high glucose), which was supplemented with 10% FBS, 1% penicillin/streptomycin and 1x MEM non-essential amino acids.

1.2.14 Confocal Laser Scanning Microscopy

Cells were imaged on a Leica TCS SP5 and a Visitron Spinning Disc microscope with a 405 nm excitation diode and emission filter 415–515 nm, as well as at 633 nm excitation using a HeNe laser and an emission filter of 643–743 nm to monitor Coumarin 343 and the nuclear stain respectively. The same laser was used for excitation of Alexa 647 (emission 657-757 nm). Furthermore, an argon laser was used for excitation at 488 nm of Annexin V (emission 498-540 nm) and propidium iodide (emission 650-750 nm). FRET was monitored by exciting at 405 nm and measuring the emission at 550-650 nm. RFP was excited at 561 nm (emission 751-671 nm) and for imaging of lysosomes (emission 506-606 nm) and nucleoli (emission 506-606 nm) a wavelength of 488 nm was used.

1.2.15 Fluorescence Microscopy

Fluorescence was imaged using a Leica DMi8 microscope using a 100x oil objective by Leica. Coumarin 343 fluorescence was imaged with 350/50 nm excitation and a 460/50 nm emission filter cube and Proteostat fluorescence was excited at 546/10 nm and the emission was recorded at 585/40 nm.

2. Synthesis

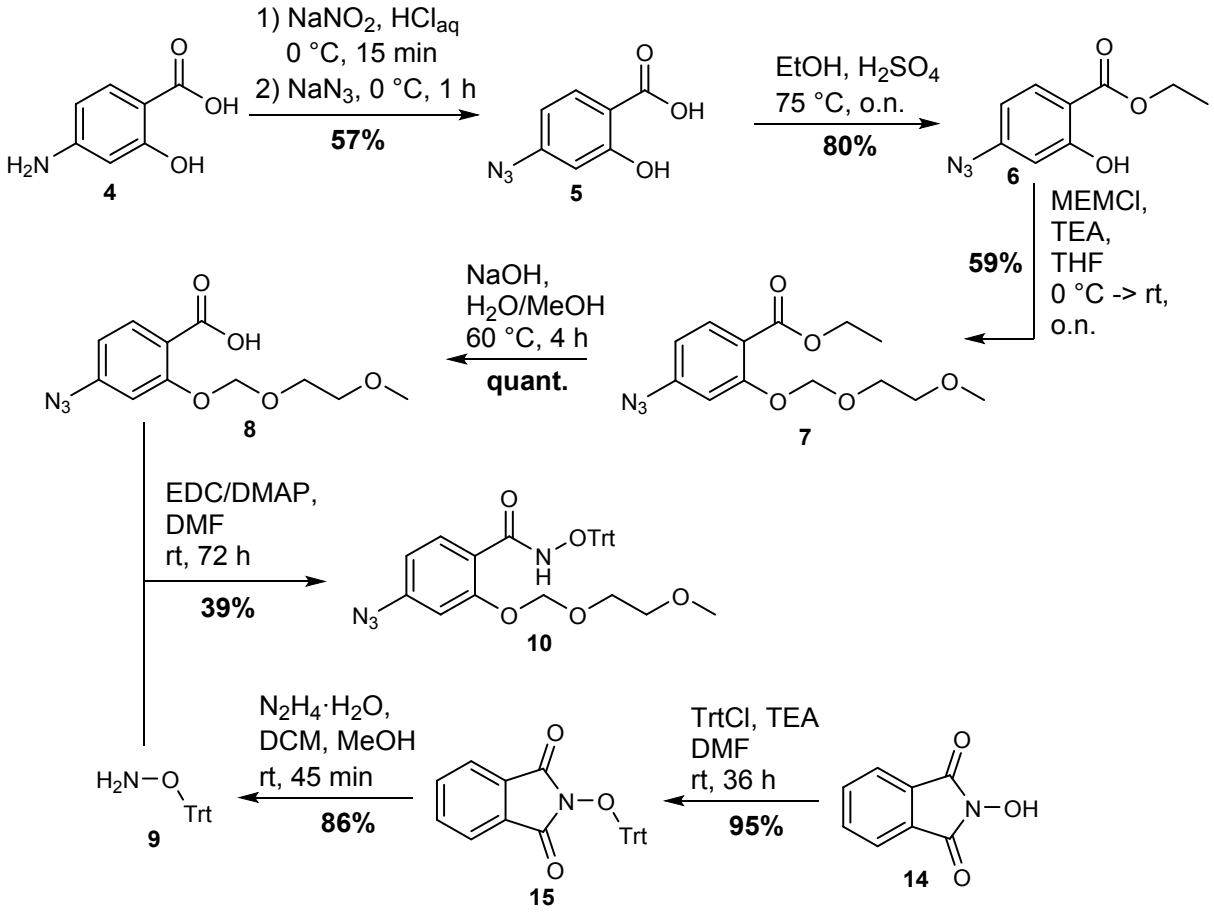

Figure S1: Synthesis of the Trt and MEM protected 4-azidosalicyl hydroxamate derivative **10** in seven steps starting from 4-amino salicylic acid **4**. After conversion of the amine into the azide **5**, the acid was protected as an ethyl ester (**6**) before the MEM protecting group was attached. Subsequently, the carboxylic acid **7** was deprotected and reacted with trityloxamine **9**, which was synthesized in two steps.

2.1 *N*-Trityloxyphthalimide

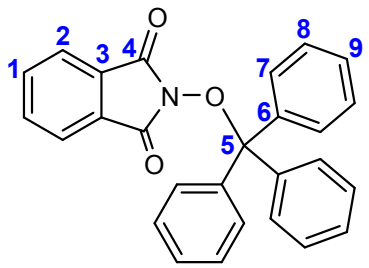

10 mL Triethylamine (72.14 mmol) were added to a solution of *N*-hydroxyphthalimide **14** (10.00 g, 61.30 mmol) in 20 mL DMF. After addition of tritylchloride (17.15 g, 61.52 mmol) the

reaction mixture was stirred for 30 min at room temperature. After the reaction proceeded for 36 h without stirring, the precipitate was suspended in 100 mL isopropanol, filtered and washed with water and saturated $NaHCO_3$ solution. After drying *in vacuo* 23.69 g (58.43 mmol, 95% yield) of the white powder **15** were received.[1]

^{1}H-NMR (300 MHz, CD_2Cl_2) δ [ppm] = 7.68-7.57 (m, 4H, 1 and 2), 7.53-7.49 (m, 6H, 8), 7.33-7.29 (m, 9H, 7 and 9).

^{13}C-NMR (75 MHz, CD_2Cl_2) δ [ppm] = 164.47 (4), 142.38 (6), 134.73 (1), 130.63 (8), 129.10 (3), 128.67 (9), 127.91 (3), 123.45 (7), 98.19 (5).

2.2 *N*-Trityloxyamine

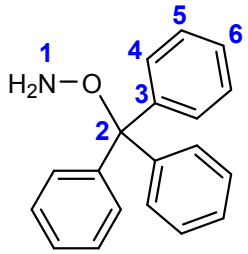

After *N*-trityloxyphthalimide (**15**, 22.07 g, 54.43 mmol) was dissolved in 135 mL DCM, a 99% hydrazine solution in water (12 mL, 0.24 mol) was diluted with 40 mL methanol and added dropwise while stirring. After 45 min stirring at room temperature, 5 M ammonium hydroxide solution was added until the precipitate dissolved. The aqueous phase was extracted three times with DCM and the organic phase was washed with brine. After drying over magnesium sulfate, the solvent was evaporated and the product **9** was recrystallized from methanol and colorless crystals (12.85 g, 46.67 mmol, 86% yield) were isolated.[1]

^{1}H-NMR (300 MHz, CD_2Cl_2) δ [ppm] = 7.46-7.43 (m, 6H, 5), 7.38-7.27 (m, 9H, 4 and 6), 4.96 (s, 2H, **1**).

^{13}C-NMR (75 MHz, CD_2Cl_2) δ [ppm] = 144.18 (3), 129.38 (5), 128.33 (4), 127.59 (6), 91.04 (2).

2.3 4-Azidosalicylic acid

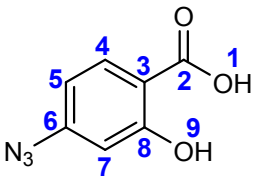

4-Aminosalicylicylic acid **4** (10.00 g, 65.30 mmol) was dissolved in a mixture of 125 mL concentrated HCl and 150 mL water. After the solution was cooled with an ice bath, sodium nitrite (6.49 g, 94.09 mmol), dissolved in 38 mL water, was added slowly. The reaction mixture was stirred for 15 min. After addition of urea the solution was stirred for 2 min and then filtered over celite while cooling.

Subsequently sodium azide (6.11 g, 93.99 mmol) was dissolved in 38 mL water and added slowly to the solution. The solution was stirred for one hour and the raw product was isolated by filtration. After recrystallization from methanol, 6.66 g (37.22 mmol, 57% yield) of brown crystals of **5** were received.[2]

^{1}H-NMR (300 MHz, DMSO-d_6) δ [ppm] = 11.56 (s, 1H, 9), 7.80 (d, J = 8.3 Hz, 1H, 4), 6.69–6.64 (m, 2H, 5 and 7).

^{13}C-NMR (75 MHz, DMSO-d_6) δ [ppm] = 171.44 (2), 162.48 (8), 146.55 (6), 132.19 (4), 110.56 (5), 109.91 (3), 106.88 (7).

MS (**ESI**, 179.03 g/mol): m/z = 178 $[M - H]^-$, 379 $[2M + Na – 2H]^-$.

2.4 4-Azidosalicylic acid ethyl ester

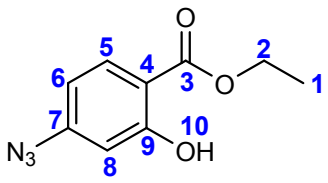

4-Azidosalicylic acid **5** (3.33 g, 18.60 mmol) was dissolved in 120 mL ethanol. After the addition of 8.5 mL concentrated sulfuric acid, the solution was stirred at 75 °C in nitrogen atmosphere overnight. After the solvent was removed *in vacuo,* the crude product was resuspended in n-hexane while stirring for 3 h. The product **6** was received after filtration and removal of the solvent, as a pale yellow powder (3.08 g, 14.88 mmol, 80% yield).[3]

^{1}H-NMR (300 MHz, $CDCl_3$) δ [ppm] = 11.03 (s, 1H, 10), 7.81 (d, J = 8.6 Hz, 1H, 5), 6.62 (d, J = 2.2 Hz, 1H, 8), 6.52 (dd, J = 8.6, 2.2 Hz, 6), 4.40 (q, 2 H, J = 7.1 Hz, 2), 1.41 (t, J = 2.1 Hz, 1).

^{13}C-NMR (75 MHz, $CDCl_3$) δ [ppm] = 169.74 (3), 163.11 (9), 147.35 (7), 131.71 (5), 110.54 (6), 109.66 (8), 107.32 (4), 61.62 (2), 14.33 (1).

MS (**APCI**, 207.0 g/mol): m/z = 208 $[M+H]^+$, 180 $[M+H-C_2H_5]^+$, 151 $[M-N_2+H]^+$.

2.5 4-Azido-2-((2-methoxyethoxy)methoxy)ethyl benzoate

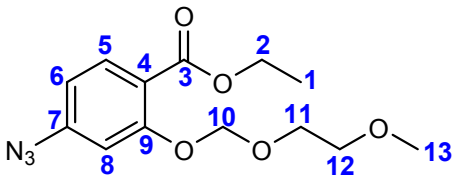

4-Azidosalicylic acid ethyl ester **6** (1.21 g, 5.84 mmol) was dissolved in 18 mL dry THF in argon atmosphere. After addition of TEA (4.86 mL, 35.06 mmol) the solution was cooled by an ice bath and MEM chloride (4.00 mL, 35.06 mmol) was added slowly. The solution was stirred

overnight, and the solvent was removed *in vacuo*. The raw product was dissolved in ethyl acetate and washed three times with water. After evaporation of the solvent the raw product was purified by column chromatography (nHex:EA 4:1). The product **7** was received as a yellow oil (1.02 g, 3.45 mmol, 59% yield).

^{1}H-NMR (300 MHz, $CDCl_3$) δ [ppm] = 7.81 (d, J = 8.4 Hz, 1H, 5), 6.88 (d, J = 2.2 Hz, 1H, 8), 6.70 (dd, J = 8.4, 2.2 Hz, 1H, 6), 5.32 (s, 2H, 10), 4.12 (d, J = 7.1 Hz, 2H, 2), 3.89–3.86 (m, 2H, 12), 3.58–3.54 (m, 2H, 11), 3.37 (s, 3H, 13), 1.36 (d, J = 7.1 Hz, 3H, 1).

^{13}C-NMR (75 MHz, $CDCl_3$) δ [ppm] = 165.30 (3), 158.44 (9), 145.23 (7), 133.21 (5), 118.12 (6), 112.18 (8), 107.65 (4), 94.32 (10), 71.58 (12), 68.24 (11), 60.94 (2), 59.14 (13), 14.33 (1).

MS (**ESI**, 295.12 g/mol): m/z = 318 $[M + Na]^+$, 334 $[M + K]^+$.

2.6 4-Azido-2-((2-methoxyethoxy)methoxy)benzoic acid

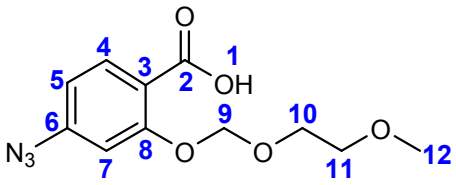

4-Azido-2-((2-methoxyethoxy)methoxy) ethyl benzoate **7** (1.02 g, 3.45 mmol) was dissolved in a mixture of methanol and 1 M NaOH (15 mL each) and heated to 60 °C for 3 h. After the solvent was removed, the raw product was extracted with ethyl acetate to remove eventually leftover educt. The aqueous phase was acidified to pH 5 using 1 M HCl and extracted with ethyl acetate. The solvent was removed and the product **8** was isolated as a yellow powder (0.92 g, 3.45 mmol, quantitative).

^{1}H-NMR (300 MHz, CD_2Cl_2) δ [ppm] = 8.11 (d, J = 8.5 Hz, 1H, **4**), 6.92 (d, J = 2.1 Hz, 1H, **5**), 6.86 (dd, J = 8.5, 2.1 Hz, 1H, **7**), 5.49 (s, 2H, **9**), 3.90-3.87 (m, 2H, **11**), 3.56–3.53 (m, 2H, **10**), 3.32 (s, 3H, **12**).

^{13}C-NMR (75 MHz, CD_2Cl_2) δ [ppm] = 164.98 (**2**), 157.81 (**8**), 147.29 (**6**), 135.38 (**4**), 115.33 (**5**), 113.74 (**7**), 106.40 (**3**), 95.58 (**9**), 72.11 (**11**), 70.07 (**10**), 59.28 (**12**).

MS (**ESI**, 267.09 g/mol): m/z = 290 $[M + Na]^+$, 306 $[M + K]^+$.

2.7 4-Azido-2-((2-methoxyethoxy)methoxy)-*N*-(trityloxy)benzamide

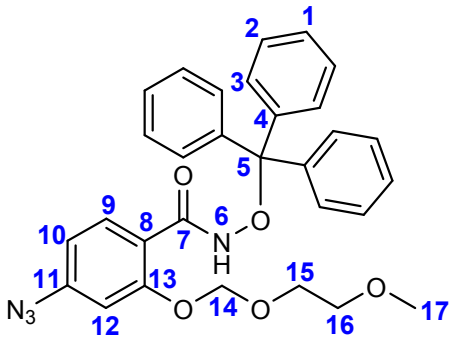

4-Azido-2-((2-methoxyethoxy)methoxy)benzoic acid **8** (629 mg, 2.35 mmol), trityloxyamine (810 mg, 2.94 mmol), EDC·HCl (564 mg, 2.94 mmol) and DMAP (36 mg, 0.29 mmol) were dissolved in DMF. The reaction mixture was stirred for 72 h under exclusion of light at room temperature. After the solvent was removed in *vacuo* the product was purified by column chromatography (silica gel, EA:nHex 1:4). The product **10** was received as a colorless powder in a yield of 39% (476 mg, 0.90 mmol).

^{1}H-NMR (300 MHz, CD_2Cl_2) δ [ppm] = 9.62 (s, 1H, **6**), 8.00 (d, J = 9.0 Hz, 1H, **9**), 7.55–7.51 (m, 6H, **2**), 7.39–7.30 (m, 9H, **1** and **3**), 6.79–6.75 (m, 2H, **10** and **12**), 4.92 (s, 2H, **14**), 3.46-3.38 (m, 4H, **15** and **16**), 3.27 (s, 3H, **17**).

^{13}C-NMR (75 MHz, CD_2Cl_2) δ [ppm] = 162.48 (**7**), 156.43 (**13**), 145.21 (**11**), 133.76 (**4**), 129.35 (**2**), 128.60 (**3**), 128.32 (**1**), 117.81 (**10**), 113.17 (**8**), 106.08 (**12**), 94.28 (**5**), 93.16 (**14**), 71.85 (**16**), 69.14 (**15**), 59.22 (**17**).

MS (**ESI**, 524.21 g/mol): m/z = 243 $[Trt]^+$, 547 $[M + Na]^+$, 1071 $[2M + Na]^+$.

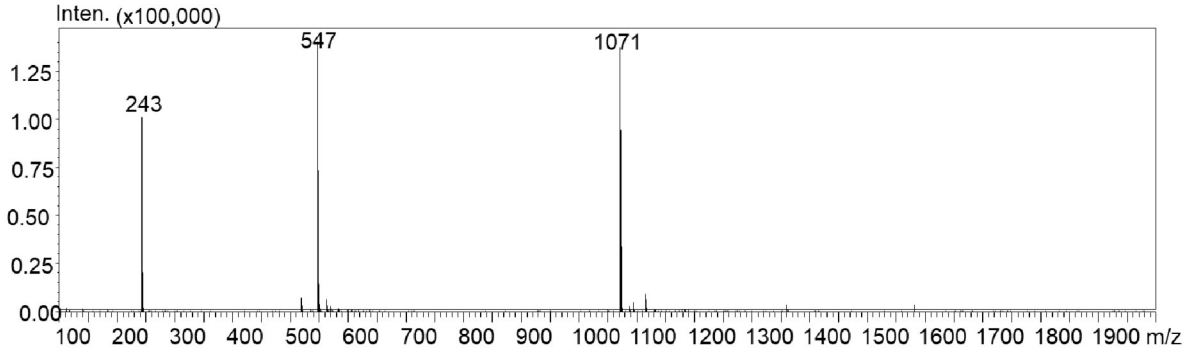

Figure S2: ESI mass (positive mode) of N_3-SHA. m/z calculated: $[M+H]^+$ = 524 g/mol, found: $[2M+Na]^+$ = 1071 g/mol, $[M+Na]^+$ = 547 g/mol, $[Trt]^+$ = 243 g/mol. Note: The acid-labile protecting group is partially removed during the measurement.

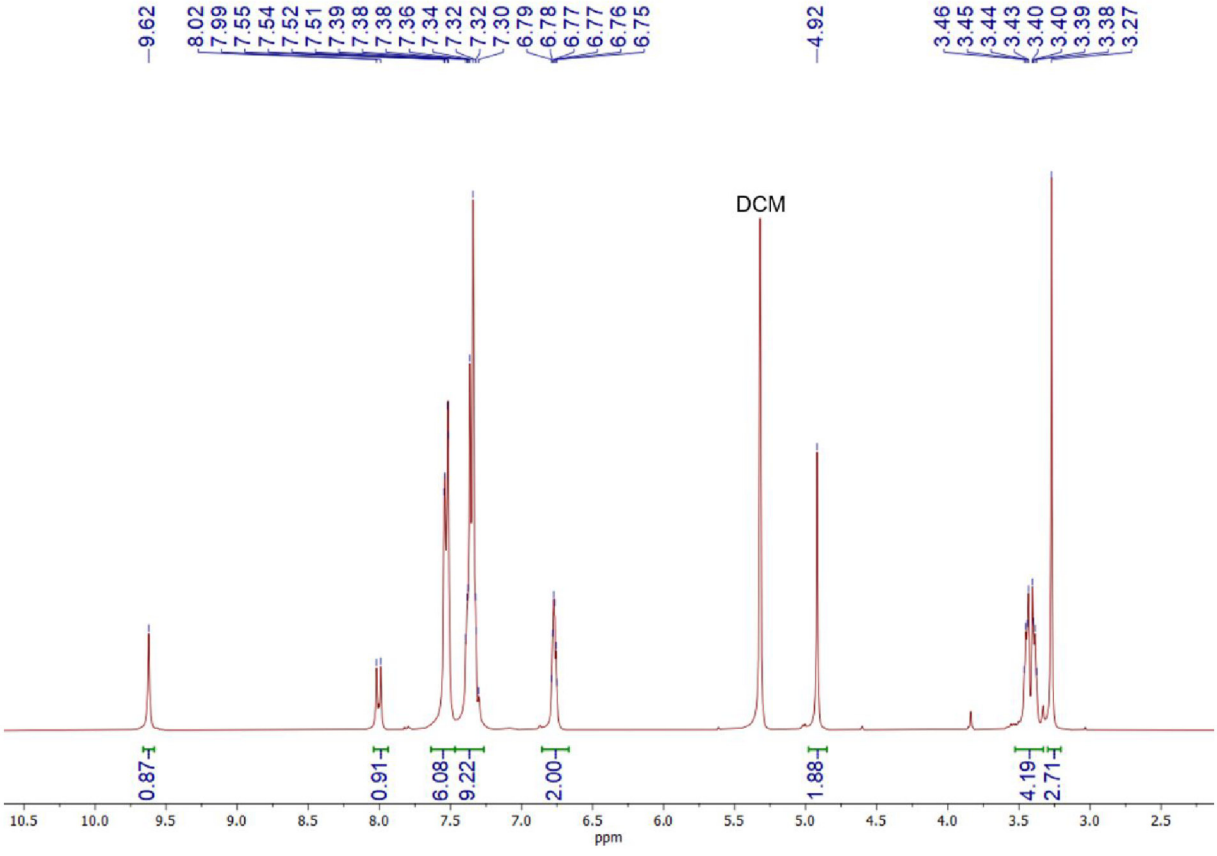

Figure S3: ^{1}H-NMR of the protected azidosalicylhydroxamate derivative measured in CD_2Cl_2.

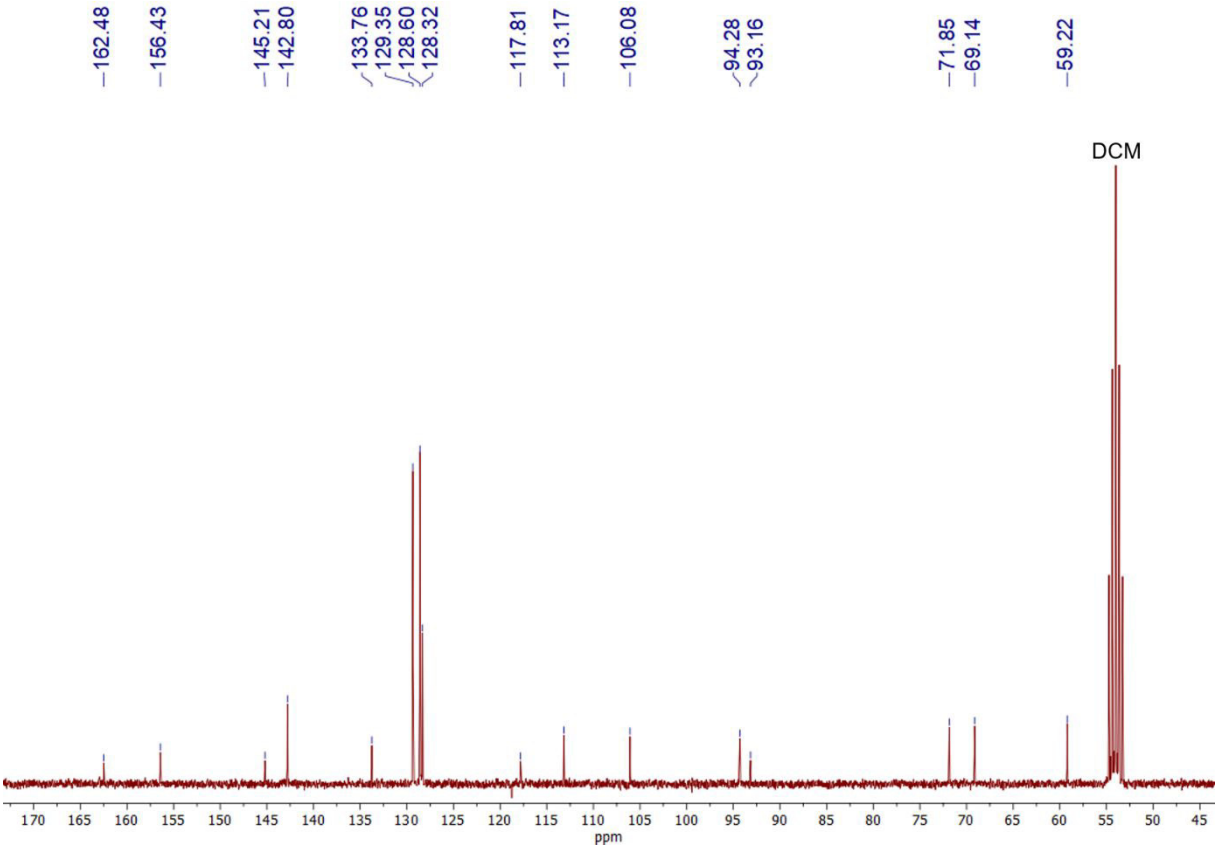

Figure S4: ^{13}C-NMR of the protected azidosalicylhydroxamate derivative **10** measured in CD_2Cl_2.

2.8 Peptide Synthesis

2.8.1 Depsi(Fmoc-I)pba-SA

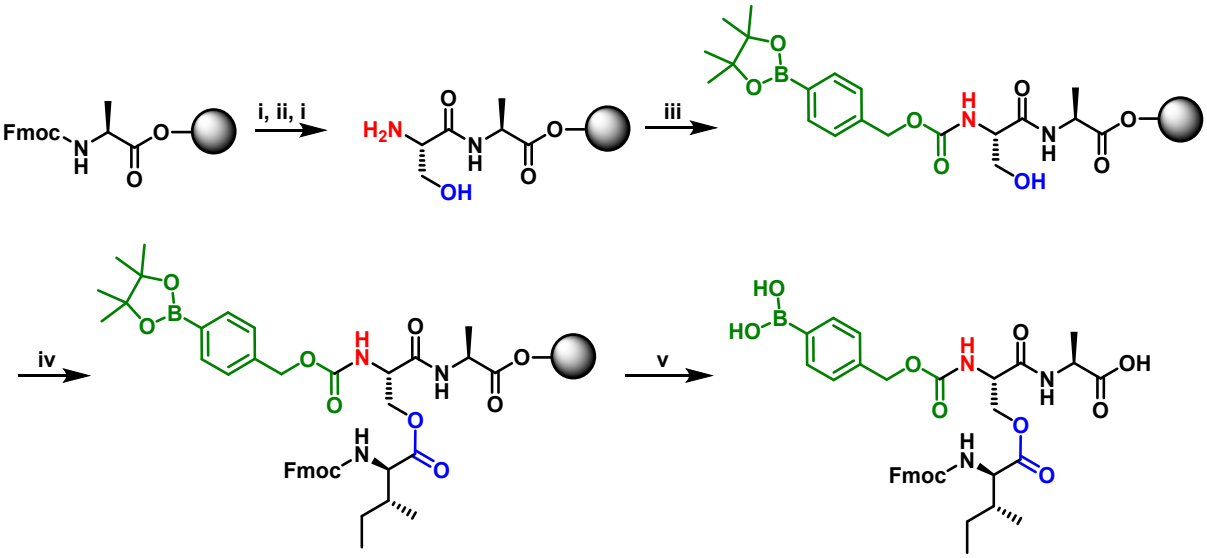

Figure S5: **i** Piperidine 20% v/v in DMF, 2 and 5 min, 75 °C, **ii** Fmoc-Ser, PyBOP, DIPEA in DMF, 20 min, 75 °C, **iii** 4-(nitrophenyl)phenylboronic acid pinacol ester, DIPEA in DMF, o.n., rt, **iv** Fmoc-Ile, DIC, 4-DMAP in DMF, 2 h and o.n., rt, **v** TFA/TIPS/H_2O 2 h, rt.

Peptides were synthesized using the Fmoc solid phase peptide synthesis strategy by Merrifield, synthesizing the peptide from *C* to *N*-terminus in a microwave assisted peptide synthesizer. Fmoc-Ala preloaded Wang resin (0.5 mmol) was swollen in DMF for 1 h before use. First, the Fmoc group was removed by two consecutive deprotection steps (2 and 5 min) with 20% piperidine in DMF (10 mL) at 75 °C (**i**). After deprotection, the resin was washed four times with DMF (7 mL). Fmoc-serine (5 equiv in 10 mL DMF) was coupled to the *N*-terminus by using the activator PyBOP (5 equiv in 4 mL DMF) and activator base DIPEA (10 equiv in 2 mL DMF) at 75 °C for 20 min (**ii**). After deprotection of the Fmoc protecting group (**i**), the *N*-terminus was modified using 4-nitrophenyl (4-(4,4,5,5-tetramethyl-1,3,2-dioxaborolan-2-yl)benzyl) carbonate (1.25 equiv) in 5 mL DMF and DIPEA (5 equiv) overnight at room temperature (**iii**). After the resin was washed with DMF and DCM, Fmoc-Ile (10 equiv in 5 mL DMF), DIC (10 equiv) and 4-DMAP (1 equiv) were added to form the ester bond in the serine

side chain. After the reaction mixture was stirred for 2 h at room temperature, fresh Fmoc-Ile, DIC and 4-DMAP were added and stirred overnight to ensure full conversion of the coupling (**iv**). After washing with DMF and DCM, the resin was dried and half of the peptide was cleaved from the solid support by using 2 mL of a cleavage cocktail (95% TFA, 2.5% TIPS, 2.5% H_2O). This step also removed the pinacol protecting group of the PBA. After 2 hours, the cleavage cocktail was removed *in vacuo* (**v**).

The peptide was purified by HPLC with the Atlantis T3 column (flowrate 10 mL/min). The gradient started with 5% ACN, which was kept constant for 1 min, then the ACN content was increased linearly to 100% within 30 min. The retention time of the product was 25.0 min. After lyophilisation, the peptide **1a** (13.12 mg, 19.03 µmol, 7.6% yield) was received as a white powder.

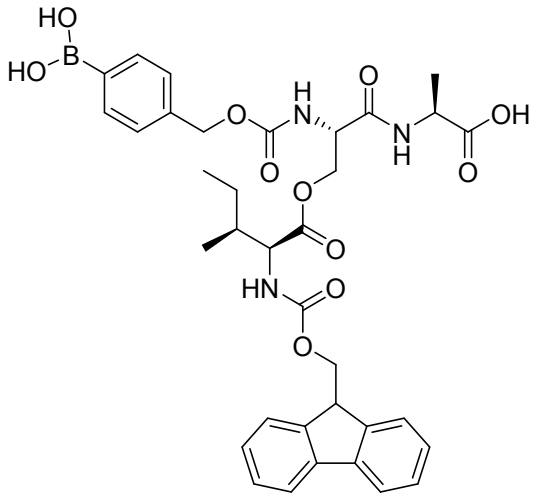

Exact Mass: 689,28

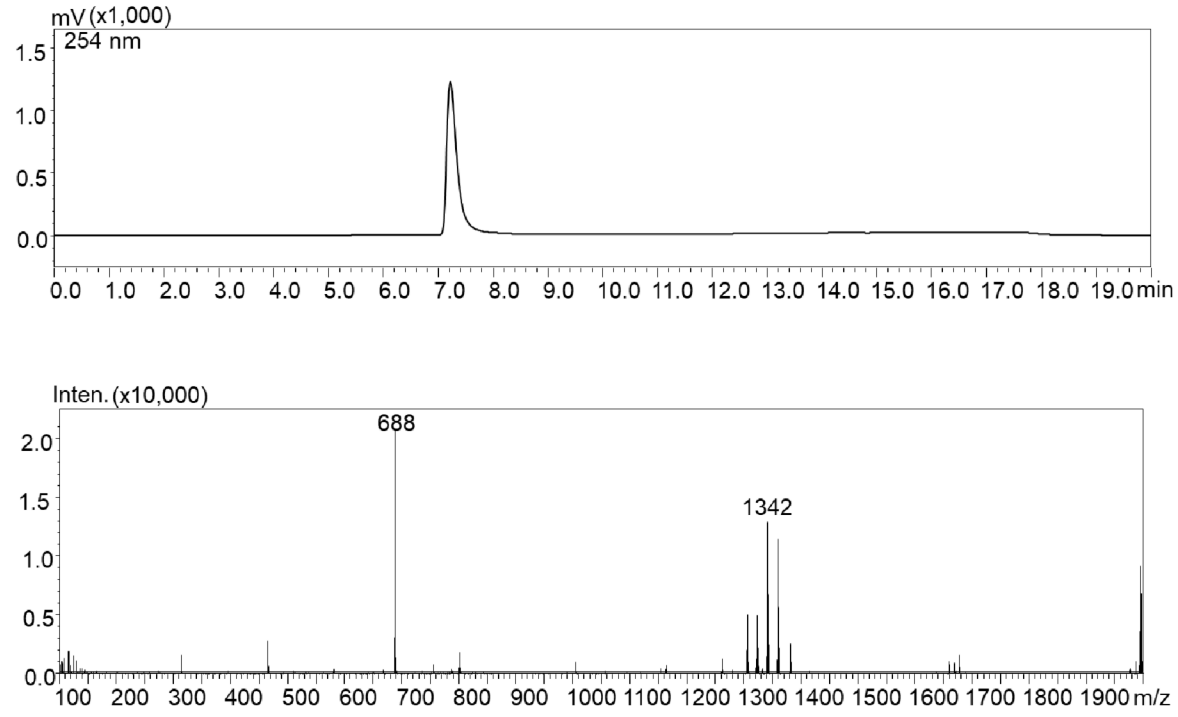

Figure S6: LC-spectrum (top) and ESI mass (negative mode, bottom) of Depsi(Fmoc-I)pba-SA. m/z calculated: $[M-H]^-$ = 688 g/mol, found: $[M-H]^-$ = 688 g/mol, $[2\ M-2\ H_2O-H]^-$ = 1342 g/mol.

2.8.2 Depsi(Fmoc-I)SA

Depsi(Fmoc-I)SA was synthesized using Boc-Ser, therefore no Fmoc deprotection was performed after the coupling of Boc-Ser. The peptide was synthesized at a scale of 0.1 mmol. After removal of the Fmoc group of alanine (3 mL of 20% v/v piperidine in DMF, 2x 5 min), Boc-Ser was coupled for 10 min at 75 °C using 5 equiv of the amino acid in 2.5 mL DMF, PyBOP (5 equiv, in 1 mL DMF) and DIPEA (10 equiv, in 0.5 mL DMF). Fmoc-Ile was coupled to the side chain of serine by heating to 75 °C for 1 h, which was repeated after addition of fresh reagents, to ensure full conversion. The same concentrations and equivalents as for Boc-Ser coupling were used. After cleavage from the solid phase as described before, the peptide was purified by HPLC using the Zorbax Eclipse column at a flowrate of 4 mL/min. The gradient started with 5% ACN in water (+0.1% TFA) and this solvent ratio was kept for 1 min, after which the ACN content was increased to 100% in 15 min. The peptide **2a** eluted from the column after 12.4 min and was received as a white powder (4.90 mg, 9.58 µmol, 9.6% yield).

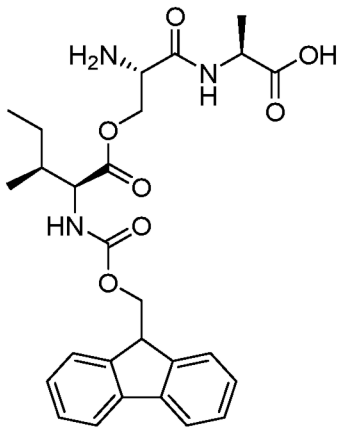

Exact Mass: 511,23

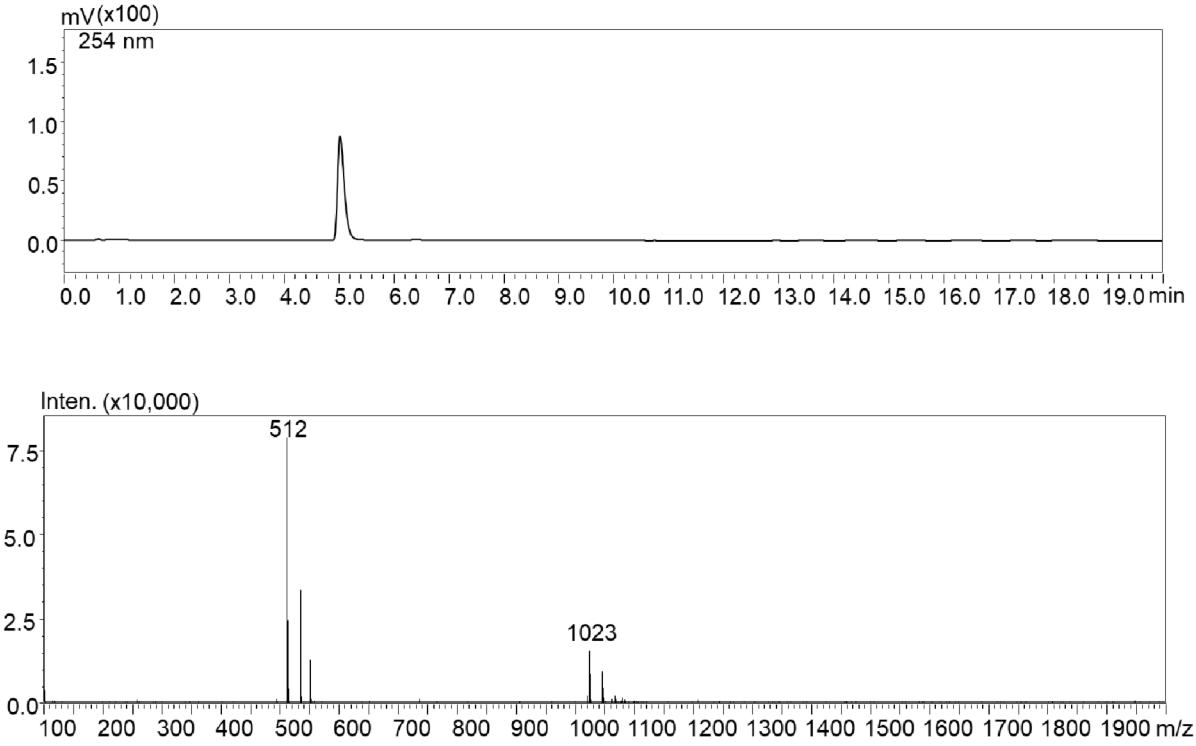

Figure S7: LC-spectrum (top) and ESI mass (positive mode, bottom) of Depsi(Fmoc-I)-SA. m/z calculated: $[M+H]^+$ = 512 g/mol, found: $[M+H]^+$ = 512 g/mol, $[2\ M+H]^+$ = 1032 g/mol.

2.8.3 Fmoc-ISA

The peptide was synthesized using a 0.1 mmol scale. After deprotection of the Fmoc group (3 mL of 20% piperidine in DMF, 2 and 5 min at 75 °C), Fmoc-Ser(tBu)/Fmoc-Ile were double coupled onto the peptide at 75 °C for 20 min. 5 equiv of the amino acids were used in 2.5 mL DMF, PyBOP (5 equiv in 1 mL DMF) and DIPEA (10 equiv in 0.5 mL) were used for the

coupling. After cleavage from the solid support, the peptide was purified by HPLC using the Atlantis T3 column (flowrate 10 mL/min) and a gradient starting from 5% ACN in water, 0.1% TFA. After keeping this solvent composition for 1 min, the amount of ACN was increased linearly within 30 min to reach 100% ACN. Fmoc-ISA **3a** eluted after 24.2 min. 13.8 mg (26.99 mmol, 27.0% yield) of the peptide were received.

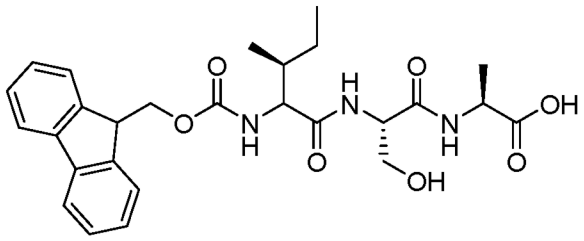

Exact Mass: 511,23

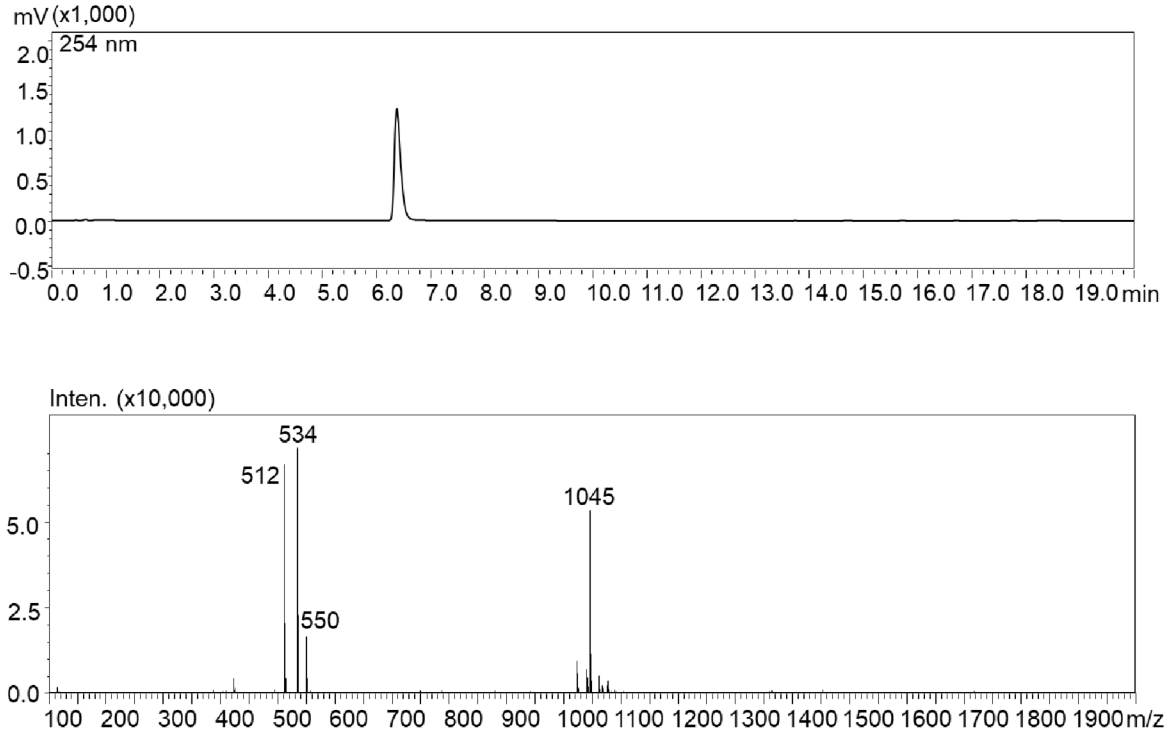

Figure S8: LC-spectrum (top) and ESI mass (positive mode, bottom) of Fmoc-ISA. m/z calculated: $[M+H]^+$ = 512 g/mol, found: $[M+H]^+$ = 512 g/mol, $[M+Na]^+$ = 534 g/mol, $[M+K]^+$ = 550 g/mol, $[2\ M+Na]^+$ = 1045 g/mol.

2.8.4 Depsi(C343-I)pba-SA

In order to synthesize Depsi(C343-I)pba-SA, Depsi(Fmoc-I)pba-SA (0.25 mmol) was not cleaved from the solid support, but instead the Fmoc group was removed in two deprotection

steps using 20% piperidine in DMF (10 min each, 5 mL) at room temperature. Coumarin 343 (1.2 equiv) was coupled onto the *N*-terminus overnight at room temperature, using PyBOP (2 equiv) and DIPEA (4 equiv) as coupling reagents. The resin was washed with DMF and DCM, dried and then the peptide was cleaved from the resin as described before. The peptide was purified by HPLC with the Atlantis T3 column at a flowrate of 10 mL/min using a gradient starting with 5% ACN and 95% water, both acidified with 0.1% TFA. The solvent composition was kept constant for 1 min and then the ACN content was increased linearly to 100% in 36 min. The retention time of the product was 28.8 min and the peptide **1b** was received as an orange powder (4.12 mg, 5.61 µmol, 2.2% yield).

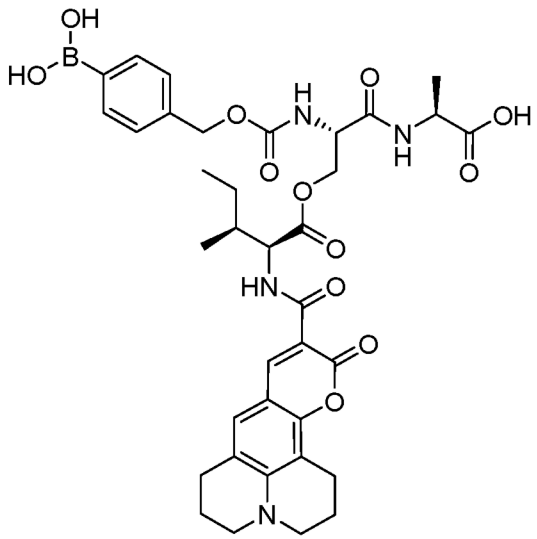

Exact Mass: 734,30

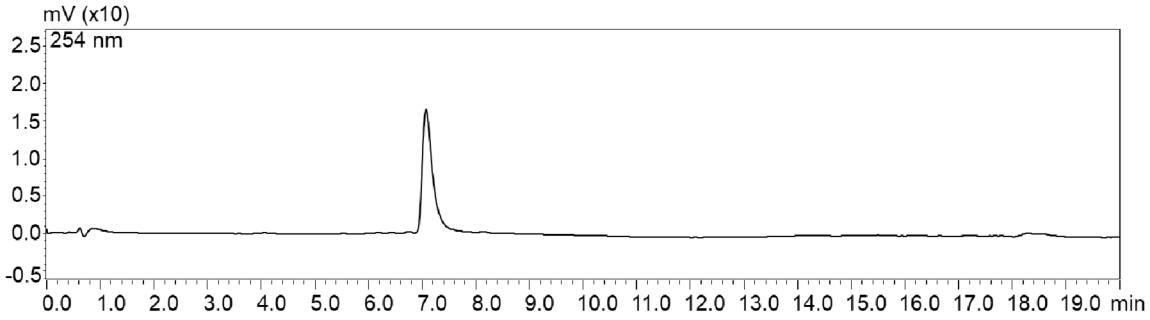

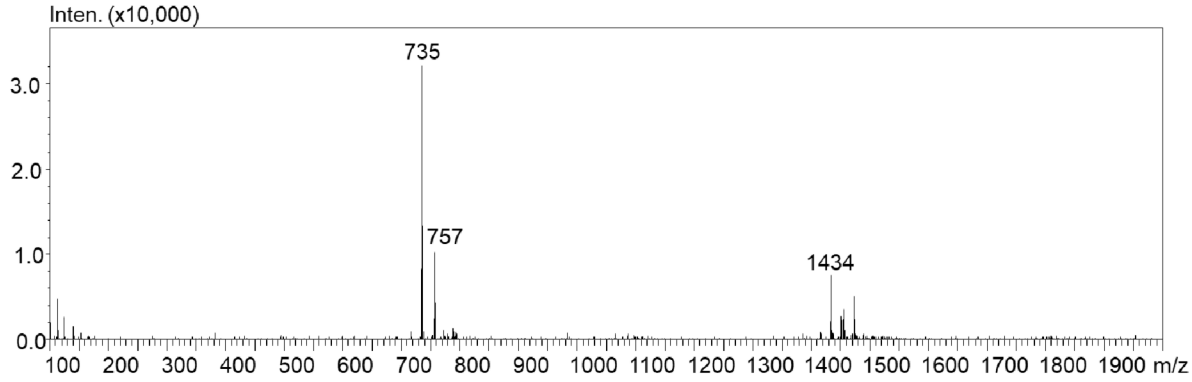

Figure S9: LC-spectrum (top) and ESI mass (positive mode, bottom) of Depsi(C343-I)pba-SA. m/z calculated: $[M+H]^+$ = 735 g/mol, found: $[M+H]^+$ = 735 g/mol, $[M+Na]^+$ = 757 g/mol, $[2\ M\text{-}2\ H_2O+H]^+$ = 1434 g/mol.

2.8.5 C343-ISA

Fmoc-ISA (0.05 mmol) bound to the Wang resin was treated with 20% piperidine in DMF for 2 and 5 min at 75 °C in order to remove the Fmoc protecting group. Coumarin 343 (C343) was coupled as described in section 2.8.4. The peptide was purified by HPLC using the Phenomenex column at a flowrate of 25 mL/min. The gradient started at 5% ACN in water (+0.1% TFA) and these conditions were kept for 1 min, after which the ACN concentration was increased to 100% in 36 min. The retention time of C343-ISA was 22.8 min. The yellow powdered peptide **3b** was received in a yield of 11.7% (3.25 mg, 5.84 µmol).

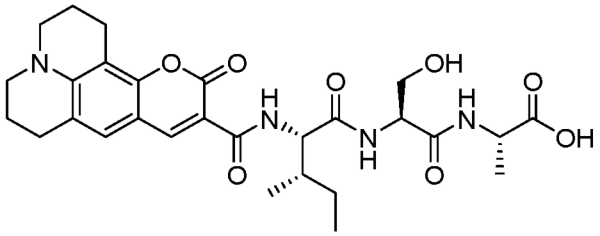

Exact Mass: 556,25

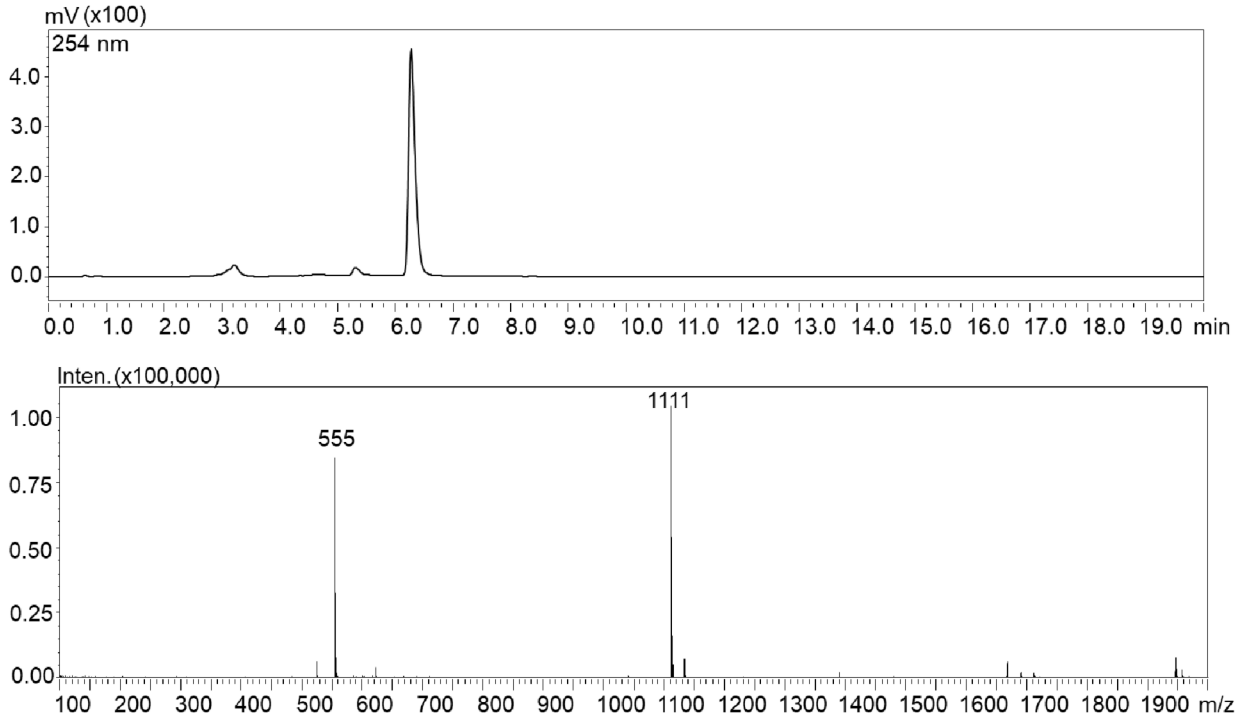

Figure S10: LC-spectrum (top) and ESI mass (negative mode, bottom) of C343-ISA. m/z calculated: $[M-H]^-$ = 555 g/mol, found: $[M-H]^-$ = 555 g/mol, $[2\ M-H]^-$ = 1111 g/mol.

2.8.6 SHA-TAT

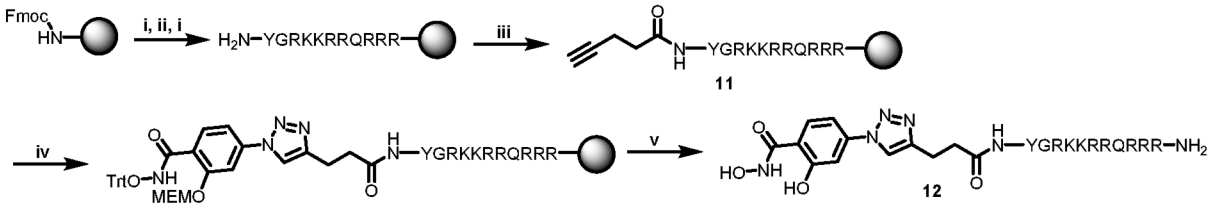

Figure S11: Synthetic scheme of the synthesis of SHA-Tat. **i** Piperidine 20% in DMF, 2 and 5 min for 75 °C, **ii** Fmoc-AA, PyBOP, DIPEA, DMF, 20 min, 75 °C, **iii** 4-pentynoic acid, PyBOP, DIPEA, DMF, overnight, rt, **iv** protected 4-azidosalicylhydroxamate, CuI, DIPEA, DMF, room temperature, overnight. **v** TFA, TIPS, H_2O, 2 h, rt.

SHA-TAT was synthesized using Rink amide resin at a scale of 0.1 mmol. Before every coupling, the Fmoc group was cleaved by two deprotection steps using 20% v/v piperidine in DMF (3 mL) for 2 and 5 min at 75 °C (**i**). Fmoc-Arg(Pbf), Fmoc-Gln(Trt), Fmoc-Lys(Boc), Fmoc-Gly and Fmoc-Tyr(tBu) (5 equiv in 2.5 mL) were coupled for 20 min using PyBOP (5 equiv in 1 mL) and DIPEA (10 equiv) in 0.5 mL DMF (**ii**). After coupling of 4-pentynoic acid using the same coupling reagents at room temperature overnight (**iii**), a CuAAC reaction was performed

overnight using protected azido-SHA (1 equiv) and CuI (0.1 equiv) as well as DIPEA (1.25 equiv) for catalysis (**iv**). The peptide was cleaved from the solid support as described before, which also removed all protecting groups (**v**). The peptide was purified by HPLC using the Atlantis T3 column at a 10 mL/min flowrate. The gradient started at a 95:5 ratio of water:ACN (+0.1% TFA) and was kept constant for 1 min, after which the ACN content was increased to 30% in 29 min. The retention time of SHA-TAT **12** was 23.0 min. The peptide was received in a yield of 7.1% (12.95 mg, 7.07 µmol).

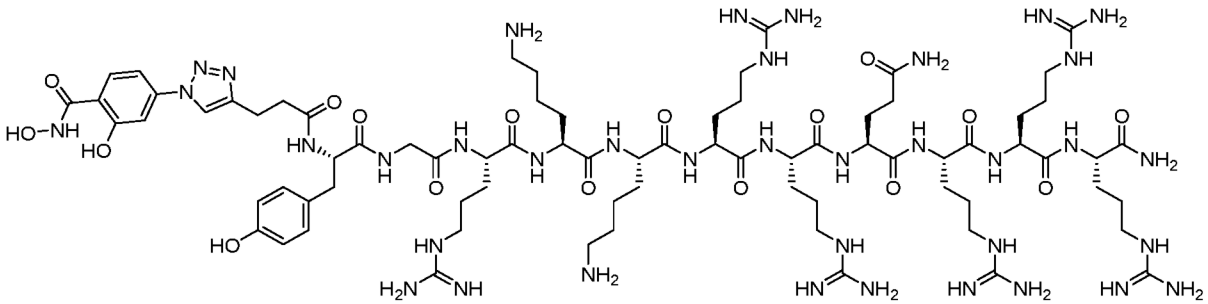

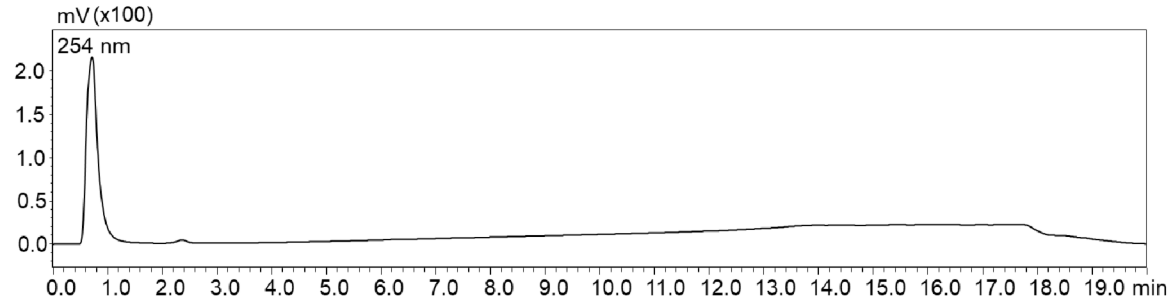

Figure S12: LC-spectrum of SHA-TAT measured at 254 nm.

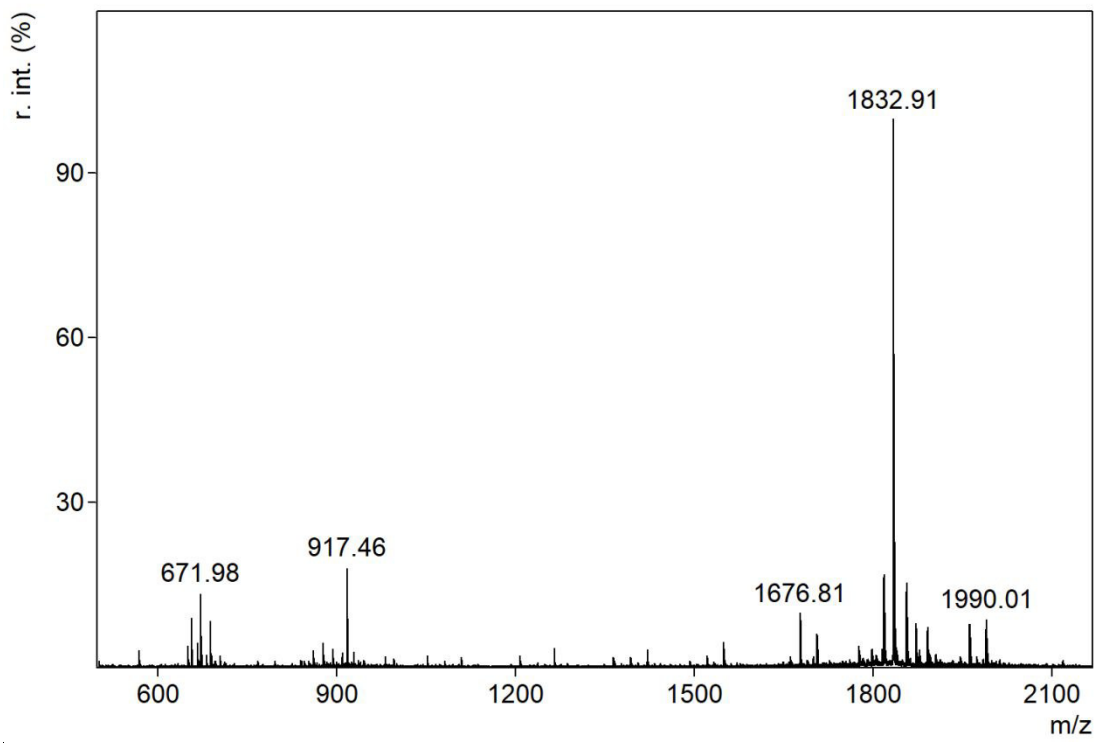

Figure S13: MALDI-TOF MS of SHA-TAT using α-cyano-4-hydroxycinnamic acid as the matrix. m/z calculated: $[M+H]^+$ = 1832 g/mol, found: $[M+TFA+3H]^{3+}$ = 671 g/mol, $[M+2H]^{2+}$ = 917 g/mol, $[M-N_3SHA+K]^+$ = 1676 g/mol, $[M+H]^+$ = 1832 g/mol, $[M+TFA+2Na-H]^+$ = 1990 g/mol. Note: SHA is partially cleaved from the peptide during the measurement.

2.8.7 SHA-Lys(5-FAM)-TAT

Fluorescent SHA-Lys(5-FAM)-TAT **14** was synthesized following the procedure described for SHA-TAT **12** in 2.8.6 at a scale of 0.025 mmol. Before coupling of 4-pentynoic acid, Fmoc-Lys(5-FAM)-OH was coupled to the TAT peptide at room temperature for 2 h using the amino acid (2.75 equiv), PyBOP (5 equiv) and DIPEA (10 equiv). After removal of the Fmoc protecting group at room temperature (2 × 20 min) using 20% piperidine in DMF and washing, 4-pentynoic acid and the salicylhydroxamate residue were attached as described before. The peptide was cleaved from the solid support with a cleavage cocktail containing TFA (95%), TIPS (2.5%) and water (2.5%) and purified by preparative HPLC using an Atlantis T3 column at a 10 mL/min flowrate. The gradient started at a 5:95 ratio of ACN: water (+0.1% TFA) and was kept constant for 1 min, after which the ACN content was increased to 30% in 29 min. The

retention time of **14** was 30.0 min. The peptide was received in a yield of 3.0% (1.74 mg, 0.75 µmol).

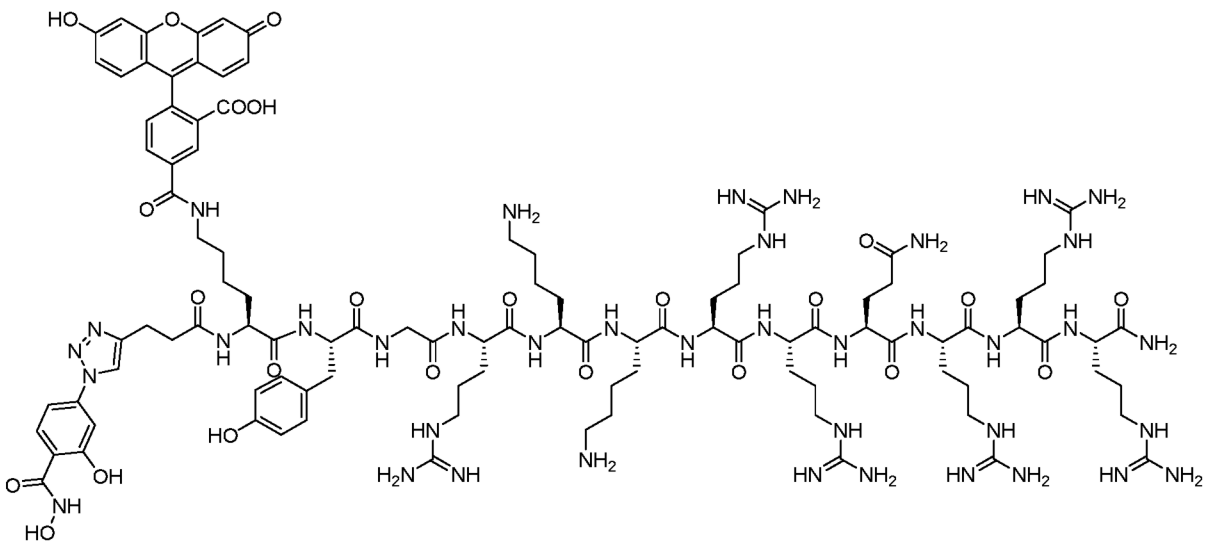

Exact Mass: 2318,18

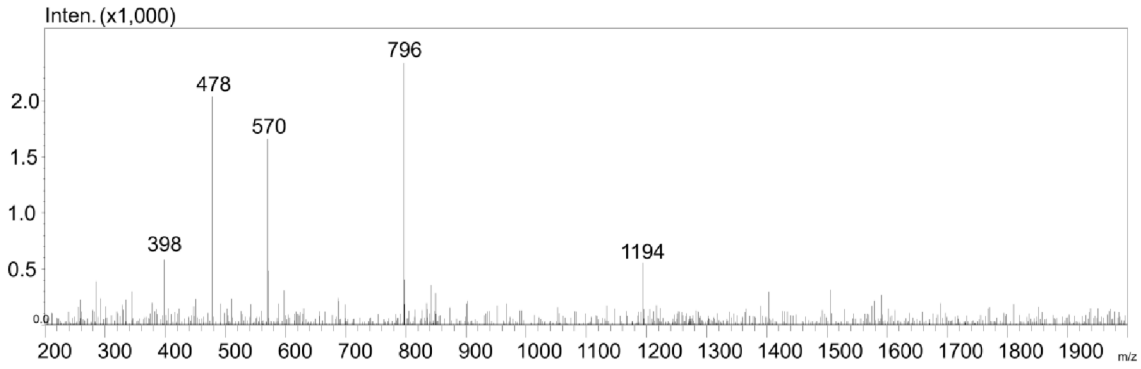

Figure S14: ESI mass spectrum (positive mode) of SHA-Lys(5-FAM)-TAT. m/z calculated: [M] = 2318 g/mol, found: $[M+3Na+3H]^{6+}$ = 398 g/mol, $[M+3Na+2H]^{5+}$ = 478 g/mol, $[M+3Na+4TFA+3Na+2H]^{5+}$ = 570 g/mol, $[M+3Na]^{3+}$ = 796 g/mol, $[M+3Na-H]^{2+}$ = 1194 g/mol.

3. Characterization

3.1 H_2O_2 induced *O, N*-Acyl Shift

Depsi(Fmoc-I)pba-SA **1a** was dissolved at a concentration of 0.1 mg·mL^{-1} in 700 µL THF and an equal amount of NH_4HCO_3 buffer 5 mM pH 7.4 was added, which either did or did not contain H_2O_2 (2 mM final concentration). At certain time points aliquots of 100 µL were analyzed using an analytical HPLC setup. The solvent gradient started at 5% ACN and 95% water, this concentration was kept for 1 min, after which the ACN content was increased to 100% linearly in 15 min. The reaction was monitored for 45 h (Figure 2 b-c).

To further confirm the identity of the product, a reaction mixture was analyzed using a LC-MS setup after incubation of 30 µg of peptide for 48 h in NH_4HCO_3 buffer 5 mM pH 7.4 mixed with methanol (1:1) with addition of 1 mM hydrogen peroxide (Figure S15).

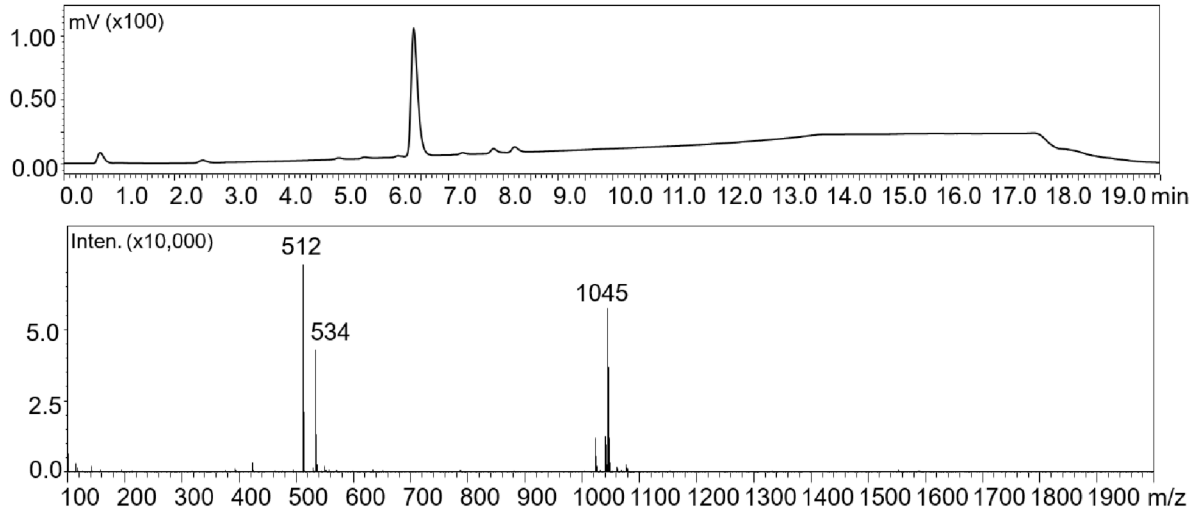

Figure S15: LC-spectrum (top) and ESI mass (positive mode, bottom) of Fmoc-ISA generated after incubation of **1a** with hydrogen peroxide. m/z calculated: $[M+H]^+$ = 512 g/mol, found: $[M+H]^+$ = 512 g/mol, $[M+Na]^+$ = 534 g/mol, $[2\ M+Na]^+$ = 1045 g/mol.

The same experiment was repeated with Depsi(C343-I)pba-SA **1b**, however the concentration and solvents were altered since a LC-MS setup was used. 30 µg of the peptide were dissolved

in 300 µL methanol and 300 µL of NH_4HCO_3 buffer 5 mM pH 7.4 were added, which either did or did not contain H_2O_2 (1 mM final concentration). At certain time points 10 µL of the solutions were analyzed by LC-MS. The solvent gradient started with 5% ACN and 95% water (+0.1% formic acid), while the ACN content was linearly increased to 95% in 12 min. The reaction was monitored for 24 h (Figure 2 d-e, Figure S16).

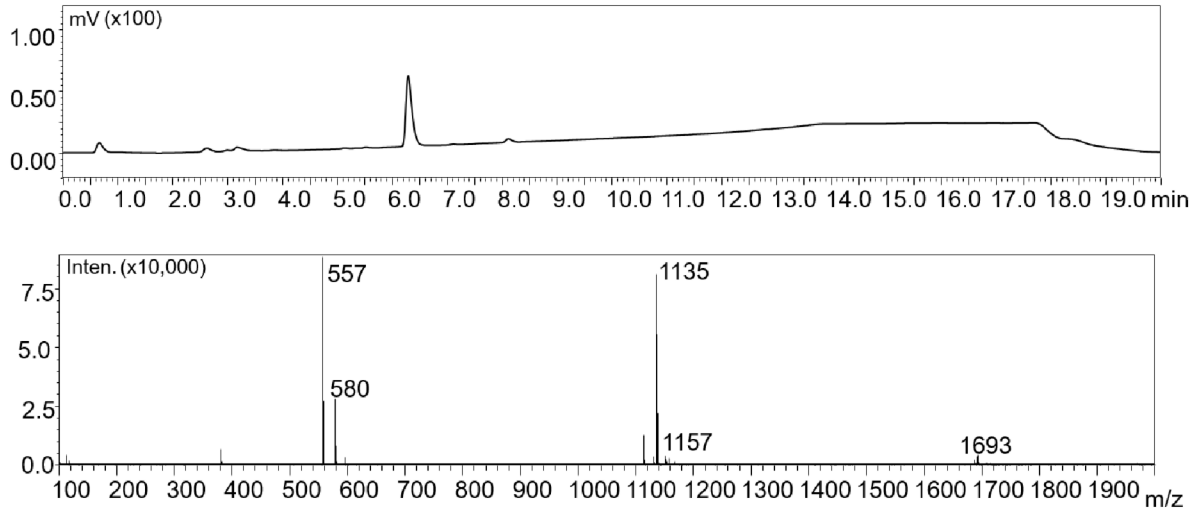

Figure S16: LC-spectrum (top) and ESI mass (positive mode, bottom) of C343-ISA **3a** generated after incubation of **1b** with hydrogen peroxide. m/z calculated: $[M+H]^+$ = 557 g/mol, found: $[M+H]^+$ = 557 g/mol, $[M+Na]^+$ = 580 g/mol, $[2\ M+Na]^+$ = 1135 g/mol, $[2\ M+2Na]^+$ = 1157 g/mol, $[3\ M+Na]^+$ = 1693 g/mol.

3.2 H_2O_2 induced Peptide Assembly

After Depsi(Fmoc-I)pba-SA **1a** or Depsi(C343-I)pba-SA **1b** were dissolved in DMSO at a concentration of 10 mM, the stock solution was diluted to 1 mM with phosphate buffer (PB) 5 mM pH 7.4, which either contained 10 mM hydrogen peroxide or did not. After 24 h incubation at room temperature, TEM measurements were performed as described above (see Figure 2 f-i). For reference C343-ISA **3b** and Fmoc-ISA **3a** were also incubated at the same conditions without addition of H_2O_2 (Figure S17 and Figure S18).

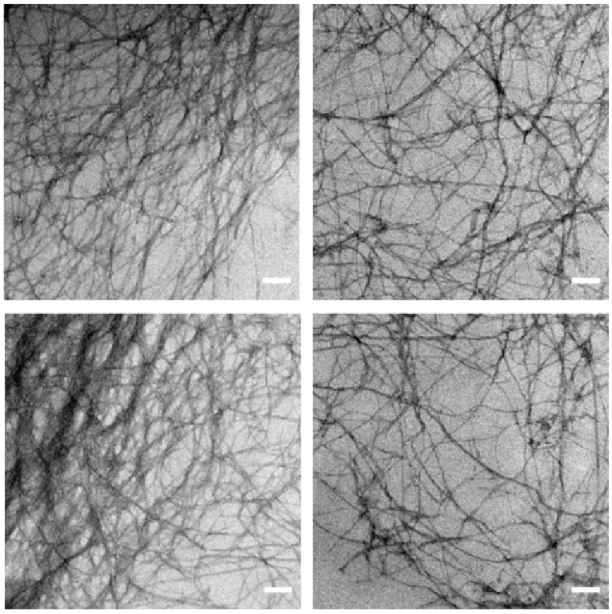

Figure S17: TEM micrographs of Fmoc-ISA **3a** incubated for 24 h in PB:DMSO 9:1. Scale bars 500 nm.

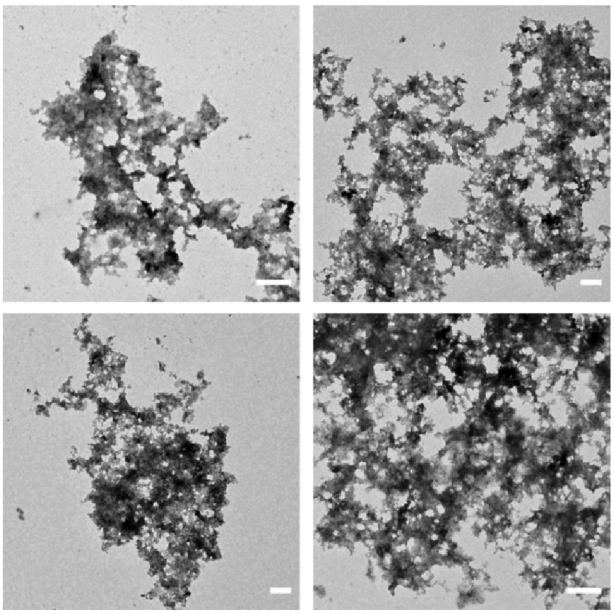

Figure S18: TEM of C343-ISA **3b** after 24 h incubation in PB:DMSO 9:1. Scale bars 500 nm.

To show that peptide fiber formation was also possible at biologically relevant hydrogen peroxide concentrations, Depsi(Fmoc-I)pba-SA **1a** was incubated with 100 µM and 10 µM H_2O_2 (Figure S19).

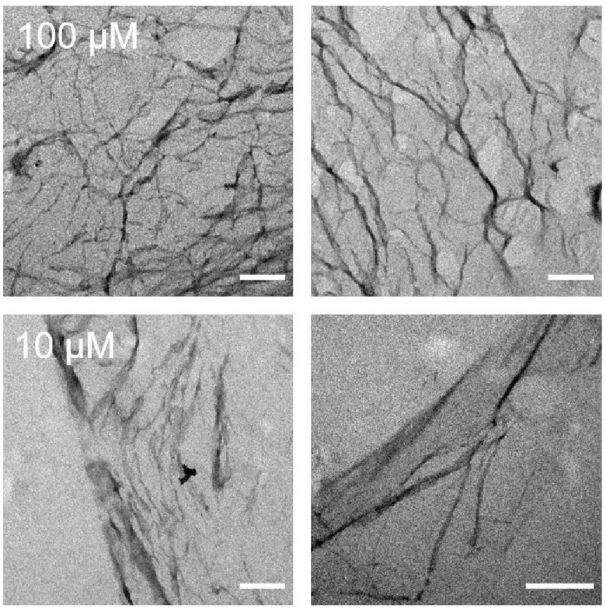

Figure S19: TEM micrographs after incubation of 1 mM Depsi(Fmoc-I)pba-SA **1a** for 24 h in PB:DMSO 9:1 with low concentrations of H_2O_2. Scale bars 500 nm.

For coincubation of the peptides, each peptide was predissolved in DMSO and they were mixed in the respective ratio. After addition of phosphate buffer pH 7.4 5 mM the solutions were incubated for 24 h at room temperature and then TEM samples were prepared as described above (Figure S20–22).

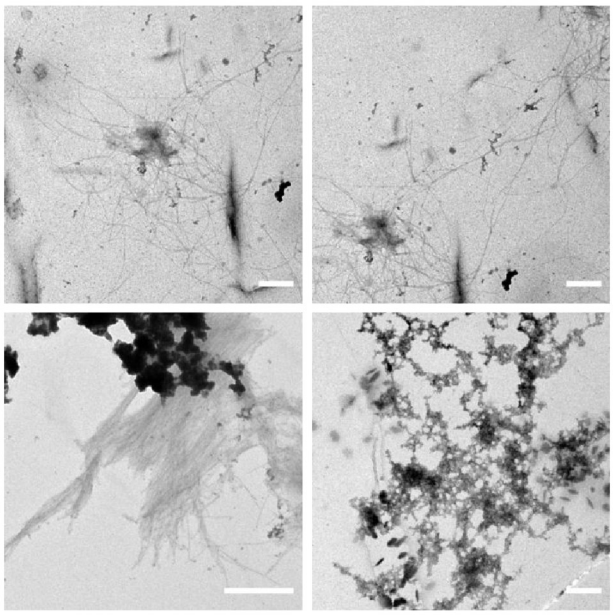

Figure S20: Incubation of Fmoc-ISA **3a** and C343-ISA **3b** at a ratio of 5:1 and a total concentration of 1 mM of peptide in PB pH 7.4 5 mM to DMSO 9:1. Scale bars 500 nm.

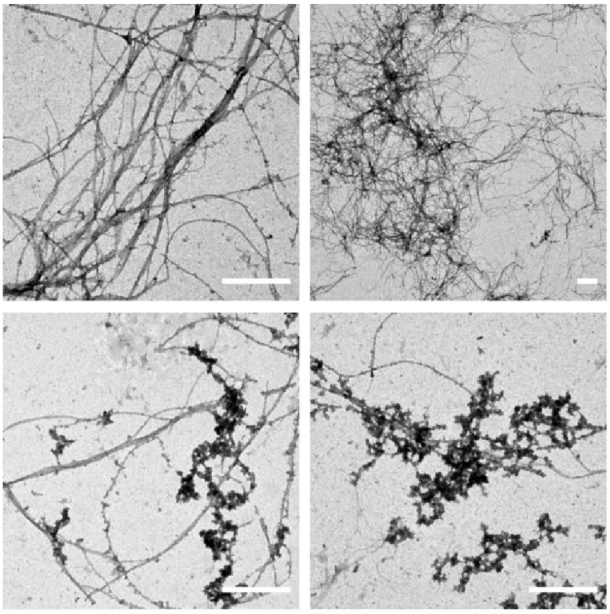

Figure S21: Incubation of Depsi(Fmoc-l)pba-SA **1a** and Depsi(C343-l)pba-SA **1b** at a ratio of 9:1 and a total concentration of 150 µM of peptide in PB pH 7.4 5 mM to DMSO 9:1 upon addition of 1 mM hydrogen peroxide. Scale bars 500 nm.

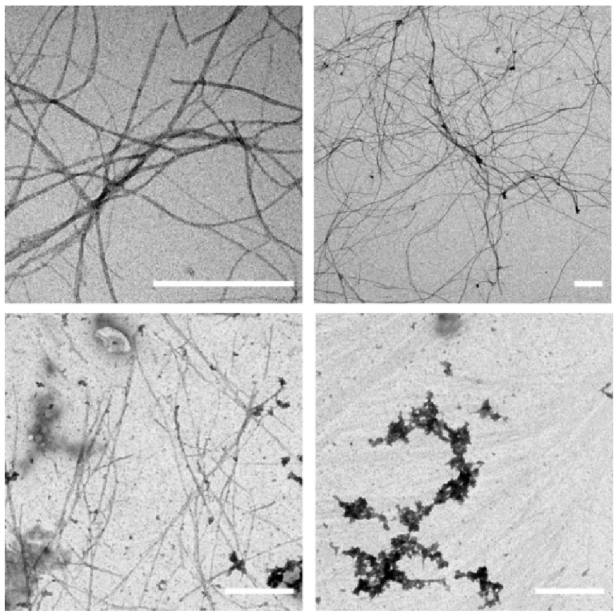

Figure S22: Incubation of Depsi(Fmoc-l)pba-SA **1a** and Depsi(C343-l)pba-SA **1b** at a ratio of 99:1 and a total concentration of 150 µM of peptide in PB pH 7.4 5 mM to DMSO 9:1 upon addition of 1 mM hydrogen peroxide. Scale bars 500 nm.

In order to see the influence of SHA-TAT **12** on structure formation, TEM images of 1 mM **13a/b** (5:1 ratio **13a**:**13b**) with or without 10 mM H_2O_2 and SHA-TAT **12** were taken after incubation overnight in phosphate buffer pH 7.4 5 mM and 10% DMSO. The results showed

that fibers were formed upon addition of hydrogen peroxide showing the conversion into **3a/b**, while small drying artifacts were observed for **12** and **13a/b**.

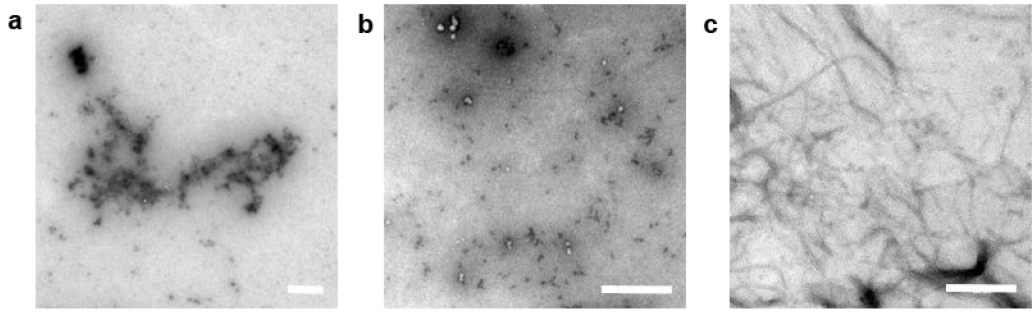

Figure S23: TEM micrograph of SHA-TAT **12** (**a**) and **13a/b** without (**b**) and with the addition of 10 mM H_2O_2 (**c**). Scale bars 500 nm.

LC-MS data confirmed the formation of the linear peptide **3a** upon incubation of **13a** for 48 h in NH_4HCO_3 buffer 5 mM pH 7.4 mixture with methanol (1:1) with addition of 1 mM hydrogen peroxide. The complex **13a** was formed 15 min before addition of H_2O_2 using **1a** (30 µg, 0.04 µmol) and **12** (80 µg, 0.04 µmol).

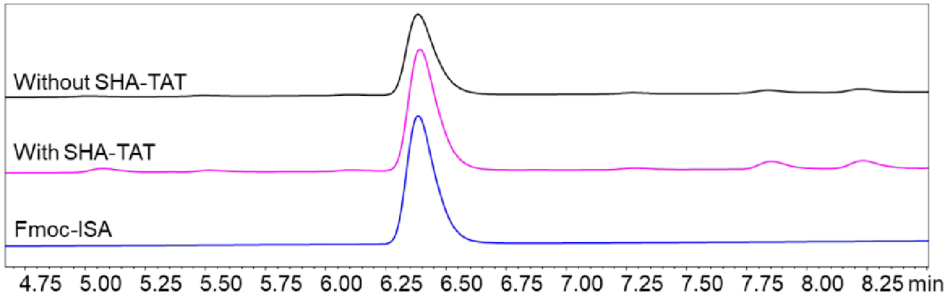

Figure S24: LC-spectra measured at 254 nm showing the conversion of **1a** (black line) and **13a** (purple line) to **3a** (control, blue line) upon treatment with hydrogen peroxide.

Furthermore, the pH dependency of the conversion of **13a/b** into **3a/b** was checked by TEM microscopy. No fibers but drying artifacts were observed upon incubation at pH 6.0 and 5.0 which indicates the pH dependency of the oxidation of boronic acids. Samples were prepared the same way as samples at pH 7.4.

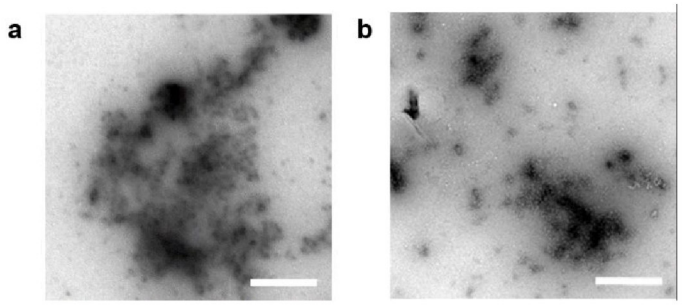

Figure S25: TEM images of structures formed after incubation of **13a/b** in phosphate buffer at pH 6.0 (a) and pH 5.0 (b).

3.3 Critical Fibrillation Concentration

A dilution series of Fmoc-ISA **3a** in PBS:DMSO (9:1) was prepared and the solutions were shaken overnight at room temperature, after which TEM grids were prepared.

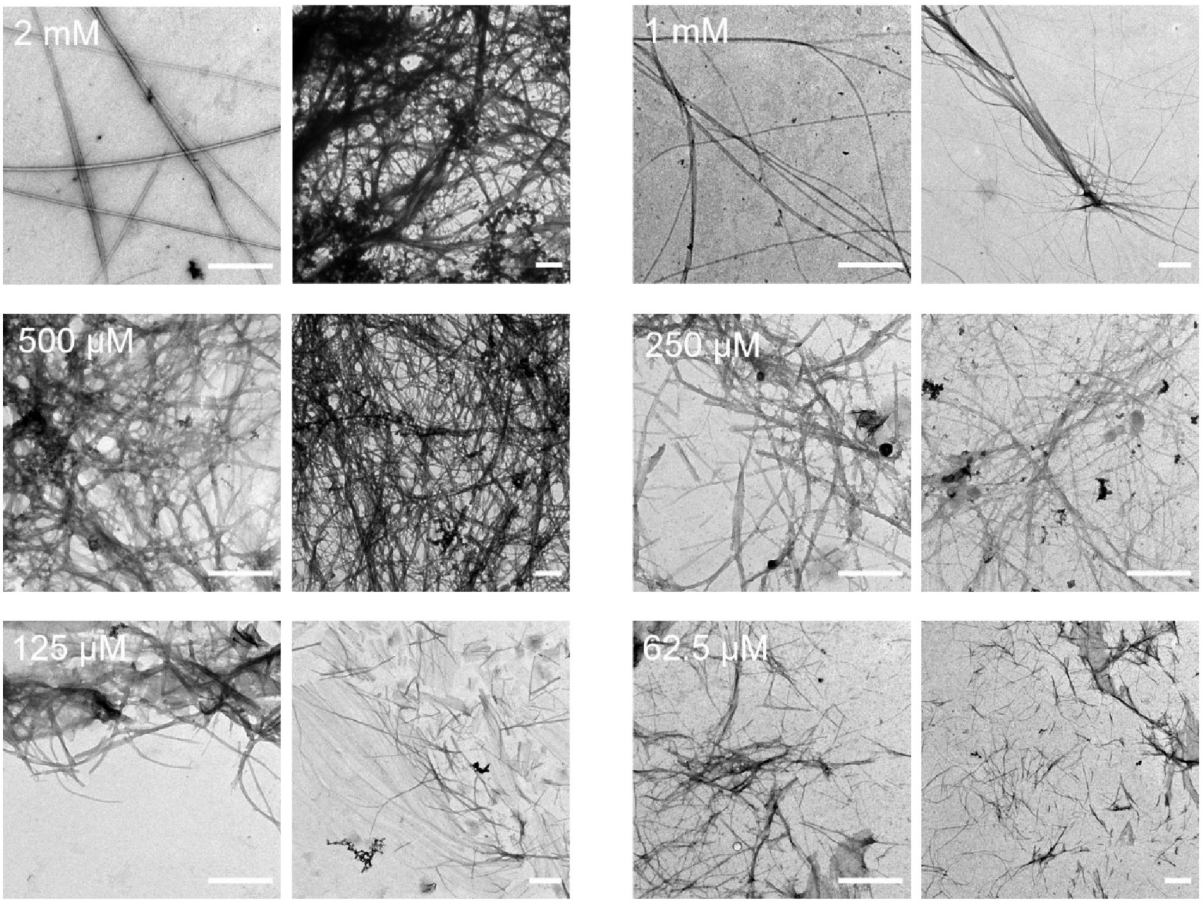

Figure S26: Determination of the critical fibrillation concentration of Fmoc-ISA **3a** by TEM. Two images of each tested concentration are displayed. Concentrations of 31.2 µM and 15.6 µM did not show fiber formation. Scale bars 500 nm.

3.4 Fluorescence Microscopy of Cofibrillized Peptides

In order to prove the staining of Fmoc-ISA peptide fibers with Proteostat, they were imaged in the fluorescence microscope (Figure S27). The sample was prepared as described before and 50 µL of 1 mM Fmoc-ISA **3a** solution (in PB:DMSO 9:1) were stained with 1 µL of Proteostat solution. The Proteostat solution was prepared according to the instructions of the supplier (*Enzo Life Sciences, Inc.*).

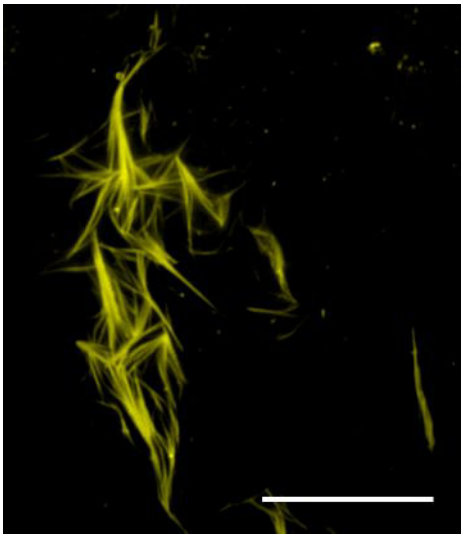

Figure S27: Proteostat stained Fmoc-ISA **3a** peptide fibers. Scale bar 20 µm.

To investigate co-assembly, Depsi(Fmoc-I)pba-SA **1a** and Depsi(C343-I)pba-SA **1b** were predissolved in DMSO and mixed at a ratio of 5:1 to achieve a peptide concentration of 10 mM. After addition of PB pH 7.4 5 mM and H_2O_2 the peptides were incubated overnight while shaking. Fibers were stained by addition of 1 µL Proteostat solution to 50 µL of fiber solution. The sample was imaged in the fluorescence microscope (Figure 2 k and Figure S28).

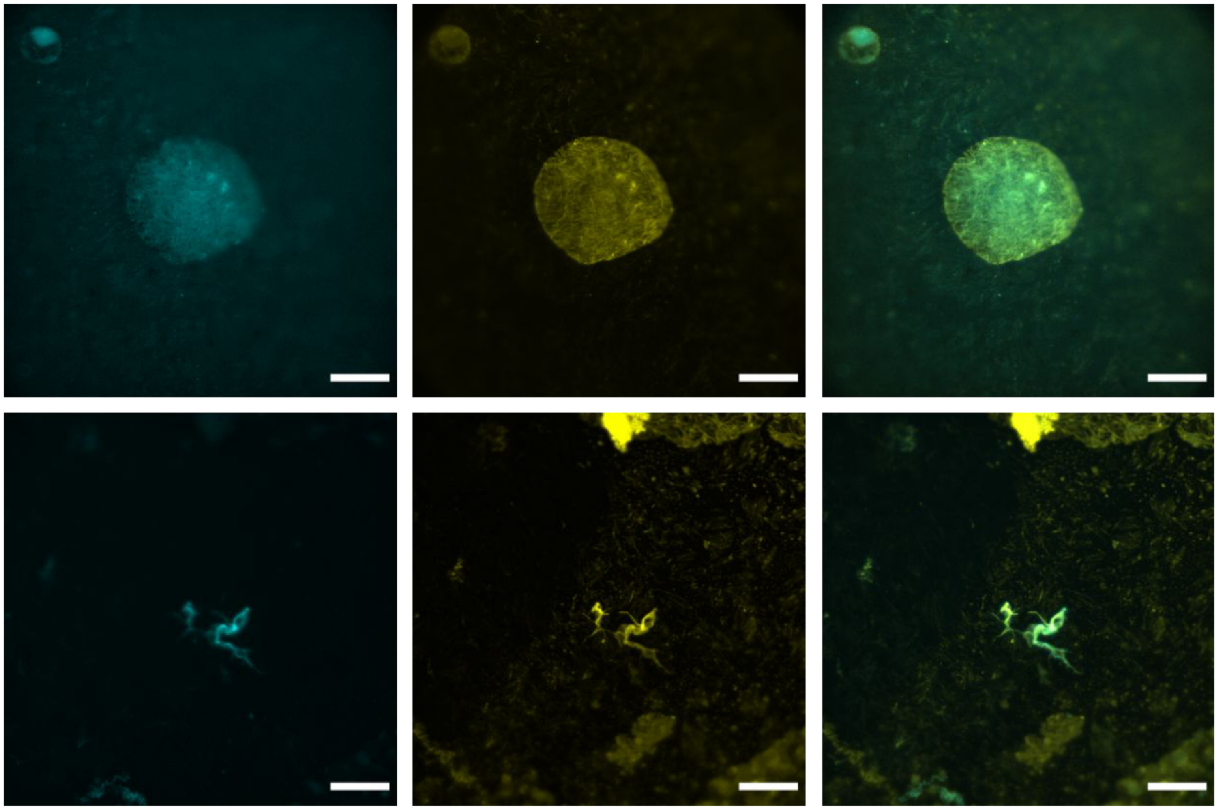

Figure S28: Cofibrillation of Fmoc-ISA **3a** and C343-ISA **3b** shown in the fluorescence microscope. Coumarin 343 fluorescence: cyan, Proteostat: yellow, colocalization: green. Scale bars 20 µm.

3.5 Fourier-Transform Infrared Spectroscopy

50 µL of either Fmoc-ISA **3a** or Depsi(Fmoc-I)pba-SA **1a** solution, incubated in DMSO:water 1:9 for 24 h, were lyophilised and FT-IR spectra were measured at wavenumbers from 400 to 4000 cm^{-1} (Figure S29). Fmoc-ISA **3a** displayed peaks typical for β-sheets (1634 cm^{-1} and either disordered or α-helical structures (1653 cm^{-1}), while the depsipeptide **1a** did not show formation of a specific structure but a very broad peak.

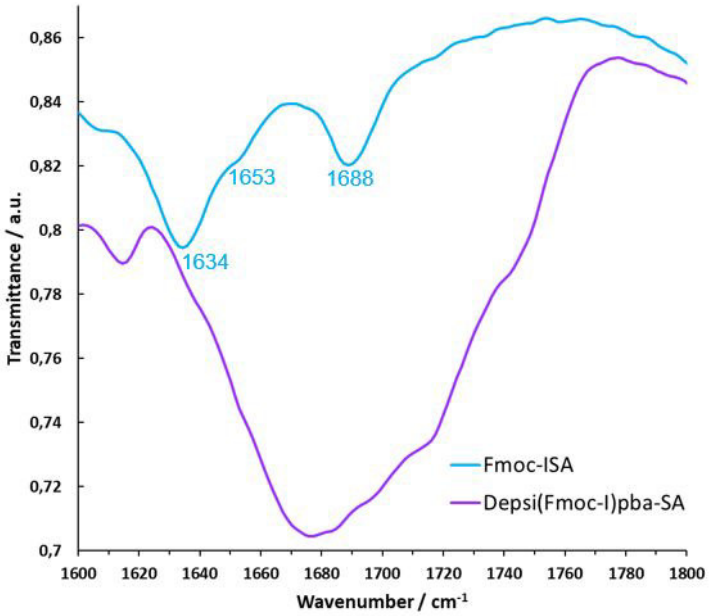

Figure S29: FT-IR spectra of Fmoc-ISA **3a** and Depsi(Fmoc-I)pba-SA **1a**.

3.6 Circular Dichroism

To show co-assembly of C343-ISA **3b** with Fmoc-ISA **3a**, CD spectra were recorded in water of both peptides separately after being self-assembled overnight, as well as CD spectra of coincubated samples (5:1 ratio **3a:3b**) and peptides which were mixed before the measurement using pre-assembled **3a** and **3b** to achieve the same concentration and ratio as for the co-assembled sample (1 mM total peptide concentration). Peptides were dissolved in MilliQ water by sonication to avoid the use of DMSO which would disturb the CD measurement. After incubation overnight, the solutions were diluted to 250 µM and circular dichroism spectra were recorded at wavelengths from 320 to 180 nm with a bandwidth of 1 nm, data pitch of 0.2 nm and scanning speed at 5 nm/min. Spectra were measured three times and accumulated (Figure 2l).

3.7 Solid-State NMR

20 mg of Fmoc-ISA **3a** were dissolved in 4 mL DMSO and the solution was diluted to a concentration of 1 mM with 36 mL MilliQ water. The solution was stirred for 24 h so peptide fibers could form and the solution was subsequently lyophilised.

A ^{13}C (^{1}H) CP-MAS NMR spectrum was recorded (Figure S30), and the peaks were assigned based on the assignment of the atoms by liquid NMR spectra of the peptide in DMSO, which is displayed below. However, NMR signals may shift due to the transition from isolated molecules in solution to the solid state.

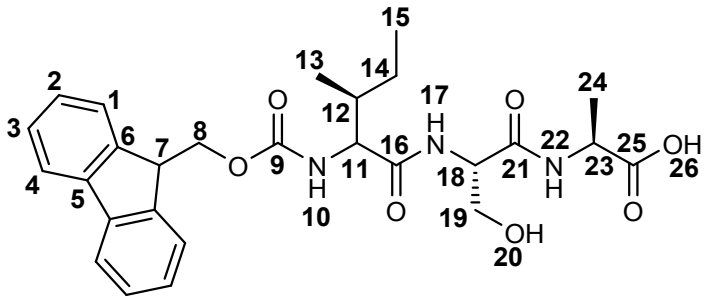

^{1}H-NMR (850 MHz, DMSO-d_6) δ [ppm] = 8.01 (d, J = 7.2 Hz, 1H, **22**), 7.95 (d, J = 7.9 Hz, 1H, **17**), 7.89 (d, J = 7.5 Hz, 2H, **4**), 7.73 (dd, J = 14 Hz, 7.5 Hz, 2H, **1**), 7.46 (d, J = 9.0 Hz, 1H, **10**), 7.41 (t, J = 7.4 Hz, 2H, **3**), 7.32 (q, J = 7.0 Hz, 2H, **2**), 4.34–4.32 (m, 1H, **18**), 4.30–4.29 (m, 1H, **8**), 4.26 - 4.17 (m, 3H, **7**, **8** and **23**), 3.95 (t, J = 8.3 Hz, 1H, **11**), 3.59–3.55 (m, 2H, **19**), 1.83–1.70 (m, 1H, **12**), 1.43–1.42 (m, 1H, **14**), 1.25 (d, J = 7.3 Hz, 3H, **24**), 1.14–1.10 (m, 1H, **14**), 0.85 (d, J = 6.8 Hz, 3H, **13**), 0.81 (t, J = 7.4 Hz, 3H, **15**).

^{13}C-NMR (75 MHz, DMSO-d_6) δ [ppm] = 174.00 (**25**), 171.23 (**16**), 169.57 (**21**), 156.07 (**9**), 143.92 (**5**), 140.72 (**6**), 127.66 (**3**), 127.10 (**2**), 125.38 (**1**), 120.11 (**4**), 65.68 (**8**), 61.70 (**19**), 59.19 (**11**), 54.85 (**18**), 47.65 (**23**), 46.70 (**7**), 36.54 (**12**), 24.36 (**14**), 17.34 (**24**), 15.35 (**13**), 10.97 (**15**).

Assignment of the peaks in the solid state was based on the following considerations: Isoleucine has many aliphatic peaks in proximity to the carbonyl position, therefore the 173 ppm peak is assigned to its C=O group. Serine contains no purely aliphatic protons, but signals above 4 ppm, which pleads for the assignment of the 171 ppm signal to the Ser carbonyl. Alanine typically displays the highest chemical shift in the carbonyl region, therefore we assign the 175 ppm to Ala. The Fmoc C=O is assigned to the two sharp and one broad peak between 157 and 160 ppm. Appearance of three peaks for Fmoc shows that there is no uniform packing of Fmoc-ISA **3a**. All carbonyl signals show multiple maxima, which further hints at the formation of different structures.

Strikingly, the serine carbonyl and the middle Fmoc carbonyl signal at 158 ppm show a correlation with the same deshielded N–H proton at 8.5 ppm (red line in Figure S25). This indicates formation of a hydrogen bond between either the N–H of Ile and C=O of serine, or alanine's N–H and the Fmoc C=O group.

The carbonyl group of alanine does not show any correlation to a deshielded proton, which together with the low intensity of the signal hints at a high mobility of the chain end (dashed red circle in Figure S25).

Comparison of the chemical shifts of Fmoc-ISA in the solid state and polypeptides to determine the secondary structure, gave the following results: The carbonyl signal of alanine (174–176 ppm) is in the region of α-helices (176 ppm) while the C_α (47 ppm) is in the β-sheet region (48 ppm). For isoleucine the carbonyl signal (172–174 ppm) covers the entire region of α-helices (175 ppm) and β-sheets (171 ppm). The chemical shift of the C_α (60–61ppm) lays between the shift of α-helices (64 ppm) and β-sheets (58 ppm) in polyisoleucine. For polyserine only the chemical shift of β-sheets (170 ppm for the carbonyl, 55 ppm for C_α) are reported, which is in accordance to the measured results (170–172 ppm for the carbonyl, 54 ppm for C_α).[4,5]

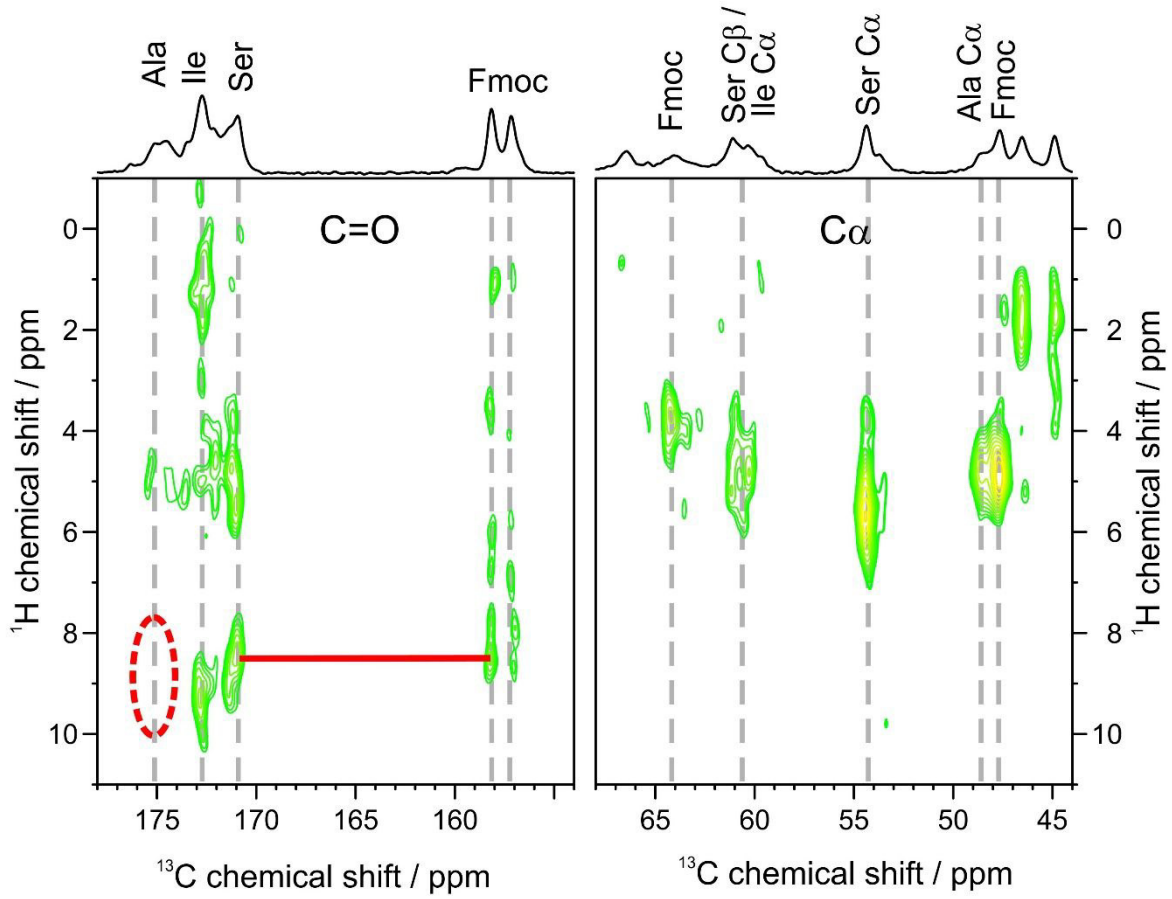

Figure S30: Carbonyl and C_α region of a ^{13}C (^1H) CP-MAS NMR spectrum of Fmoc-ISA **3a**.

3.8 MALDI-TOF of Depsi-TAT Complexes

SHA-TAT **12** and either Depsi(Fmoc-I)pba-SA **1a** or Depsi(C343-I)pba-SA **1b** (predissolved in DMSO) were conincubated for 30 min in NH_4HCO_3 buffer 5 mM pH 7.4 (buffer: DMSO 9:1). The concentration of both peptides was 1 mM. MALDI samples were prepared by mixing 2 µL of peptide solution at a ratio of 1:1 with saturated CHCA solution in water/acetonitrile (Figure 3 b).

3.9 Fluorescence Quenching

Depsi(C343-I)pba-SA **1b** was used as the fluorescent binding partner, dissolved in DMSO and diluted with phosphate buffer (PB, 5 mM, pH 7.4, PB:DMSO 99:1) to a concentration of 2 µM.

SHA-TAT **12** was used as the ligand and a dilution series was prepared by diluting the stock solution each time with PB 1:1 till 16 dilutions were received. Ligand concentrations ranged from 6.00 mM to 0.18 µM. For the experiment, each ligand solution (10 µL) was mixed with 10 µL of Depsi(C343-I)pba-SA **1b**, which led to a final concentration of fluorescently labelled peptide of 1.00 µM and final ligand concentrations ranging from 3.00 mM to 0.09 µM. After 1 h incubation in the dark at room temperature, approximately 8 µL of each solution was filled into Monolith NT Standard Treated Capillaries (NanoTemper Technologies GmbH). Thermophoresis/fluorescence was measured using the Monolith NT.115 instrument (NanoTemper Technologies GmbH) at 25 °C with 5 s/ 30 s/ 5 s laser off/on/off, respectively. Instrument parameters were adjusted to 60% LED power, medium MST power and fluorescence excitation and emission were performed by using the “blue channel” of the device (excitation: 465–490 nm, emission: 500–550 nm). Data of three independently pipetted measurements were analyzed (NT.Analysis software, NanoTemper Technologies GmbH) using the fluorescence signal (Figure 3 c).

In order to show the release of boronic acid compounds which are complexed to SHA-TAT **12** upon acidification, a phenylboronic acid modified BODIPY (PBA-BDP) was complexed with **12** for 15 min at a final concentration of 150 µM by being predissolved in DMSO and mixed with **12** which was dissolved in phosphate buffer pH 7.4 5 mM. Fluorescence spectra of this sample as well as a sample which was acidified to pH 5.0 with HCl_{aq} and further incubated for 10 min, and control spectra of PBA-BDP at both pH values were recorded at the emission maximum of 516 nm after excitation at 475 nm. All measurements were performed in triplicates. Complete recovery of the fluorescence and hence release of the molecules at pH 5.0 was observed (Figure S31).

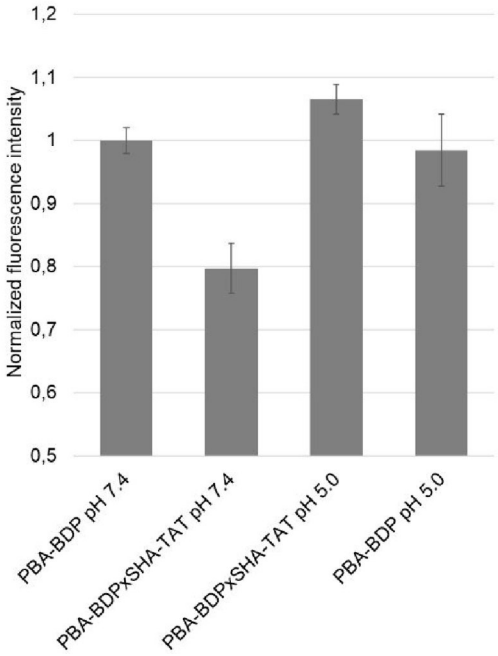

Figure S31: Fluorescence recovery of PBA-BDP upon cleavage of its complex with SHA-TAT at pH 5.0.

PBA-BDP was used as a model compound to show fluorescence recovery instead of Depsi(C343-I)pba-SA **1b** due to the quenching of fluorescence of **1b** upon acidification to pH 5.0 (Figure S32).

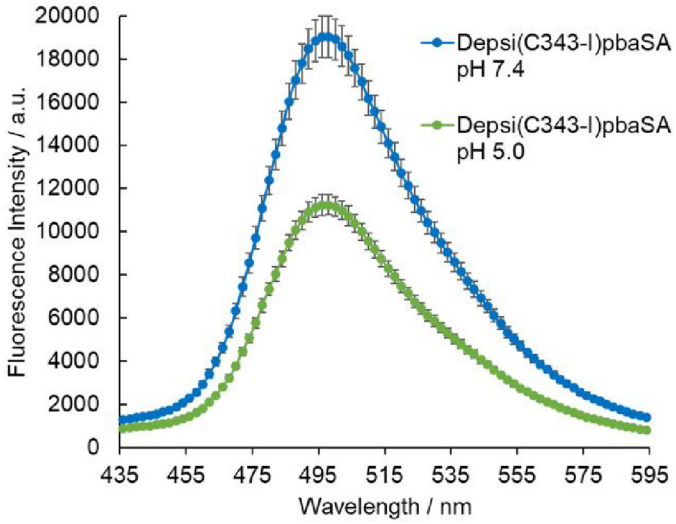

Figure S32: Fluorescence quenching of **1b** due to acidification. Spectra were recorded (excitation 405 nm) in triplicates after incubation of the peptide for 15 min at a concentration of 150 µM in a 9:1 mixture of phosphate buffer 5 mM pH 7.4 or 5.0 and DMSO.

3.10 Optical Properties

To check the influence of peptide fiber formation on coumarin 343 fluorescence, the peptides were dissolved in DMSO at a ratio of 5:1 of **1a** to **1b** or **3a** to **3b** and diluted with PBS or TAT containing PBS to 150 µM (ratio PBS:DMSO 9:1). To allow fiber formation samples were incubated overnight. To check fluorescence of monomeric peptides **3a/b** the peptides were incubated only in DMSO overnight at the same concentration. The control sample contained only PBS/DMSO. Emission was recorded at 435-600 nm (step size 2 nm) with a bandwidth of 20 nm. Samples were excited at 405 nm, bandwidth 10 nm (Figure S33). Measurements were performed in triplicates.

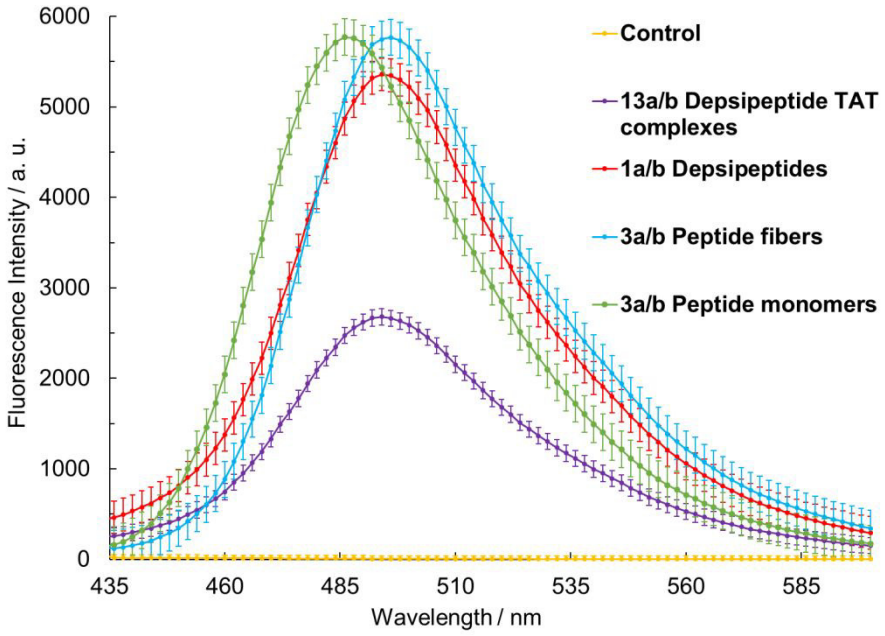

Figure S33: Fluorescence spectra of peptide mixtures after excitation at 405 nm in PBS/DMSO 9:1. In order to get a fluorescence spectrum of **3a/b** in the monomeric state, the peptides were incubated in DMSO without PBS to prevent assembly.

4. Cell Experiments

A549 cells were cultured in DMEM medium containing 10% fetal bovine serum and 1% penicillin/streptomycin as well as 1% MEM non-essential amino acids. Cells were seeded into confocal or well plates and left overnight to adhere at 37 °C, 5% CO_2.

4.1 Cell Uptake

Cells were seeded at a density of 15,000 cells/well in an 8-well confocal plate. After adhering for 24 h, cells were treated with the sample for different time points at 37 °C. Samples were preincubated to form the SHA-PBA complex **13a** and **13b** by dissolving the PBA-Depsi peptides **1a** and **1b** in DMSO and mixing with an equimolar amount of SHA-TAT **12**, which was dissolved in Dulbecco's PBS (PBS:DMSO 9:1). Sample solutions were diluted 1:4 with DMEM and incubated with the cells. Some samples were coincubated with the cells by addition of PMA (100 nM) in order to upregulate the hydrogen peroxide production in the cells. After the incubation time was over, the nucleus was stained with HCS NuclearMask Deep Red Stain for 30 min at 37 °C. The staining solution was removed, and fresh medium was added to the cells before they were imaged by confocal laser scanning microscopy (Figure 4 a and Figure S34).

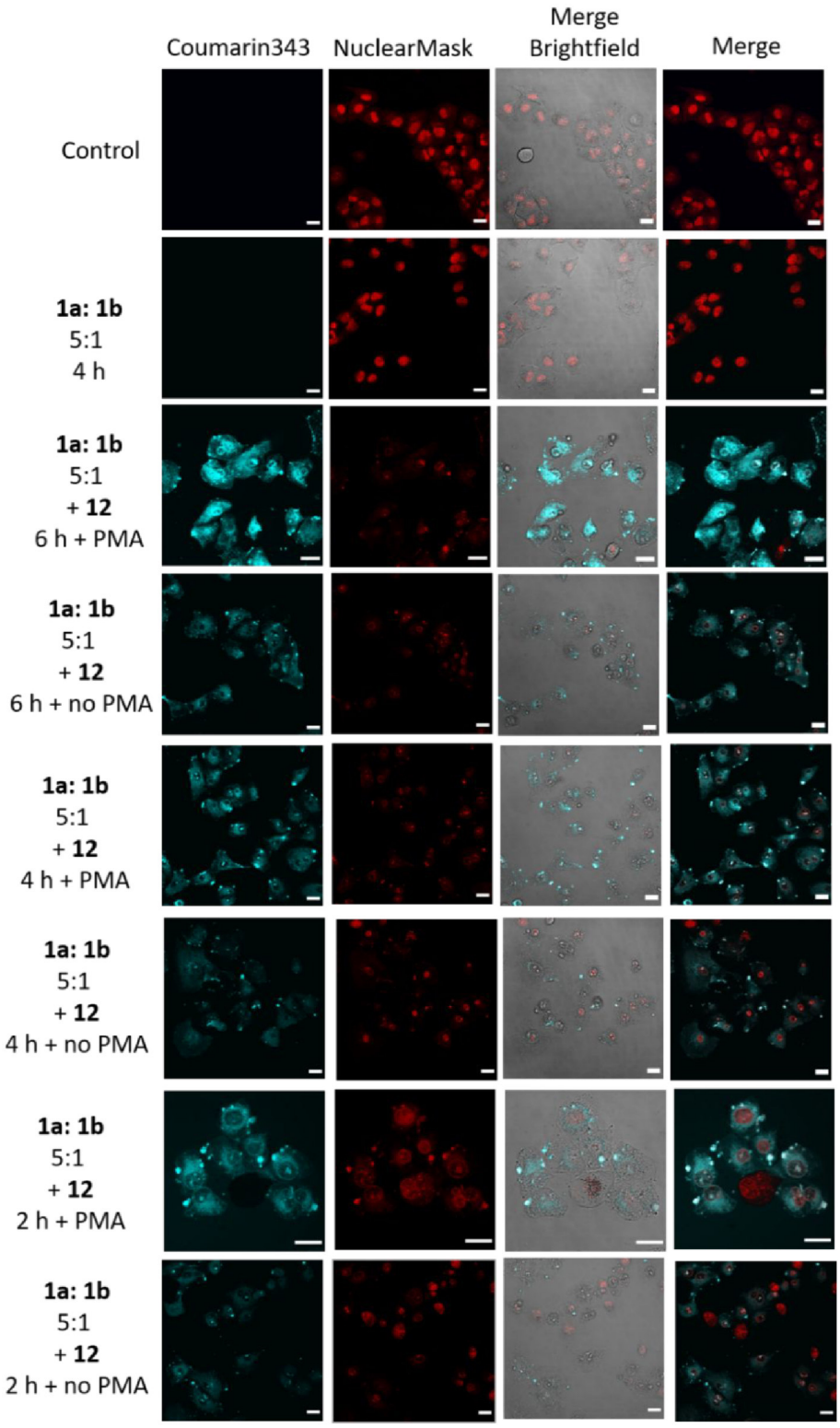

Figure S34: Confocal microscopy images of A549 cells incubated with peptides for different times with and without the addition of PMA. Peptide concentration was 150 µM in all samples. Scale bars 20 µm.

For imaging in the fluorescence microscope, cells that were incubated with the samples as described above were fixed with 4% paraformaldehyde solution for 20 min at room temperature (Figure S35).

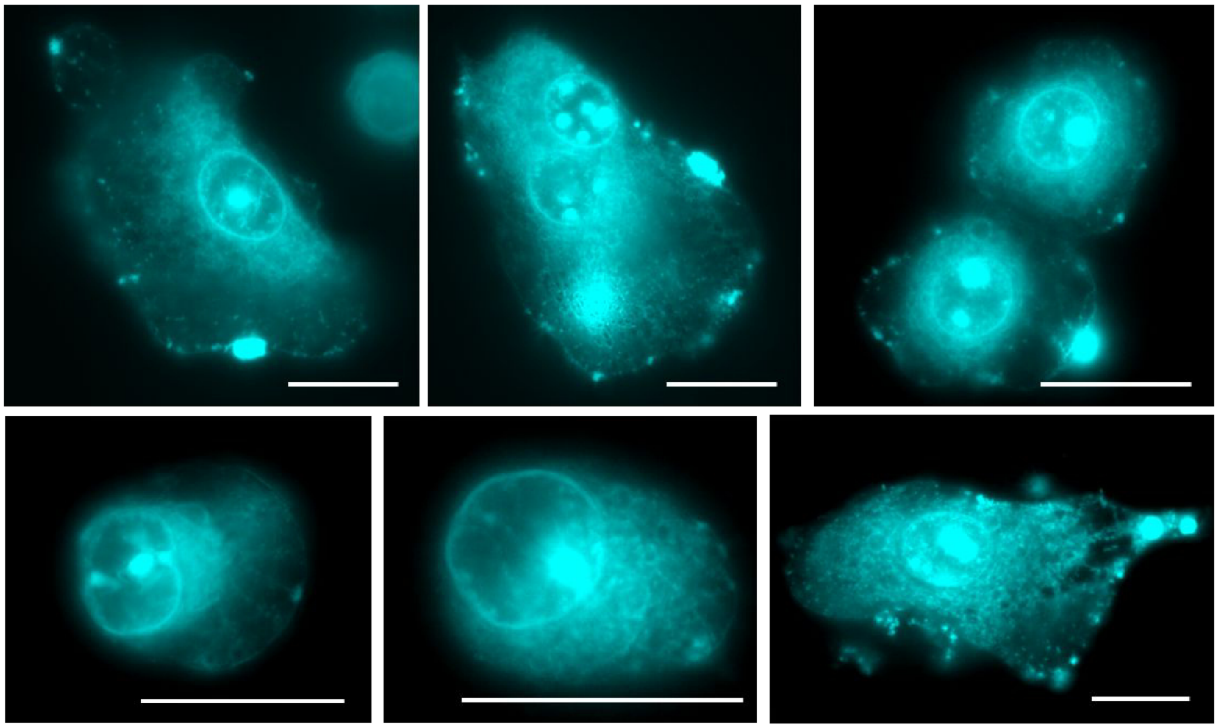

Figure S35: Fluorescence microscope images of **13a/b** treated A549 cells monitoring Coumarin 343. Scale bars 20 µm.

4.2 Staining of Cell Compartments

To elucidate the intracellular localization and uptake mechanism of the peptides confocal images were taken after staining of cell compartments. Cells were coincubated with 150 µM solutions of **13a/b** and 100 nM PMA as described before in Section 4.1. Cells were seeded at a concentration of 15,000 cells/well the day before the experiment and left to adhere, with the exception of endosomal staining, where cells were seeded two days prior to the experiment at 7,500 cells/well.

4.2.1 Staining of Endosomes and Lysosomes

After incubation with **13a/b** cells were washed and stained with 50 nM LysoTracker Green DND-26 for 5 min and washed before imaging by confocal microscopy (Figure S36). The peptides were found to be localized in lysosomes to a small extent.

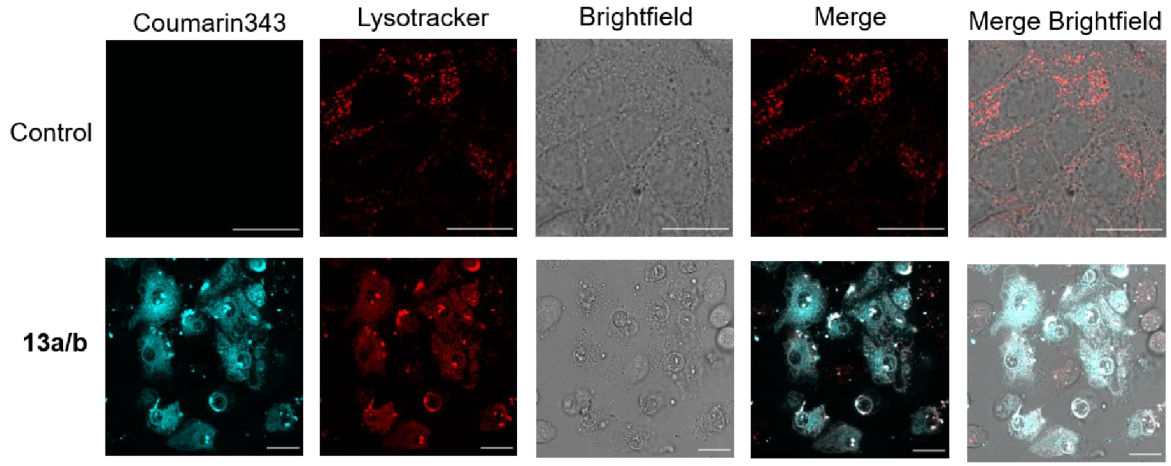

Figure S36: Confocal microscopy images of control cells and **13a/b** treated cells which were stained to visualize lysosomes. Scale bars 20 µm.

In order to proof the localization of the peptides in endosomes, adherent cells were transducted with either CellLight Early Endosomes-RFP or CellLight Late Endosomes-RFP one day after seeding and further incubated for 16 h for gene expression before the experiment was conducted. 4.5 µL of CellLight reagents were used for each well. After removal of the solution, **13a/b** was added as described before, after 4 h cells were washed with PBS once before imaging (Figure S37). Peptides were partial localized in endosomes, which indicates an endocytic pathway for cellular uptake.

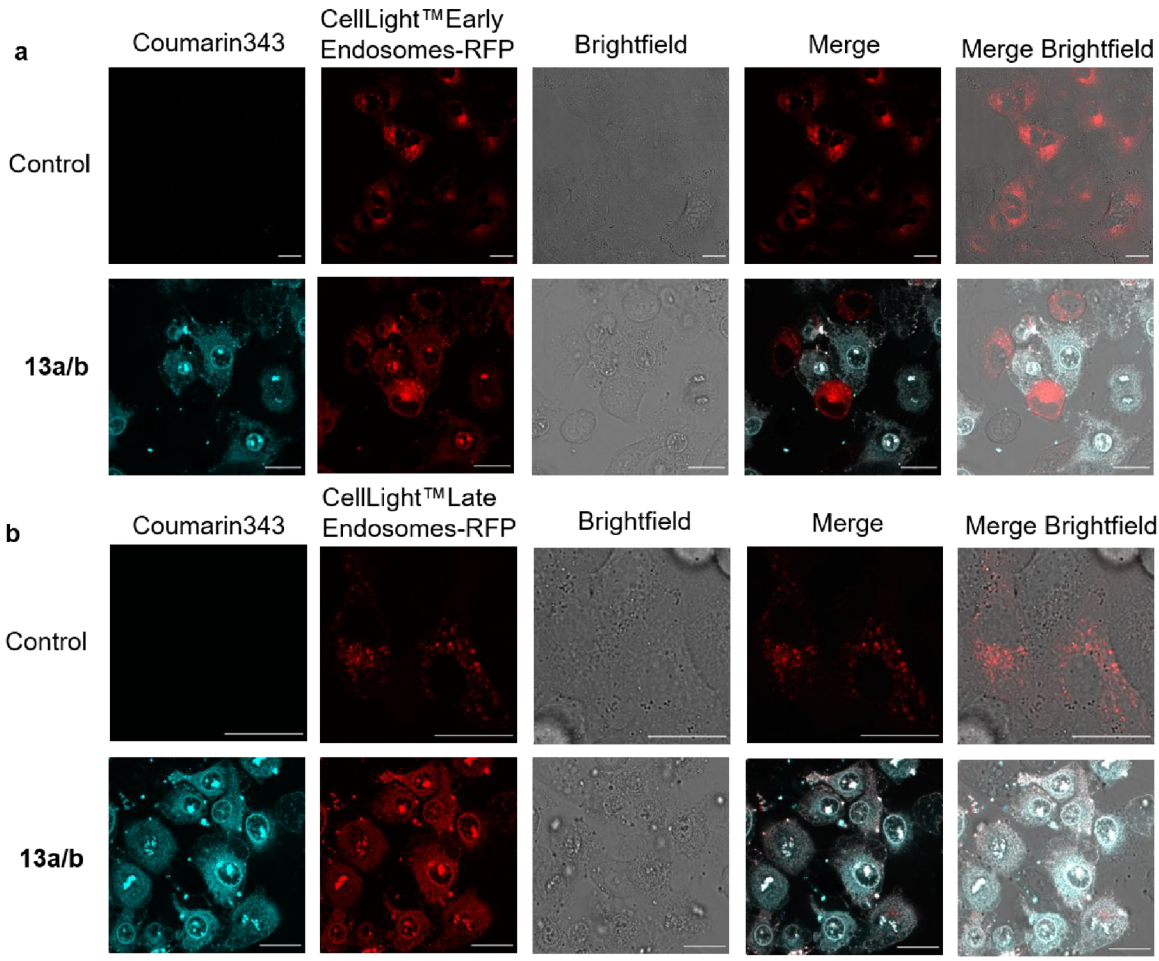

Figure S37: Confocal images of **13a/b** treated and control cell with fluorescently stained early and late endosomes. Scale bars 20 µm.

4.2.2 Staining of Nuclei and Determination of Nucleus Size

After incubation with **13a/b** cells were washed and stained with HCS NuclearMask Deep Red stain (after 250x dilution of the commercial stock solution) for 30 min and washed with PBS before imaging by confocal microscopy (Figure S38).

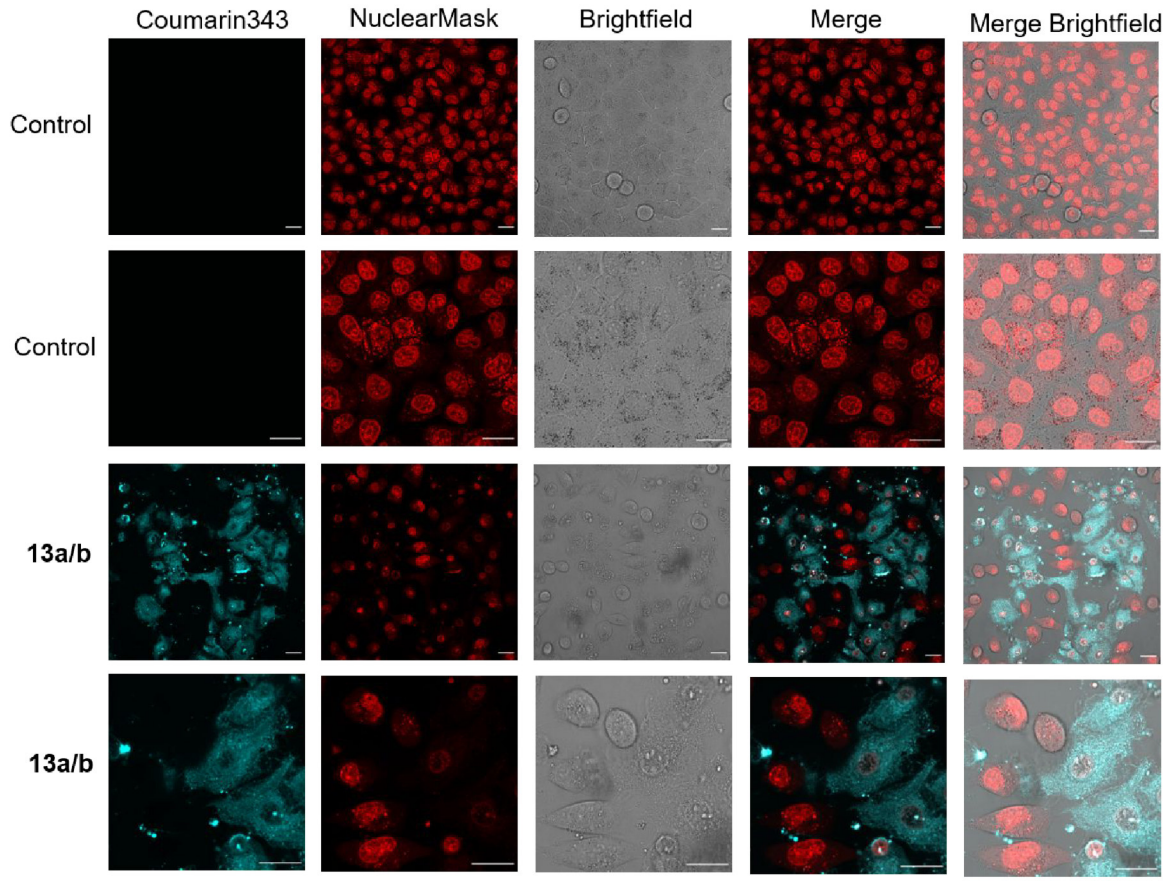

Figure S38: Confocal images of control cells and cells treated with **13a/b** for 4 h. Nuclei were visualized by staining. Scale bars 20 µm.

In order to quantify the changes in size of the nucleus upon peptide treatment, the nuclei of 20 cells of each control cells and peptide treated cells were measured at their widest point using ImageJ. The results showed that the average size of non-treated cells is 15.87±1.71 µm, while peptide treated cells had nuclei of a size of 9.28±2.23 µm (Figure S39).

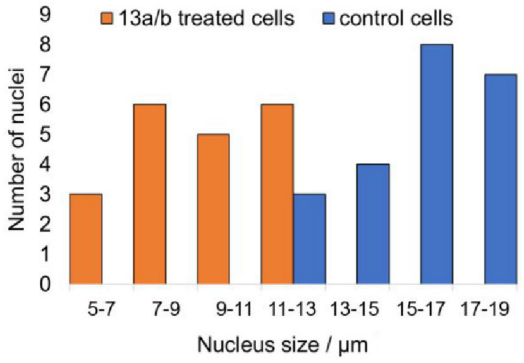

Figure S39: Distribution of nuclei size in untreated control cells and **13a/b** treated cells.

4.2.3 Staining of Nucleoli

After treatment of cells with **13a/b** and PMA as described above, the peptide solution was removed and cells were washed with PBS, after which they were fixed at -20 °C using methanol (10 min). After washing 2x with PBS, nucleoli were stained by incubation with 500 nM SYTO RNASelect Green for 20 min. Cells were imaged after washing two times with PBS. z-Stack images showed the localization of the peptides inside nucleoli (Figure S40).

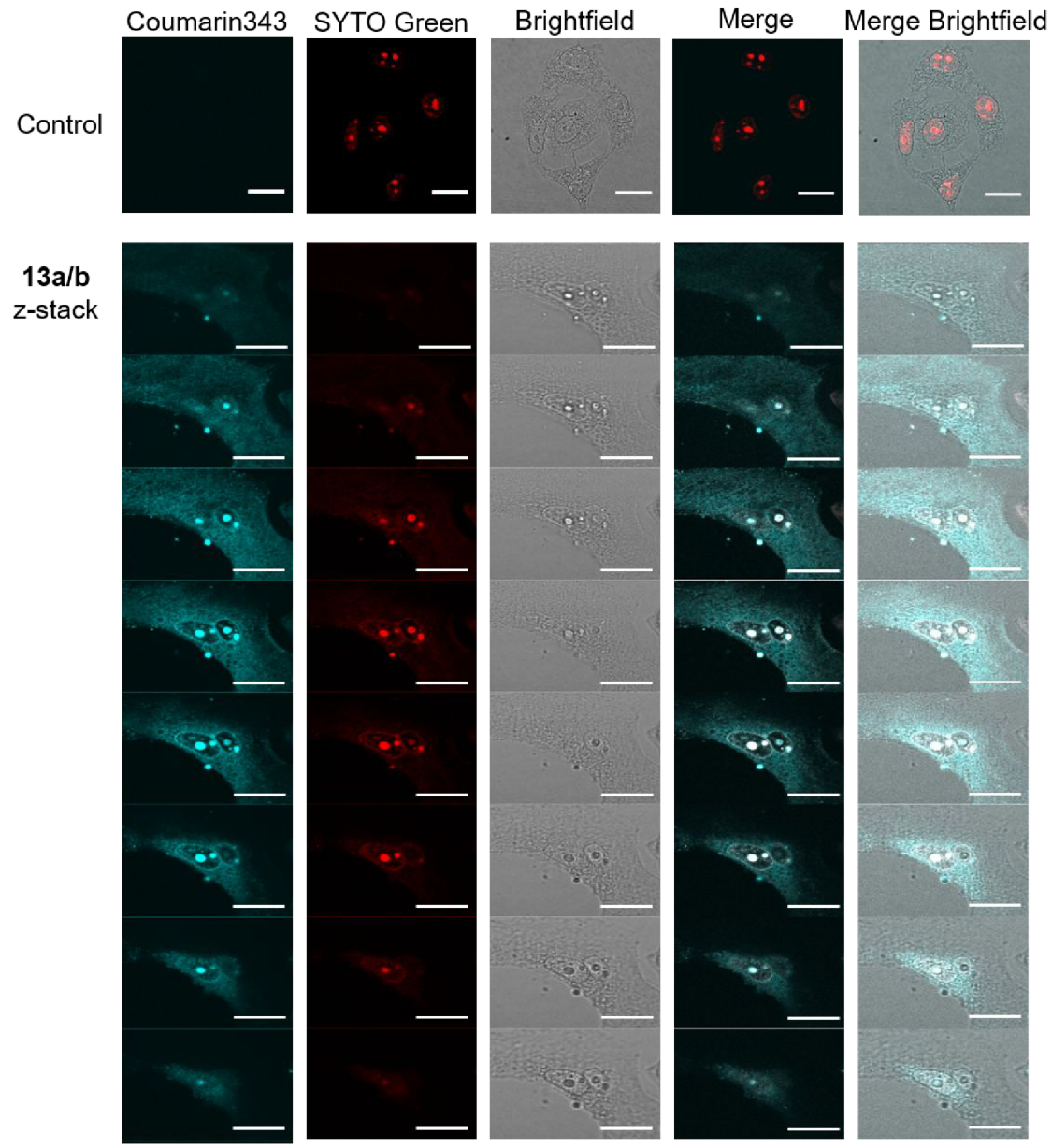

Figure S40: Confocal images of control cells and z-stack of **13a/b** treated cells showing the localization of the compounds inside nucleoli. Scale bars 20 µm.

4.2.4 Staining of the Cytoskeleton

To visualize the changes in morphology of cells upon fiber formation the cytoskeleton of control cells and **13a/b** cells were stained using Alexa Fluor 647 Phalloidin. After incubation with **13a/b** for 4 h, the cells were washed with PBS and fixed in 4% paraformaldehyde, after which the cells were incubated with the stain (330 nM in PBS) for 15 min. Cells were imaged with the confocal microscope after washing with PBS (Figure S41).

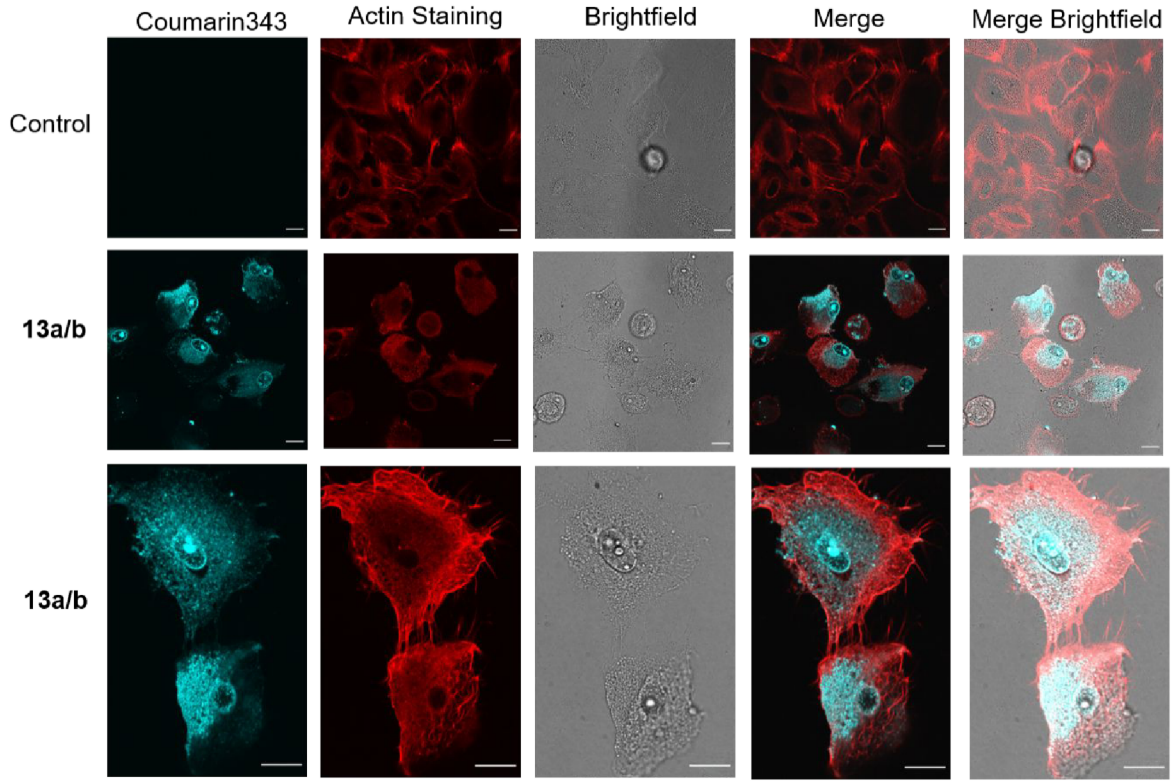

Figure S41: Confocal images of A549 cells after treatment with **13a/b** for 4 h and images of control cells. The cytoskeleton was stained using Alexa Fluor 647 Phalloidin. Scale bars 20 µm.

4.3 FRET inside Cells

For visualization of the disassembly of **13a/b** in confocal microscopy Förster resonance energy transfer between **1b** and fluorescent SHA-(Lys-5-FAM)-TAT **14** inside cells was imaged.

Cell were seeded in an 8-well confocal plate (7,500 cells/well) 2 days prior to the experiment and were left to adhere in an incubator as described before. Cells were coincubated with PMA and preformed complexes of **1a/b** with **14** to generate the boronic acid complexes with salicylhydroxamate **15a/b** following the protocol described before for generation of **13a/b**. After incubation with the peptides, cells were washed with PBS once and confocal imaging was performed (Figure S42).

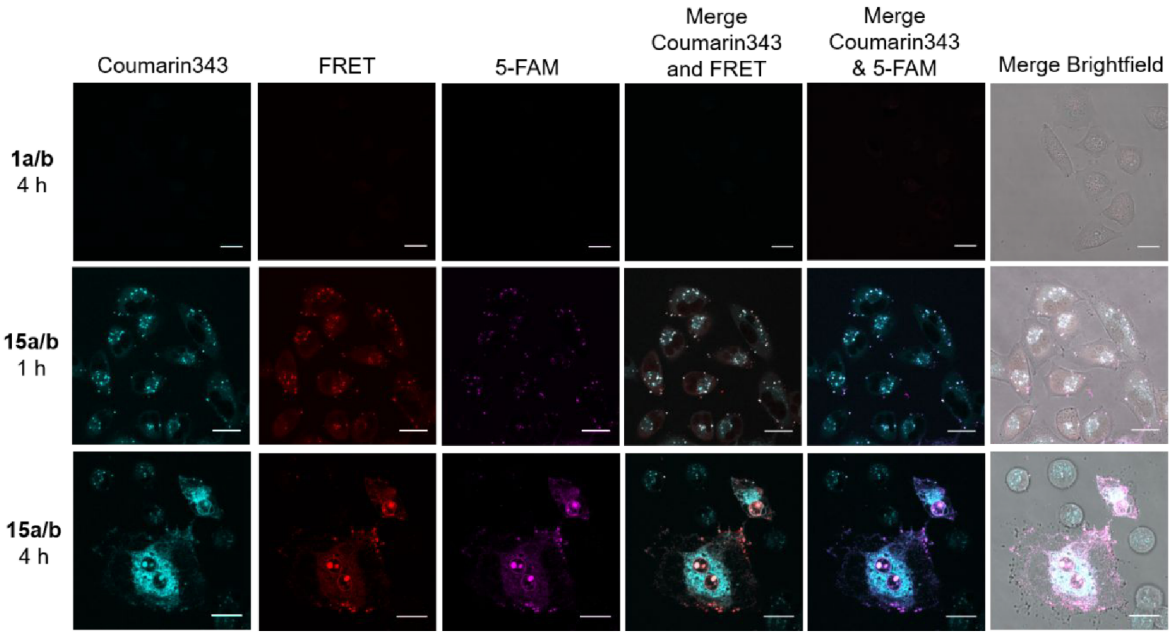

Figure S42: Confocal images of cells which were treated **1a/b** (top row) and **15a/b** (middle and bottom row). Scale bars 20 µm.

4.4 Isolation of Peptide Fibers by Cell Lysis

After cells were incubated in a confocal plate (8-well, 15,000 cells/well) and treated with a mixture of Depsi(Fmoc-I)pba-SA : Depsi(C343-I)pba-SA 5:1 (150 µM total) + 150 µM TAT as well as 100 nM PMA for 4 h, cells were washed with PBS three times and lysed using 100 µL RIPA buffer on ice for 5 min. Cells were treated using a cell scraper and the cell lysate was transferred into a PCR tube. After 5 min centrifugation, the upper part of the solution was transferred to another PCR tube to get a separation of the parts of the cell that were centrifuged down. Both fractions were analyzed in TEM (Figure 6 d and Figure S43). Grids were prepared as described above. For a control, A549 cells which were not treated with the peptides were also lysed and analyzed with TEM (Figure S44).

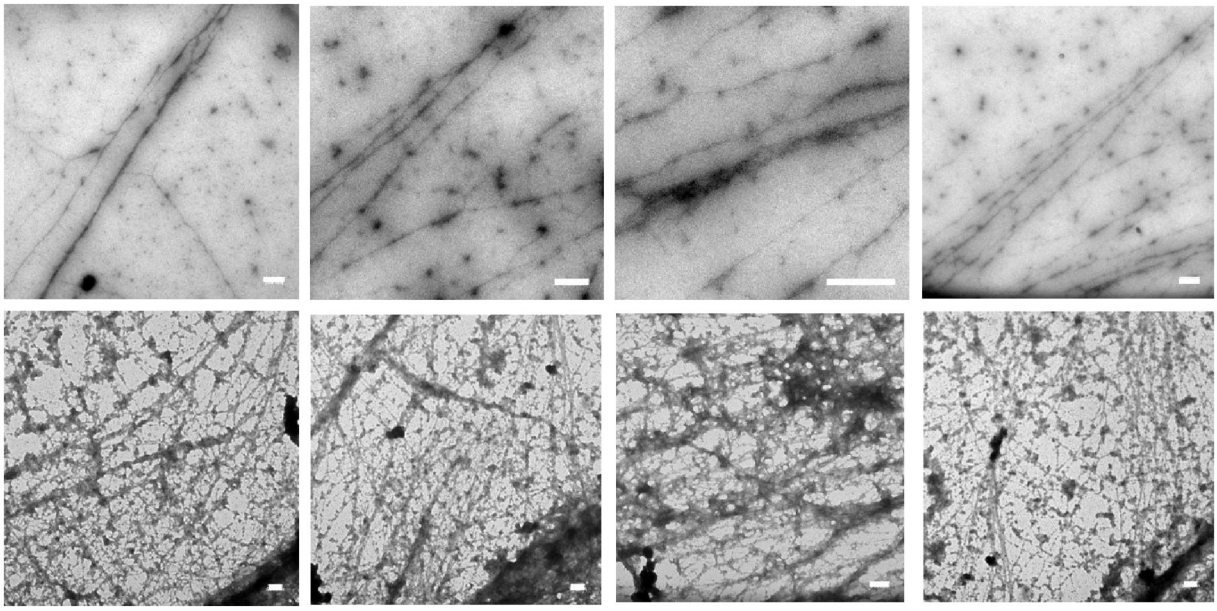

Figure S43: Peptide fibers isolated out of A549 cells. Top: lower density fraction after centrifugation. Bottom: higher density fraction. Scale bars 500 nm.

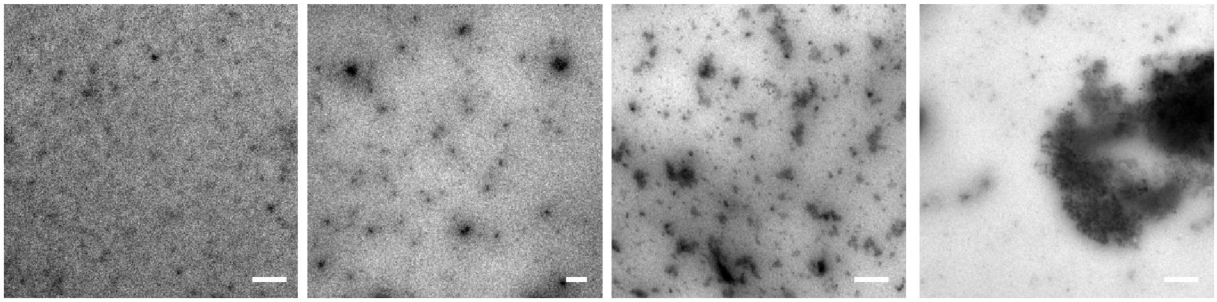

Figure S44: TEM images reflective of typical structures found in lysates of A549 cells. Scale bars 500 nm.

The fractions of peptide treated cells were also analyzed in the fluorescence microscope and the confocal microscope, with and without staining with Proteostat (1 µL of Proteostat solution, prepared as described before, in 20 µL of cell lysate).

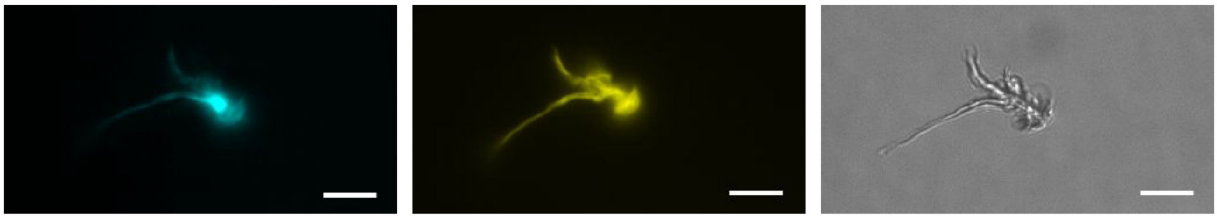

Figure S45: Fibrillar structures isolated by lysis from depsipeptide treated A549 cells. Cyan: Coumarin 343 fluorescence, yellow: Proteostat fluorescence, grey: brightfield image. Scale bars 10 µm.

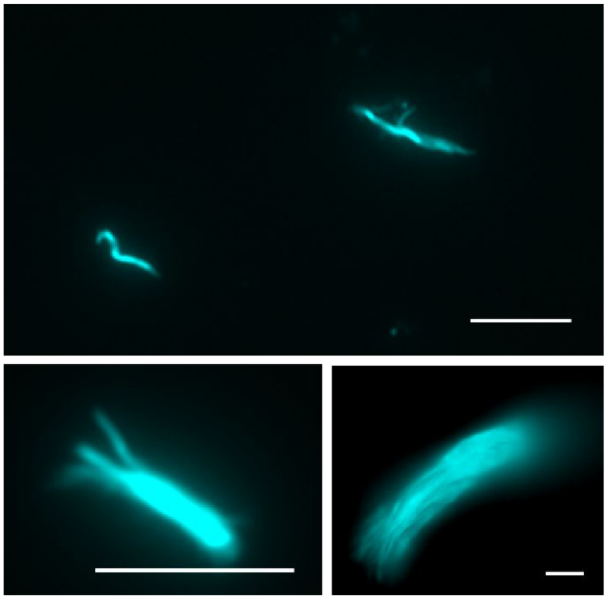

Figure S46: Fibrillar structures isolated by lysis from depsipeptide treated A549 cells. Cyan: Coumarin 343 fluorescence. Scale bar 10 µm.

The same experiment was repeated without the addition of PMA to show that the natural hydrogen peroxide production of A549 cells is sufficient to induce fiber formation (Figure S47 and Figure S48).

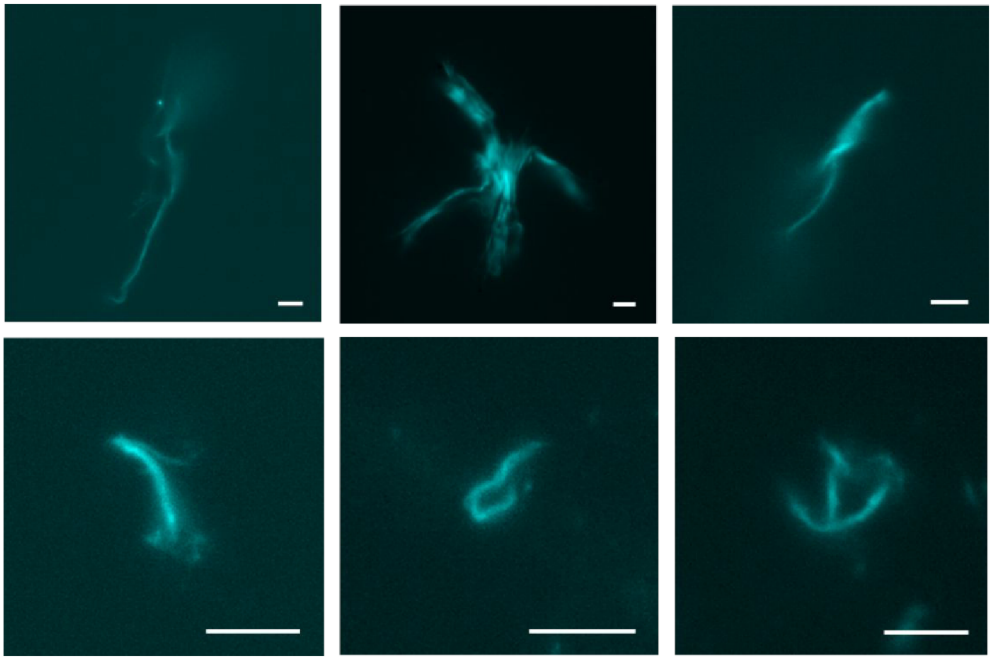

Figure S47: Fluorescence microscopy images of peptide fibers found in A549 cell lysate after incubation with **13a/b** for 4 h without addition of PMA. Images were taken in the coumarin 343 channel. Scale bars 5 µm.

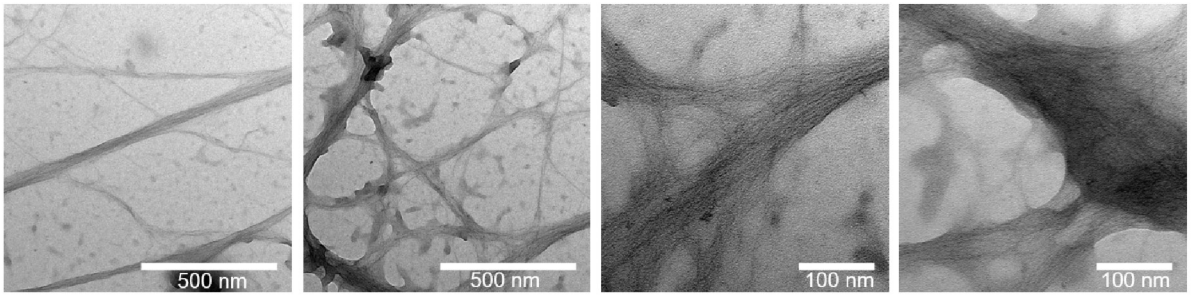

Figure S48: TEM images of peptide fibers in cell lysate of A549 cells, which were treated with **13a/b** for 4 h without addition of PMA.

4.5 Intracellular Linearization of Depsipeptides

Cells were seeded and treated with **13a/b** and PMA for 4h and lysed as described in Section 4.4. 100 µL of cell lysate were mixed with 400 µL methanol to precipitate proteins from the lysate. After centrifugation at 13,000 rpm at 4 °C for 20 min to remove the proteins and cellular debris, 180 µL of the supernatant was analyzed by analytical HPLC with a gradient starting from 5% ACN, which was kept constant for 1 min, after which the ACN content was increased linearly for 16 min to 100% ACN and kept constant for 5 min. An analytical ZORBAX Eclipse, XDB-C18, 80Å, 5 µm, 4.6 × 250 mm column was used.

The results showed that the linear peptide **3b** was formed inside cells (Figure S49).

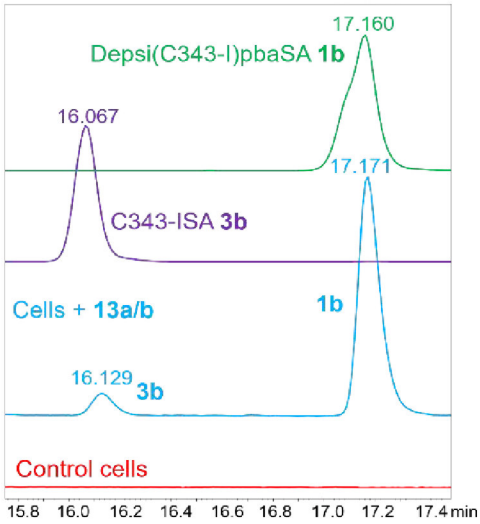

Figure S49: HPLC were spectra measured at 443 nm to monitor coumarin343 fluorescence of **1b** and **3b** in cell lysate of cells which were treated with **13a/b** (blue) or control cells which were not treated with the peptides (red)

and peptide solutions as controls to identify the peaks (green and purple). The retention times are indicated above the peaks.

4.6 TEM of Cells

Cells were seeded and grown on carbon pre-coated sapphire disks (3 mm; M. Wohlwend GmbH), which were autoclaved and freshly etched (30 s at 20% oxygen content) before use. After incubation with peptide, each sapphire disk was collected and slightly immersed into 1-hexadecene before placing them between two aluminum plates (3 mm, Plano). The aluminum plates with the sample were placed into a specimen holder for high pressure freezing in a Wohlwend HPF Compact 01 high pressure freezer with a pressure of 2100 bar for 2–3 s. The specimen holder was withdrawn from the freezer and immersed into liquid nitrogen to release the sample. The frozen sample was then labeled and stored in a container filled with liquid nitrogen. Subsequently, freeze substitution of the sample was carried out in a 0.5 mL Eppendorf tube using an AFS2 automated freeze substitution unit (Leica). Each tube contained 1 mL of freeze substitution solution, consisting of 0.2wt/vol% osmium tetroxide, 0.1wt/vol% uranyl acetate, and 5% distilled water in acetone. The tubes were firstly kept at –90 °C and slowly warmed up to 0 °C in 24 h. After keeping at room temperature for 1 h, the substitution solution was removed, and the samples were washed 3 times with acetone. Each sample was infiltrated in an ascending epoxy resin series (30%, 50%, and 75% in acetone) for 1 h before finally infiltration in 100% epoxy resin overnight. Finally, each sample was transferred into a new Eppendorf tube containing freshly prepared pure epoxy resin for polymerization at 60 °C for 24 h. After polymerization, sample blocks were kept at room temperature until their sectioning. Sample blocks for each time point were trimmed and sectioned into 100 nm sections by a 45º diamond knife (Diatome) in EM UC6 ultramicrotome (Leica). Sections were

then carefully placed onto 300-mesh carbon coated copper grid for standard bright-field imaging in Tecnai F20 200 kV transmission electron microscope (TEM) by FEI. Bright-field TEM micrographs were obtained with a Gatan US1000 2k CCD camera.

The TEM images (Figure S51) were stitched to show the entire cell (Figure 5 a and Figure S50).

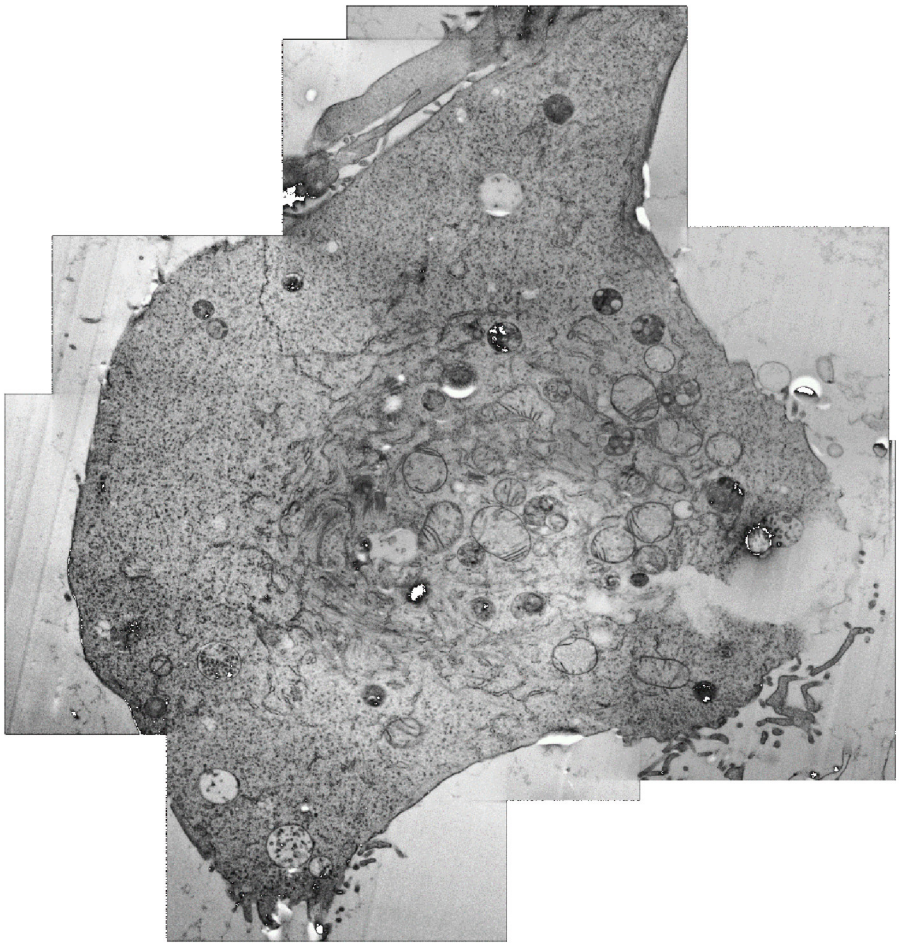

Figure S50: Stitched TEM image of an A549 cell showing intracellular peptide fiber formation.

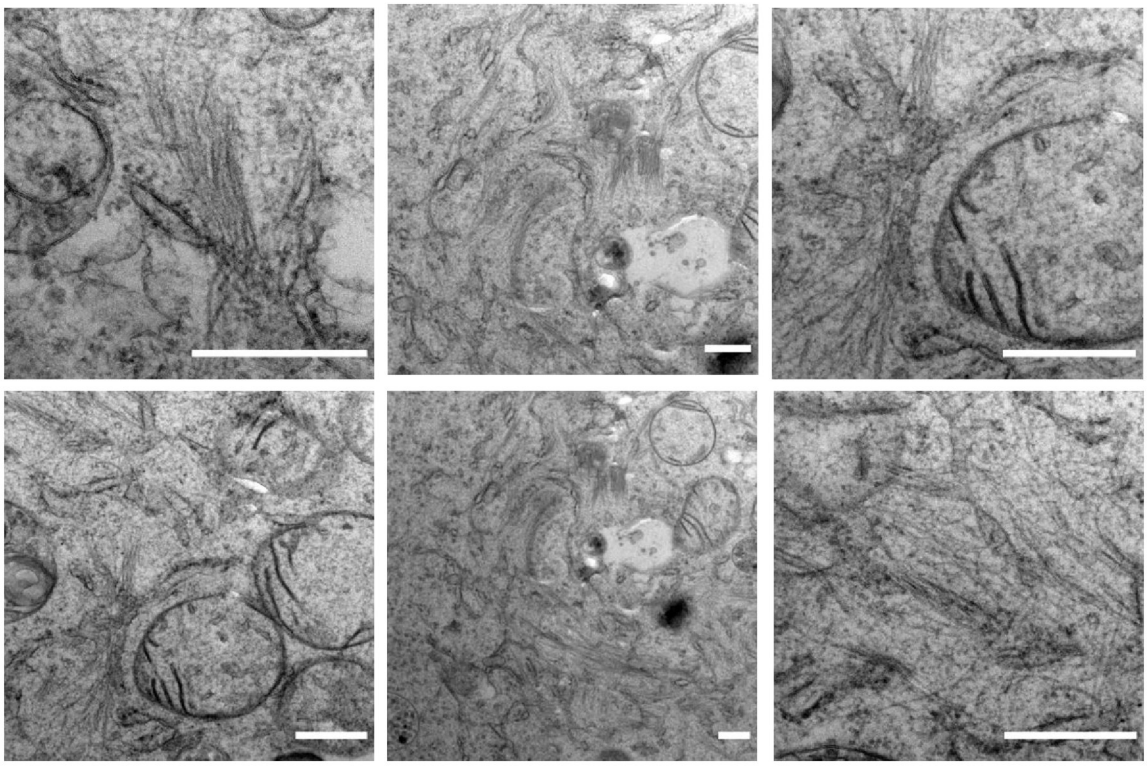

Figure S51: TEM images of peptide fibers inside an A549 cell. Scale bars 500 nm.

Furthermore, images of another cell were taken (Figure 5 b, Figure S52 and Figure S53).

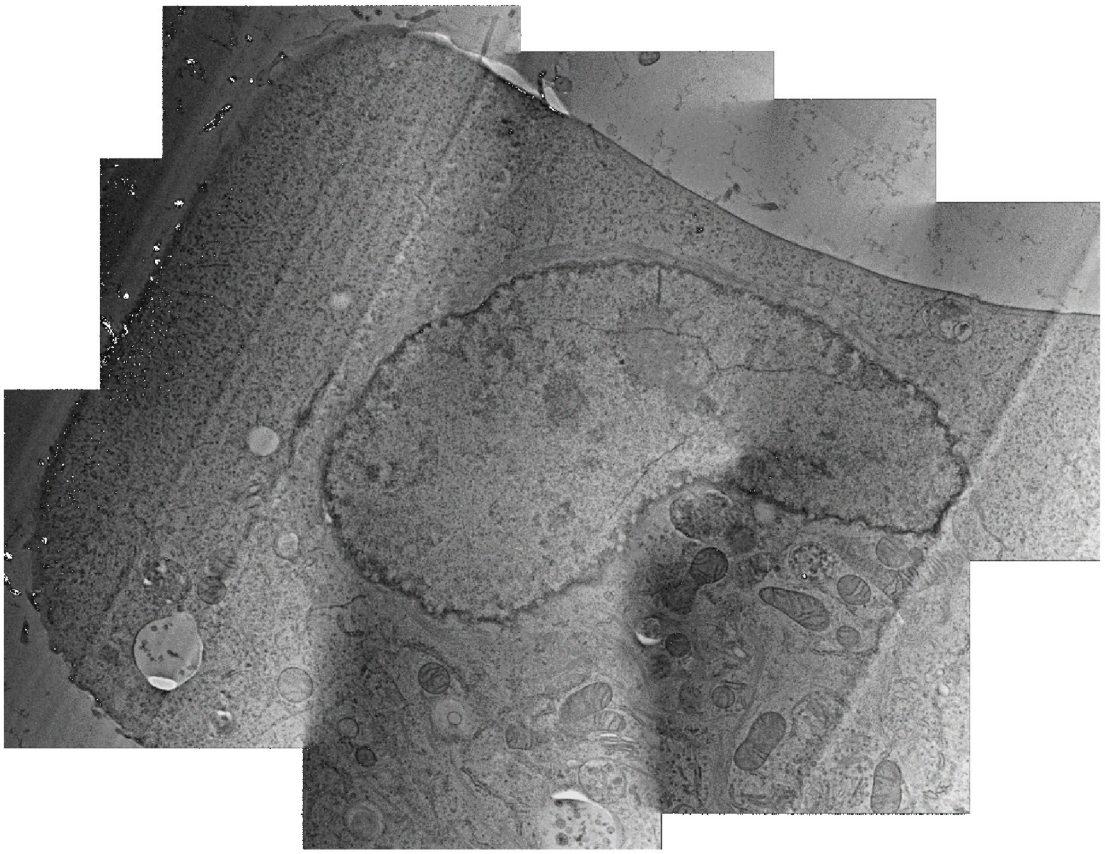

Figure S52: TEM image of the nucleus of an A549 cell, which was received after stitching TEM micrographs.

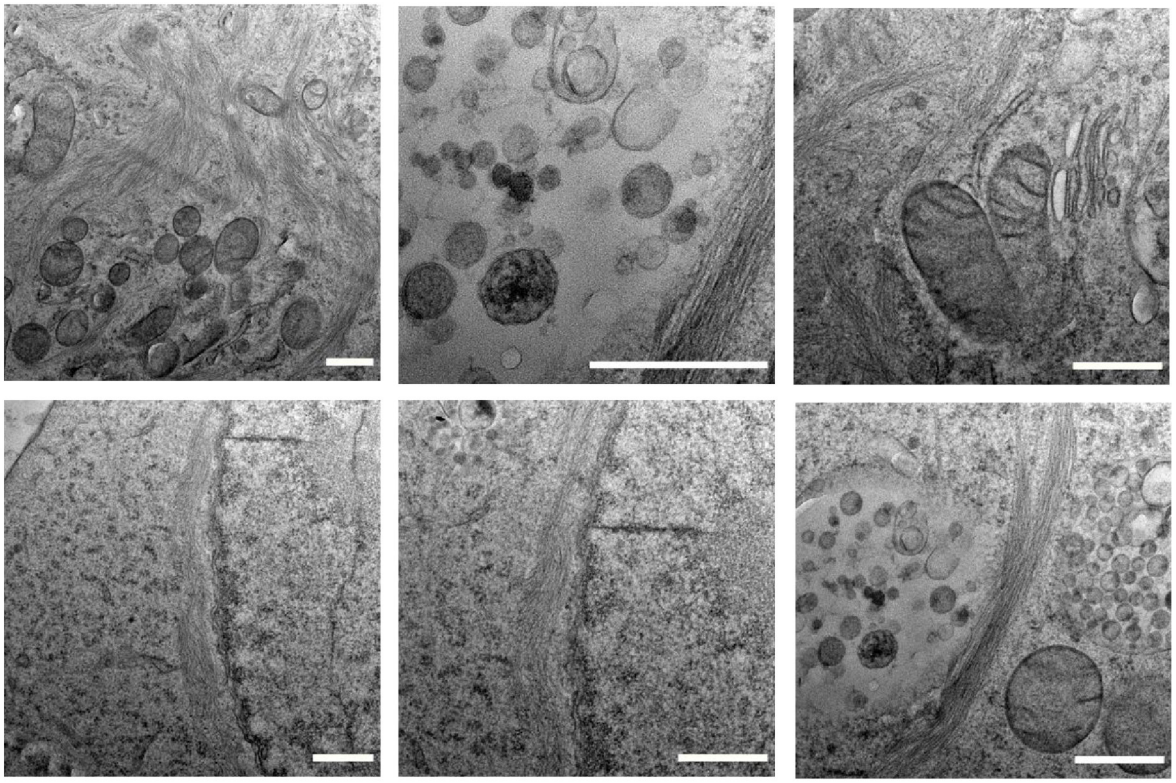

Figure S53: TEM images of peptide fibers inside an A549 cell. Scale bars 500 nm.

As a control, A549 cells which were not treated with the peptides were prepared as above and analyzed by TEM to show that the fibrillar structures derive from the peptides. No fibers were observed inside the cells (Figure S54 and Figure S55).

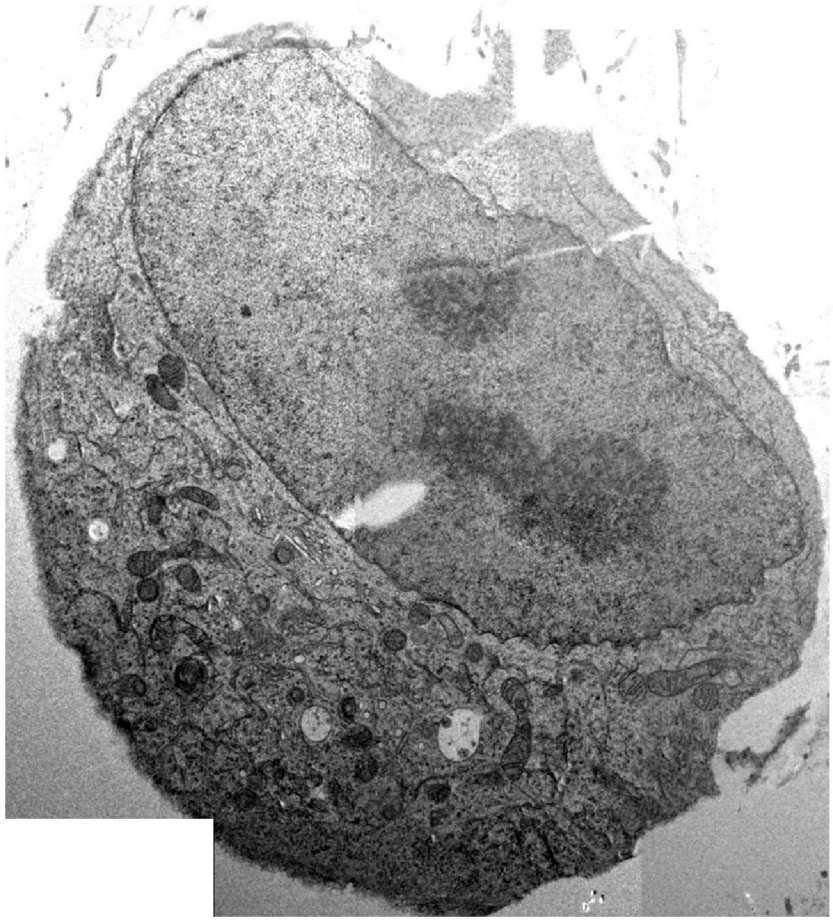

Figure S54: TEM image of a control A549 cell that was not treated with **13a/b** after stitching TEM micrographs. No fibers were observed in control cells, which were not incubated with peptides.

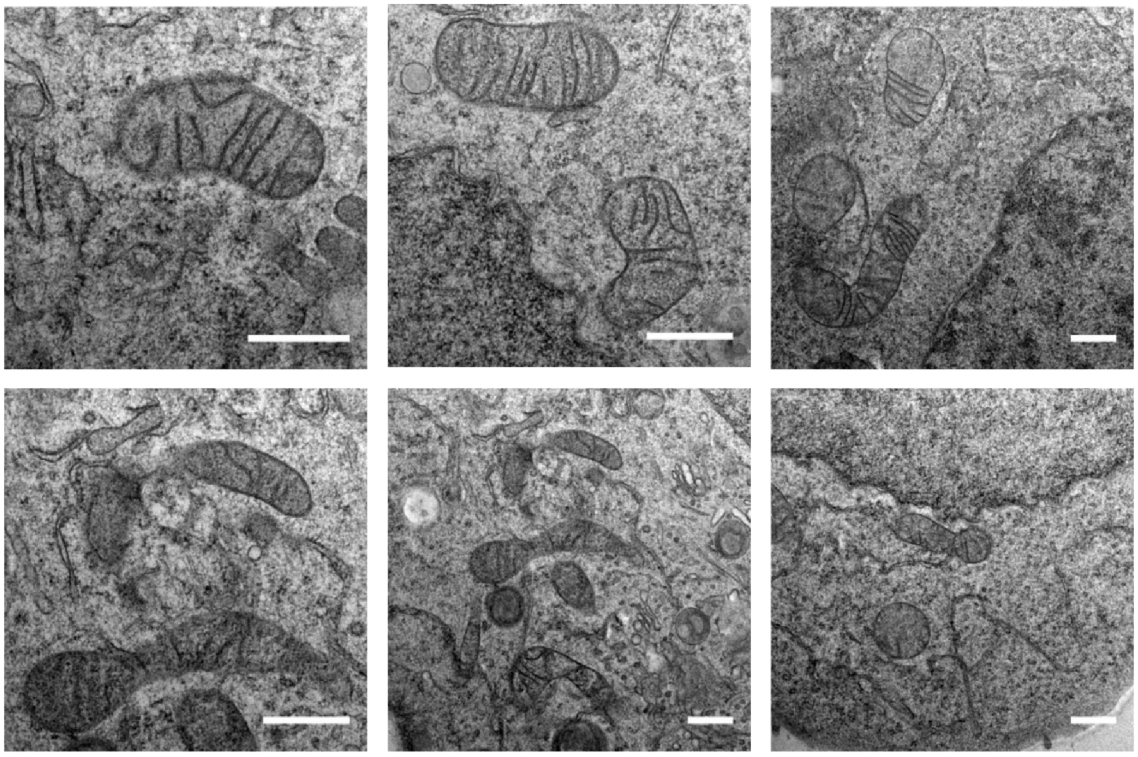

Figure S55: TEM micrographs of control A549 cells (scale bars 500 nm) which were not treated with the peptides.

4.7 Cytotoxicity

Cells were seeded at a concentration of 8000 cells/well in a white 96 half area well plate and were left to adhere overnight. Cells were treated with 50 µL sample solutions that were prepared as described before with different incubation times. After the incubation was finished, the same volume of CellTiterGlo Assay solution (prepared according to the protocol of the supplier) was added to the sample. After incubation for 10 min at room temperature, the luminescence was read out using the well plate reader Promega GloMax®-Multi Detection System, using the settings the instrument was supplied with. The assay was performed twice in triplicates (Figure 4c).

To investigate the influence of PMA coincubation on cell viability, A549 cells were incubated with 150 µM sample solutions of **13a/b** for 4 h with and without coincubation of 100 nM PMA (Figure S56). Each experiment was performed four times.

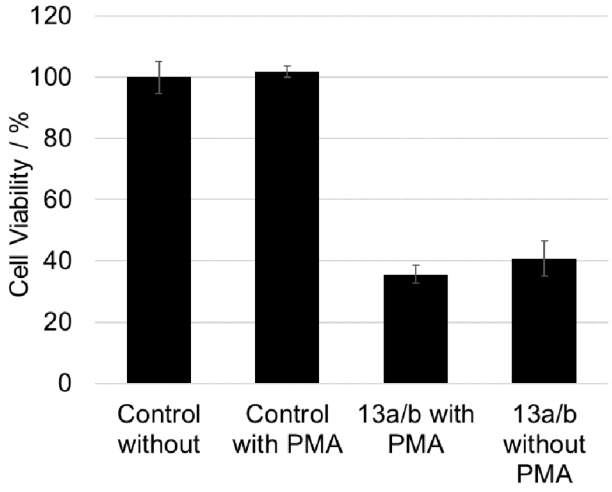

Figure S56: Cytotoxicity of **13a/b** towards A549 cells after 4 h incubation time with and without addition of PMA.

Apoptosis of **13a/b** treated cells was further visualized by Annexin V staining (Figure 5a). Here, cells were stained using Annexin V FITC and propidium iodine (PI) from the Annexin V Apoptosis Detection Kit FITC by Invitrogen. Cells were seeded at a density of 15,000 cells/well the day prior to the experiment and treated with **13a/b** and PMA following the protocol described in Section 4.1 for 2 and 4 h. After the incubation time was over, samples were removed and replaced with 200 µL of binding buffer from the assay kit and 5 µL of each Annexin V FITC and PI were added to each well. After 15 min of incubation at room temperature in the dark, the staining solution was removed and replaced with fresh binding buffer before imaging.

4.8 Intracellular hydrogen peroxide concentration

The intracellular hydrogen peroxide concentration of cells which were treated with PMA and cells which were not treated with PMA was determined using the Intracellular Hydrogen Peroxide Assay Kit by Sigma-Aldrich. Cells were seeded in a black cell culture 96 well plate

with clear bottom at a density of 8000 cells per well and were left to adhere overnight. Three wells of cells were prepared for each sample (PMA treated and non-treated control cells). To enhance the intracellular hydrogen peroxide concentration cells were treated with 100 nM PMA for 4 h. In order to measure the H_2O_2 concentration the fluorescent peroxide sensor was prepared following the protocol of the vendor and added to the cells after washing them with PBS. After incubation in the dark for 30 min cells were washed with PBS and fluorescence intensity was recorded using a well plate reader at 525 nm after excitation at 490 nm (bandwidth 10 nm each). To determine the concentration of H_2O_2 inside cells, a standard curve was generated by measuring the fluorescence intensity of a dilution series of hydrogen peroxide at the concentrations of 5, 2.5, 1.25, 0.625, 0.3125, 0.15625 and 0 µM (background blank) after incubation with the fluorescent sensor for 30 min in the dark following the vendor's protocol. All measurements for the standard curve and cells were performed in triplicates and the background blank was subtracted from all values. The intracellular H_2O_2 concentration of PMA treated cells was determined to be 2.45 ± 0.37 µM and non-treated cells had a concentration of 1.64 ± 0.16 µM (Figure S57).

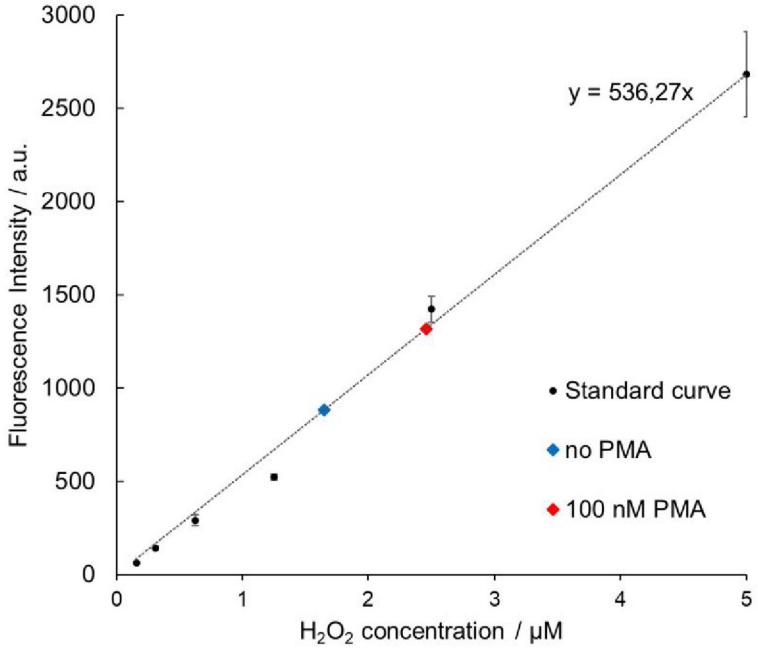

Figure S57: Standard curve for determination of the intracellular hydrogen peroxide concentration.

5. Literature

1. Bella, A. F.; Slawin, A. M. Z.; Walton, J. C., Approach to 3-aminoindolin-2-ones via oxime ether functionalized carbamoylcyclohexadienes. *J. Org. Chem.* **2004,** *69* (18), 5926-5933.

2. Husain, S. N.; Gentile, B.; Sauers, R. R.; Eichholz, A., Synthesis of photoaffinity labeling derivatives of D-glucose and D-galactose. *Carbohydrate Research* **1984,** *118*, 57-63.

3. Hockey, S. C.; Barbante, G. J.; Francis, P. S.; Altimari, J. M.; Yoganantharajah, P.; Gibert, Y.; Henderson, L. C., A comparison of novel organoiridium(III) complexes and their ligands as a potential treatment for prostate cancer. *Eur J Med Chem* **2016,** *109*, 305-313.

4. Kricheldorf, H. R.; Mueller, D., Secondary structure of peptides. 3. Carbon-13 NMR cross polarization/magic angle spinning spectroscopic characterization of solid polypeptides. *Macromolecules* **1983,** *16* (4), 615-623.

5. Shoji, A.; Ozaki, T.; Saito, H.; Tabeta, R.; Ando, I., Conformational characterization of solid polypeptides by carbon-13 NMR recorded by the cross polarization-magic angle spinning method: conformation-dependent carbon-13 chemical shifts of oligo- and poly(γ-benzyl L-glutamates) and sequential copolymers of γ-benzyl and γ-methyl L-glutamates and qualitative evaluation of side-chain orientation. *Macromolecules* **1984,** *17* (8), 1472-1479.

8.3 Sequence Programming with Dynamic Boronic Acid / Catechol Binary Codes

Marco Hebel[+], Andreas Riegger, Maksymilian M. Zegota, Gönül Kizilsavas, Jasmina Gačanin, Michaela Pieszka, Thorsten Lückerath, Jaime A. S. Coelho, Manfred Wagner, Pedro M. P. Gois, David Y. W. Ng[‡] and Tanja Weil[‡]

[+]first author, [‡]corresponding author

Published in *Journal of the American Chemical Society* **2019**, *141* (36), 14026-14031.

Date of Publication: 22. August 2019

Copyrights

Abstract

The development of a synthetic code that enables a sequence programmable feature like DNA represents a key aspect toward intelligent molecular systems. We developed herein the well-known dynamic covalent interaction between boronic acids (BAs) and catechols (CAs) into synthetic nucleobase analogs. Along a defined peptide backbone, BA or CA residues are arranged to enable sequence recognition to their complementary strand. Dynamic strand displacement and errors were elucidated thermodynamically to show that sequences are able to specifically select their partners. Unlike DNA, the pH dependency of BA/CA binding enables the dehybridization of complementary strands at pH 5.0. In addition, we demonstrate the sequence recognition at the macromolecular level by conjugating the cytochrome c protein to a complementary polyethylene glycol chain in a site-directed fashion.

Contributions

Marco Hebel: Synthesis and characterization of compounds. Design, planning and execution of experiments and analysis of data.

Andreas Riegger: Partially synthesized the boronic acid amino acid and some peptides. Contributed to MALDI, ^{1}H-NMR, binding assays and bioconjugation studies.

Maksymilian M. Zegota: Upscaling of many mixed sequence peptides in larger scale for NMR studies.

Gönül Kizilsavas: Executed 2D-NMR experiments and contributed to manuscript writing.

Manfred Wagner: Executed 2D-NMR experiments and contributed to manuscript writing.

Jasmina Gačanin: Was involved in scientific discussions. Performed and analyzed structural studies with FT-IR, this includes method development and optimization, and contributed to writing of the manuscript.

Michaela Pieszka: Performed CD spectroscopy measurements.

Thorsten Lückerath: Performed AFM measurements.

Jaime A. S. Coelho: Performed computational studies.

Pedro M. P. Gois: Performed computational studies.

David Y. W. Ng: Project and experiment design, supervision of experiments and discussion of the results, writing of the manuscript.

Tanja Weil: Acquiring funding for this project, project and experiment design, discussion of results and writing the manuscript.

JACS JOURNAL OF THE AMERICAN CHEMICAL SOCIETY

Communication

Cite This: J. Am. Chem. Soc. 2019, 141, 14026−14031

pubs.acs.org/JACS

Sequence Programming with Dynamic Boronic Acid/Catechol Binary Codes

Marco Hebel,[†,‡] Andreas Riegger,[‡] Maksymilian M. Zegota,[†,‡] Gönül Kizilsavas,[†] Jasmina Gačanin,[†,‡] Michaela Pieszka,[†,‡] Thorsten Lückerath,[†,‡] Jaime A. S. Coelho,[§] Manfred Wagner,[†] Pedro M. P. Gois,[§] David Y. W. Ng,*[,†] and Tanja Weil*[,†,‡]

[†]Max Planck Institute for Polymer Research, Ackermannweg 10, 55128 Mainz, Germany

[‡]Institute of Inorganic Chemistry I, Ulm University, Albert-Einstein-Allee 11, 89081 Ulm, Germany

[§]Research Institute for Medicines (iMed.ULisboa), Faculty of Pharmacy, Universidade de Lisboa, 1649-003 Lisbon, Portugal

Supporting Information

ABSTRACT: The development of a synthetic code that enables a sequence programmable feature like DNA represents a key aspect toward intelligent molecular systems. We developed herein the well-known dynamic covalent interaction between boronic acids (BAs) and catechols (CAs) into synthetic nucleobase analogs. Along a defined peptide backbone, BA or CA residues are arranged to enable sequence recognition to their complementary strand. Dynamic strand displacement and errors were elucidated thermodynamically to show that sequences are able to specifically select their partners. Unlike DNA, the pH dependency of BA/CA binding enables the dehybridization of complementary strands at pH 5.0. In addition, we demonstrate the sequence recognition at the macromolecular level by conjugating the cytochrome c protein to a complementary polyethylene glycol chain in a site-directed fashion.

Molecular interactions in Nature are often involved in a complex network of energy landscapes where individual components, from small molecules to organelles, form transient systems on demand.[1] Proteins have their origin within the genome, where molecular information is encoded and translated based on precise complexation and spatially controlled chemistry. In this respect, there has been much progress in the creation of artificial DNA prototypes to program molecular functions,[2,3] adapting both supramolecular[4−8] and dynamic covalent interactions.[9−12] Despite these successes in pursuit of artificial life, the advent of synthetic chemistry in this field remains far slower than their biochemistry counterparts.[13−16]

The development of synthetic DNA-type systems is deceptively challenging. On the sequence level, it is necessary that the interacting motifs are small so that both sterical demand and synthesis are not compromised by increasing sequence length. Molecularly, the binding event should be selective for complementary sequences while remaining dynamic and exchangeable in mild aqueous conditions. At first glance, synthetic functional groups in supramolecular chemistry (e.g., cyclodextrin,[17] curcubituril,[18] ureido-pyrimidinones[19]) or dynamic covalent chemistry (e.g., spiropyran,[20] diarylethenes[21]) seem to satisfy the above criteria. However, most motifs are either sterically bulky, offer too high binding constants already for the first binding event and/or they are laborious to be incorporated along a sequence.

Unlike most recognition motifs, the interaction between boronic acids (BAs) and electron rich vicinal diols such as catechols (CAs) fulfills these criteria well.[22] The binding complex is equipped with (1) small spatial requirement, (2) fast binding kinetics and (3) pH-responsiveness within the physiological range (5.0−7.4).[23] Hence, its dynamic covalent binding capabilities have been applied broadly in therapeutics,[24] biosensors,[25,26] stimulus responsive ligation tools[27] and as self-regenerative materials.[28,29] Herein, we propose that BA/CA motifs in a binary sequence would encode molecular recognition in a stimulus responsive fashion.

The permutation between binary "**1**/**0**" events and the length of the backbone defines the coding space (Figure 1). Inspired by peptide nucleic acids, a peptide backbone was designed to ensure greater hydrolytic stability.[30] Moreover, existing peptide synthesis methodologies facilitate the preparation of longer sequences, installation of customizable end groups and flexibility of spacer groups, i.e., lysine or alanine to control solubility, steric demand or surface charges. As a demonstration in a broader context, a protein (cytochrome c) and a polymer (polyethylene glycol) were conjugated via these dynamic covalent tags to demonstrate recognition specificity at the macromolecular level.

The unnatural amino acid **7** containing the BA was synthesized based on a protocol for iodo-phenylalanine (Scheme 1).[31] L-Phenylalanine was iodinated to afford **1**, with the carboxylic acid and the amine groups protected by the methyl ester (**2**) and the boc group (**3**), respectively. Suzuki−Miyaura borylation was conducted to install the BA pinacol ester moiety (**4**) with a subsequent global deprotection to yield the boronated L-phenylalanine **5**. Here, a switch in protecting groups is necessary because the pinacol ester is sensitive to microwave conditions. Additionally, longer sequences containing multiple BA cause aggregation on the solid phase. Thus, after the installation of the fmoc moiety (**6**), the BA was protected with a highly bulky pinanediol to afford **7**. The

Received: March 28, 2019
Published: August 22, 2019

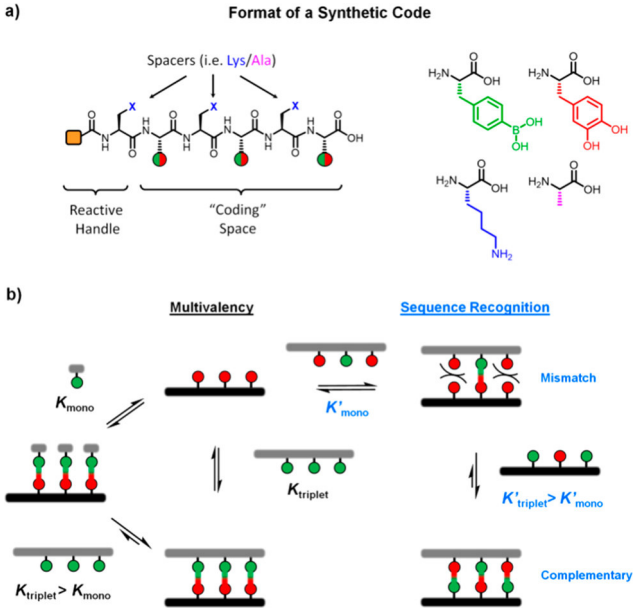

Figure 1. (a) Peptide scaffold to code a binary BA/CA pairing. (b) Thermodynamic processes involved in multivalent effects, complementary and mismatched sequences.

corresponding CA containing amino acid, dihydroxy-L-phenylalanine, was commercially available.

Peptide sequences containing all permutations of BA and CA in a hexa/octa-peptide format were synthesized to elucidate the influence of sequence, length and positional defects. The amino acids that do not participate in the coding segment are filled by lysines (**X**) to improve water solubility. To demonstrate the chemical versatility, the N-terminus was modified with reactive functionalities, i.e., amine, thiol or maleimide (Scheme 1). In this way, oligopeptides containing one, two and three BA [$(\mathbf{AX})_1$, $(\mathbf{AX})_2$, $(\mathbf{AX})_3$] as well as their complementary CA counterparts [$(\mathbf{BX})_1$, $(\mathbf{BX})_2$, $(\mathbf{BX})_3$] were synthesized. The binding affinities of the dynamic covalent interactions between $(\mathbf{AX})_1$-$(\mathbf{BX})_1$, $(\mathbf{AX})_2$-$(\mathbf{BX})_2$, $(\mathbf{AX})_3$-$(\mathbf{BX})_3$ were evaluated by fluorescence microscale thermophoresis in 300 mM phosphate buffer, pH 7.4 (Figure 2a).

In each series, fluorescein labeled BA peptides act as the template strand and are titrated with their complementary CA peptides. For a single BA/CA binding event, $(\mathbf{AX})_1$-$(\mathbf{BX})_1$, a binding affinity of 1300 ± 300 M^{-1} was observed, which is consistent with published data.[32] By increasing the binding event to divalent $(\mathbf{AX})_2$-$(\mathbf{BX})_2$ and trivalent $(\mathbf{AX})_3$-$(\mathbf{BX})_3$, a respective 10-fold (12 500 ± 1100 M^{-1}) and 70-fold (81 400 ± 7300 M^{-1}) increase were observed. Importantly, the absence of binding errors to form unstructured aggregates was supported by the defined fluorescence decay and dynamic light scattering (Figure S4). The binding of $(\mathbf{AX})_3$-$(\mathbf{BX})_3$ was also confirmed independently by Förster resonance energy transfer (FRET) (Figure S5). The lesser increase in binding affinity with each subsequent binding code suggests that energy is required to compensate the backbone structure in the bound state. By bringing the findings into perspective of DNA hybridization,

Scheme 1. Synthesis of BA Containing Amino acid 7 and the Chemical Structures of a Small Library of BA/CA Peptide Codes

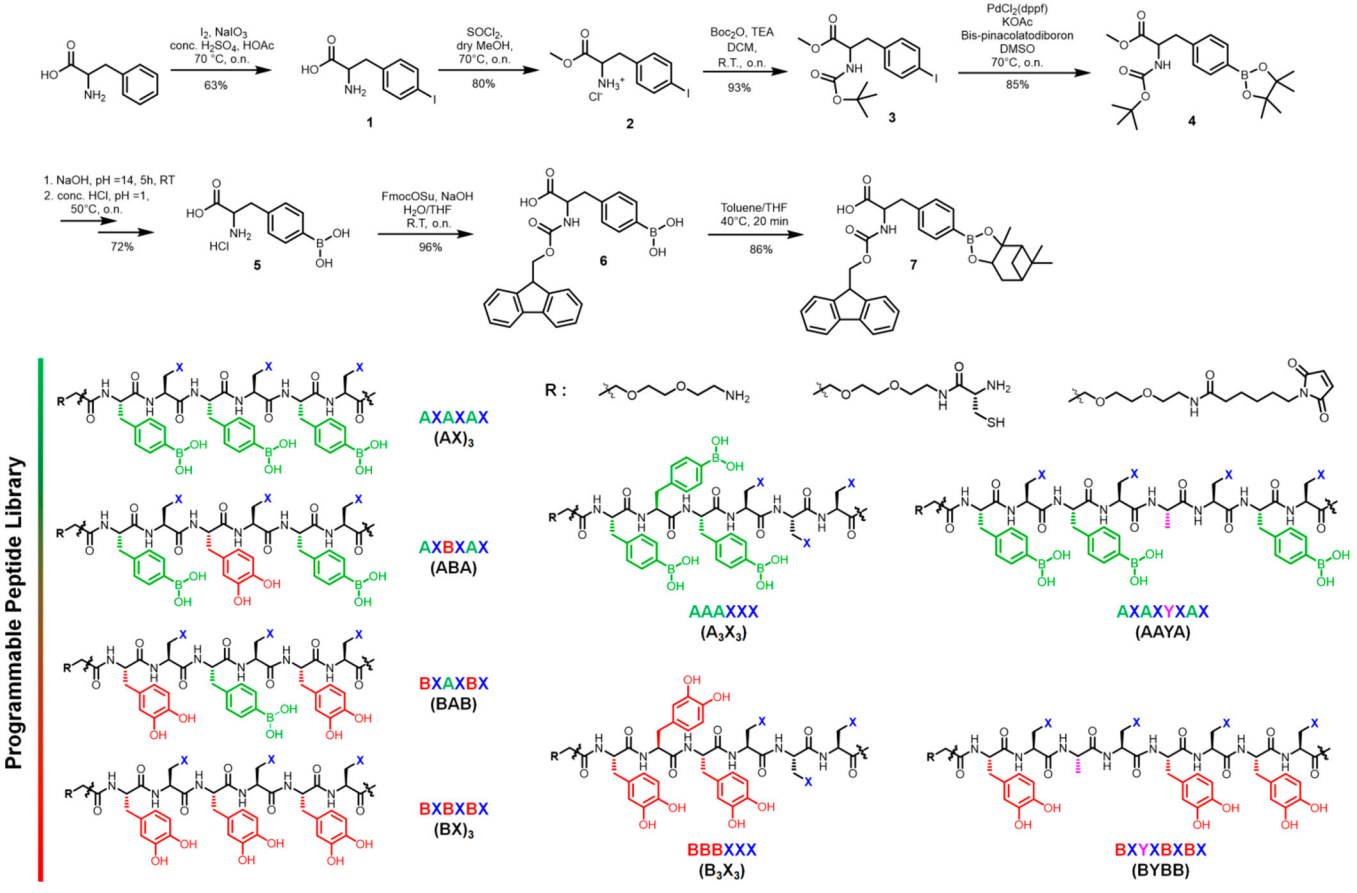

DOI: 10.1021/jacs.9b03107
J. Am. Chem. Soc. 2019, 141, 14026−14031

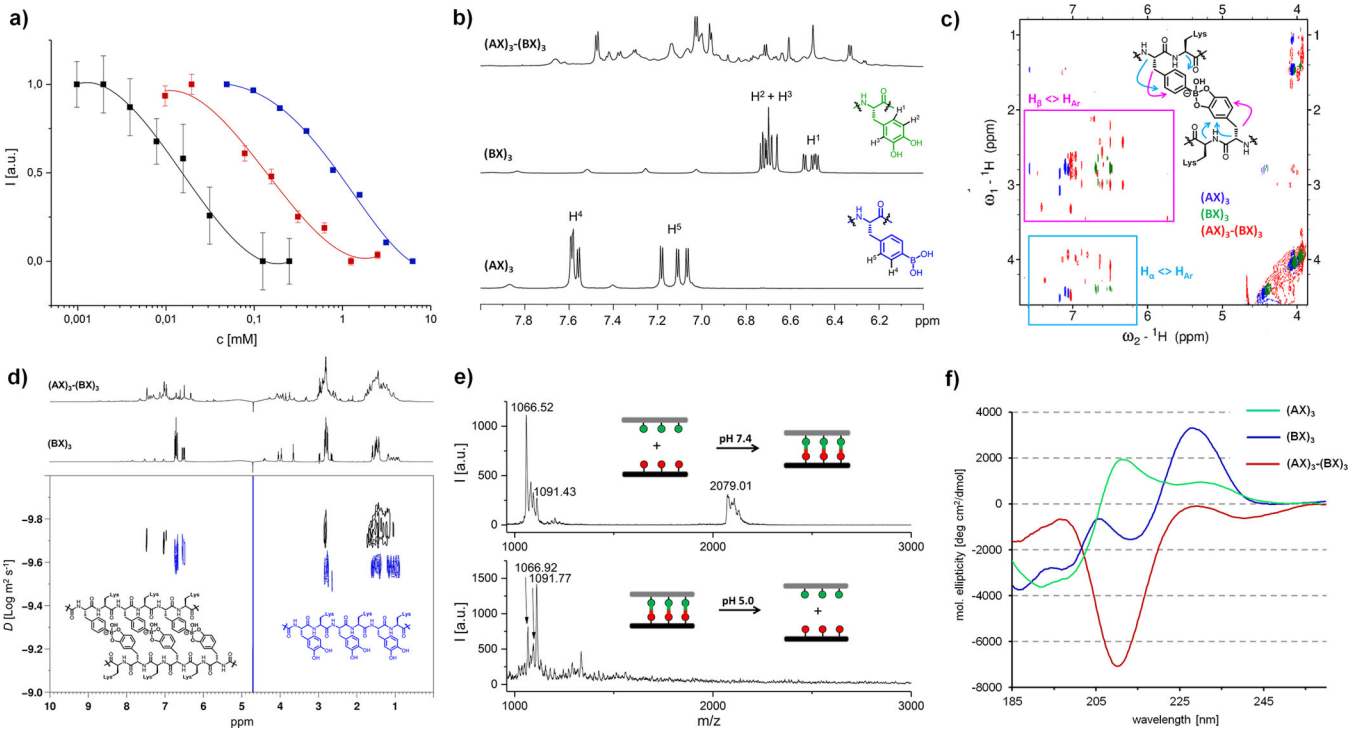

Figure 2. Characterization of multivalent binding of complementary BA/CA codes. (a) Binding affinity determination of $(\mathbf{AX})_1$-$(\mathbf{BX})_1$ (monovalent, blue), $(\mathbf{AX})_2$-$(\mathbf{BX})_2$ (divalent, red) and $(\mathbf{AX})_3$-$(\mathbf{BX})_3$ (trivalent, black) by fluorescence microscale thermophoresis in 300 mM phosphate buffer, pH 7.4. (b) ^{1}H NMR and (c) ^{1}H NOESY of $(\mathbf{AX})_3$, $(\mathbf{BX})_3$ and $(\mathbf{AX})_3$-$(\mathbf{BX})_3$ complex in 300 mM phosphate buffer, pH 7.4, 9:1 (H_2O:D_2O), 298 K. (d) DOSY of the $(\mathbf{AX})_3$-$(\mathbf{BX})_3$ complex against $(\mathbf{BX})_3$ in 300 mM phosphate buffer, pH 7.4, 9:1 (H_2O:D_2O), 298 K. (e) MALDI-TOF of $(\mathbf{AX})_3$-$(\mathbf{BX})_3$ at pH 7.4 (top) and pH 5.0 (bottom). (f) Circular dichroism spectroscopy of $(\mathbf{AX})_3$-$(\mathbf{BX})_3$ and their separate components at phosphate buffer pH 7.4, 298 K.

the binding affinity of $(\mathbf{AX})_3$-$(\mathbf{BX})_3$ is comparable to about eight base pairs (with 50% G-C content) on a DNA level.[33,34]

The binding structure of the $(\mathbf{AX})_3$-$(\mathbf{BX})_3$ complex was characterized by multidimensional ^{1}H NMR spectroscopy. The binding of the boronic acids and catechols leads to the complete transformation of the chemical environment, shifting the ^{1}H aromatic signals of the components (Figure 2b, S6). Resonance peaks of the boronic acids $^1H_{AR}$ in the total correlation spectroscopy (TOCSY) were shifted into high-field confirming that the boron center becomes less electron withdrawing upon binding (Figures S7 and S8). Nuclear Overhauser effect spectroscopy (NOESY) analysis of $(\mathbf{AX})_3$-$(\mathbf{BX})_3$ shows many additional and shifted intramolecular through space ^{1}H-couplings compared to the separate components (Figures 2c, S9 and S10). These new interactions ascertain the formation of chemical environments that increase the intramolecular through space interactions between the aromatic groups and the H_α, H_β of the boronic acid or catechols. Diffusion ordered NMR (DOSY) confirms the binding event as an increase in the diffusion time of the complex (Figures 2d and S11). Additionally, the monovalent complexes are stable to heat up to 70 °C at the using variable temperature NMR (Figures S15–S19).

The observed BA–CA interaction was supported independently by matrix-assisted laser desorption/ionization-time of flight (MALDI-TOF) MS, where the formation of $(\mathbf{AX})_3$-$(\mathbf{BX})_3$ was characterized by an m/z value at 2079.01 at pH 7.4 (Figure 2e, top). Noteworthy, significant fragmentation of the complex occurs due to the acidic nature of the matrix (α-cyano-4-hydroxycinnamic acid, α-CHCA). At pH 5.0, only separate components of $(\mathbf{AX})_3$ and $(\mathbf{BX})_3$ were found (Figure 2e, bottom). In the Fourier-transform infrared (FTIR) of $(\mathbf{AX})_3$-$(\mathbf{BX})_3$, the vibrational mode at 1289 cm^{-1} was lost while a new peak was observed at 1495 cm^{-1}, suggesting an increase in bond energy and C=C character for the dynamic covalent interaction (Figure S20).[35,36] The electron deficient boron withdraws electrons through the vicinal diols, which reduces the electron density of the catechol aromatic system.

Circular dichroism spectroscopy found that, at pH 7.4, the $(\mathbf{AX})_3$-$(\mathbf{BX})_3$ complex shows a strong negative molar ellipticity at 210 nm, corresponding to the n-π^* transition of the carbonyl group (Figure 2f, S21). Together with the absence of Cotton effects, these observations imply that the tetrahedral boron center has a strong through-space effect on the C=O bond. Density functional theory (DFT) calculations confirmed that hydrogen bonding interactions between the hydroxyl groups of the tetrahedral boron and the carboxyl groups of lysines contribute to lowering the electronic energy of $(\mathbf{AX})_3$-$(\mathbf{BX})_3$ (Figures 3a, S23 and S24). The combination of these observations seems to corroborate the shifts associated with the TOCSY, NOESY cross-peaks. In contrast, at pH 5.0, there is no interaction between the complementary sequences (Figure S21). Here, DFT calculations using a simplified structure revealed a low activation energy (10 kcal mol^{-1}) for the first boron–oxygen (catechol) bond breaking step, representing the fast hydrolysis of the tetrahedral boron observed at acidic pH (Figure S26).

Interestingly, sequences containing consecutive BA/CA residues without the alternating spacers ($\mathbf{A_3X_3}$, $\mathbf{B_3X_3}$) do not bind to their complementary partners ≤500 μM (Table 1, Figure S22, S27). Above this concentration, precipitation of $\mathbf{A_3X_3}$ occurs, indicating the importance of the lysine spacer in

DOI: 10.1021/jacs.9b03107
J. Am. Chem. Soc. 2019, 141, 14026–14031

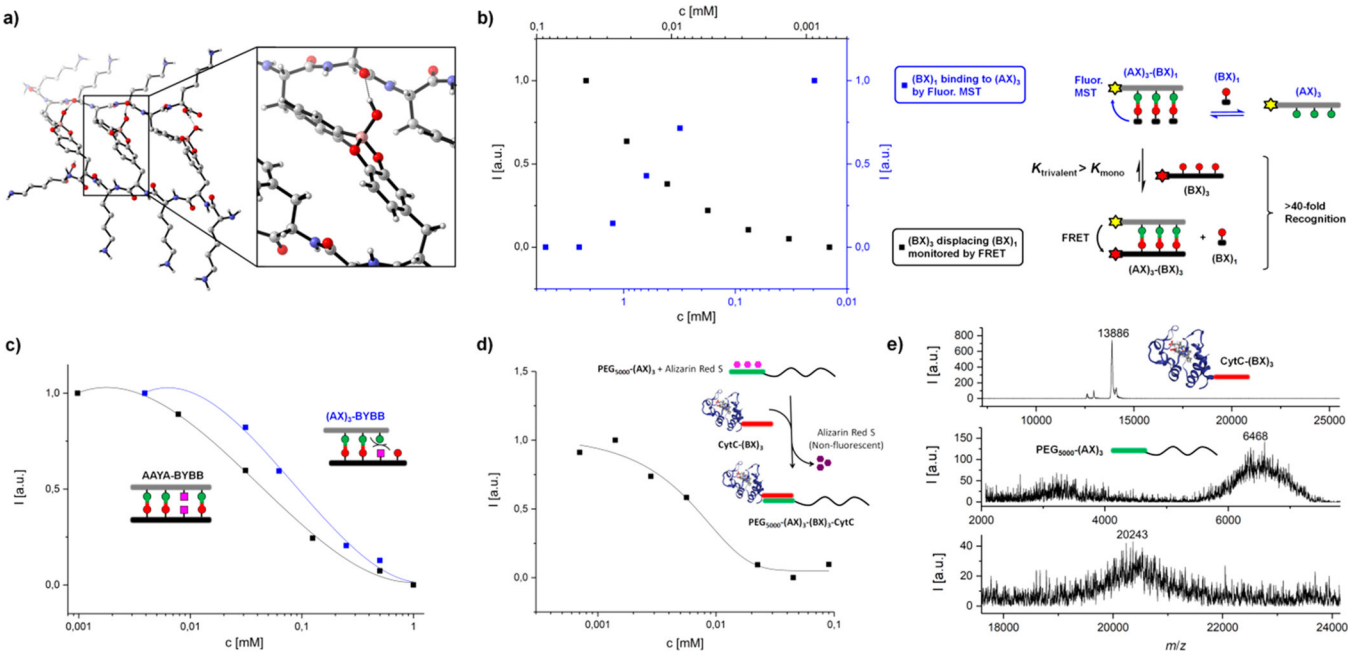

Figure 3. (a) Model of the DFT optimized structure of $(AX)_3$-$(BX)_3$ at (B3LYP/6-31G(d) theory level (see Supporting Information). (b) Displacement reaction on a fluorescein-$(AX)_3$ template: Monovalent $(BX)_1$ was titrated to achieve maximum binding (fluorescence, blue) followed by the addition of increasing amounts of Dylight650-$(BX)_3$ to displace $(BX)_1$ (FRET, black). (c) Sequence dependent discrimination between complementary **AAYA-BYBB** and mismatching $(AX)_3$-**BYBB** peptide based on titration. (d) Quantification of binding of PEG_{5000}-$(AX)_3$ with **CytC**-$(BX)_3$ at 100 μM using Alizarin Red S assay. (e) Characterization of the recognition by **CytC**-$(BX)_3$ (13 886 g mol^{-1}) with PEG_{5000}-$(AX)_3$ (6468 g mol^{-1}) yielding PEG_{5000}-$(AX)_3(BX)_3$-**CytC** (calcd. MW: 20 036 g mol^{-1}, detected MW 20 243 g mol^{-1}, matrix CHCA) using MALDI-TOF MS.

the alternating (**AX**) arrangement providing both solubility and relief of steric constraints for the binding event.

Next, we encoded a sequence specific binding event by using (1) mixed sequences (**ABA** and **BAB**) and (2) inclusion of a nonbinding event **Y**. Importantly, mixed sequences contain partially complementary parts, whereas the nonbinding event provides an "error" in the sequence. We observed that the **ABA-BAB** interacts with a binding affinity of 79 400 ± 5200 M^{-1}, which is comparable to the homogeneous $(AX)_3$-$(BX)_3$ pairs (Table 1). However, the interaction took significantly longer (about 8 h) suggesting that error correction requires a certain time frame, similar to DNA.[37,38] On the other hand, sequence hybridization can be weakened correspondingly by **AAYA-BYBB**, where **Y** is a nonbinding, noninteracting amino acid (alanine). The increase in the chain length also increases the energy needed to compensate, resulting in a lower binding affinity (21 100 ± 6100 M^{-1}) to a divalent level. Mismatched partners such as $(AX)_3$-**BYBB** further weaken complementarity. Taking another mismatch pair of identical length, **BAB**-$(BX)_3$, nonbinding residues appear in ^{1}H NMR (Figure S12), indicating very weak interactions.

Since strand displacement dynamics is an important tool in DNA nanotechnology,[38−40] we investigate the displacement dynamics of our conjugate by the binding of monovalent $(BX)_1$ and a trivalent $(BX)_3$ against a $(AX)_3$ template. The fluorescein-$(AX)_3$ was first titrated with $(BX)_1$ until binding saturation (Figure 3b, black). Displacement and sorting was then achieved by titrating the $(AX)_3$-$(BX)_1$ against Dylight650-$(BX)_3$, monitored independently by FRET. The intersection between the measurements indicates a stoichiometric ratio where $(BX)_1$ and $(BX)_3$ can competitively displace each other by at least 50% (Figure 3b). For $(BX)_1$ to displace $(BX)_3$ by 50%, a stoichiometric factor of >4000 mol % is required. On the other hand, $(BX)_3$ would only require >2.5 mol % due to its multivalent effect.

Table 1. Summary of Association Constants of Different Matching/Mismatching Sequences

Binding Partner	K_a (M^{-1})	Type	Binary Code
$(AX)_1$-$(BX)_1$	1300 ± 300	Monovalent	1
$(AX)_2$-$(BX)_2$	12 500 ± 1100	Divalent	11
$(AX)_3$-$(BX)_3$	81 400 ± 7300	Trivalent	111
A_3X_3-B_3X_3	<2000	No Spacer	111
ABA-BAB	79 400 ± 5200	Mixed Trivalent	111
$(BX)_3$-**BAB**	–	–	Mismatch
AAYA-BYBB	21 100 ± 6100	Divalent (Spaced)	1101
$(AX)_3$-**BYBB**	9400 ± 800	Divalent	Mismatch

Based on these findings, the established binary codes could be used to enable recognition of macromolecules, i.e., proteins and polymers. As PEGylation of proteins remain an important aspect in protein therapeutics,[41,42] we functionalized PEG_{5000} and yeast cytochrome c (CytC) with $(AX)_3$ and $(BX)_3$, respectively. The conversion to PEG_{5000}-$(AX)_3(BX)_3$-**CytC** was quantified by a fluorogenic sensor, Alizarin Red S in a titration assay (Figure 3d). The construct was characterized additionally with MALDI-TOF MS albeit with partial dissociation of the construct due to the acidic matrix (Figure 3e). Additionally, topological height increases due to complexation was visualized by atomic force microscopy (Figure S19).[43]

In summary, we have demonstrated, to the best of our knowledge, the first application of boronic acid chemistry in molecular sequence programming under physiological conditions. By combining the recognition and binding customization of boronic acid/catechol chemistry with a peptide

DOI: 10.1021/jacs.9b03107
J. Am. Chem. Soc. 2019, 141, 14026−14031

scaffold, synthetic binary codes were created, in which binding and dynamic displacement was directed in a predictable and logical manner. In addition, the pH responsiveness of the chemistry adds an extra trigger to control the hybridization process. Assisted by the burgeoning field of site-selective protein chemistry,[44] the application of complementary sequences to the protein cytochrome c and PEG_{5000} further underlines the potential to create defined and dynamic macromolecular assemblies. We envision that the technology provides a synthetic platform for programming macromolecular architectures to possess complex dynamic features.

■ ASSOCIATED CONTENT

Supporting Information

The Supporting Information is available free of charge on the ACS Publications website at DOI: 10.1021/jacs.9b03107.

Materials and methods, characterization techniques and instrumentation as well as supporting figures (PDF)

■ AUTHOR INFORMATION

Corresponding Authors

*david.ng@mpip-mainz.mpg.de
*weil@mpip-mainz.mpg.de

ORCID

Jaime A. S. Coelho: 0000-0002-7459-0993
Pedro M. P. Gois: 0000-0002-7698-630X
David Y. W. Ng: 0000-0002-0302-0678
Tanja Weil: 0000-0002-5906-7205

Notes

The authors declare no competing financial interest.

■ ACKNOWLEDGMENTS

The project was funded by the Deutsche Forschungsgemeinschaft (DFG, German Research Foundation) − Project number 316249678 − SFB 1279 (C01) and Project number: 318290668 − SPP 1923 as well as by an ERC Synergy Grant under grant agreement No. 319130 (BioQ). M. M. Zegota thanks the Marie Curie International Training Network Protein Conjugates for a research scholarship.

■ REFERENCES

(1) Grzybowski, B. A.; Huck, W. T. S. The nanotechnology of life-inspired systems. *Nat. Nanotechnol.* **2016**, *11*, 585−592.
(2) Hirao, I.; Kimoto, M.; Yamashige, R. Natural versus Artificial Creation of Base Pairs in DNA: Origin of Nucleobases from the Perspectives of Unnatural Base Pair Studies. *Acc. Chem. Res.* **2012**, *45*, 2055−2065.
(3) Liu, Y.; Lehn, J.-M.; Hirsch, A. K. H. Molecular Biodynamers: Dynamic Covalent Analogues of Biopolymers. *Acc. Chem. Res.* **2017**, *50*, 376−386.
(4) Swain, J. A.; Iadevaia, G.; Hunter, C. A. H-Bonded Duplexes based on a Phenylacetylene Backbone. *J. Am. Chem. Soc.* **2018**, *140*, 11526−11536.
(5) Stross, A. E.; Iadevaia, G.; Núñez-Villanueva, D.; Hunter, C. A. Sequence-Selective Formation of Synthetic H-Bonded Duplexes. *J. Am. Chem. Soc.* **2017**, *139*, 12655−12663.
(6) Gong, B. Molecular Duplexes with Encoded Sequences and Stabilities. *Acc. Chem. Res.* **2012**, *45*, 2077−2087.
(7) Zhang, Y.; Cao, R.; Shen, J.; Detchou, C. S. F.; Zhong, Y.; Wang, H.; Zou, S.; Huang, Q.; Lian, C.; Wang, Q.; Zhu, J.; Gong, B. Hydrogen-Bonded Duplexes with Lengthened Linkers. *Org. Lett.* **2018**, *20*, 1555−1558.
(8) Makiguchi, W.; Tanabe, J.; Yamada, H.; Iida, H.; Taura, D.; Ousaka, N.; Yashima, E. Chirality- and sequence-selective successive self-sorting via specific homo- and complementary-duplex formations. *Nat. Commun.* **2015**, *6*, 7236.
(9) Iida, H.; Ohmura, K.; Noda, R.; Iwahana, S.; Katagiri, H.; Ousaka, N.; Hayashi, T.; Hijikata, Y.; Irle, S.; Yashima, E. Double-Stranded Helical Oligomers Covalently Bridged by Rotary Cyclic Boronate Esters. *Chem. - Asian J.* **2017**, *12*, 927−935.
(10) Yashima, E.; Ousaka, N.; Taura, D.; Shimomura, K.; Ikai, T.; Maeda, K. Supramolecular Helical Systems: Helical Assemblies of Small Molecules, Foldamers, and Polymers with Chiral Amplification and Their Functions. *Chem. Rev.* **2016**, *116*, 13752−13990.
(11) Sisco, S. W.; Moore, J. S. Homochiral Self-Sorting of BINOL Macrocycles. *Chem. Sci.* **2014**, *5*, 81−85.
(12) Epstein, E. S.; Martinetti, L.; Kollarigowda, R. H.; Carey-De La Torre, O.; Moore, J. S.; Ewoldt, R. H.; Braun, P. V. Modulating Noncovalent Cross-links with Molecular Switches. *J. Am. Chem. Soc.* **2019**, *141*, 3597−3604.
(13) Powell, K. How biologists are creating life-like cells from scratch. *Nature* **2018**, *563*, 172−175.
(14) Göpfrich, K.; Platzman, I.; Spatz, J. P. Mastering Complexity: Towards Bottom-up Construction of Multifunctional Eukaryotic Synthetic Cells. *Trends Biotechnol.* **2018**, *36*, 938−951.
(15) Xu, C.; Hu, S.; Chen, X. Artificial cells: from basic science to applications. *Mater. Today* **2016**, *19*, 516−532.
(16) Seeman, N. C.; Sleiman, H. F. DNA nanotechnology. *Nat. Rev. Mater.* **2017**, *3*, 17068.
(17) Crini, G. Review: A History of Cyclodextrins. *Chem. Rev.* **2014**, *114*, 10940−10975.
(18) Barrow, S. J.; Kasera, S.; Rowland, M. J.; del Barrio, J.; Scherman, O. A. Cucurbituril-Based Molecular Recognition. *Chem. Rev.* **2015**, *115*, 12320−12406.
(19) Webber, M. J.; Appel, E. A.; Meijer, E. W.; Langer, R. Supramolecular biomaterials. *Nat. Mater.* **2016**, *15*, 13−26.
(20) Klajn, R. Spiropyran-based dynamic materials. *Chem. Soc. Rev.* **2014**, *43*, 148−184.
(21) Kathan, M.; Eisenreich, F.; Jurissek, C.; Dallmann, A.; Gurke, J.; Hecht, S. Light-driven molecular trap enables bidirectional manipulation of dynamic covalent systems. *Nat. Chem.* **2018**, *10*, 1031−1036.
(22) Brooks, W. L. A.; Sumerlin, B. S. Synthesis and Applications of Boronic Acid-Containing Polymers: From Materials to Medicine. *Chem. Rev.* **2016**, *116*, 1375−1397.
(23) Akgun, B.; Hall, D. G. Boronic Acids as Bioorthogonal Probes for Site-Selective Labeling of Proteins. *Angew. Chem., Int. Ed.* **2018**, *57*, 13028−13044.
(24) Santos, F. M. F.; Matos, A. I.; Ventura, A. E.; Gonçalves, J.; Veiros, L. F.; Florindo, H. F.; Gois, P. M. P. Modular Assembly of Reversible Multivalent Cancer-Cell-Targeting Drug Conjugates. *Angew. Chem., Int. Ed.* **2017**, *56*, 9346−9350.
(25) Wu, X.; Li, Z.; Chen, X.-X.; Fossey, J. S.; James, T. D.; Jiang, Y.-B. Selective sensing of saccharides using simple boronic acids and their aggregates. *Chem. Soc. Rev.* **2013**, *42*, 8032−8048.
(26) Sun, X.; James, T. D.; Anslyn, E. V. Arresting "Loose Bolt" Internal Conversion from − B(OH)2 Groups is the Mechanism for Emission Turn-On in ortho-Aminomethylphenylboronic Acid-Based Saccharide Sensors. *J. Am. Chem. Soc.* **2018**, *140*, 2348−2354.
(27) Seidler, C.; Zegota, M. M.; Raabe, M.; Kuan, S. L.; Ng, D. Y. W.; Weil, T. Dynamic Core−Shell Bioconjugates for Targeted Protein Delivery and Release. *Chem. - Asian J.* **2018**, *13*, 3474−3479.
(28) Seidler, C.; Ng, D. Y. W.; Weil, T. Native protein hydrogels by dynamic boronic acid chemistry. *Tetrahedron* **2017**, *73*, 4979−4987.
(29) Smithmyer, M. E.; Deng, C. C.; Cassel, S. E.; LeValley, P. J.; Sumerlin, B. S.; Kloxin, A. M. Self-Healing Boronic Acid-Based Hydrogels for 3D Co-cultures. *ACS Macro Lett.* **2018**, *7*, 1105−1110.
(30) Uhlmann, E. Peptide nucleic acids (PNA) and PNA-DNA chimeras: from high binding affinity towards biological function. *Biol. Chem.* **1998**, *379*, 1045−1052.
(31) Lei, H.; Stoakes, M. S.; Schwabacher, A. W.; Herath, K. P. B.; Lee, J. Efficient Synthesis of a Phosphinate Bis-Amino Acid and Its

Use in the Construction of Amphiphilic Peptides. *J. Org. Chem.* **1994**, *59*, 4206−4210.
(32) Martínez-Aguirre, M. A.; Villamil-Ramos, R.; Guerrero-Alvarez, J. A.; Yatsimirsky, A. K. Substituent Effects and pH Profiles for Stability Constants of Arylboronic Acid Diol Esters. *J. Org. Chem.* **2013**, *78*, 4674−4684.
(33) Kibbe, W. A. OligoCalc: an online oligonucleotide properties calculator. *Nucleic Acids Res.* **2007**, *35*, W43−W46.
(34) Ratilainen, T.; Holmén, A.; Tuite, E.; Haaima, G.; Christensen, L.; Nielsen, P. E.; Nordén, B. Hybridization of Peptide Nucleic Acid. *Biochemistry* **1998**, *37*, 12331−12342.
(35) Zhang, H.-Y.; Sun, Y.-M.; Wang, X.-L. Substituent Effects on O-H Bond Dissociation Enthalpies and Ionization Potentials of Catechols: A DFT Study and Its Implications in the Rational Design of Phenolic Antioxidants and Elucidation of Structure−Activity Relationships for Flavonoid Antioxidants. *Chem. - Eur. J.* **2003**, *9*, 502−508.
(36) Gulley-Stahl, H.; Hogan, P. A.; Schmidt, W. L.; Wall, S. J.; Buhrlage, A.; Bullen, H. A. Surface Complexation of Catechol to Metal Oxides: An ATR-FTIR, Adsorption, and Dissolution Study. *Environ. Sci. Technol.* **2010**, *44*, 4116−4121.
(37) Zhang, J. X.; Fang, J. Z.; Duan, W.; Wu, L. R.; Zhang, A. W.; Dalchau, N.; Yordanov, B.; Petersen, R.; Phillips, A.; Zhang, D. Y. Predicting DNA hybridization kinetics from sequence. *Nat. Chem.* **2018**, *10*, 91−98.
(38) Platnich, C. M.; Hariri, A. A.; Rahbani, J. F.; Gordon, J. B.; Sleiman, H. F.; Cosa, G. Kinetics of Strand Displacement and Hybridization on Wireframe DNA Nanostructures: Dissecting the Roles of Size, Morphology, and Rigidity. *ACS Nano* **2018**, *12*, 12836−12846.
(39) Fern, J.; Schulman, R. Modular DNA strand-displacement controllers for directing material expansion. *Nat. Commun.* **2018**, *9*, 3766.
(40) Machinek, R. R. F.; Ouldridge, T. E.; Haley, N. E. C.; Bath, J.; Turberfield, A. J. Programmable energy landscapes for kinetic control of DNA strand displacement. *Nat. Commun.* **2014**, *5*, 5324.
(41) Mummidivarapu, V. V. S.; Rennie, M. L.; Doolan, A. M.; Crowley, P. B. Noncovalent PEGylation via Sulfonatocalix[4]arene−A Crystallographic Proof. *Bioconjugate Chem.* **2018**, *29*, 3999−4003.
(42) Nischan, N.; Hackenberger, C. P. R. Site-specific PEGylation of Proteins: Recent Developments. *J. Org. Chem.* **2014**, *79*, 10727−10733.
(43) Takeda, K.; Uchihashi, T.; Watanabe, H.; Ishida, T.; Igarashi, K.; Nakamura, N.; Ohno, H. Real-time dynamic adsorption processes of cytochrome c on an electrode observed through electrochemical high-speed atomic force microscopy. *PLoS One* **2015**, *10*, e0116685−e0116685a.
(44) Krall, N.; da Cruz, F. P.; Boutureira, O.; Bernardes, G. J. L. Site-selective protein-modification chemistry for basic biology and drug development. *Nat. Chem.* **2016**, *8*, 103−113.

DOI: 10.1021/jacs.9b03107
J. Am. Chem. Soc. 2019, 141, 14026−14031

Supporting Information

Sequence Programming with Dynamic Boronic Acid/Catechol Binary Codes

Marco Hebel,[1,2] Andreas Riegger,[2] Maksymilian M. Zegota,[1,2] Gönül Kizilsavas,[1] Jasmina Gačanin,[1,2] Michaela Pieszka,[1,2] Thorsten Lückerath,[1,2] Jaime A. S. Coelho,[3] Manfred Wagner,[1] Pedro M. P. Gois,[3] David Y. W. Ng,[1,*] and Tanja Weil[1,2,*]

[1]Max Planck Institute for Polymer Research, Ackermannweg 10, 55128 Mainz, Germany

[2]Institute of Inorganic Chemistry I, Ulm University, Albert-Einstein-Allee 11, 89081 Ulm, Germany

[3]Research Institute for Medicines (iMed.ULisboa), Faculty of Pharmacy, Universidade de Lisboa, Lisbon, Portugal

Contents

1. Index of Abbreviations

FITC	fluorescein isothiocyanate
Bor- (in peptide sequence)	*para*-borono-phenylalanine
Cat- (in peptide sequence)	L-3,4-dihydroxyphenylalanine
Mal- (in peptide sequence)	6-maleimidohexanoic acid
PEG5000-maleimide	methoxypolyethylene glycol maleimide
TCEP	tris(2-carboxyethyl)phosphine hydrochloride
AEEAc	8-amino-3,6-dioxaoctanoic acid
Fmoc-	Fluorenylmethyloxycarbonyl-
Boc	*tert*-Butyloxycarbonyl-

2. Experimental Procedures

2.1 Synthesis of protected borono-phenylalanine

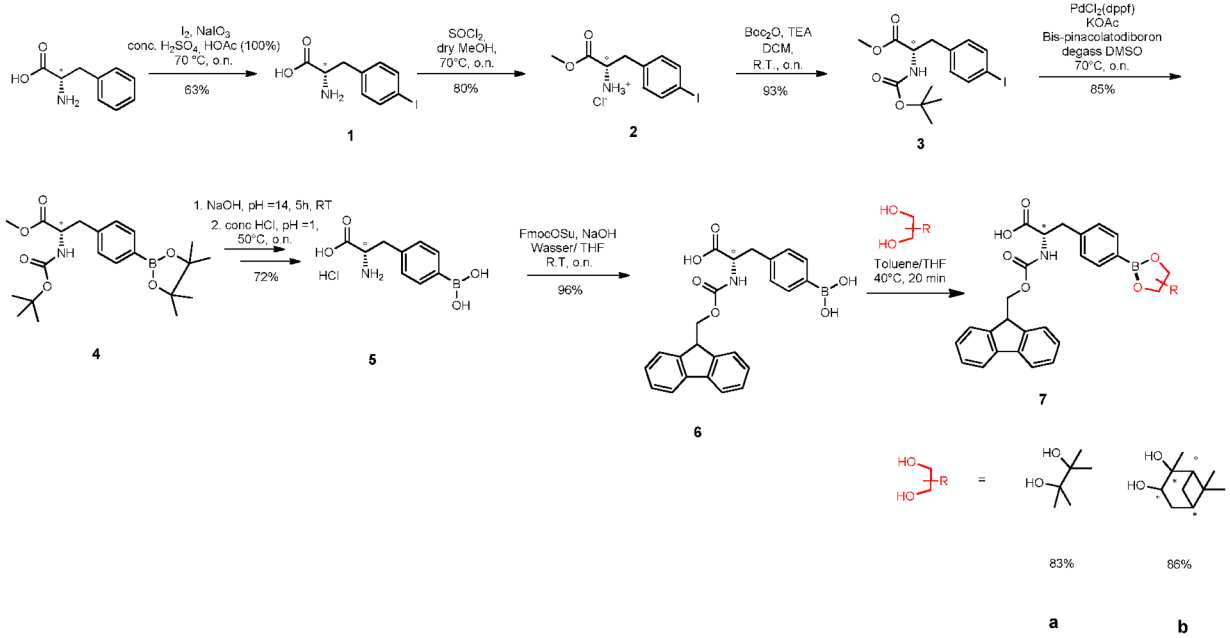

NMR spectra were recorded on a Bruker 400 or 500 MHz NMR spectrometer. Signals are reported in parts per million (ppm) with respect to residual solvent peak ($CDCl_3$, DMSO-d_6, CD_3OD, D_2O). LC-MS was recorded on or Shimadzu LC-MS 2020. The MALDI-TOF mass spectra were obtained from Bruker Reflex III (MALDI-TOF) and Bruker Solarix (FTICR) spectrometer. All chemical reagents were obtained from commercial suppliers and were used without further purification unless otherwise noted. Thin layer chromatography (TLC, Merck 60 F254) was used to monitor the reactions. TLC plates were stained with $KMnO_4$, ninhydrine, iodine. Acros Organics silica gel was used for column chromatography (0.035 nm – 0.070 nm, 60 Å).

4-Iodo-L-phenylalanine (1)

Phenylalanine (1 equiv.), was dissolved in a mixture of acetic and sulfuric acid (5:1). Then iodine (0.4 equiv.) and sodium periodate (0.23 equiv.) were added. The mixture was heated to 70 °C, stirred overnight and concentrated under vacuum. Water and DCM (4:1) were added to dissolve the solid. The two layers were separated and the aqueous layer was washed with DCM and Et_2O. Subsequently, activated charcoal was added to the aqueous layer, stirred for one hour and filtered. By adjusting the pH of the solution to 4, the white product was precipitated. After filtration the solid was dried under vacuum (Yield: 86%). The NMR data was accordance with the literature.[1] **^{1}H-NMR** (400 MHz, CD_3OD): δ (ppm) = 3.05 (dd, 1H), 3.28 (dd, 1H), 3.91 (dd, 1H), 7.13 (d, 2H), 7.73 (d, 2H). **^{13}C-NMR** (125 MHz, CD_3OD): δ (ppm) = 37.67, 55.74, 95.28,

133.41, 136.03, 140.19, 171.12. **HR-ESI-MS**: m/z = 291.98290 $[M + H]^+$, (calcd. mass: 291.98345 $[M + H]^+$, formula: $C_9H_{10}INO_2$).

4-Iodo-L-phenylalaninemethylester (2)

4-Iodopenylalanine (1 equiv.) was dissolved in dry MeOH. The solution was cooled to 0 °C and thionylchloride (3 equiv.) was added dropwise. The mixture was heated to 70 °C, and stirred overnight. The solvent was partially evaporated to concentrate the solution, which was added to cold Et_2O causing the white product to precipitate. The product was filtered and dried in vacuum (Yield: 94%). The NMR data was in accordance with the literature.[1] **^{1}H-NMR** (400 MHz, CD_3OD): δ (ppm) = 3.10 – 3.22 (m, 2H), 3.81 (s, 3H), 4.33 (dd, 1H), 7.07 (d, 2H), 7.73 (d, 2H). **^{13}C-NMR** (125 MHz, CD_3OD): δ (ppm) = 36.81, 53.63, 54.87, 94.12, 132.55, 135.16, 139.34, 170.26. **HR-ESI-MS**: m/z = 307.00581 $[M + H]^+$, (calcd. mass: 307.00693 $[M + H]^+$, formula: $C_{10}H_{12}INO_2$).

***N*-(*tert*-butyloxycarbonyl)-4-Iodo-L-phenylalaninemethylester (3)**

4-Iodophenylalaninemethylester (1 equiv.) was dissolved in DCM. Then di-*tert*-butyldicarbonat (1.2 equiv.) and TEA (3 equiv.) were added. The solution was stirred overnight and concentrated under vacuum. The crude was purified with column chromatography (*n*-hexane/ethylacetate, 3:1) to afford a clear, highly-viscous oil (Yield: 92%). The NMR was in accordance with the literature.[1] **^{1}H-NMR** (400 MHz, $CDCl_3$): δ (ppm) = 1.42 (s, 9H), 2.92 - 3.10 (m, 2H), 3.71 (s, 3H), 4.56 (dd, 1H), 4.97 (d, 1H), 6.87 (d, 2H), 7.61 (d, 2H). **^{13}C-NMR** (125 MHz, $CDCl_3$): δ (ppm) = 28.41, 52.48, 54.40, 80.23, 92.67, 131.46, 135.85, 137.73, 155.20, 172.28. **LC-MS (ESI)**: m/z = 406 $[M + H]^+$, (calcd. mass: 406 $[M + H]^+$, formula: $C_{15}H_{20}INO_4$).

***N*-(*tert*-butyloxycarbonyl)-4-(pinacolylborono)-L-phenylalaninemethylester (4)**

Potassium acetate (3 equiv.) was placed in a round bottom flask and was dried under vacuum. Then *N*-(*tert*-butyloxycarbonyl)-4-Iodophenylalaninemethylester (1 equiv.), the Pd catalyst ($PdCl_2$dppf, 0.03 equiv.) and bis-pinacolatodiboron (1.3 equiv.) were added, followed by dry DMSO. The clear solution was degassed (4x), heated to 80 °C, and stirred overnight. After removal of the solvent in vacuum, water and DCM were added to the black solid. The aqueous layer was washed with additional DCM (3x). The combined organic layers were dried and concentrated in vacuum. Column chromatography (EA/*n*-hexane, 1:3) was used to isolate the pure product as white solid

(Yield: 87%). The data NMR was in accordance with literature.[2] **^{1}H-NMR** (400 MHz, CD_3OD): δ (ppm) = 1.34 (s, 12H), 1.42 (s, 9H), 2.95 - 3.15 (m, 2H), 3.70 (s, 3H), 4.58 (dd, 1H), 4.95 (d, 1H), 7.12 (d, 2H), 7.73 (d, 2H). **^{13}C-NMR** (125 MHz, CD_3OD): δ (ppm) = 25.00, 28.43, 31.38, 38.53, 52.38, 54.46, 80.08, 83.93, 128.85, 135.15, 139.34, 155.19, 172.36. **LC-MS (ESI)**: m/z = 428 $[M + Na]^+$, (calcd. mass: 428 $[M + Na]^+$, formula: $C_{21}H_{32}BNO_6$).

4-Borono-L-phenylalanine (5)

N-(*tert*-butyloxycarbonyl)-4-(pinacolylborono)-phenylalaninemethylester (1 equiv.) was dissolved in acetone. Concentrated sodium hydroxide solution (10 equiv.) was added and the solution was stirred overnight. The next day, the pH of the solution was adjusted to 0 using concentrated HCl. Then the solution was heated to 50 °C and stirred overnight. The solution was concentrated by partial removal of the solvent and the pH was adjusted to 4 causing the product to precipitate. After filtration the white solid was washed with cold water, Et_2O and dried in vacuum (yield: 81%). The NMR was in accordance with the literature.[3] **^{1}H-NMR** (400 MHz, CD_3OD): δ (ppm) = 2.65 - 2.85 (m, 2H), 3.81 – 3.87 (m, 1H), 6.79 (d, 2H), 7.17 (d, 2H). **^{13}C-NMR** (125 MHz, CD_3OD): δ (ppm) = 44.85, 62.61, 103.19, 141.64, 144.34, 147.03, 179.89.

***N*-(9*H*-Fluorenylmethoxycarbonylamino)-4-borono-L-phenylalanine (6)**

4-Boronophenylalanine (1 equiv.) was suspended in water. Then the pH was adjusted to 11 by adding NaOH. A solution of *N*-(9-Fluorenylmethoxycarbonyloxy)succinimide (1.2 equiv.) was added dropwise to the resulting clear aqueous solution and stirred overnight. The reaction mixture was washed with EA (3x) before the pH was adjusted to 1. Another potion of EA was added (3x) to extract the product. The combined organic layers were dried and concentrated under vacuum to afford a white solid (yield: 69%). **^{1}H-NMR** (400 MHz, $CDCl_3$): δ (ppm) = 3.07 - 3.14 (m, 2H), 4.15 - 4.23 (m, 2H), 4.29 (dd, 1H), 4.44 (dd, 1H), 7.22 - 7.31 (m, 4H), 7.33 - 7.40 (m, 2H), 7.48 - 7.54 (d, 2H), 7.56 - 7.62 (d, 2H), 7.75 - 7.80 (m, 2H). **^{13}C-NMR** (125 MHz, $CDCl_3$): δ (ppm) = 26.29, 38.66, 56.74, 68.00, 120.88, 126.25, 126.36, 128.18, 128.76, 129.62, 135.01, 142.53, 145.22, 158.39, 174.92, 175.28. **LC-MS (ESI)**: m/z = 432 $[M + H]^+$, (calcd. mass: 432 $[M + H]^+$, formula: $C_{24}H_{22}BNO_6$).

General protocol for the protection of the boronic acid

Fmoc-Boronic acid (1 equiv.) was dissolved in a toluene/THF (1:1) mixture. Then (1S,2S,3R,5S)-(+)-pinanediol or pinacol (1 equiv.) was added. The solution was stirred for 15 min before the solvent was completely removed in vacuum. Then another portion of toluene/THF was added, the solution was stirred for another 10 min and solvent again evaporated (repeated 3x). Column chromatography (*n*-hexane/ THF, 4:1 up to 1:2 + 2% FA) was used to isolate the products as white solids.

***N*-(9*H*-Fluorenylmethoxycarbonylamino)-4-(pinacolatoborono)-L-phenylalanine (7a)**

Synthesis was conducted according to the general protocol above. Yield: 83%. The NMR data was in accordance with the literature.[4] **^{1}H-NMR** (400 MHz, MeOH-d_4): δ (ppm) = 1.30 (s, 12H), 2.90 – 3.00 (m, 1H), 3.20 – 3.30 (m, 1H), 4.05 – 4.15 (m, 1H), 4.30 – 4.40 (m, 2H), 7.20- 7.30 (m, 6H), 7.32 – 7.39 (m, 2H), 7.48 - 7.55 (m, 2H), 7.61 – 7.66 (d, 2H), 7.73 – 7.79 (d, 2H). **^{13}C-NMR** (125 MHz, $CDCl_3$): δ (ppm) = 25.17, 36.63, 48.27, 55.20, 67.26, 84.97, 120.82, 126.15, 126.30, 126.36, 128.15, 128.68, 128.70, 129.83, 129.92, 135.86, 142.36, 145.19, 156.20, 174.36. **LC-MS (ESI)**: m/z = 514 $[M+H]^+$, (calcd. mass: 514 $[M+H]^+$, formula: $C_{30}H_{32}BNO_6$).

***N*-(9*H*-Fluorenylmethoxycarbonylamino)-4-(pinandiolborono)-L-phenylalanine (7b)**

Synthesis was conducted according to the general protocol above. Yield: 80% **^{1}H-NMR** (400 MHz, $CDCl_3$): δ (ppm) = 0.85 (s, 3H), 0.98 (d, 1H), 1.26 (s, 3H), 1.39 (s, 3H), 1.73 – 1.75 (m, 1H), 1.83 – 1.89 (m, 1H), 2.05 (t, 1H), 2.09 – 2.17 (m, 1H), 2.30 – 2.40 (m, 1H), 2.79 (t, 1H), 2.85 – 2.95 (m, 1H), 3.10 – 3.18 (m, 1H), 4.14 – 4.17 (m, 1H), 4.17 – 4.25 (m, 2H), 4.47 (dd, 1H), 7.20- 7.40 (m, 6H), 7.59 (d, 2H), 7.60 – 7.62 (m, 2H), 7.75 (d, 2H), 7.89 (d, 2H). **^{13}C-NMR** (125 MHz, $CDCl_3$): δ (ppm) = 23.67, 24.46, 25.17, 26.06, 26.87, 28.43, 35.15, 36.75, 37.79, 39.02, 46.58, 50.90, 55.41, 65.66, 67.06, 77.25, 85.81, 120.09, 120.11, 125.19, 125.36, 127.06, 127.57, 127.62, 128.83, 134.49, 140.68, 140.72, 141.61, 143.76, 155.92, 1732.32. **HR-MS (MALDI-TOF, DHB)**: m/z = 566.27053 $[M+H]^+$, 588.25246 $[M + Na]^+$, (calcd. mass: 566.27085 $[M+H]^+$, 588.25279 $[M+ Na]^+$, formula: $C_{34}H_{36}BNO_6$).

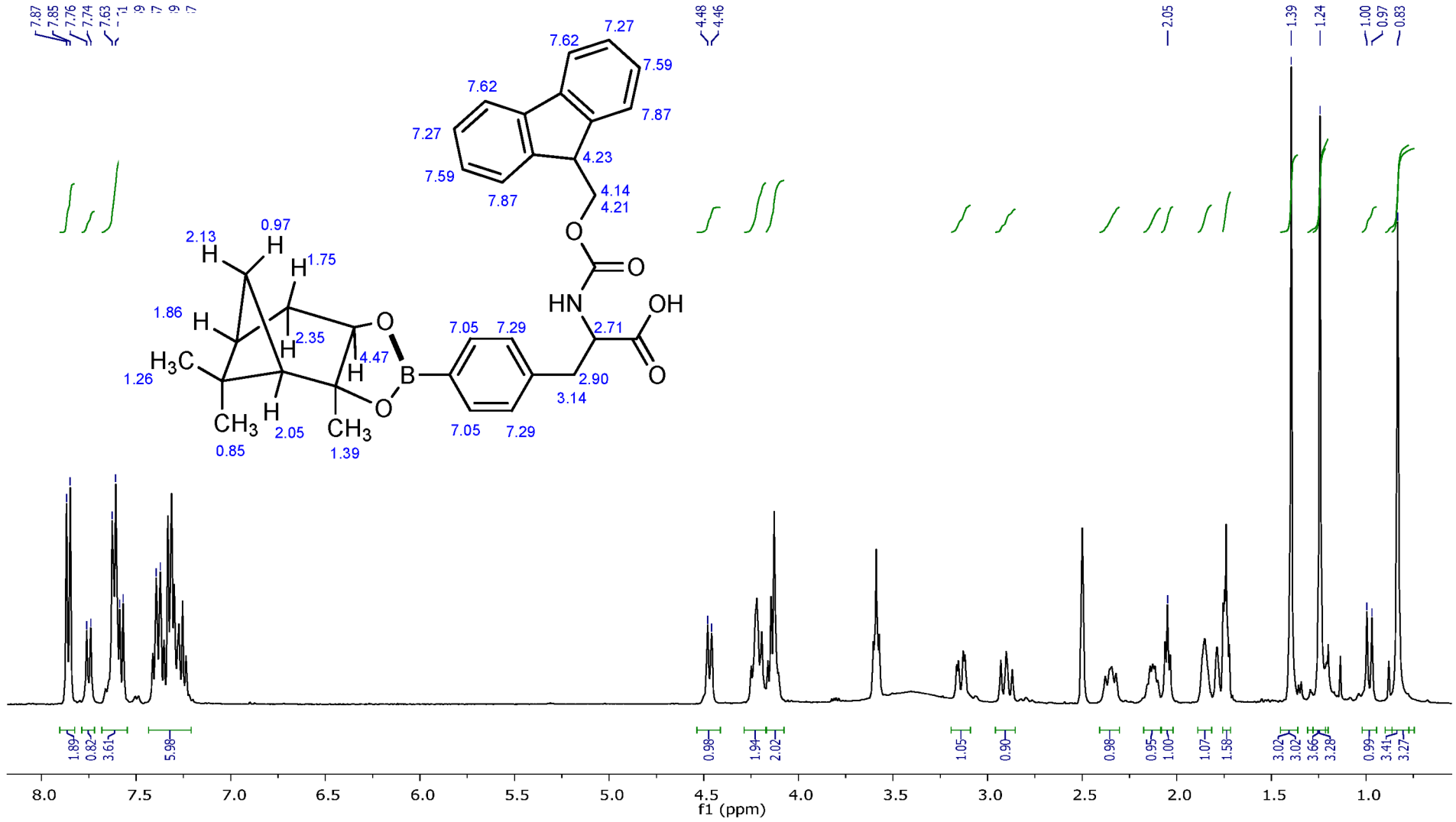

Figure S1. ^{1}H-NMR of *N*-(9*H*-Fluorenylmethoxycarbonylamino)-4-(pinandiolborono)-L-phenylalanine (7b).

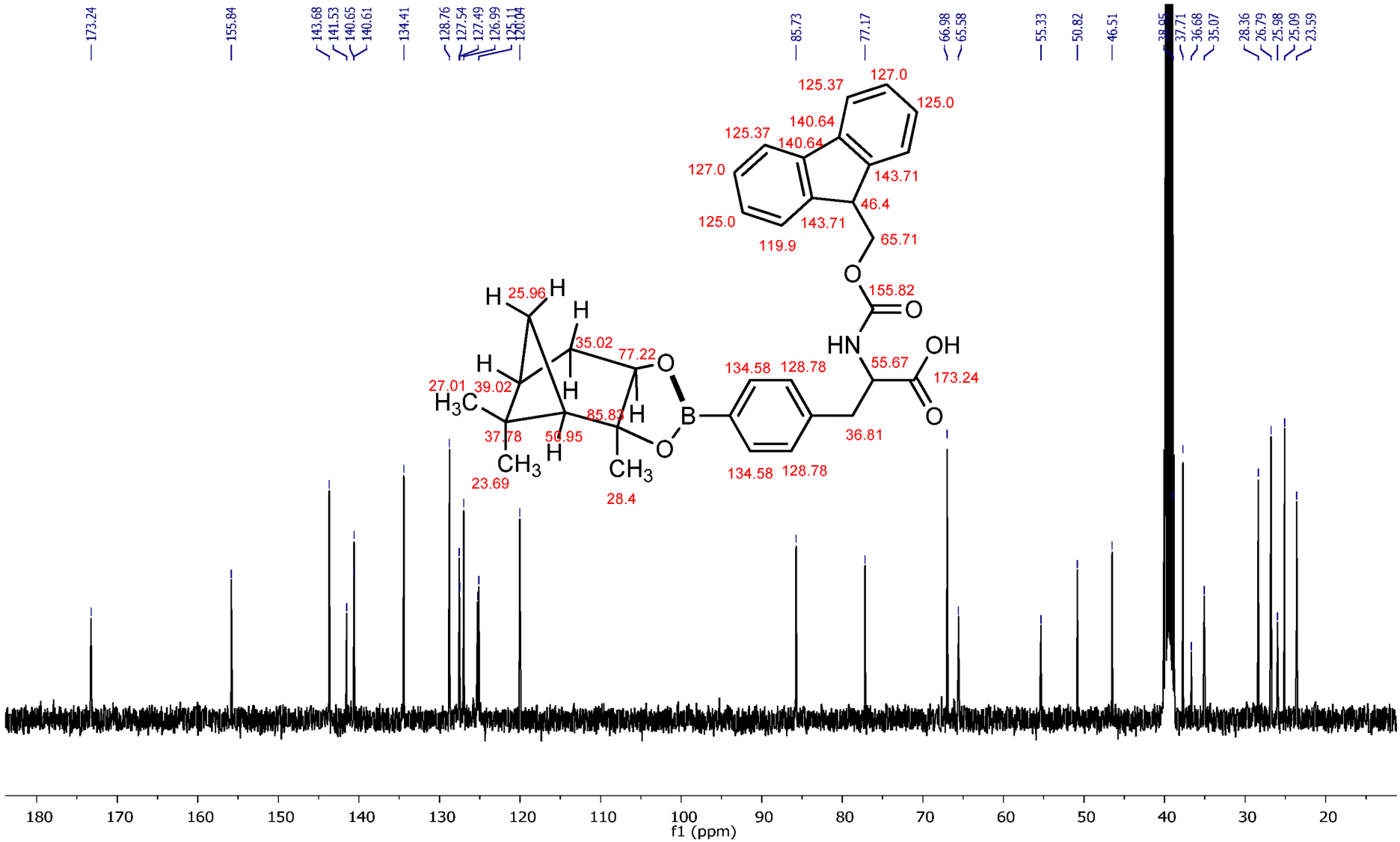

Figure S2. ^{13}C-NMR of *N*-(9*H*-Fluorenylmethoxycarbonylamino)-4-(pinandiolborono)-L-phenylalanine (7b).

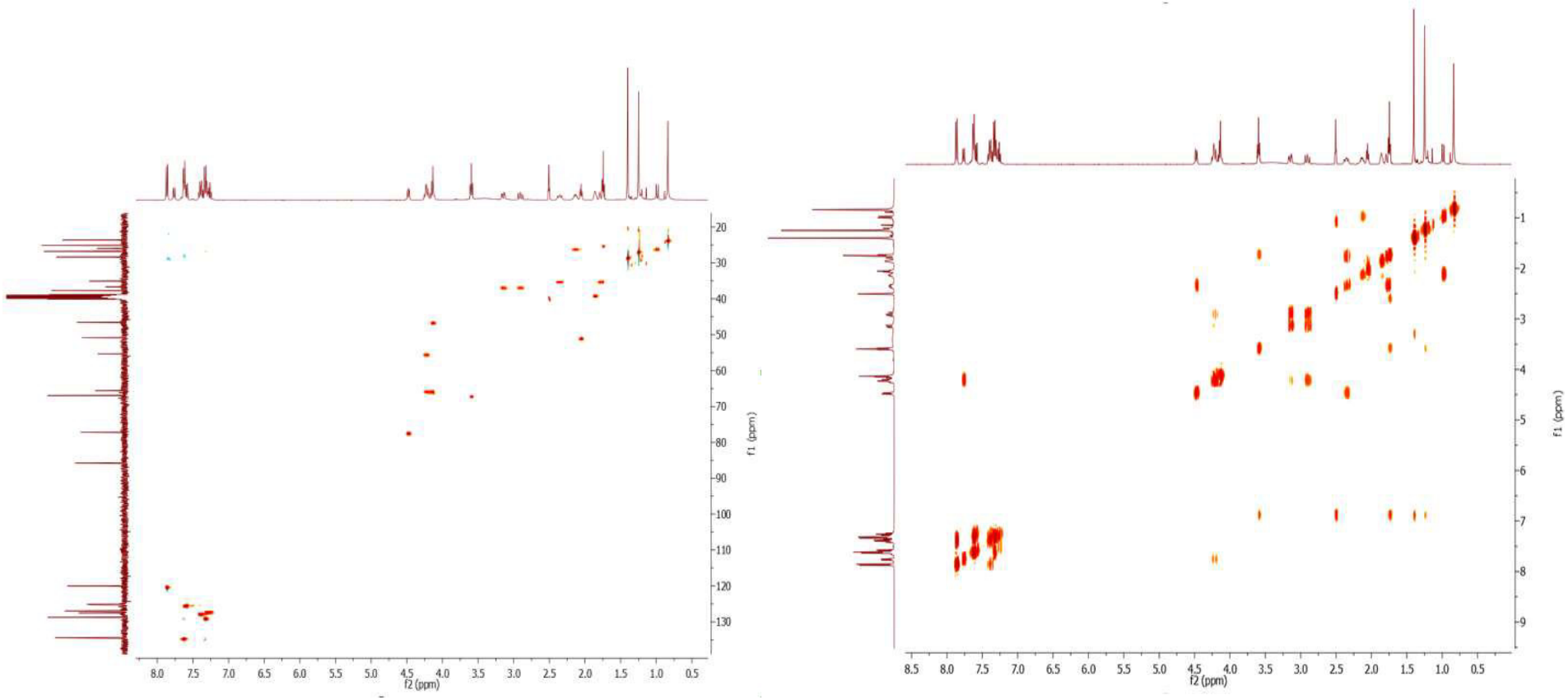

Figure S3. HSQC (left) and H,H COSY (right) of *N*-(9*H*-Fluorenylmethoxycarbonylamino)-4-(pinandiolborono)-L-phenylalanine (7b).

2.2 Solid-phase-peptide-synthesis

Peptides were synthesized using standard fmoc solid phase peptide synthesis (Fmoc-SPPS). Preloaded resins (catechol containing peptides: Wang Resin, boronic acid containing peptides: tentagel resin) were swelled overnight (DMF, 4°C) and used after 3 washes with fresh DMF (peptide grade):

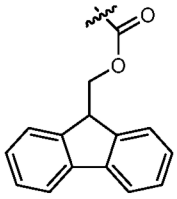

Fmoc

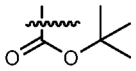

Boc

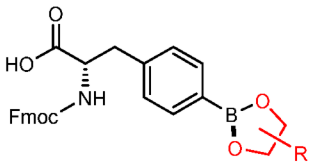

Borono-phenylalanine

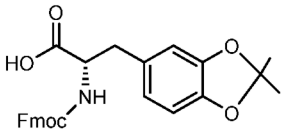

L-DOPA (acetonide protected)

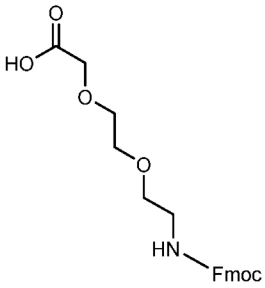

AEEAc

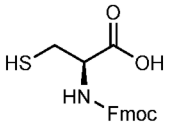

Cysteine

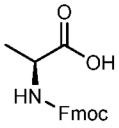

Alanine

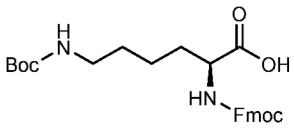

Lysine

The deprotection, coupling and final cleavage conditions are given in the protocol listed below.

Deprotection:

- Deprotection #1 (25% Piperidine in DMF, 3 min, R.T.)
- Deprotection #2 (25% Piperidine in DMF, 10 min, R.T.)
- Wash (4x DMF)

Coupling:

- Add reagents (5 equiv. amino acid, 5 equiv. PyBoP, 10 equiv. DIPEA)
- Microwave (5 min, 75°C), for boronic acid containing peptides increase the reaction time subsequently (2 min/boronic acid)

- Wash (4x DMF)

Final cleavage from the solid phase:

For catechol containing peptides: Treat the peptide, which is still bound to the solid phase with 95% TFA, 2.5% TIPS, 2.5% H_2O, 2 h, R.T.
After the final cleavage, the peptides were precipitated by dropping the peptide solution into cold ether. Subsequently, the peptides were purified with HPLC and characterized with mass spectrometry.

For boronic acid containing peptides: Treat the peptide, which is still bound to the solid phase with 95% TFA, 2.5% TIPS, 2.5% H_2O, 2 h, R.T.
After that the peptides were precipitated by dropping the peptide solution into cold ether. In the next steps the following synthesis strategy was used:

1) Excess PBA (5 equiv.) in hydrochloric acid (4 N), add Et_2O (2 Phases), 30 min, exchange the organic phase steadily (3 times), then remove all the solvent.
3) Add conc. hydrochloric acid and stir for 30 min, then remove the hydrochloric acid.

After the final cleavage the peptides were precipitated by dropping the peptide solution into cold ether. Subsequently, the peptides were purified with HPLC and characterized with mass spectrometry.

2.3 Labeling of peptides with fluorescent dyes

DyLight®650-Cys-AEEAc-Cat-Lys-Cat-Lys-Cat-Lys

The catechol peptide with the sequence Cys-AEEAc-Cat-Lys-Cat-Lys-Cat-Lys (0.1926 mg, 0.1634 µmol, 1.1 equiv.) was dissolved in 100 µL degassed phosphate buffer (pH 6.8, 200 mM). TCEP (4.67 mg, 16.34 µmol, 100 equiv.) was added and stirred for 2 h under argon atmosphere. Then DyLight®650-maleimide (0.1621 mg, 0.1485 µmol, 1.0 equiv.) was added as a 10 mg/mL DMF-solution and the mixture was stirred at room temperature overnight under argon atmosphere. The resulting crude solution was purified by HPLC (chapter 5).

Fluorescein-Cys-AEEAc-Bor-Lys-Bor-Lys-Bor-Lys

The boronic acid peptide with the sequence Cys-AEEAc-Bor-Lys-Bor-Lys-Bor-Lys (0.250 mg, 0.2044 µmol, 1.0 equiv.) was dissolved in 500 µL degassed phosphate buffer (pH 7.1, 200 mM). TCEP (2.923 mg, 10.22 µmol, 50 equiv.) was added and stirred for 2 h under argon atmosphere. Then fluorescein-maleimide (2.18 mg, 5.110 µmol, 25 equiv.) was added as a 10 mg/mL DMF-solution and the mixture was stirred at room temperature overnight under argon atmosphere. The resulting crude solution was purified by HPLC (Refer to Section 5).

Fluorescein-Cys-AEEAc-Bor-Lys-Bor-Lys-Ala-Lys-Bor-Lys

The boronic acid peptide with the sequence Cys-AEEAc-Bor-Lys-Bor-Lys-Ala-Lys-Bor-Lys (0.646 mg, 0.4540 µmol, 1.0 equiv.) was dissolved in 1000 µL degassed phosphate buffer (pH 7.1, 200 mM). TCEP (6.492 mg, 22.70 µmol, 50 equiv.) was added and stirred for 2 h under argon atmosphere. Then fluorescein-maleimide (4.850 mg, 11.35 µmol, 25 equiv.) was added as a 10 mg/mL DMF-solution and the mixture was stirred at room temperature overnight under argon atmosphere. The resulting crude solution was purified by HPLC (Refer to Section 5).

2.4 Synthesis of protein/polymer conjugates

Synthesis of Cytochrome-C-Catechol Peptide-Conjugate (CytC-B3)

CytC (3.120 mg, 0.20479 µmol, 1.0 equiv.) was dissolved in 700 µL degassed phosphate buffer (pH 7.4, 200 mM). TCEP (24.79 µg, 0.099 µmol, 0.4 equiv., 19 µL PB-solution) was added and stirred for 2 h under argon atmosphere. Then the maleimide-functionalized catechol peptide (0.317 mg, 0.248 µmol, 1.0 equiv., 156 µL PB-solution) was added and the mixture was stirred at room temperature overnight under argon atmosphere. The resulting crude solution was purified by Vivaspin® 500 Centrifugal Concentrator (Cut-off of 3000 MW) by six-times washing with water.

Synthesis of PEG_{5000}-Boronic Acid Peptide-Conjugate (PEG_{5000}-A3)

The boronic acid peptide with the sequence Cys-AEEAc-Bor-Lys-Bor-Lys-Bor-Lys (0.250 mg, 0.2044 µmol, 1.0 equiv.) was dissolved in 250 µL degassed phosphate buffer (pH 7.1, 200 mM). TCEP (2.713 mg, 9.485 µmol, 50 equiv., 70 µL PB-solution) was added and stirred for 2 h under argon atmosphere. PEG_{5000}-maleimide (9.591mg,

1.900 µmol, 10 equiv.) was dissolved in 1000 µL degassed phosphate buffer (pH 7.4, 200 mM) was added and the mixture was stirred at room temperature overnight under argon atmosphere. The resulting crude solution was purified by HPLC.

2.5 Mass Spectrometry and High-Performance Liquid Chromatography

The catechol containing peptide tags were characterized via LC-MS or MALDI-FTICR using HCCA matrix. Typically, a sample solution (c = 1 mg/mL) was mixed (1:1) with a saturated HCCA matrix solution (50% ACN/ 50% H_2O) and spotted on the steel plate. Then an additional aliquot of the HCCA solution was added to dilute the sample and spotted again (repeat 3x). Spectra can be obtained in positive and negative mode.

Boronic acid containing peptide tags were characterized via MALDI-FTICR measurements. Spectra can be obtained in positive mode.

Preparation A: A sample solution (c = 1 mg/mL) was mixed (1:1) with a saturated DHB matrix solution (50% ACN/ 50% H_2O) and spotted on the steel plate. Then an additional aliquot of the DHB solution was added to dilute the sample and spotted again (repeat 3x).

Preparation B: A saturated DHB matrix solution (50% ACN/ 50% H_2O) was spotted on the steel plate. After drying, a droplet of the sample solution (c = 1 mg/mL) was added on top of the DHB crystals. After drying, another droplet of saturated DHB matrix solution was added.

The complexes of boronic acid containing peptides and catechol containing peptides were characterized via MALDI-FTICR using SA matrix in the case of the cytochrome c-PEG5000 complex and using HCCA matrix in the case of the simple peptide tag-complexes. Typically, a sample solution (c = 1 mg/mL) was mixed (1:1) with a saturated matrix solution (50% ACN/ 50% H_2O) and spotted on the steel plate. Then an additional aliquot of the HCCA solution was added to dilute the sample and spotted again (repeat 3x). Spectra can be obtained mainly in negative mode.

Alanine-based Peptide Tags

Catechol Tags

Ala-Cat-Ala

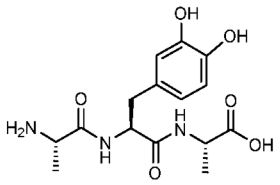

LC-MS: m/z = 340 $[M + H]^+$, (calcd. mass: 340 $[M + H]^+$, formula: $C_{15}H_{21}N_3O_6$).

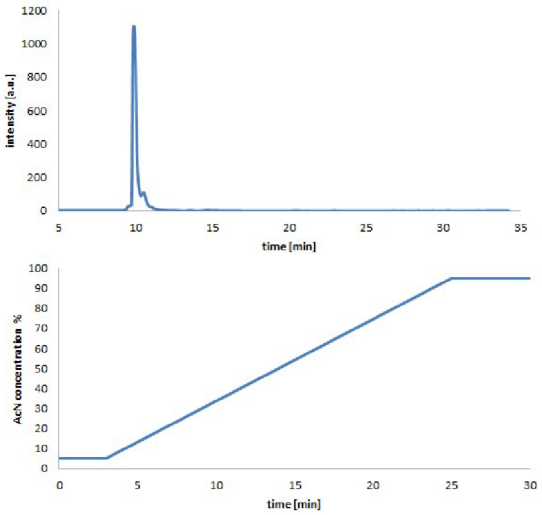

Ala-Cat-Ala-Cat-Ala

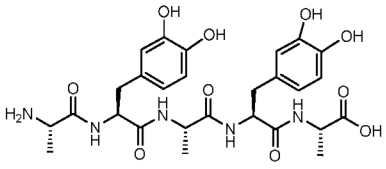

HR-MS (MALDI-TOF, HCCA): m/z = 590.24565 $[M + H]^+$, (calcd. mass: 590.24567 $[M + H]^+$, formula: $C_{27}H_{35}N_5O_{10}$).

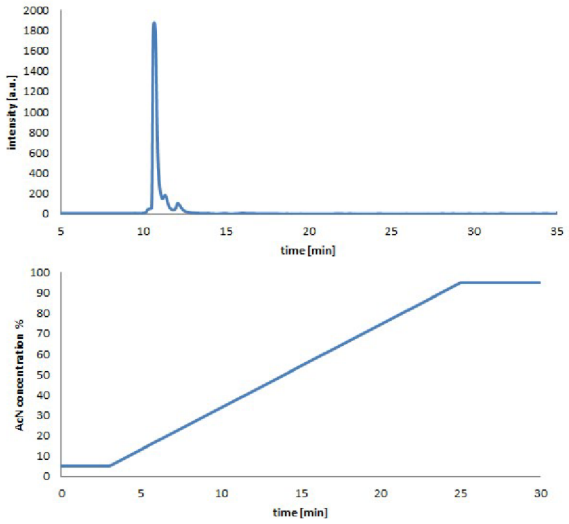

Bor-Tags

Only the main signal of the mass spectra are recorded here. Other detected species resulted from deborylation and water-addition during the measurement with DHB.

FITC-AEEAc-Bor-Ala

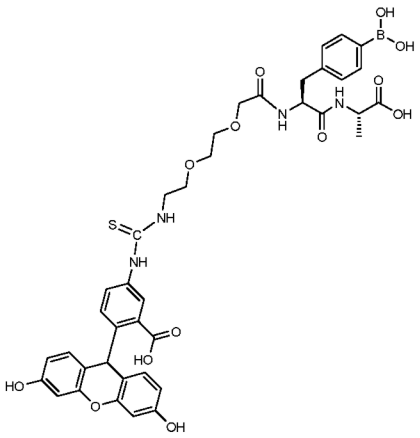

HR-MS (MALDI-TOF, DHB): m/z = 815.23959 $[M + H]^+$, (calcd. mass: 815.24070 $[M + H]^+$, formula: $C_{39}H_{39}BN_4O_{13}S$).

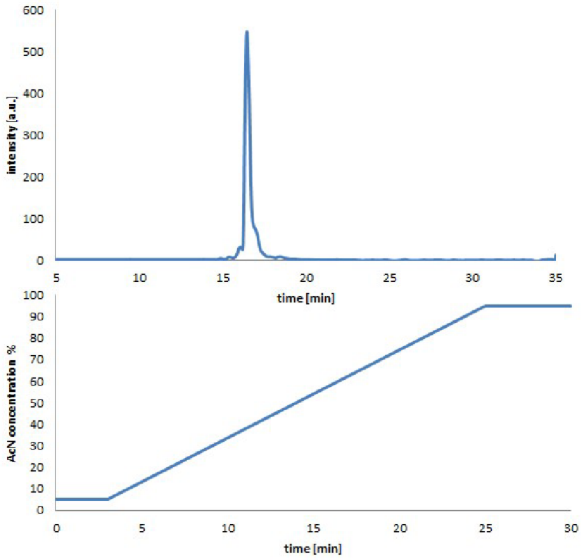

FITC-AEEAc-Bor-Ala-Bor-Ala

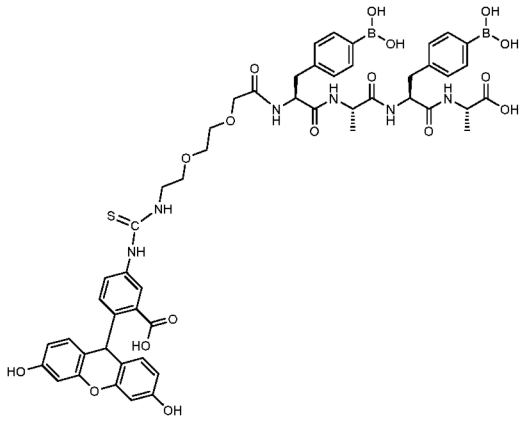

HR-MS (MALDI-TOF, DHB): m/z = 1059.34259 $[M - H_2O + H]^+$, (calcd. mass: 1059.34344 $[M - H_2O + H]^+$, formula: $C_{51}H_{52}B_2N_6O_{16}S$).

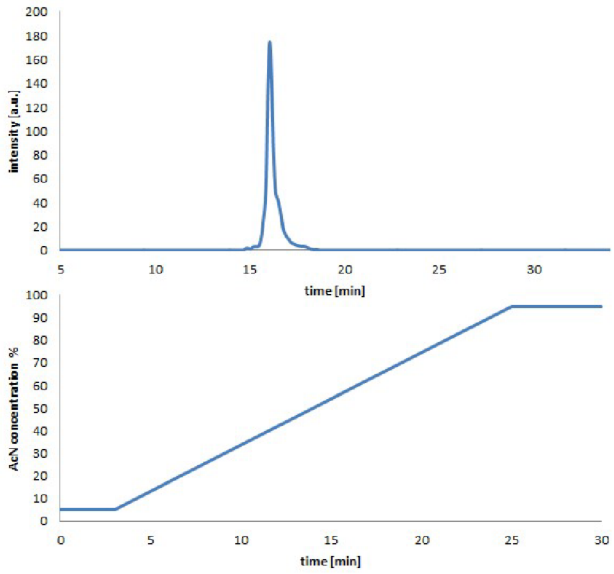

Lysine-based Peptide Tags

Cat-Tags

Lys-Cat-Lys

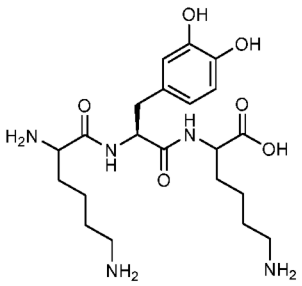

MS (MALDI-TOF, CHCA): m/z = 454.844 $[M + H]^+$, (calcd. mass: 454.2660 $[M + H]^+$, formula: $C_{21}H_{35}N_5O_6$).

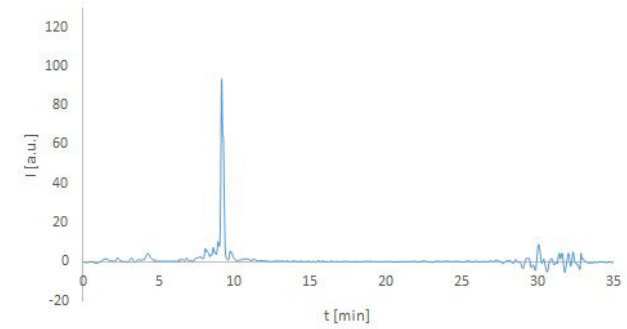

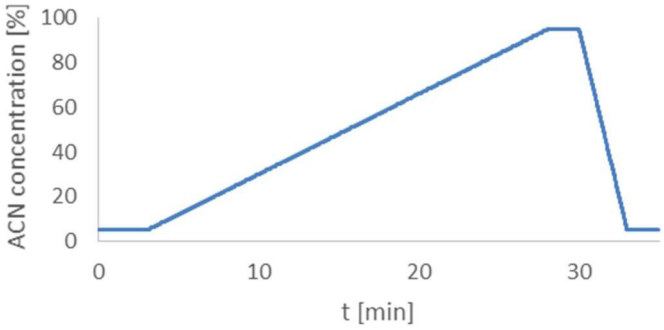

Lys-Cat-Lys-Cat-Lys-Cat-Lys

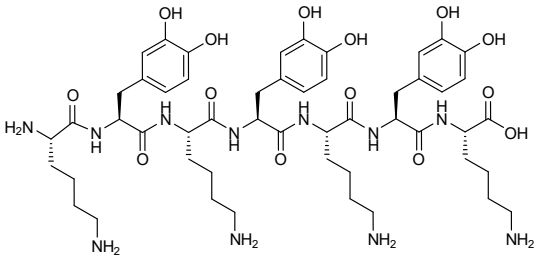

MS (MALDI-TOF, CHCA): m/z = 1066.409 $[M-H]^-$, (calcd. mass: 1066.5579 $[M-H]^-$, formula: $C_{51}H_{77}N_{11}O_{14}$).

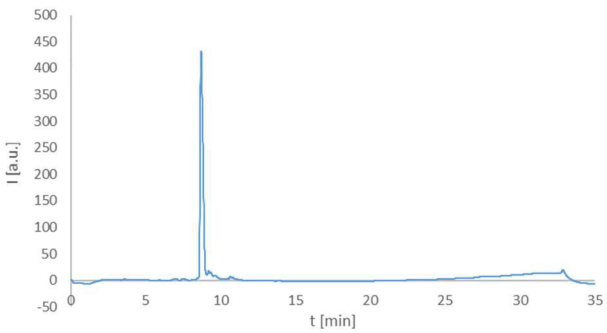

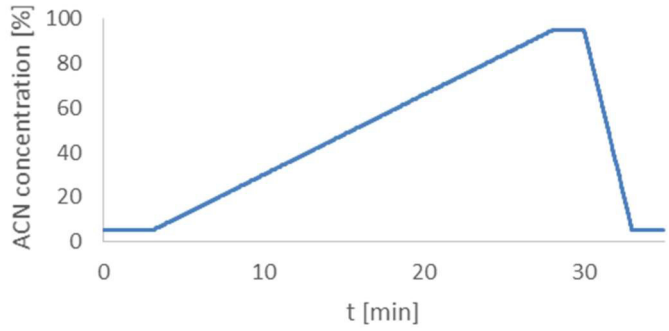

Maleimide-AEEAc-Cat-Lys-Cat-Lys-Cat-Lys

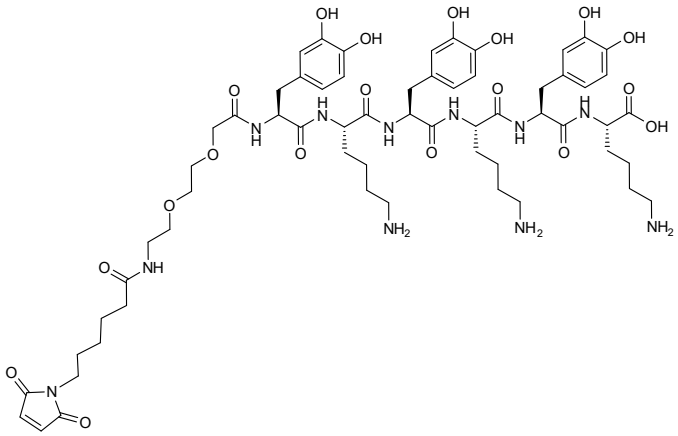

MS (MALDI-TOF, CHCA): m/z = 1276.647 $[M-H]^-$, (calcd. mass: 1276.6107 $[M-H]^-$, formula: $C_{61}H_{87}N_{11}O_{19}$).

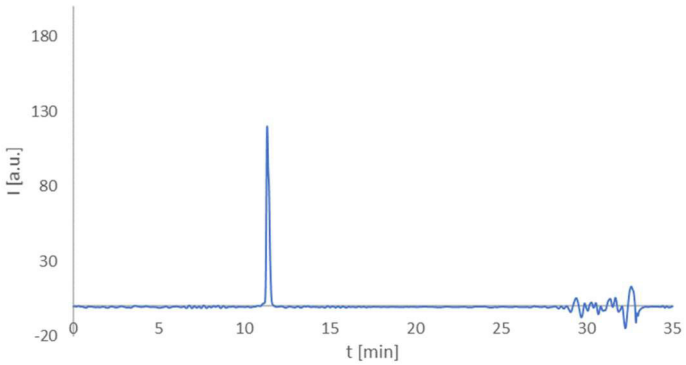

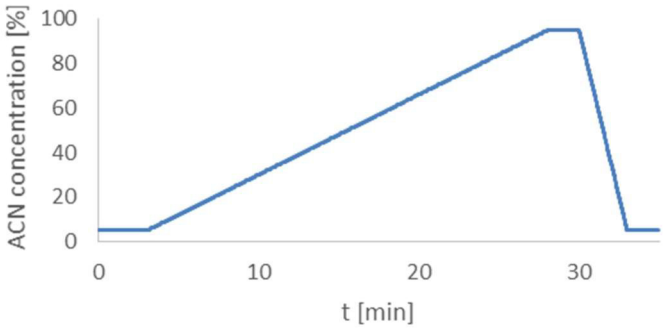

Lys-Cat-Lys-Ala-Lys-Cat-Lys-Cat-Lys

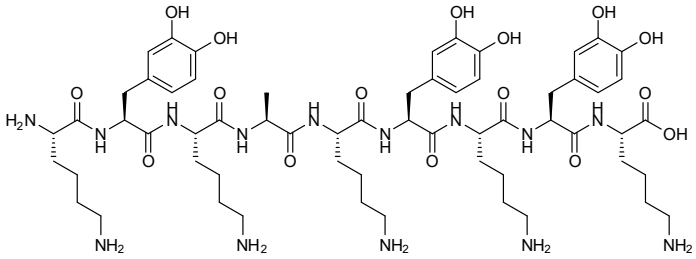

MS (MALDI-TOF, CHCA): m/z = 1265.688 $[M-H]^-$, (calcd. mass: 1265.6899 $[M-H]^-$, formula: $C_{60}H_{94}N_{14}O_{16}$).

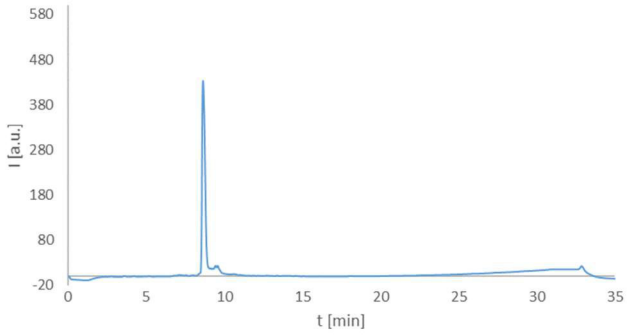

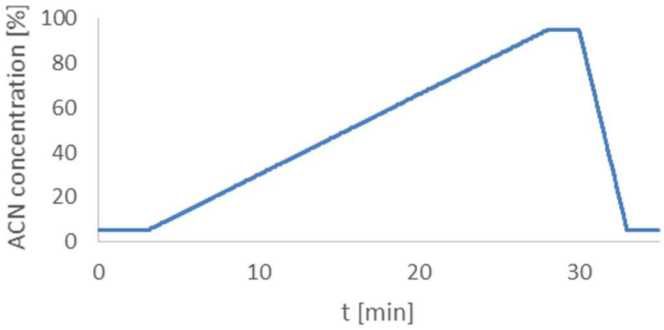

DyLight®650-Cys-AEEAc-Cat-Lys-Cat-Lys-Cat-Lys

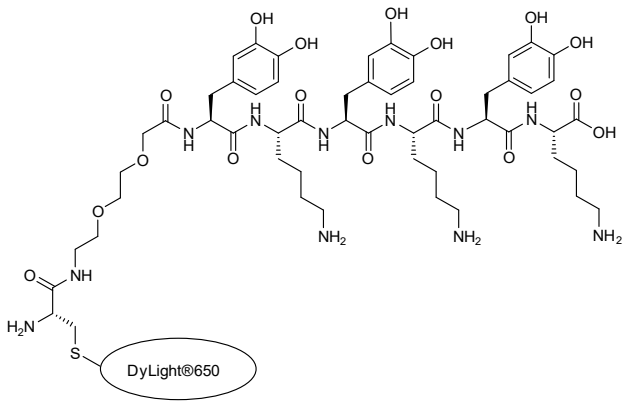

MS (MALDI-TOF, DHB): m/z = 2277.131 $[M-H]^-$, (calcd. mass: 2277.546 $[M-H]^-$, formula: formula cause of DyLight®650 not calculable.

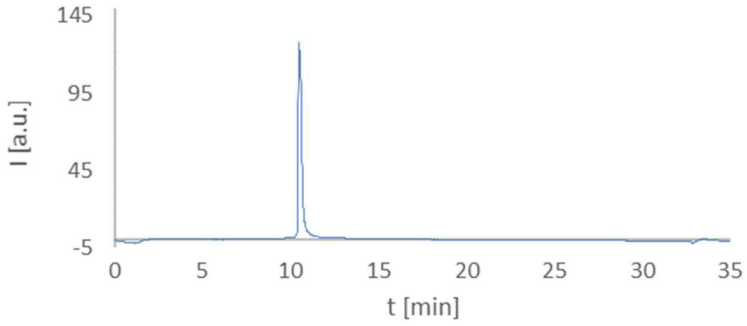

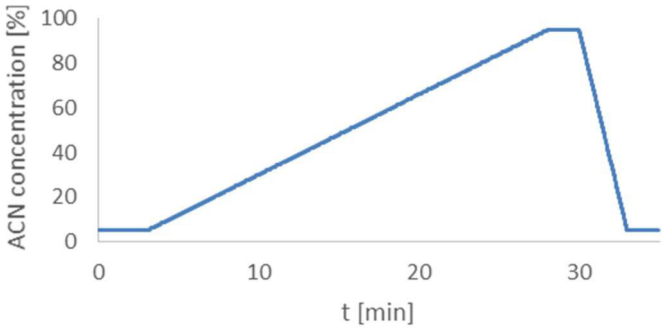

Cys-Lys-Lys-Lys-Cat-Cat-Cat

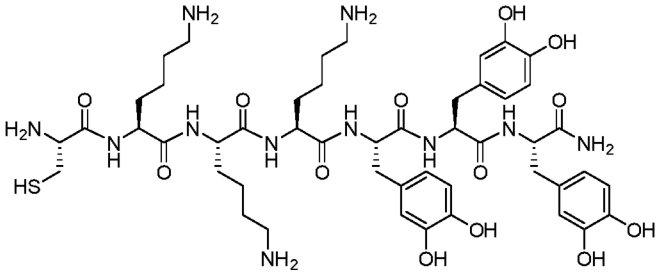

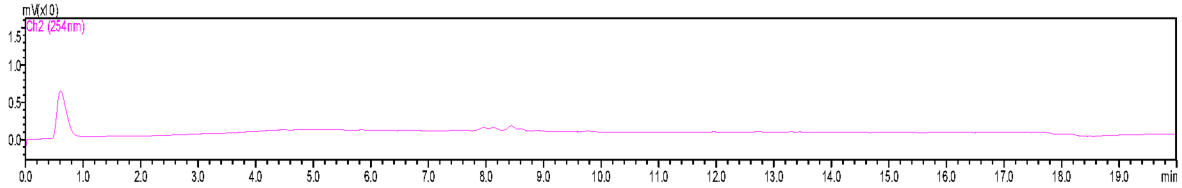

MS (MALDI-TOF, DHB): m/z = 1042.541 $[M+H]^+$ (calcd. mass: 1042.503 $[M-H]^-$ formula: $C_{48}H_{71}N_{11}O_{13}S$)

FITC-Cys-Lys-Lys-Lys-Cat-Cat-Cat

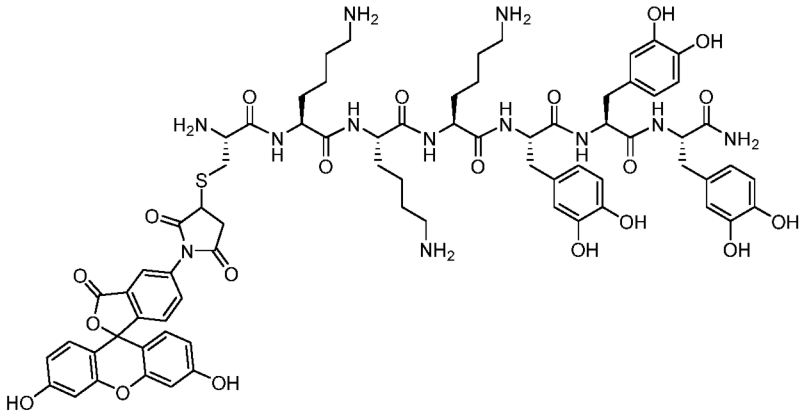

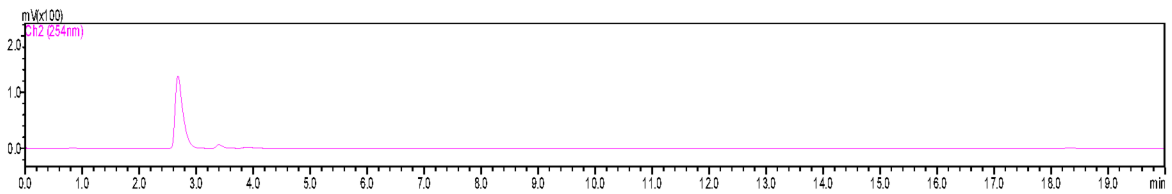

MS (MALDI-TOF, DHB): m/z = 1469.496 $[M+H]^+$ (calcd. mass: 1469.572 $[M+H]^+$ formula: $C_{72}H_{84}N_{12}O_{20}S$)

Bor-Tags

Only the main signal of the mass spectra are recorded here. Other detected species resulted from deborylation and water-addition during the measurement with DHB.

Cys-AEEAc-Bor-Lys-Bor-Lys-Bor-Lys

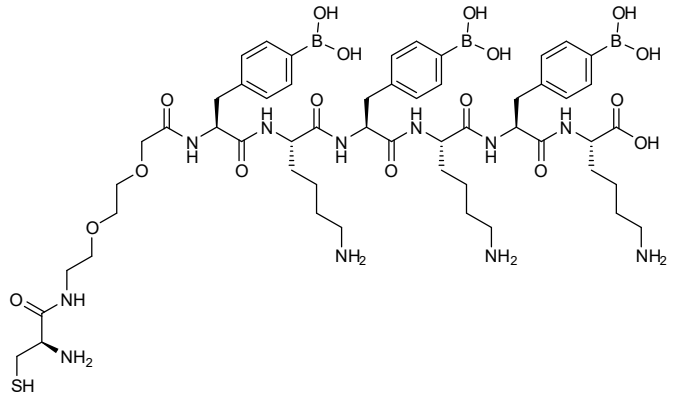

MS (MALDI-TOF, DHB): m/z = 1578.996 $[M + 3\ DHB - 6\ H_2O + H]^+$, (calcd. mass: 1578.6284 $[M + 3\ DHB - 6\ H_2O + H]^+$, formula: $C_{54}H_{84}B_3N_{11}O_{17}S$).

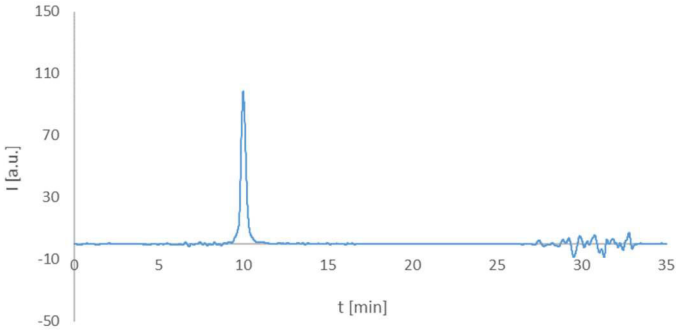

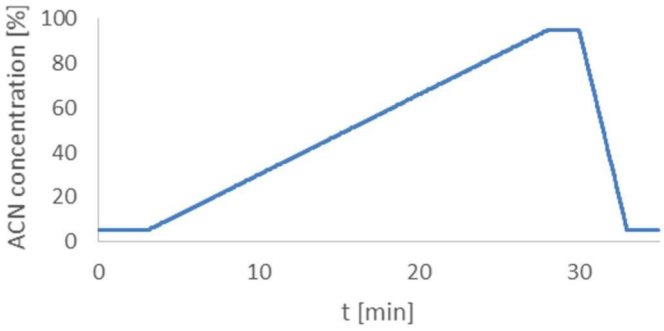

AEEAc-Bor-Lys-Bor-Lys-Bor-Lys

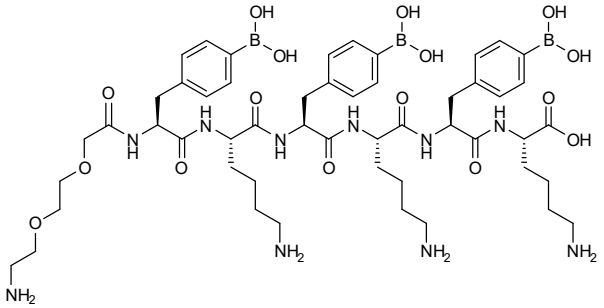

MS (MALDI-TOF, DHB): m/z = 1475.723 [M + 3 DHB – 6 H_2O + H]$^+$, (calcd. mass: 1475.6192 [M + 3 DHB – 6 H_2O + H]$^+$, formula: $C_{51}H_{79}B_3N_{10}O_{16}$).

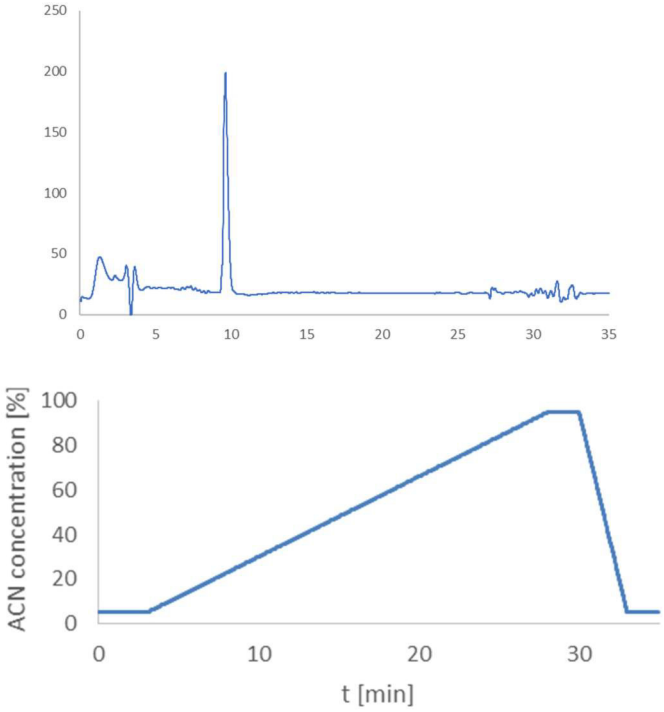

Fluorescein-Cys-AEEAc-Bor-Lys-Ala-Lys-Bor-Lys-Bor-Lys

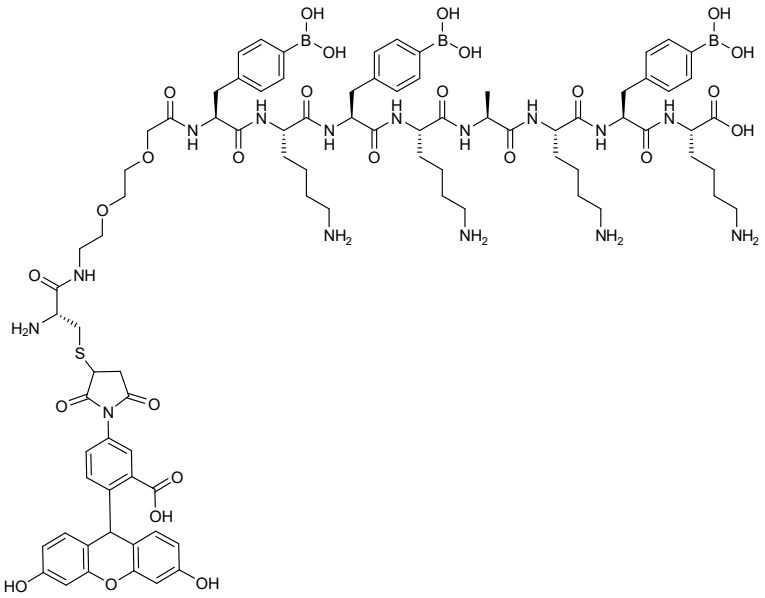

MS (MALDI-TOF, DHB): m/z = 2206.640 [M + 3 DHB – 6 H_2O + H]$^+$, (calcd. mass: 2206.8453 [M + 3 DHB – 6 H_2O + H]$^+$, formula: $C_{87}H_{116}B_3N_{15}O_{26}S$).

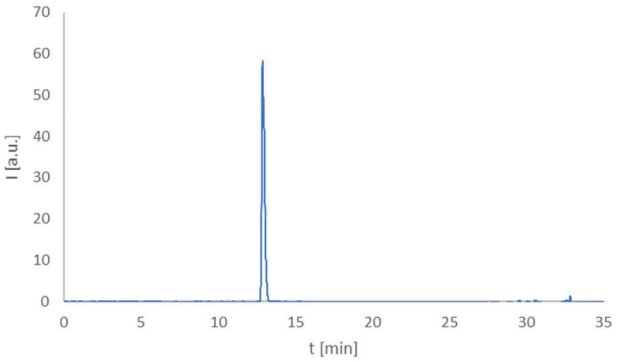

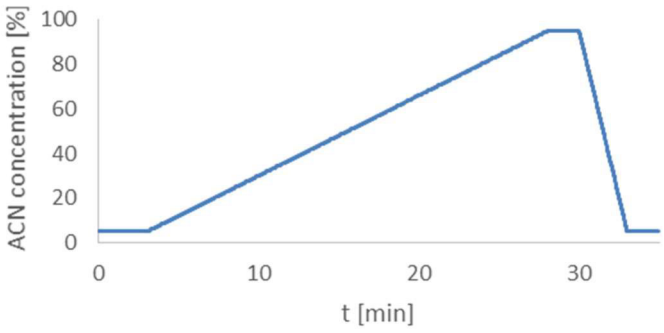

Fluorescein-Cys-AEEAc-Bor-Lys-Bor-Lys-Bor-Lys

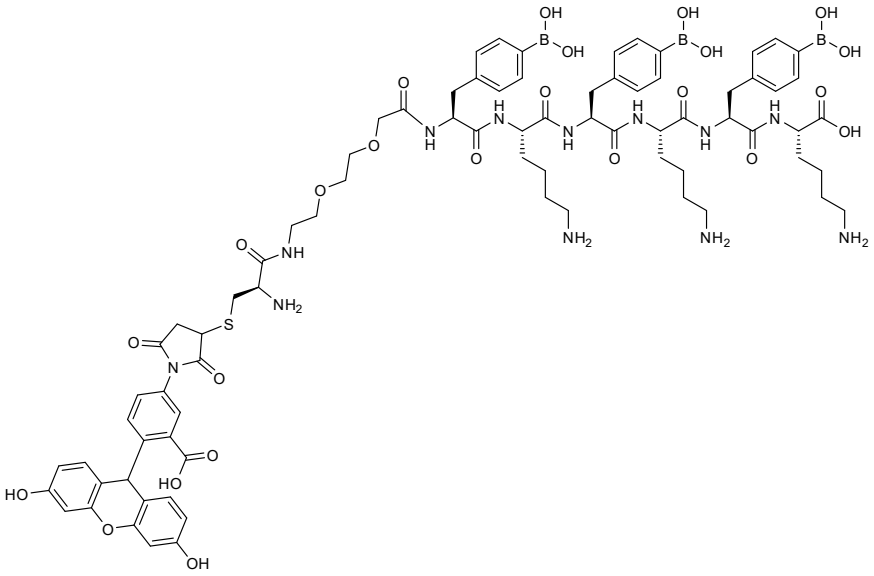

MS (MALDI-TOF, DHB): m/z = 2007.906 [M + 3 DHB – 6 H_2O + H]$^+$, (calcd. mass: 2007.7132 [M + 3 DHB – 6 H_2O + H]$^+$, formula: $C_{78}H_{99}B_3N_{12}O_{24}S$).

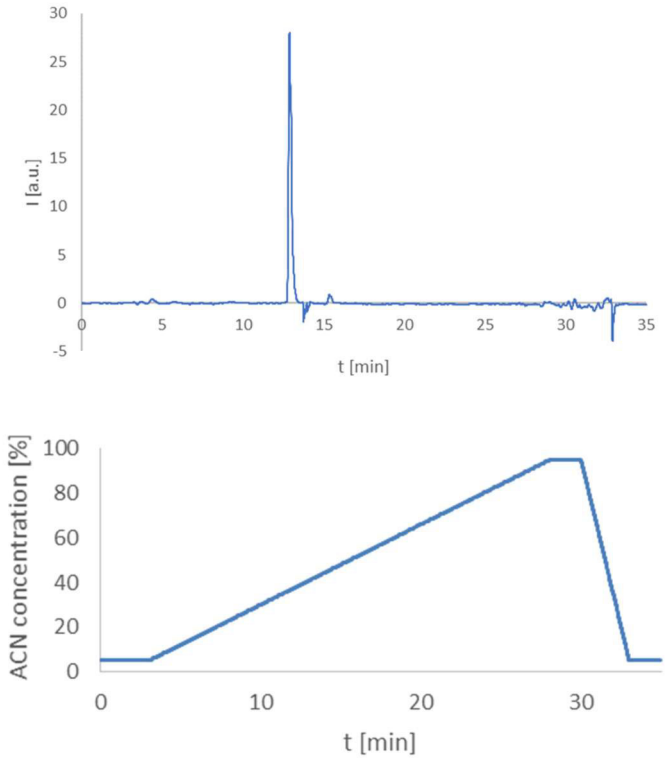

Lys-Lys-Lys-Bor-Bor-Bor

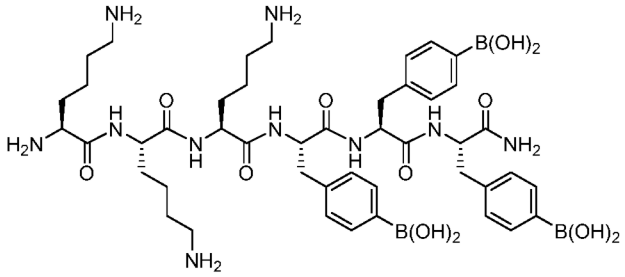

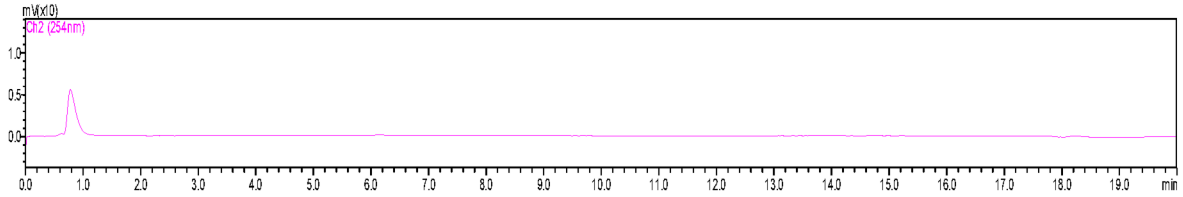

MS (MALDI-TOF, DHB): m/z = 975.563 $[M + H]^+$, (calcd. mass: 975.545 $[M + H]^+$, formula: $C_{45}H_{69}B_3N_{10}O_{12}$).

Lys-Bor-Lys-Cat-Lys-Bor-Lys

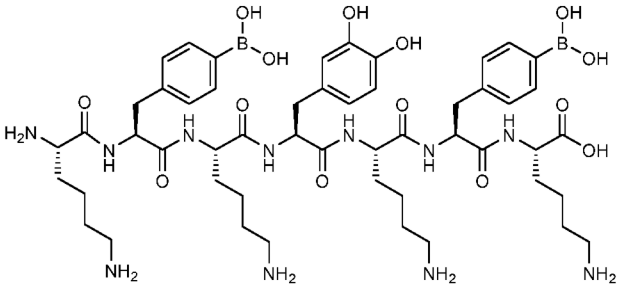

MS (MALDI-TOF, DHB): m/z = 1328.61826 $[M + 3\ DHB - 6\ H_2O + H]^+$, (calcd. mass: 1328.62 $[M + 3\ DHB - 6\ H_2O + H]^+$, formula: $C_{51}H_{79}B_2N_{11}O_{14}$).

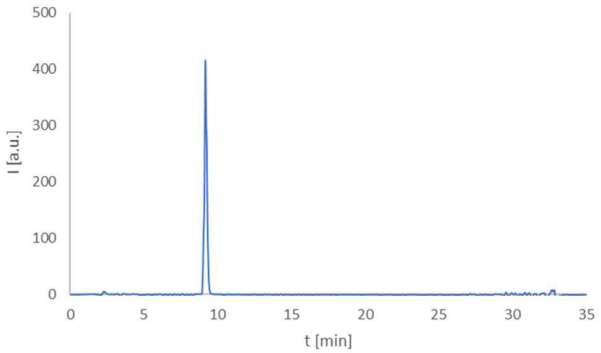

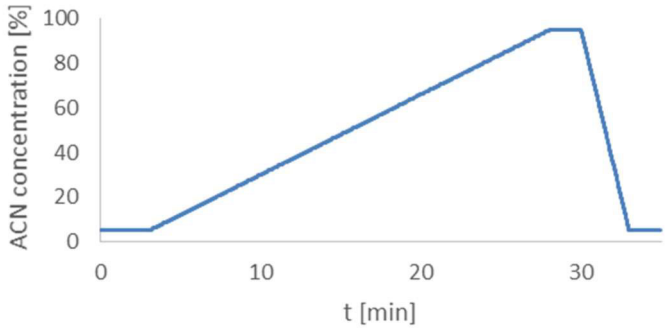

Cys-AEEAc-Cat-Lys-Bor-Lys-Cat-Lys

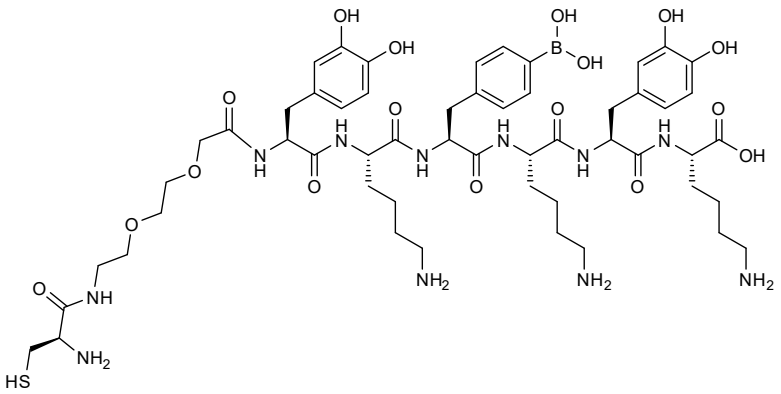

MS (MALDI-TOF, DHB): m/z = 1318.58346 [M + 1 DHB – 2 H_2O + H]$^+$, (calcd. mass: 1318.58 [M + 1 DHB – 2 H_2O + H]$^+$, formula: $C_{54}H_{82}BN_{11}O_{17}S$).

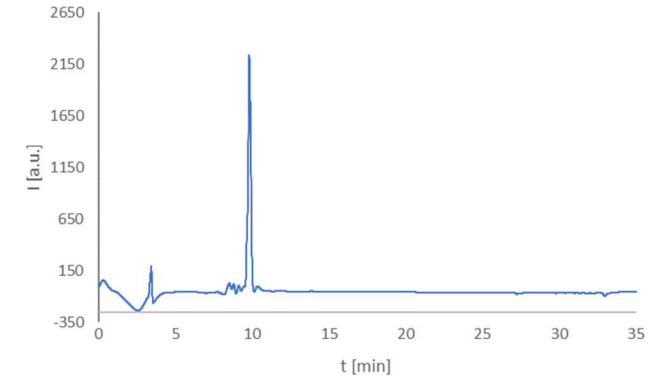

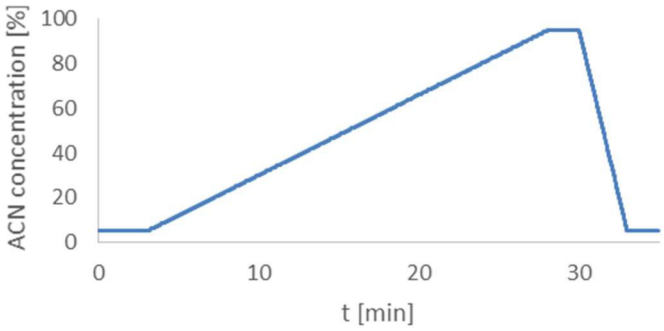

Fluorescein-Cys-AEEAc-Cat-Lys-Bor-Lys-Cat-Lys

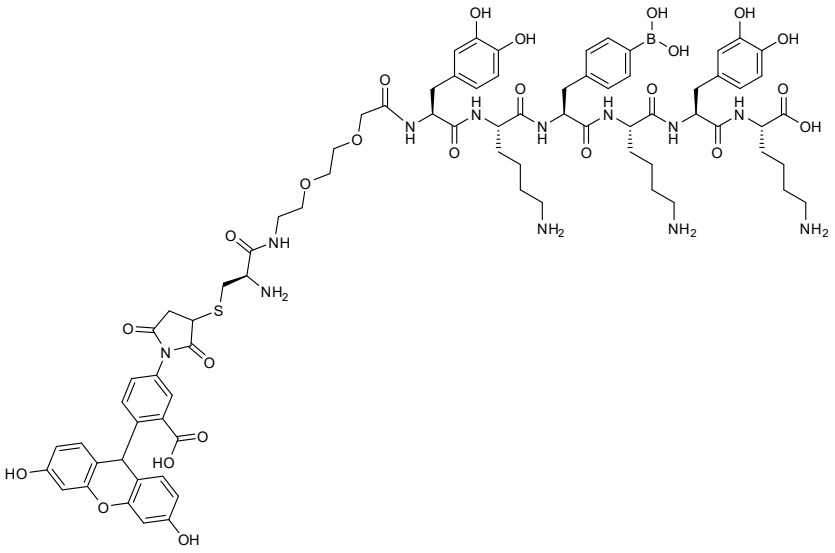

MS (MALDI-TOF, DHB): m/z = 1747.65660 $[M + 1\ DHB - 2\ H_2O + H]^+$, (calcd. mass: 1747.67 $[M + 1\ DHB - 2\ H_2O + H]^+$, formula: $C_{78}H_{97}BN_{12}O_{24}S$).

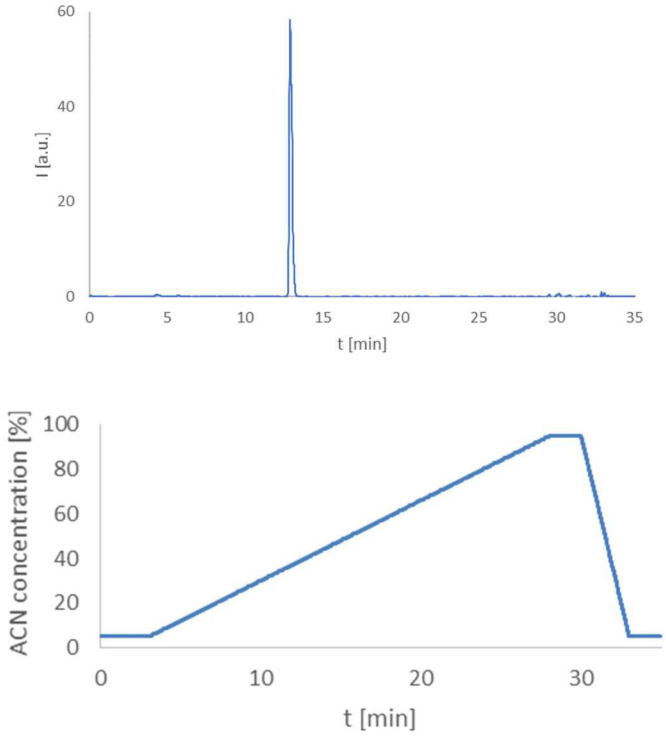

2.6 Binding Affinity Analysis (Fluorescence Quenching Assay)

General procedure:

Fluorescence spectra were recorded on an Infinite® M1000 PRO microplate reader (Tecan®) and on a microscale thermophoresis device (Monolith NT.115 of NanoTemper Technologies GmbH). 20 µL of different concentrations of the non-labeled compound were served (dilutions series with factor of 2 for each step, phosphate buffer 300 mM, pH 7.4). To this a constant amount of the fluorescein-labeled compound (vol. 20 µL, phosphate buffer 300 mM, pH 7.4) below the lowest amount in the dilution series of the non-labeled one was added. After mixing for 2 h at 450 rpm, 35 µL of every mixture was placed in black UV Star® 384 microliter well-plates (Greiner bio-one®) or 10 µL was sucked in a capillary for the microscale thermophoresis device (Monolith NT.115 Capillaries). After 15 min of equilibration time, the fluorescence emission was recorded at 520 nm upon excitation at 488 nm with multiple reads per well (3x3) or with the green/red laser device with a laser power of 20% on the settings of the microscale thermophoresis device.

Exemplary described procedure (of the measurement with Fluorescein-**(AX)$_3$** and **(BX)$_3$**):

At the beginning, the serial dilution of the catechol peptide tag was produced. For that, 8 solutions with a volume of 20 µL each (phosphate buffer 300 mM, pH 7.4) were prepared. Furthermore, one solution with the starting concentration of 0.5 mM of the catechol peptide tag in 40 µL (phosphate buffer 300 mM, pH 7.4) was mixed. 20 µL of the solution was diluted with 20 µL and is iterated for the 8 prepared solutions. At the end the catechol peptide serial dilution has 9 solutions with 20 µL volume each and the following concentrations:

Dilution of catechol peptide	Concentration [mM]
1	0.50000
2	0.25000
3	0.12500
4	0.06250
5	0.03125
6	0.01562
7	0.00781
8	0.00390
9	0.00195

To each of these solutions, 20 µL of a prepared 0.00048 mM fluorescein-boronic acid peptide solution (phosphate buffer 300 mM, pH 7.4) was introduced.

The resulting catechol-boronic acid mixtures (after mixing every solution contained half of the prepared concentrations) were then shaken for 2 h at 450 rpm. In the next step, 35 µL of the solutions were pipetted in the wells/capillaries for fluorescence spectroscopy (general procedure describes settings of the device).

Used peptide sequences:

Fluorescein-Cys-AEEAc-Bor-Lys-Bor-Lys-Bor-Lys	+	Lys-Cat-Lys-Cat-Lys-Cat-Lys
Fluorescein-Cys-AEEAc-Bor-Lys-Bor-Lys-Bor-Lys	+	Lys-Cat-Lys-Ala-Lys-Cat-Lys-Cat-Lys
Fluorescein-Cys-AEEAc-Bor-Lys-Ala-Lys-Bor-Lys-Bor-Lys	+	Lys-Cat-Lys-Ala-Lys-Cat-Lys-Cat-Lys
Fluorescein-Cys-AEEAc-Cat-Lys-Bor-Lys-Cat-Lys	+	Lys-Bor-Lys-Bor-Lys-Bor-Lys
FITC-AEEAc-Bor-Ala-Bor-Ala	+	Ala-Cat-Ala-Cat-Ala
FITC-AEEAc-Bor-Ala	+	Ala-Cat-Ala
Lys-Lys-Lys-Bor-Bor-Bor	+	FITC-Cys-Lys-Lys-Lys-Cat-Cat-Cat

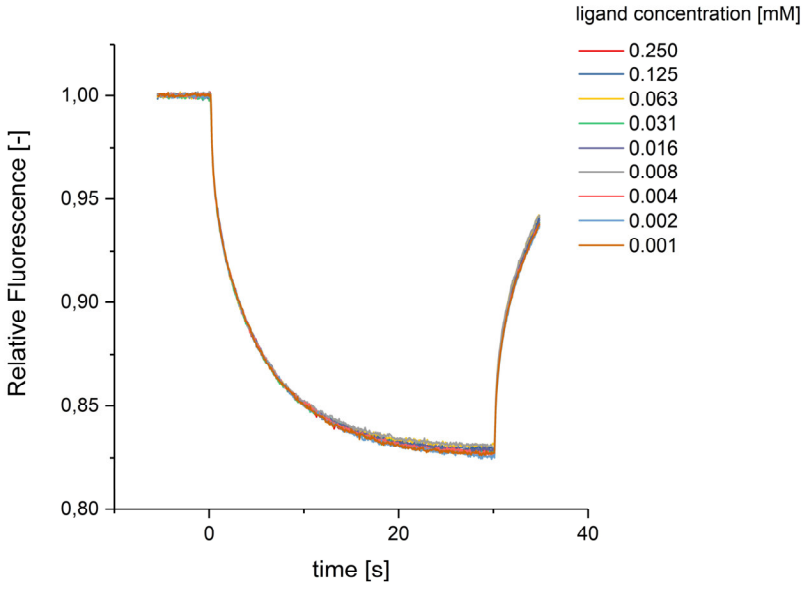

Figure S4. Fluorescence decay as a result of thermophoresis of **(AX)$_3$-(BX)$_3$** binding demonstrating the absence of aggregates and higher ordered structures.

Statistics and reproducibility

The concentration dependent fluorescence data points were plotted in OriginPro 2017G. To compare the binding concentrations (or K_a), the points of inflection were calculated by the OriginPro 2017G software by using sigmoidal fitting according to the Boltzmann function. Each individual experiment was conducted in triplicates with a different batch of synthesized peptides. Three sets of experiments were conducted to obtain the data in Figure 2a of the main manuscript. The point of inflection values of the different experiments were used to determine the arithmetic average binding concentrations (or K_a) and standard deviations. The standard deviation points for **(AX)-(BX)** (blue in Figure 2a) is smaller than the represented square itself and thus not graphically observable.

2.7 Dynamic light scattering

Dynamic light scattering on the **(AX)$_3$-(BX)$_3$** binding complex in 300 mM PB buffer, pH 7.4, was performed using Nano-ZetaSizer (Malvern Instruments). The 173° backscatter was measured using a 633 nm laser at 25 °C. No aggregates were detected.

2.8 FRET experiment

Fluorescence spectra were recorded on an Infinite® M1000 PRO microplate reader (Tecan). 30 µL of the boronic acid peptide tag (Fluorescein-Cys-AEEAc-Bor-Lys-Bor-Lys-Bor-Lys), 30 µL of the catechol peptide tag (Dyelight650®-AEEAc-Cat-Lys-Cat-Lys-Cat-Lys) and 30 µL of the mixture of both (every solution has a concentration of 1 mM of the peptide and was produced with phosphate buffer (300 mM, pH 7.4)) were placed in a black UV Star® 384 microliter well-plate (Greiner bio-one), each. The mixtures were stirred for 2 h at 450 rpm and measured with an excitation wavelength of 488 nm and the emission was recorded 550 nm – 850 nm.

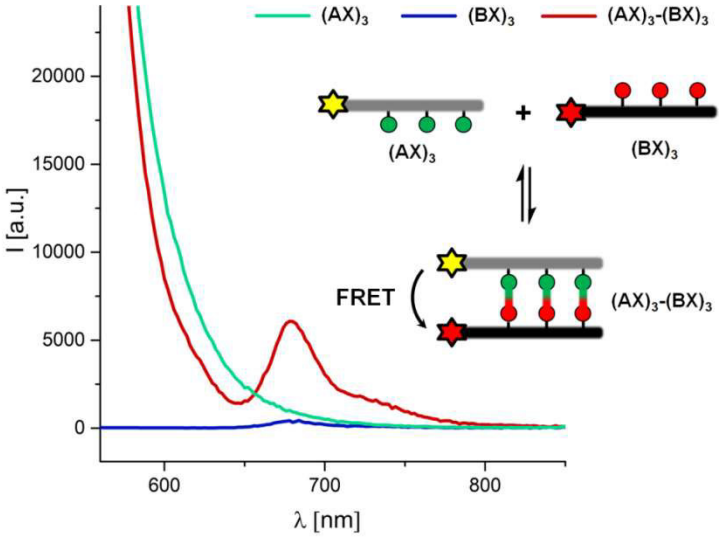

Figure S5. FRET of **$(AX)_3$-$(BX)_3$** binding in phosphate buffer pH 7.4

2.9 ^{1}H NMR Spectroscopy: TOCSY, NOESY, DOSY

The ^{1}H NMR data of **$(AX)_3$**, **$(BX)_3$** and **$(AX)_3$-$(BX)_3$** as well as **BAB** and **BAB-$(BX)_3$** were acquired on a Bruker Avance 850 MHz spectrometer equipped with a 5 mm TXI with a Z gradient. The measurements were performed at 298 K with a sample concentration of 2 mM in 300 mM phosphate buffer, pH 7.4, 9:1 (H_2O:D_2O). Chemical shifts were recorded in parts per million (ppm), using ^{1}H NMR resonance of H_2O to reference the ^{1}H NMR spectrum with the methyl resonance of TMS at 0.0 ppm, according to IUPAC recommended method.[5] Two-dimensional NMR spectra were analyzed using NMRFAM-SPARKY.[6] The proton resonances were assigned manually

with the standard method of using TOCSY (Total Correlations Spectroscopy)[7] fingerprints of the amino acids. Unfortunately, the backbone amide protons were not detectable, thus a sequential assignment was not possible. Additionally, the side chain amine protons of the Lysine groups were also not detectable. The numbering of the assigned groups is to differentiate between the individual amino acids, but shall not indicate the position of this amino acid in the peptide. Additionally, the assigned aromatic protons do not necessarily need to belong to the same numbered group of the H_α and side chain protons, due to the lack of scalar couplings between those two regions in the respective amino acids.

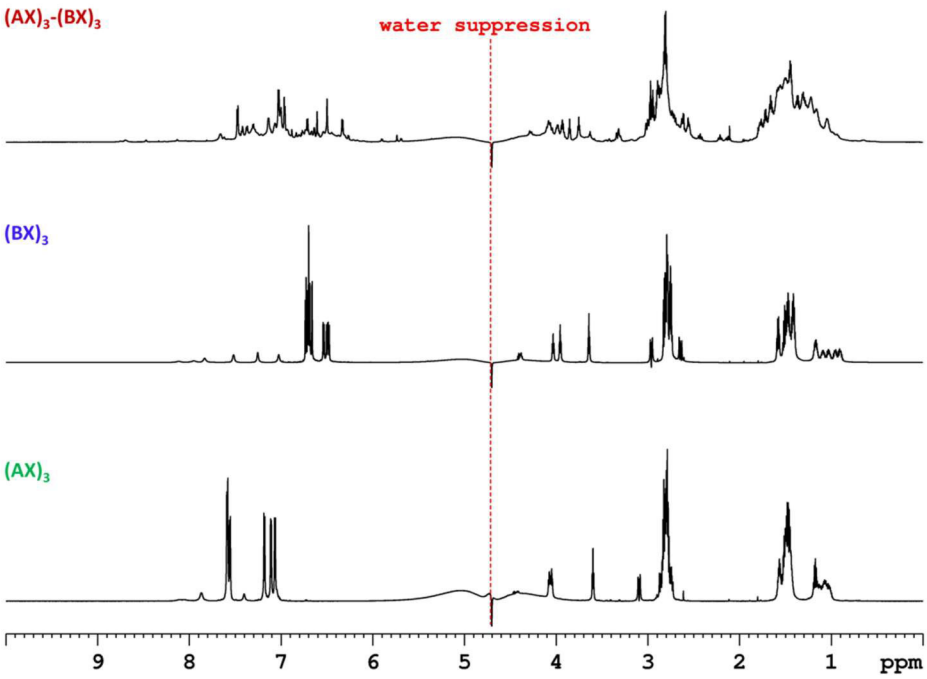

Figure S6. ^{1}H NMR of **$(AX)_3$-$(BX)_3$** and its separate constituents in phosphate buffer pH 7.4 H_2O/D_2O 9/1 with water suppression.

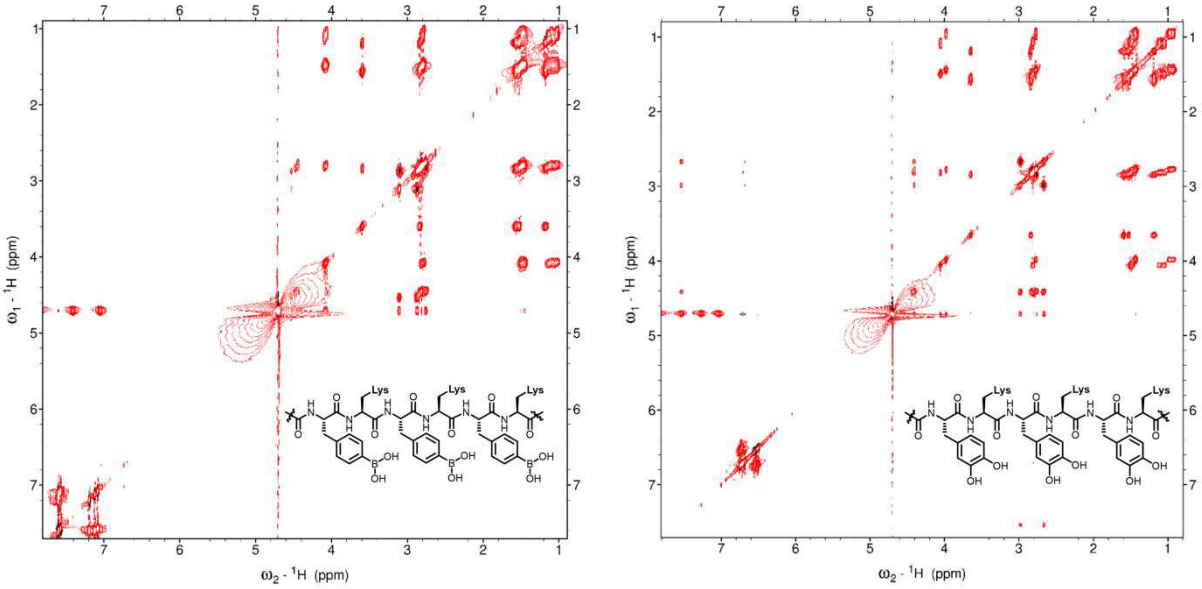

Figure S7. ^{1}H TOCSY NMR of **$(AX)_3$** (left) and **$(BX)_3$** (right) in phosphate buffer pH 7.4 H_2O/D_2O 9/1 with water suppression.

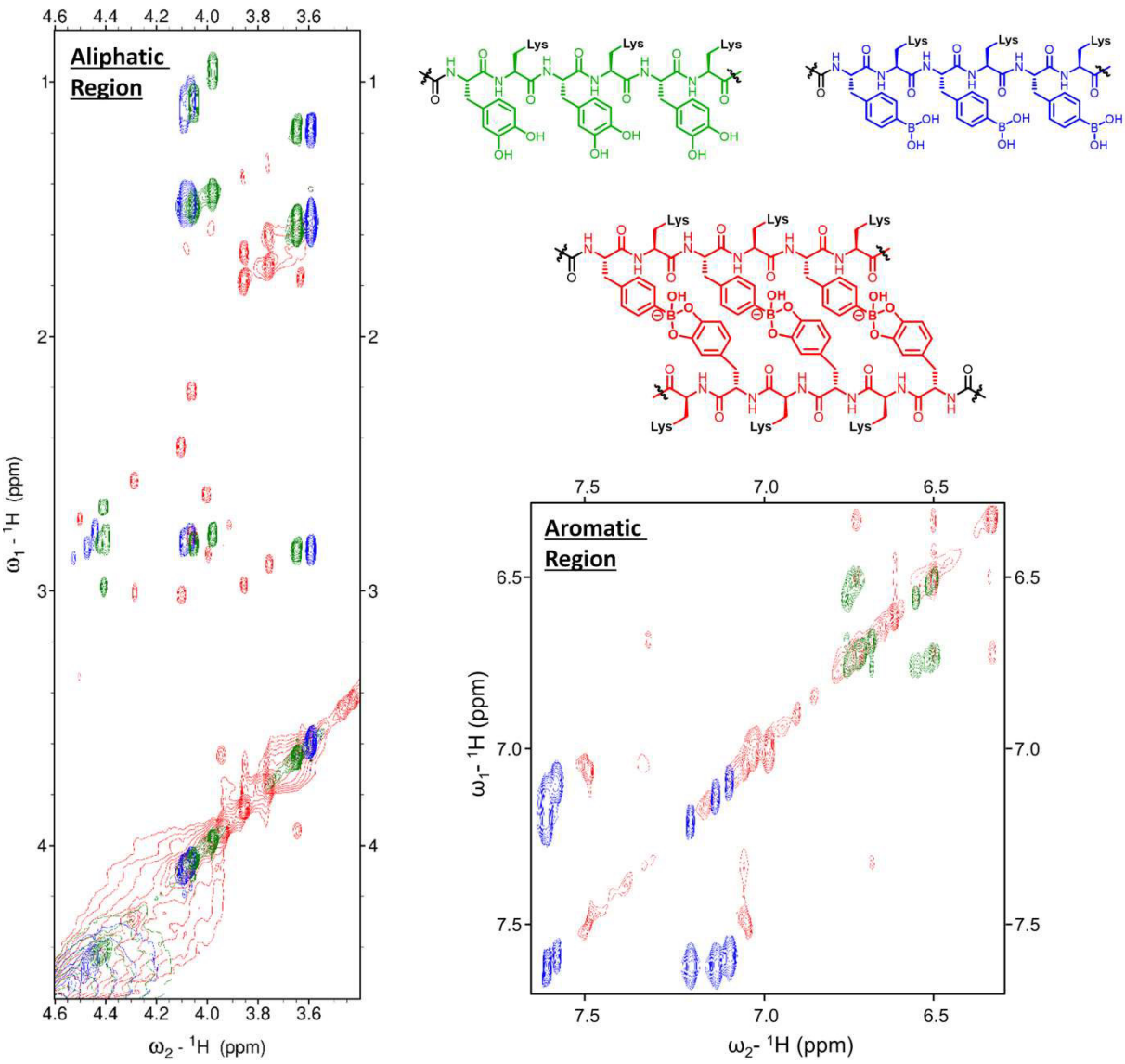

Figure S8. ^{1}H TOCSY NMR of **(AX)$_3$-(BX)$_3$** and its separate constituents in phosphate buffer pH 7.4 H_2O/D_2O 9/1 with water suppression.

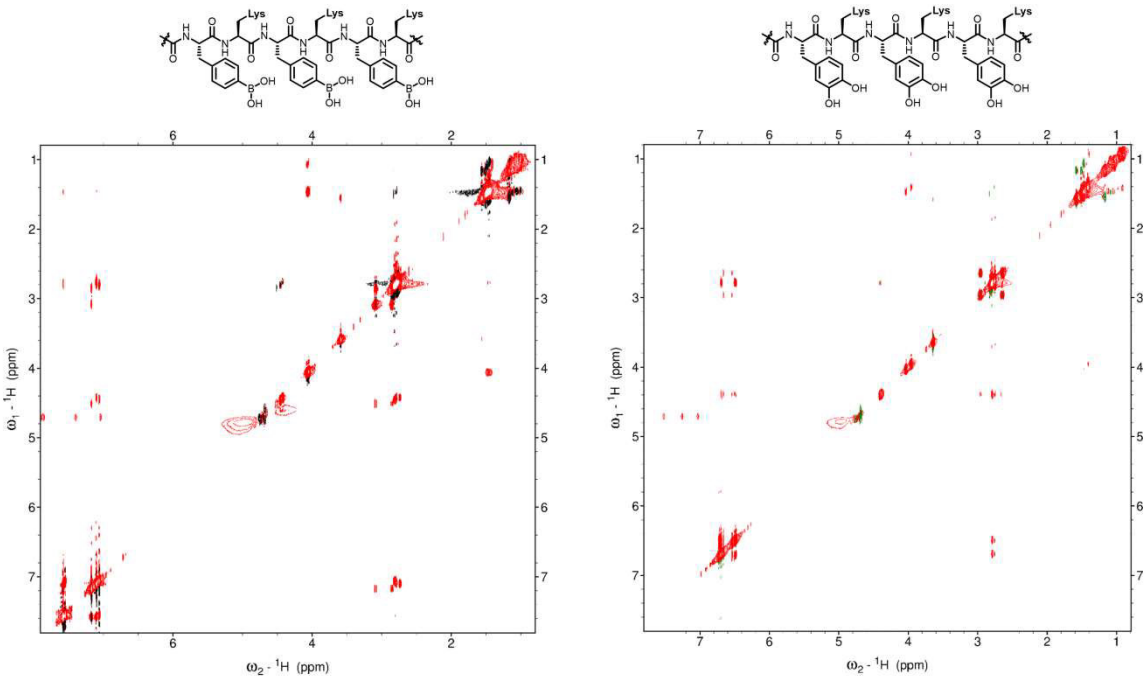

Figure S9. ^{1}H NOESY NMR of **(AX)$_3$** (left) and **(BX)$_3$** (right) in phosphate buffer pH 7.4 H_2O/D_2O 9/1 with water suppression.

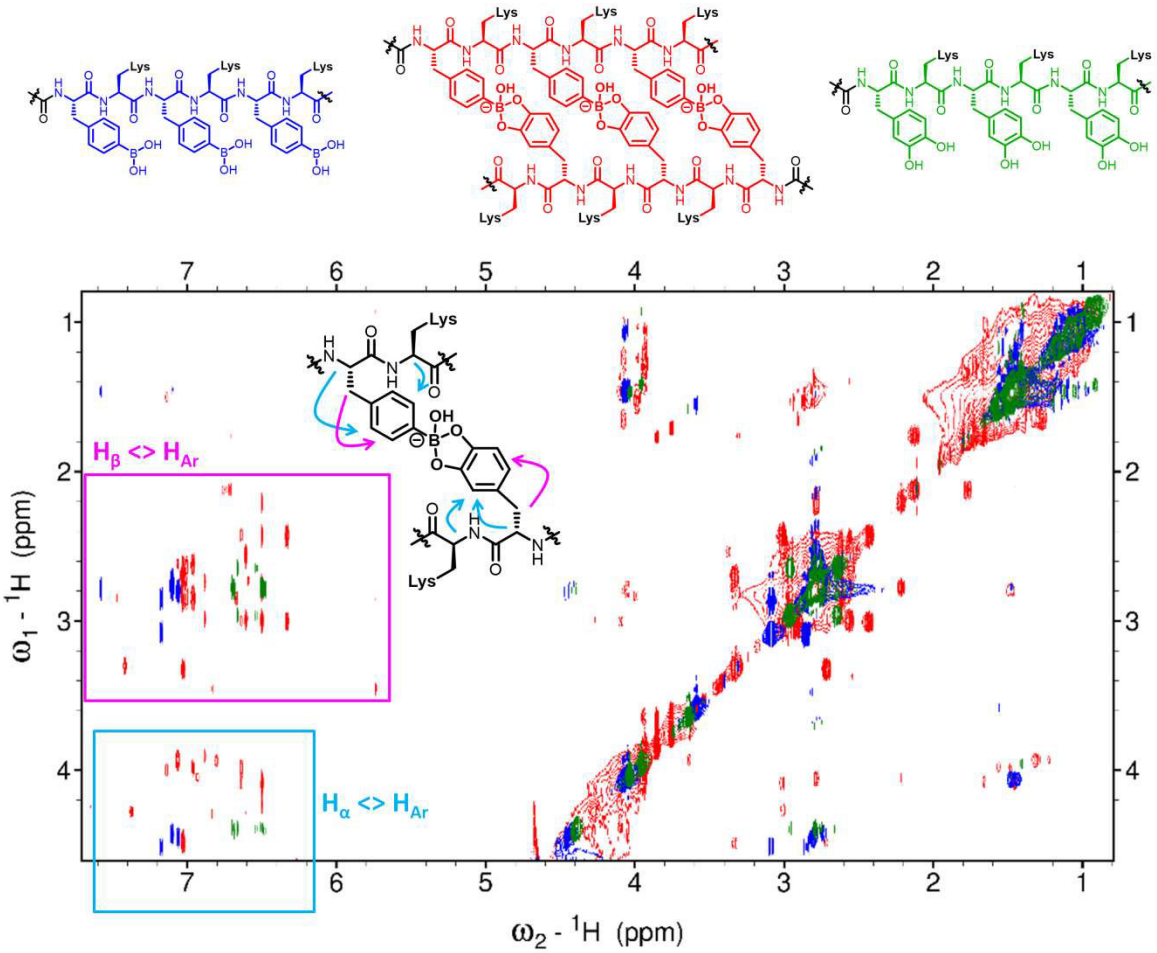

Figure S10. ^{1}H NOESY NMR of **(AX)$_3$-(BX)$_3$** and its separate constituents in phosphate buffer pH 7.4 H_2O/D_2O 9/1 with water suppression.

Proton resonance assignment of $(AX)_3$:

Group	Atom	Nuc	Shift
BA1	HA	1H	4.532
BA1	HB1	1H	3.106
BA1	HB2	1H	2.871
BA1	HD#	1H	7.117
BA1	HE#	1H	7.597
K1	HA	1H	4.092
K1	HB#	1H	1.477
K1	HE#	1H	2.808
K1	HG#	1H	1.085
BA2	HA	1H	4.476
BA2	HB#	1H	2.829
BA2	HD#	1H	7.188
BA2	HE#	1H	7.602
K2	HA	1H	4.067
K2	HB#	1H	1.479
K2	HE#	1H	2.789
K2	HG#	1H	1.056
BA3	HA	1H	4.444
BA3	HB#	1H	2.765
BA3	HD#	1H	7.079
BA3	HE#	1H	7.572
K3	HA	1H	3.594
K3	HB#	1H	1.555
K3	HE#	1H	2.836
K3	HG#	1H	1.181

Proton resonance assignment of $(BX)_3$:

Group	Atom	Nuc	Shift
Cat1	HA	1H	4.428
Cat1	HB1	1H	2.812
Cat1	HB2	1H	2.773
Cat1	HD#	1H	6.557
Cat1	HE	1H	6.746
K1	HA	1H	4.056
K1	HB#	1H	1.493
K1	HD#	1H	1.116
K1	HE#	1H	2.817
K1	HG#	1H	1.053

Cat2	HA	1H	4.408
Cat2	HB1	1H	2.981
Cat2	HB2	1H	2.665
Cat2	HD#	1H	6.52
Cat2	HE	1H	6.72
K2	HA	1H	3.978
K2	HB#	1H	1.436
K2	HD#	1H	0.966
K2	HE#	1H	2.777
K2	HG#	1H	0.938
Cat3	HD#	1H	6.502
Cat3	HE	1H	6.709
K3	HA	1H	3.649
K3	HB1	1H	1.594
K3	HB2	1H	1.532
K3	HD#	1H	1.187
K3	HE#	1H	2.842

Diffusion Ordered NMR (DOSY)

The DOSY experiments with water suppression (stebpgp1s19) were executed with a 5 mm TXI $^{1}H/^{13}C/^{15}N$ z-gradient probe and a gradient strength of 5.516 [G/mm] on the 850 MHz spectrometer. The gradient strength was calibrated the diffusion coefficient of a sample of $^{2}H_2O/^{1}H_2O$ at a defined temperature of 298K and compared with the literature.

The temperature was defined with a standard ^{1}H methanol NMR sample. The control of the temperature was realized with a VTU (variable temperature unit) and an accuracy of +/- 0,1K, which was checked with the standard Bruker Topspin 3.6 software.

In this work, the gradient strength was varied in 32 steps from 2% to 100% and for each gradient 64 number of scans was used. The diffusion time d20 was optimised to 50 ms and the gradient length p30 was kept at 1.4 ms.

The 2D NMR sequences for measuring diffusion coefficient using echoes for convection compensation and longitudinal eddy current delays to store the magnetization in the z-axis, and only be dependent on T_1-relaxation. The calculation of the diffusion value was automatically done with the mono exponential function:

$$\ln\left(\frac{I(G)}{I(0)}\right) = -\gamma^2\delta^2G^2\left(\Delta - \frac{\delta}{3}\right)D,$$

where I(G) and I(0) are the intensities of the signals with and without gradient, γ the gyromagnetic ratio of the nucleus (^{1}H in this measurements), G is the gradient strength, δ the duration of the pulse field gradient (PFG), D the diffusion value in m^2/s and Δ the "diffusion time" between the beginning of the two gradient pulses. The relaxation delay between the scans was 3s.

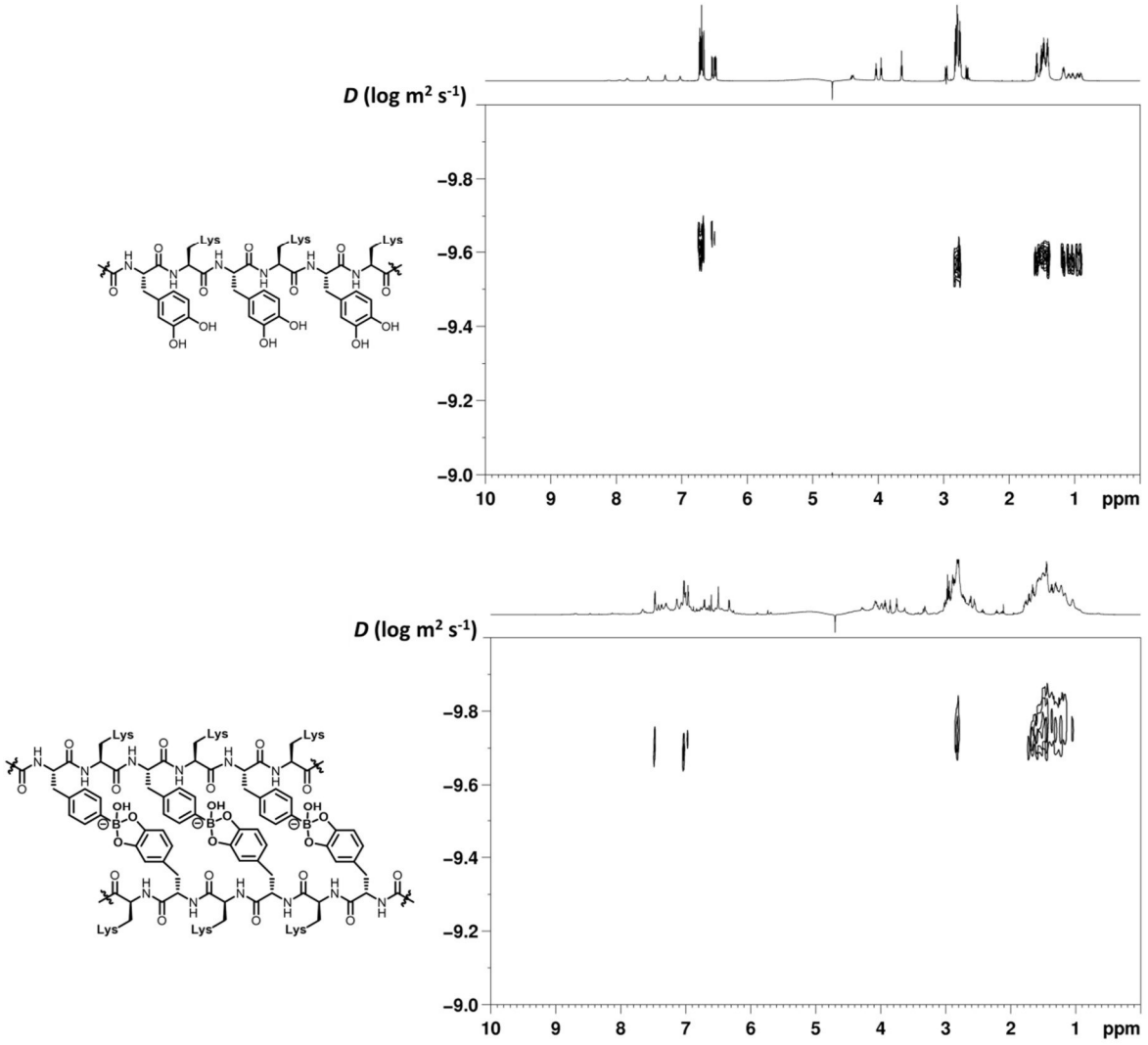

Figure S11. ^{1}H DOSY NMR of **(BX)$_3$ (top)** and **(AX)$_3$-(BX)$_3$** (bottom) in phosphate buffer pH 7.4 H_2O/D_2O 9/1 with water suppression.

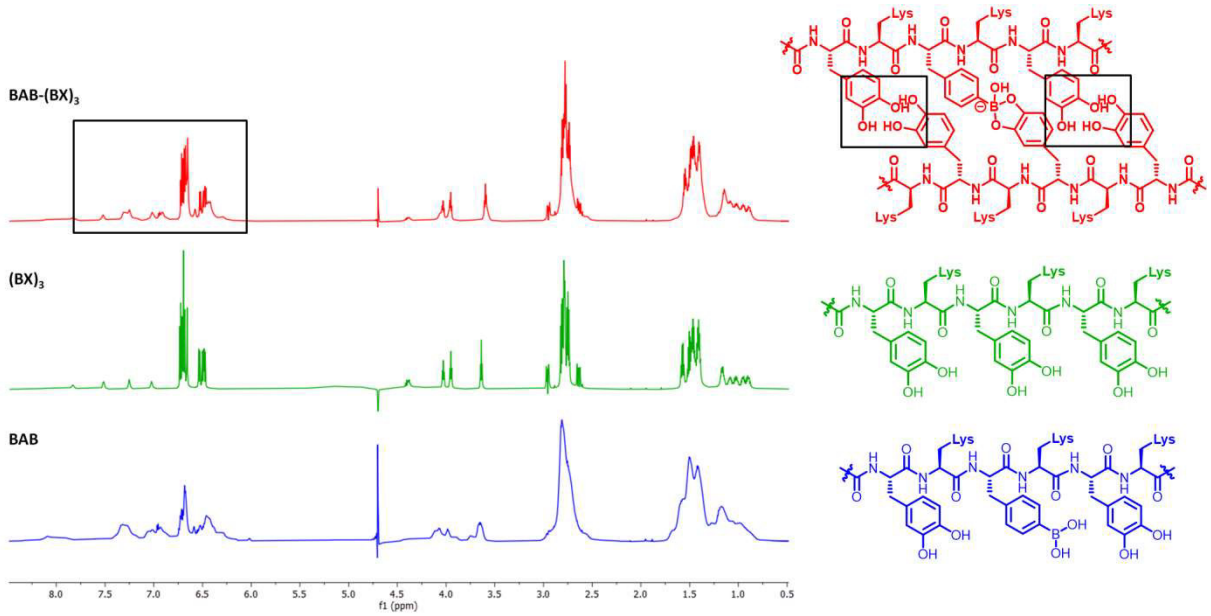

Figure S12. ^{1}H NMR of **BAB**, **(BX)$_3$** and the mismatched **BAB-(BX)$_3$** sequence in phosphate buffer pH 7.4 H_2O/D_2O 9/1 with water suppression.

2.10 ^{11}B NMR Spectroscopy

^{11}B NMR Spectroscopy was conducted using a Bruker 700 MHz NMR Spectrometer at 298K. Samples were prepared at a concentration 25 mM in 300 mM phosphate buffer at pH 2.0, 5.0, 7.4, 10.0 or in DMSO-d_6. Background subtraction of the boro-silicate NMR tube was made using solvents without samples.

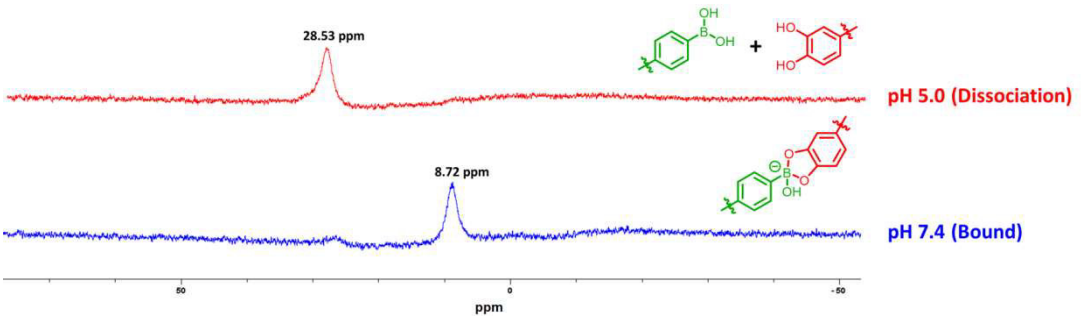

Figure S13. ^{11}B NMR of the pH-responsiveness of the boronic acid/catechol interaction.

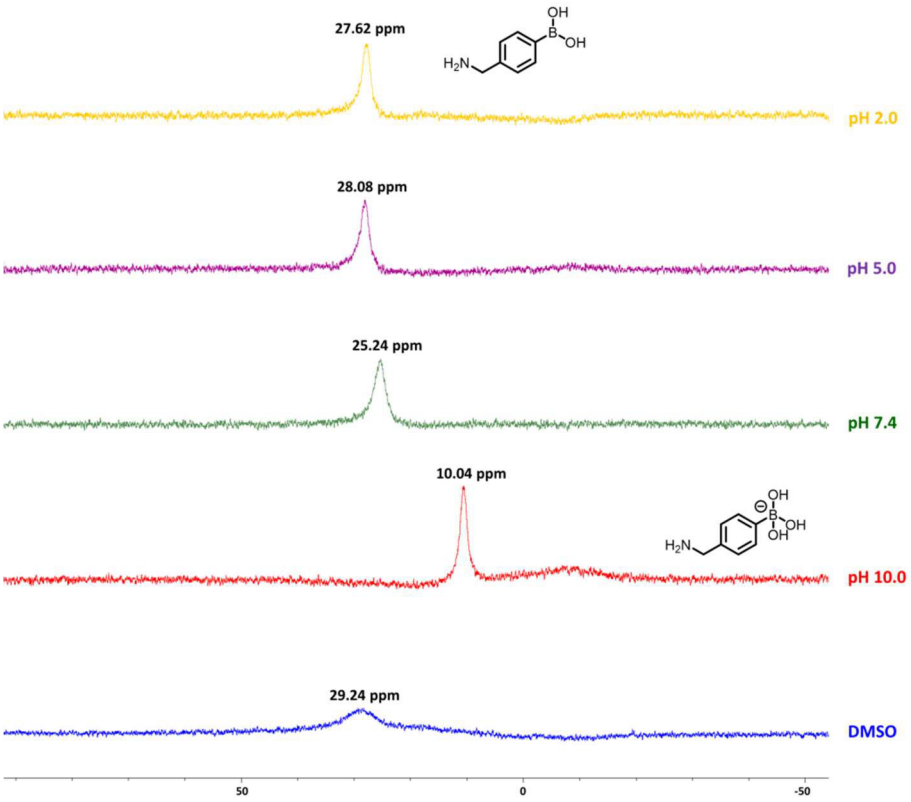

Figure S14. ^{11}B NMR of a water-soluble reference boronic acid (4-aminomethylphenylboronic acid) in different pH and solvents.

2.11 Variable Temperature ^{1}H NMR

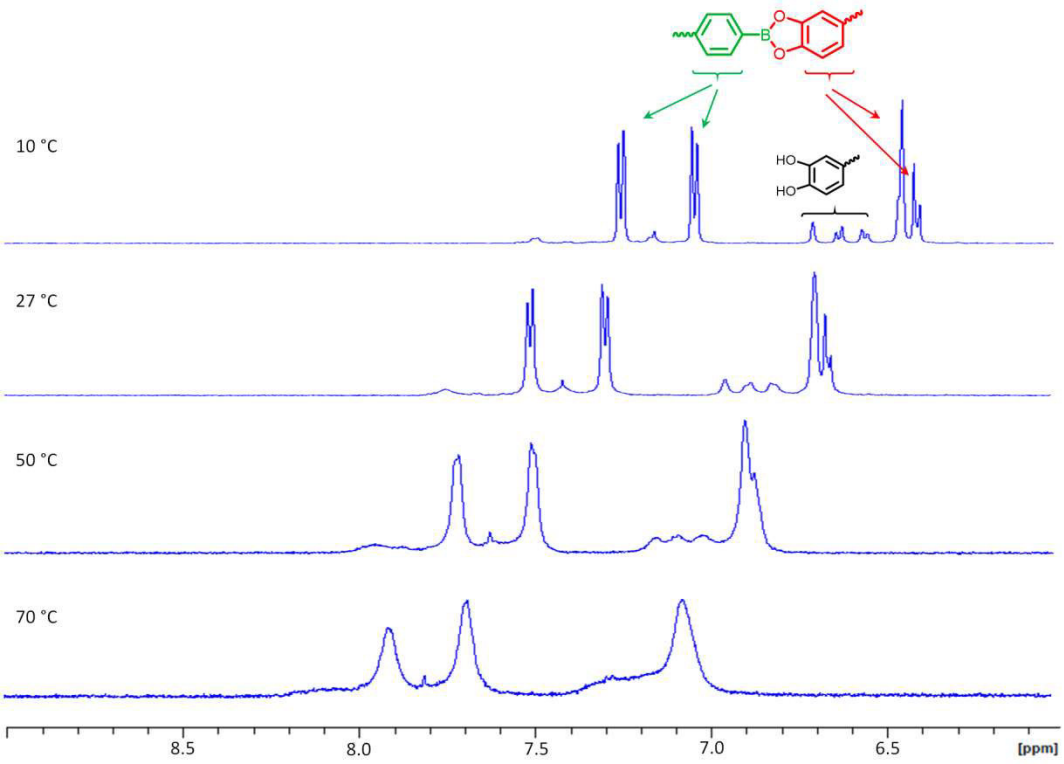

Figure S15. Variable temperature ^{1}H NMR of **(AX)$_1$-(BX)$_1$**.

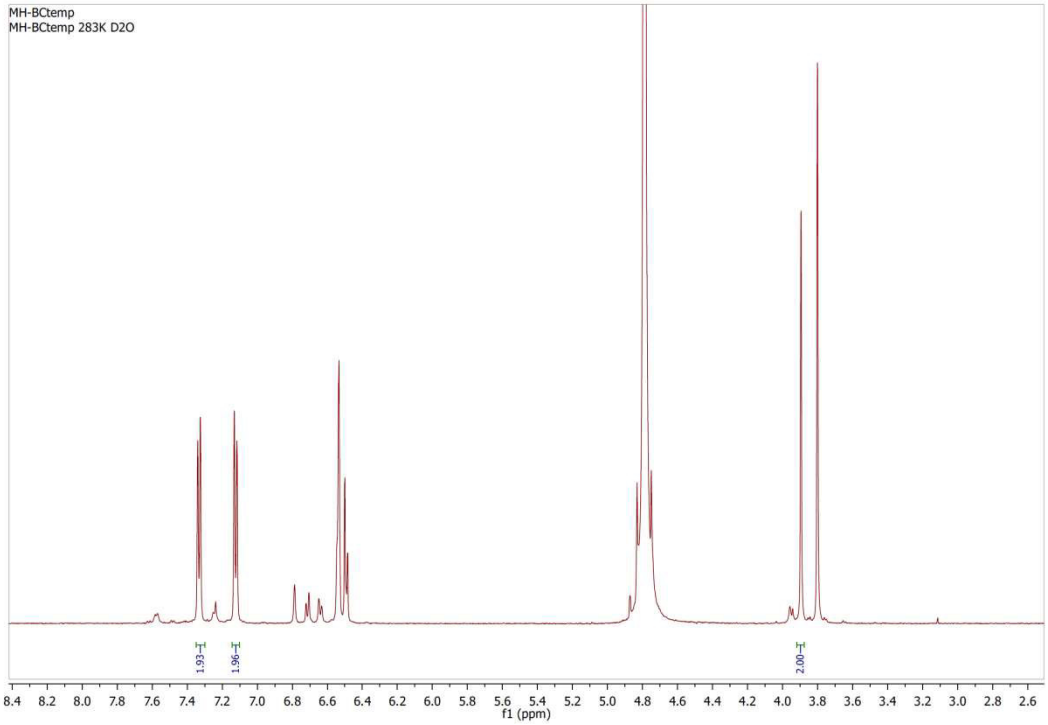

Figure S16. ^{1}H NMR of **(AX)$_1$-(BX)$_1$** at 283 K, 10 °C.

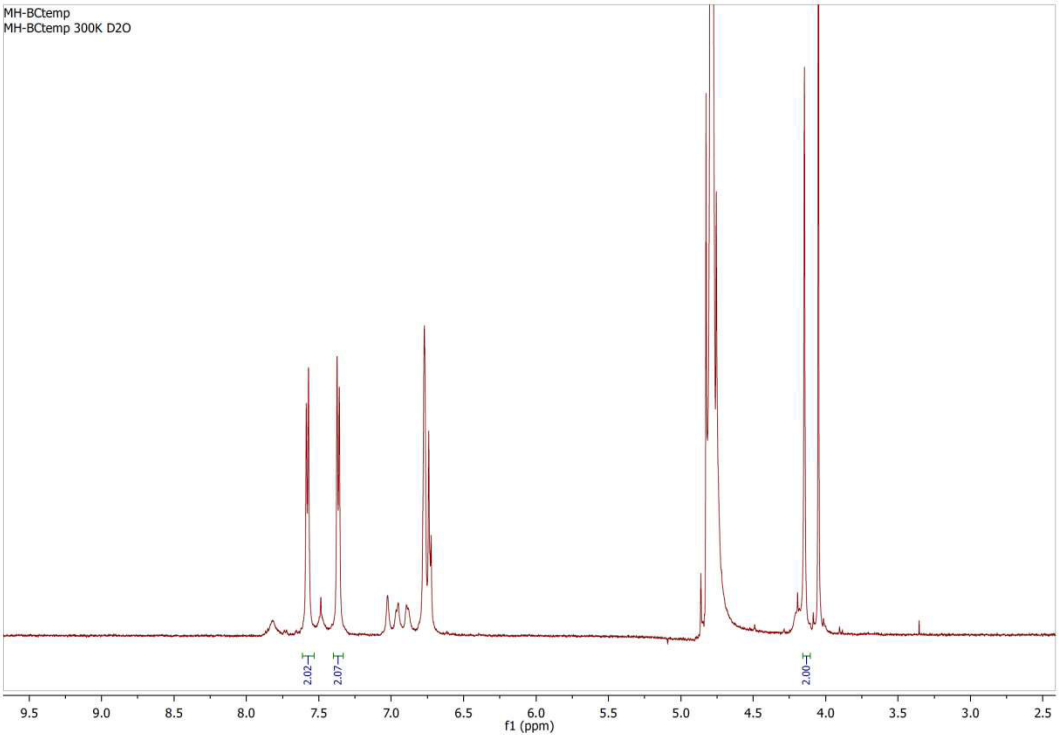

Figure S17. ^{1}H NMR of **(AX)$_1$-(BX)$_1$** at 300 K, 27 °C.

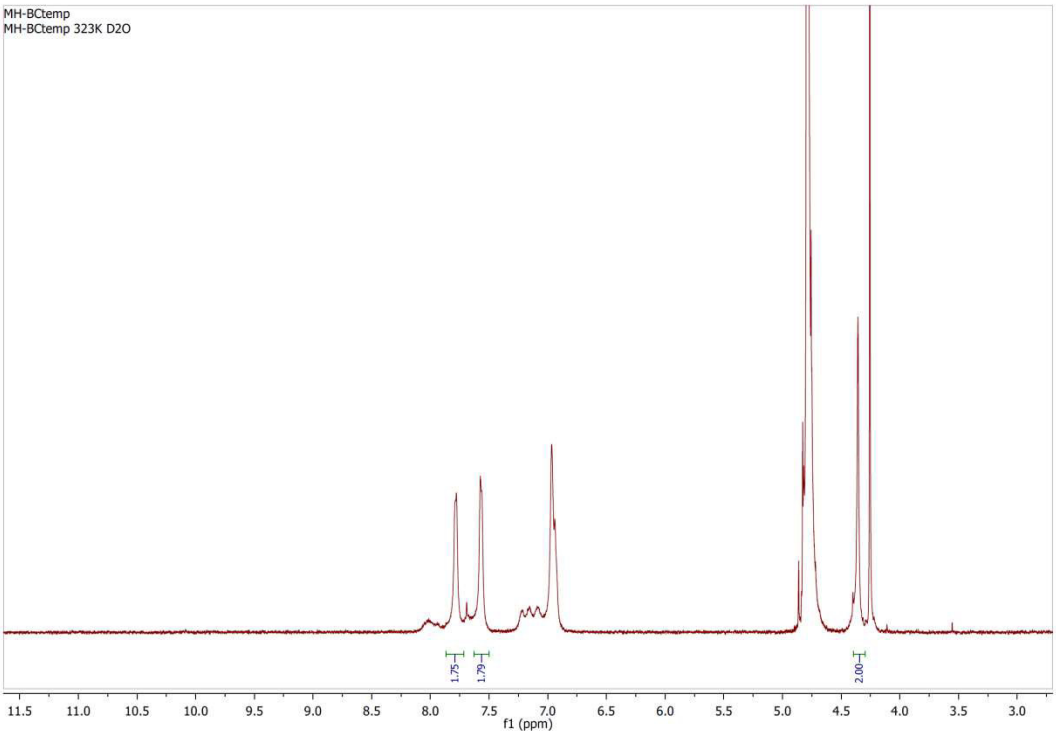

Figure S18. ^{1}H NMR of **(AX)$_1$-(BX)$_1$** at 323 K, 50 °C.

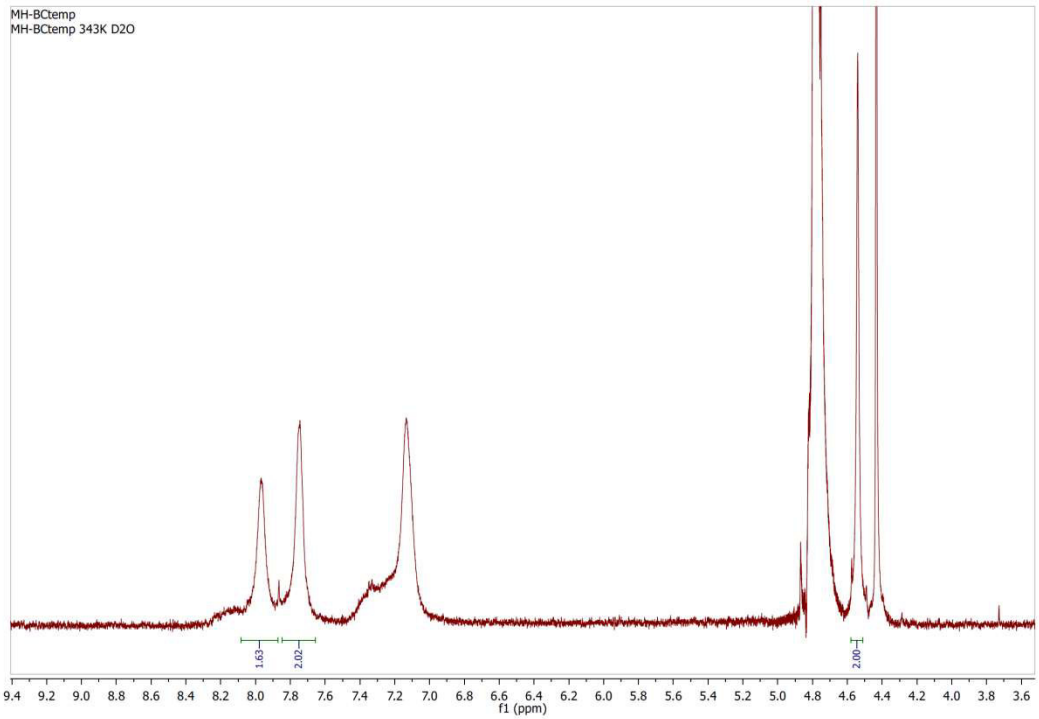

Figure S19. ^{1}H NMR of **(AX)$_1$-(BX)$_1$** at 343 K, 70 °C.

2.12 ATR FT-IR

For analysis of the binding by IR spectroscopy, a mixture of the trivalent peptides Lys-Cat-Lys-Cat-Lys-Cat-Lys and AEEAc-Bor-Lys-Bor-Lys-Bor-Lys (concentration of 0.462 mmol/L for each tag, equiv. 1:1) and a mixture of boronic acid **8** and catechol **9** (concentration of 3.57 mmol/L for each tag, equiv. 1:1) was stirred for 1 h phosphate buffer solution (100 mM, pH 7.4). The same process was done before the measurement of the separate (not mixed) peptides Lys-Cat-Lys-Cat-Lys-Cat-Lys and AEEAc-Bor-Lys-Bor-Lys-Bor-Lys. After the mixing the samples were frozen in liquid nitrogen and lyophilized. The ATR FT-IR spectra of the solid samples were recorded using a Bruker Tensor 27 spectrometer equipped with a diamond crystal as ATR element (PIKE Miracle™) with a spectral resolution of 1 cm^{-1}, each spectrum was an average of 20 scans.

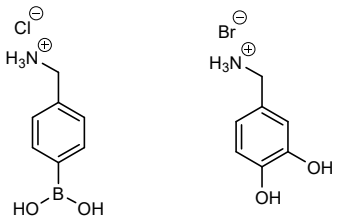

8 **9**

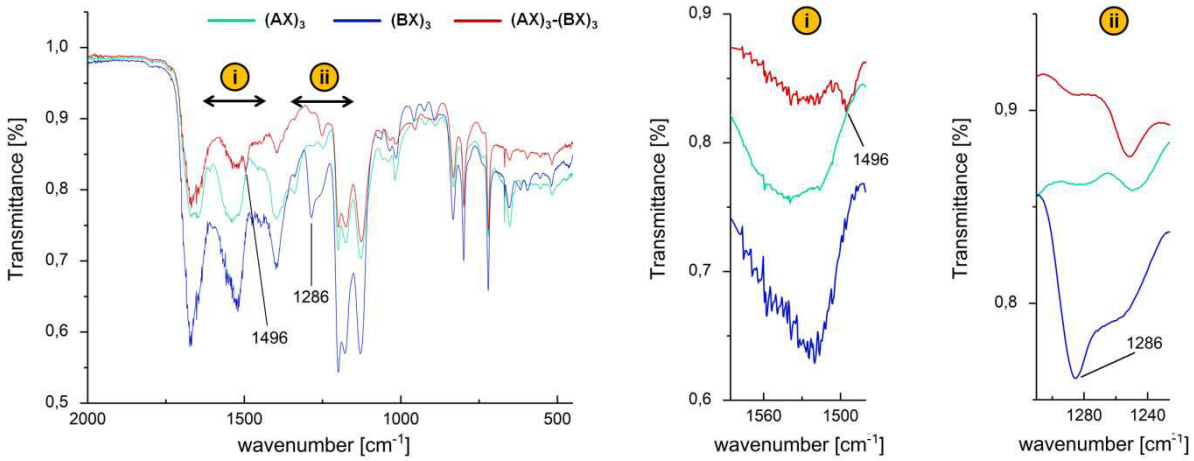

Figure S20. FTIR spectra of **$(AX)_3$-$(BX)_3$** and its separate constituents in phosphate buffer pH 7.4 H_2O/D_2O 9/1 with water suppression.

2.13 Circular Dichroism Spectroscopy

Solutions of **A_3X_3**, **B_3X_3**, **A_3X_3-B_3X_3** as well as **$(AX)_3$**, **$(BX)_3$**, **$(AX)_3$-$(BX)_3$** were each prepared at a concentration of 200 µM in 10 mM phosphate buffer, separately at pH 5.0 and 7.4. The solutions for the binding mixture **A_3X_3-B_3X_3** and **$(AX)_3$-$(BX)_3$** were incubated for at least 1 h at room temperature before measurement to ensure binding is complete. Measurements was conducted using the following parameters on a JASCO-1500 Circular Dichroism Spectrometer.

Path length: 0.1 mm
Scan rate: 5 nm/min
Scan range: 260 nm – 180 nm
Data pitch: 0.2 nm
Data Integration Time: 2 sec

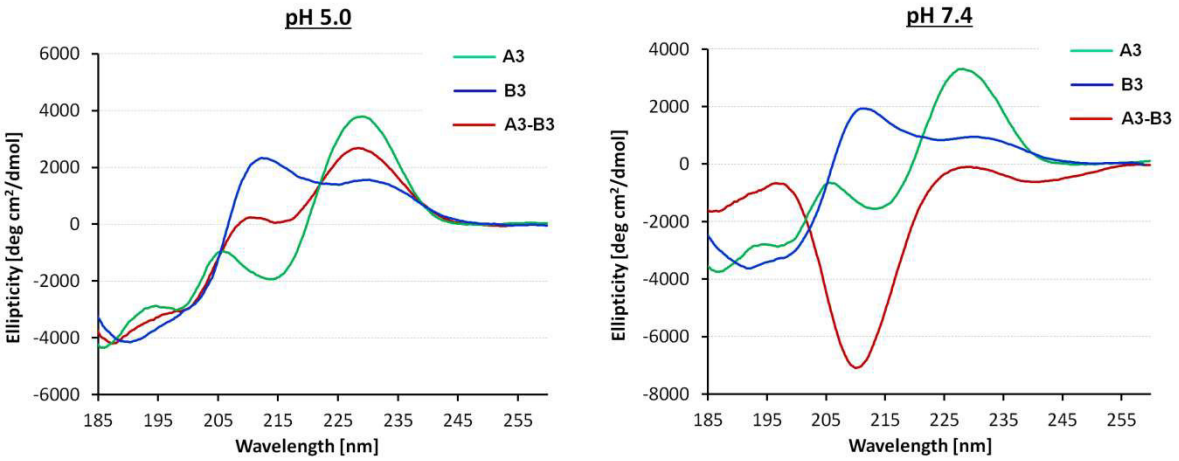

Figure S21. CD spectra of **(AX)$_3$**, **(BX)$_3$** and **(AX)$_3$-(BX)$_3$** at pH 5.0 (left) and pH 7.4 (right).

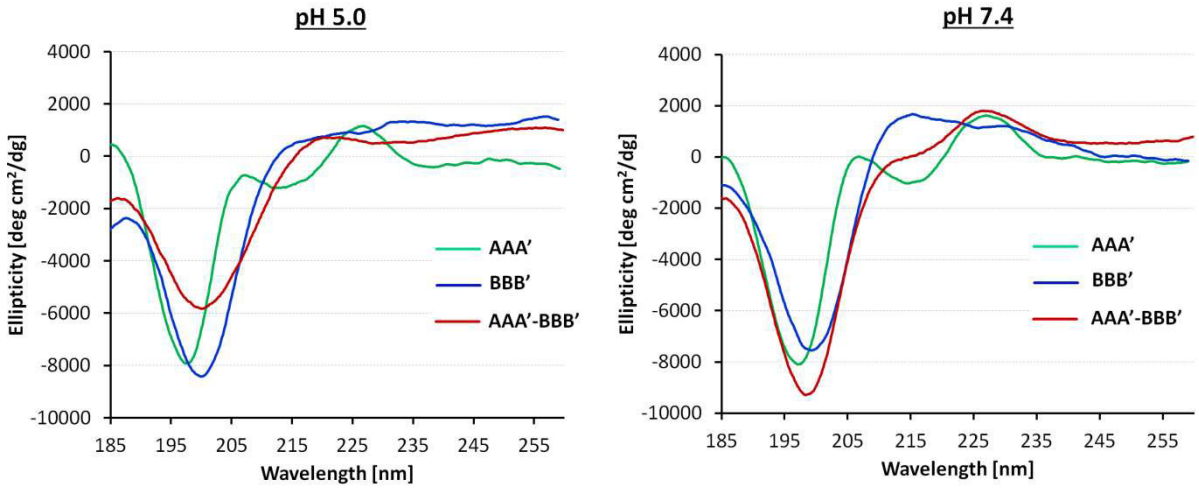

Figure S22. CD Spectra of A_3X_3, B_3X_3 and A_3X_3-B_3X_3 at pH 5.0 (left) and pH 7.4 (right)

2.14 DFT Calculations

DFT calculations were performed using the Gaussian 09 software package[8] and structural representations were generated with *CYLview*[9]. All the geometry optimizations were carried out at the B3LYP/6-31G(d) level of theory. All of the optimized geometries were verified by frequency computations as minima (zero imaginary frequencies) or transition states (a single imaginary frequency corresponding to the desired reaction coordinate). Single-point energy calculations on

the optimized geometries were then evaluated using the functional ωB97X-D[10] and def2-TZVPP basis set, with solvent effects (water) calculated by means of the Polarizable Continuum Model (PCM) initially devised by Tomasi and coworkers,[11] with radii and non-electrostatic terms of the SMD solvation model, developed by Truhler and co-workers.[12]

$(AX)_3$-$(BX)_3$ Structure

	ΔE (H) B3LYP/6-31G(d)	ΔE (H) ωB97X-D /def2-TZVPP/SMD(water)
$(AX)_3$-$(BX)_3$-i	-7136.40814413	-7137.69450679 (0.0)
$(AX)_3$-$(BX)_3$-ii	-7136.39862443	-7137.68553871 (5.6)
ABA-BAB-i	-7136.41072008	-7137.68930710 (3.3)

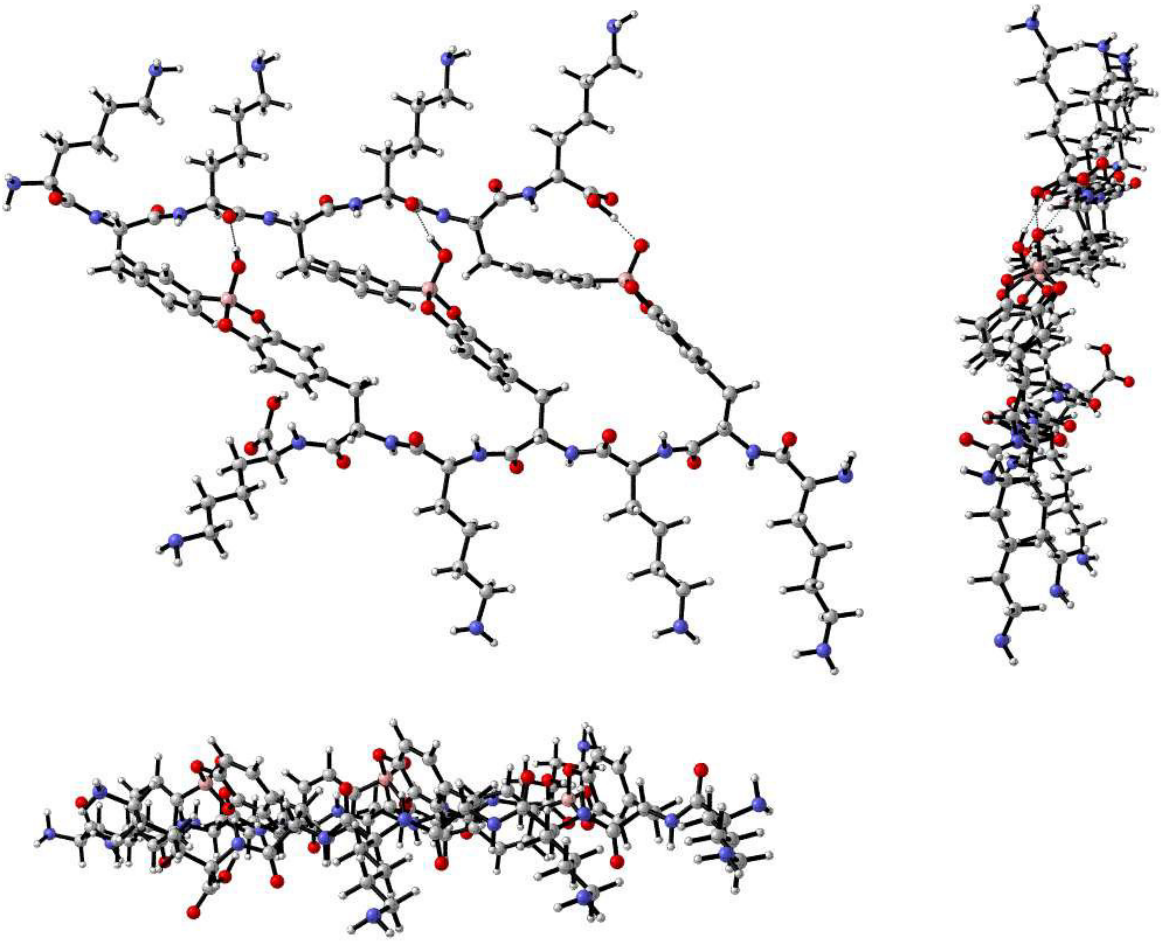

Figure S23. DFT optimized structure of (**$(AX)_3$-$(BX)_3$-i** (B3LYP/6-31G(d), side and bottom views included.

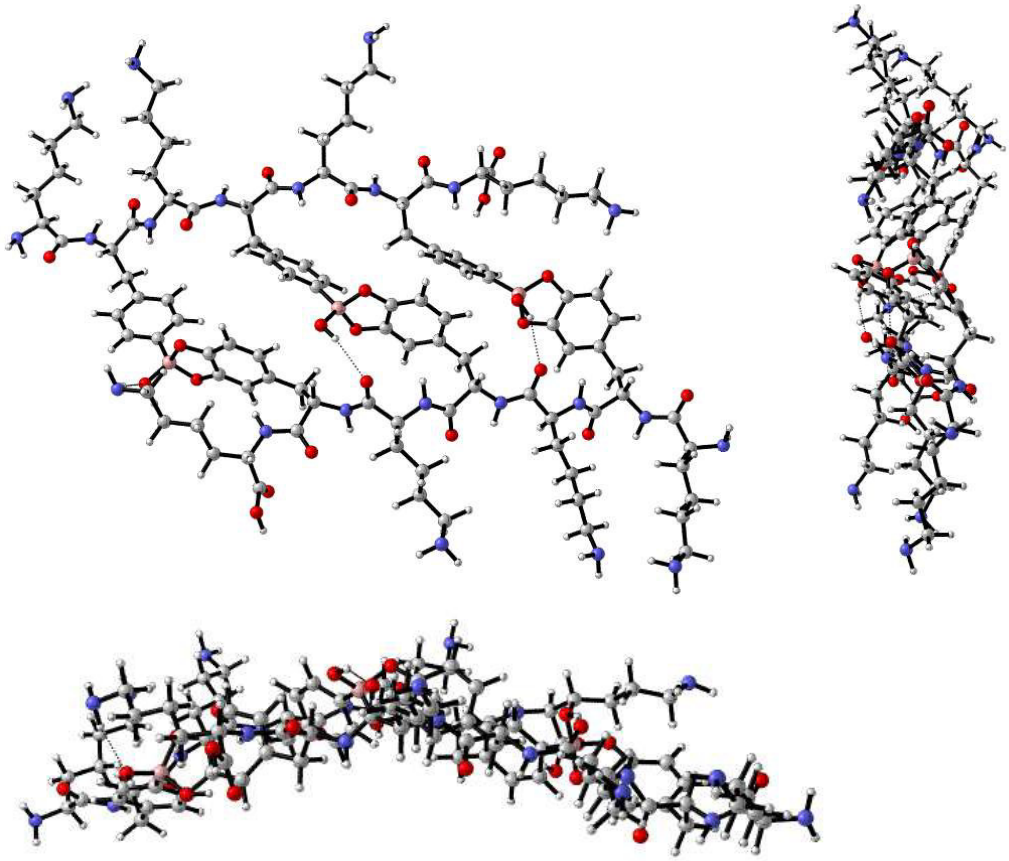

Figure S24. DFT optimized structure of **(AX)$_3$-(BX)$_3$-ii** (B3LYP/6-31G(d), side and bottom views included.

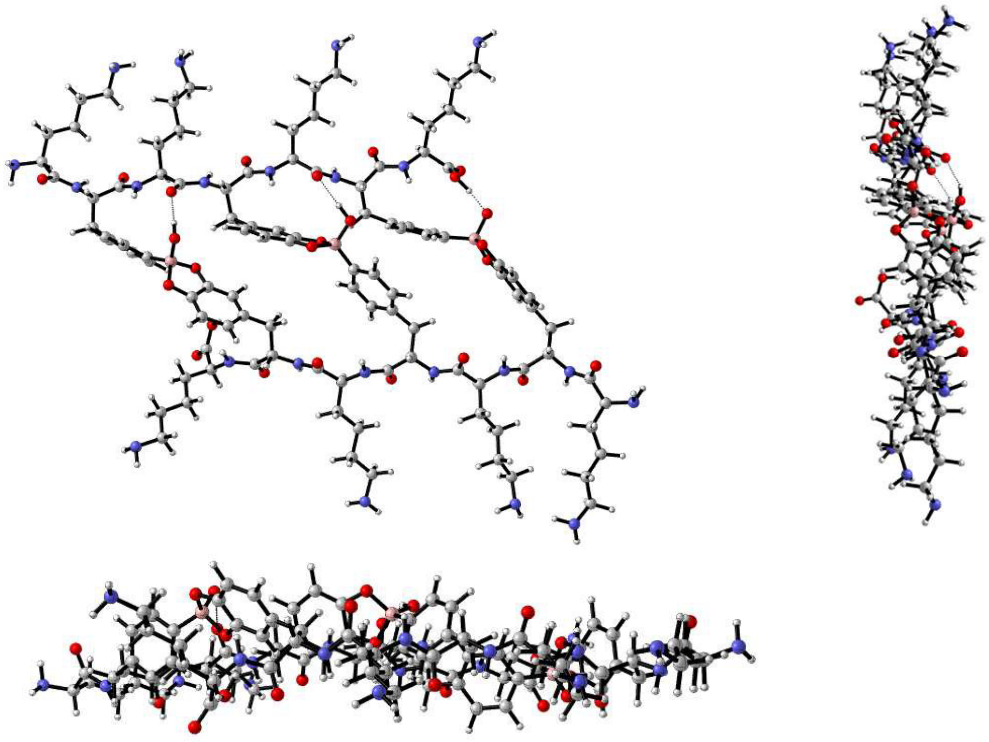

Figure S25. DFT optimized structure of **ABA-BAB-i** (B3LYP/6-31G(d), side and bottom views included.

Study of the dissociation mechanism (model structure)

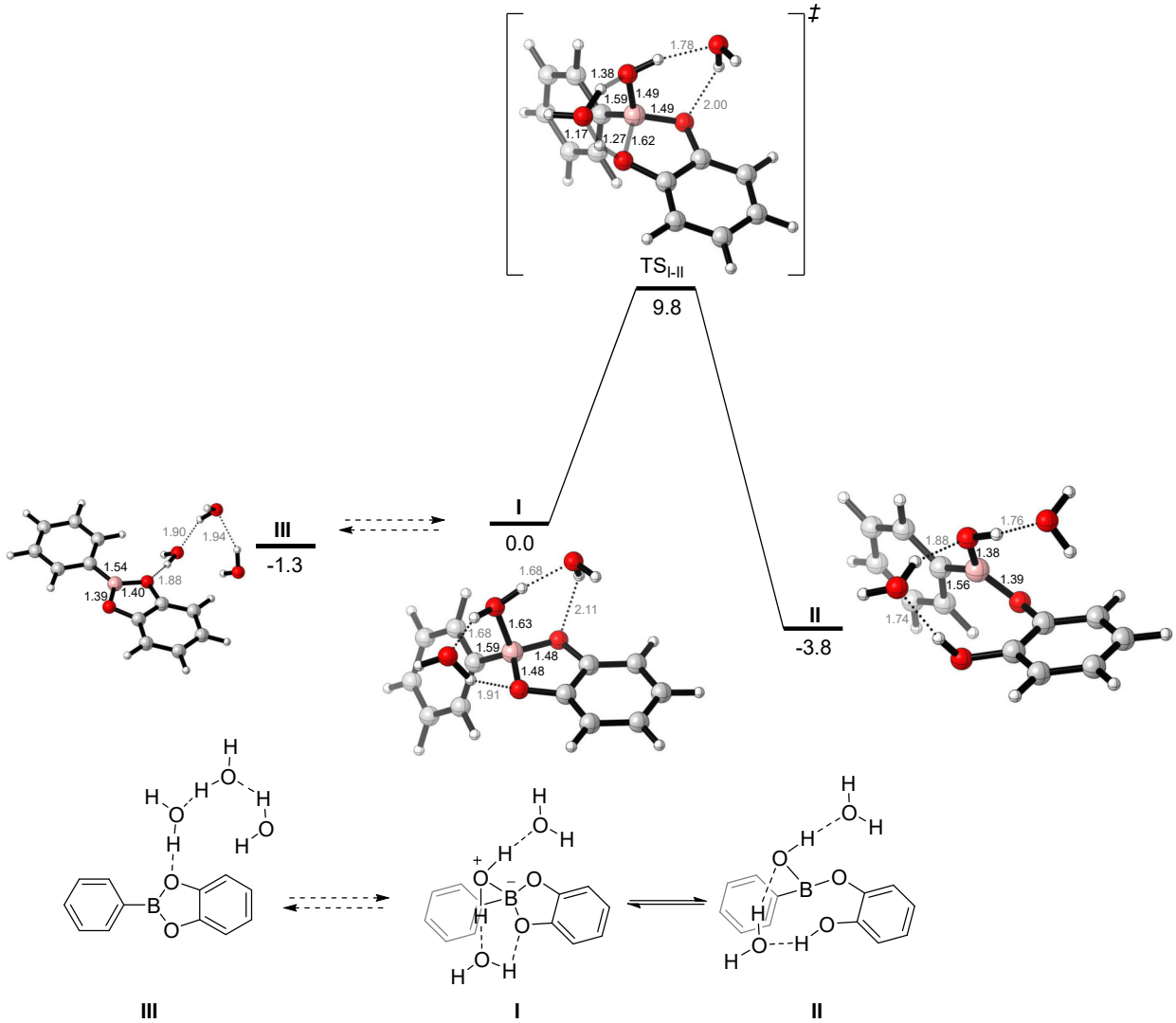

III I II

Level of Theory		I	TS$_{I-II}$	II	III
B3LYP/6-31G(d)	**ΔE (H)**	-867.3838826	-867.3642104	-867.3827210	-867.3797646
	ΔG (H)	-867.169240	-867.153706	-867.170955	-867.170602
	ΔG rel (kcal mol^{-1})	0.0	9.7	-1.1	-0.9
ωB97X-D/ def2-TZVPP/ SMD(water)	**sp E (H)**	-867.502185137	-867.482401348	-867.505424349	-867.498778601
	ΔG$^{solv, corr}$ (H)	-867.287542565	-867.271896904	-867.293658391	-867.289615986
	ΔG^{solv} rel (kcal mol^{-1})	**0.0**	**9.8**	**-3.8**	**-1.3**

Figure S26. Free energy profile for the dissociation of I**.** DFT calculations were performed at the ωB97X-D /def2-TZVPP/SMD(water)//B3LYP/6-31G(d) level of theory. The distances shown are in Å, and energies are in kcal mol^{-1}.

Optimized Cartesian Coordinates

$(AX)_3$-$(BX)_3$-i

C	9.405461000	-17.658200000	-6.827205000
N	8.152797000	-17.159843000	-6.912273000
C	10.364134000	-16.885510000	-5.892238000
O	9.812786000	-18.632661000	-7.462554000
C	7.091819000	-17.667105000	-7.787678000
C	6.308213000	-16.406434000	-8.193230000
N	6.073347000	-16.234504000	-9.510534000
C	5.344537000	-15.098432000	-10.059129000
C	6.220404000	-18.704430000	-7.037363000
O	6.011871000	-15.575278000	-7.327038000
C	6.263781000	-13.901369000	-10.407615000
C	5.126719000	-19.370975000	-7.849778000
C	5.418894000	-20.048324000	-9.038060000
C	4.419621000	-20.723626000	-9.766763000
C	3.123972000	-20.722814000	-9.271597000
C	2.817356000	-20.055191000	-8.061694000
C	3.799350000	-19.372142000	-7.358615000
O	2.029289000	-21.290885000	-9.801303000
C	4.674627000	-15.596944000	-11.358826000
O	5.183168000	-16.517916000	-12.000595000
N	11.366039000	-17.779365000	-5.296889000
C	11.063616000	-15.773159000	-6.700690000
C	6.970257000	-13.246219000	-9.214649000
C	7.798001000	-12.019885000	-9.622448000
C	8.454711000	-11.325920000	-8.428423000
O	1.512517000	-20.180963000	-7.762057000
C	11.918235000	-14.835459000	-5.841219000
C	12.683856000	-13.797034000	-6.670559000
C	13.446598000	-12.785039000	-5.814721000
N	3.579797000	-14.909513000	-11.736764000
C	2.729468000	-15.263114000	-12.872964000
C	1.850492000	-14.026418000	-13.123102000
N	1.428624000	-13.838904000	-14.395415000
C	0.473332000	-12.797315000	-14.758102000
C	1.896414000	-16.531694000	-12.541295000
O	1.590212000	-13.250573000	-12.195901000
C	1.153121000	-11.462889000	-15.157448000
C	0.880758000	-16.958929000	-13.577289000
C	1.242177000	-17.264866000	-14.894318000
C	0.295530000	-17.752055000	-15.821508000
C	-1.011991000	-17.951189000	-15.397636000
C	-1.383954000	-17.630854000	-14.067202000

C	-0.460514000	-17.125637000	-13.167379000
O	-2.051017000	-18.448978000	-16.080357000
C	-0.313759000	-13.291397000	-15.987825000
O	0.229026000	-13.987620000	-16.843050000
C	1.947314000	-10.764381000	-14.048011000
C	2.497405000	-9.403634000	-14.496361000
C	3.274237000	-8.682261000	-13.394608000
N	3.774785000	-7.380006000	-13.868747000
O	-2.674368000	-17.906785000	-13.850339000
N	9.269940000	-10.179576000	-8.864763000
N	14.219842000	-11.862811000	-6.660360000
C	-18.516147000	-19.626717000	-20.287216000
C	-18.135018000	-20.006625000	-18.853773000
N	-18.354702000	-21.440770000	-18.604623000
N	-1.582279000	-12.829653000	-16.077285000
C	-2.420797000	-12.994442000	-17.254572000
C	-3.359781000	-11.772372000	-17.282757000
N	-4.080900000	-11.610540000	-18.427751000
C	-4.989057000	-10.493656000	-18.616319000
C	-3.166925000	-14.363630000	-17.250464000
O	-3.430904000	-10.983874000	-16.338824000
C	-5.140010000	-10.155226000	-20.112124000
C	-4.124335000	-14.579633000	-18.407772000
C	-3.687559000	-14.576483000	-19.737506000
C	-4.581591000	-14.805163000	-20.812112000
C	-5.915958000	-15.060236000	-20.531413000
C	-6.372390000	-15.046210000	-19.184795000
C	-5.500581000	-14.783043000	-18.132454000
O	-6.910498000	-15.366528000	-21.375622000
C	-6.391638000	-10.666539000	-17.989761000
O	-7.098879000	-9.695225000	-17.821238000
C	-3.842851000	-9.646265000	-20.753360000
C	-4.023242000	-9.222975000	-22.216452000
C	-2.736090000	-8.682082000	-22.841238000
N	-2.960689000	-8.273236000	-24.236524000
O	-7.672189000	-15.332108000	-19.122987000
O	-6.809694000	-11.895086000	-17.672786000
C	-16.671836000	-16.188703000	-22.536838000
N	-15.996276000	-15.778217000	-21.435112000
C	-18.209079000	-16.286235000	-22.399744000
O	-16.128648000	-16.493841000	-23.600275000
C	-14.553007000	-15.931172000	-21.271828000
C	-14.363947000	-16.527592000	-19.858037000
N	-13.223908000	-17.201122000	-19.618901000
C	-12.970617000	-17.844023000	-18.333251000
C	-13.799542000	-14.588004000	-21.494570000
O	-15.269542000	-16.417765000	-19.016890000
C	-13.762840000	-19.173480000	-18.248342000
C	-12.299228000	-14.728089000	-21.363505000
C	-11.608432000	-14.149597000	-20.293178000

C	-10.252337000	-14.417895000	-20.085539000
C	-9.533252000	-15.294417000	-20.913176000
C	-10.227861000	-15.820388000	-22.019166000
C	-11.573807000	-15.537820000	-22.253819000
B	-8.062963000	-15.869544000	-20.522267000
C	-11.451789000	-18.075828000	-18.232635000
O	-10.784076000	-18.232519000	-19.258347000
N	-18.874289000	-15.912327000	-23.656823000
C	-18.609209000	-17.732489000	-22.024040000
C	-13.882273000	-19.790347000	-16.849185000
C	-14.719921000	-21.075564000	-16.870910000
C	-14.930742000	-21.697435000	-15.491037000
C	-18.273985000	-18.139885000	-20.581688000
N	-15.761669000	-22.910730000	-15.599227000
N	-10.958951000	-18.125065000	-16.981399000
C	-9.570159000	-18.416043000	-16.645651000
C	-9.607398000	-19.173606000	-15.303798000
N	-8.510530000	-19.896105000	-14.995086000
C	-8.315677000	-20.500927000	-13.679300000
C	-8.732205000	-17.104790000	-16.557882000
O	-10.602019000	-19.097186000	-14.567614000
C	-9.045513000	-21.862138000	-13.573006000
C	-7.277211000	-17.359103000	-16.247314000
C	-6.725794000	-16.990466000	-15.015565000
C	-5.409961000	-17.329215000	-14.692733000
C	-4.600416000	-18.076229000	-15.563708000
C	-5.152527000	-18.386239000	-16.820566000
C	-6.456732000	-18.030703000	-17.169372000
B	-3.179060000	-18.677883000	-15.074800000
C	-6.794688000	-20.685430000	-13.493208000
O	-6.107074000	-21.032098000	-14.453833000
C	-9.103878000	-22.424664000	-12.146666000
C	-9.741620000	-23.817885000	-12.074155000
C	-9.776012000	-24.373807000	-10.649969000
N	-10.366851000	-25.724906000	-10.625739000
N	-6.329093000	-20.460922000	-12.242836000
C	-4.976755000	-20.757533000	-11.773593000
C	-5.109321000	-21.806411000	-10.649212000
N	-4.005744000	-22.545501000	-10.376574000
C	-3.926669000	-23.393987000	-9.185701000
C	-4.278626000	-19.451035000	-11.279356000
O	-6.173402000	-21.936799000	-10.029908000
C	-4.222654000	-24.870809000	-9.529596000
C	-2.908748000	-19.687366000	-10.683205000
C	-1.849968000	-20.135929000	-11.489722000
C	-0.627232000	-20.485419000	-10.911516000
C	-0.399754000	-20.400744000	-9.527230000
C	-1.445833000	-19.874746000	-8.750314000
C	-2.677830000	-19.532074000	-9.310425000
B	0.905649000	-21.053772000	-8.841721000

C	-2.551592000	-23.249692000	-8.515843000
O	-2.427018000	-23.100769000	-7.309777000
C	-4.259608000	-25.789188000	-8.301104000
C	-4.569190000	-27.249301000	-8.654639000
C	-4.566075000	-28.173776000	-7.436771000
N	-4.887140000	-29.558534000	-7.824748000
O	-1.557480000	-23.349279000	-9.383684000
H	7.869590000	-16.367063000	-6.347171000
H	9.791528000	-16.420267000	-5.077801000
H	7.572623000	-18.133828000	-8.650162000
H	6.211860000	-16.995390000	-10.171033000
H	4.593554000	-14.782305000	-9.326704000
H	6.925574000	-19.449788000	-6.641821000
H	5.780891000	-18.193684000	-6.171737000
H	7.004815000	-14.247802000	-11.140644000
H	5.646367000	-13.150430000	-10.920218000
H	6.443870000	-20.080845000	-9.405128000
H	4.650519000	-21.237245000	-10.695736000
H	3.547668000	-18.852185000	-6.437075000
H	10.893330000	-18.379776000	-4.619676000
H	11.633404000	-18.419885000	-6.049652000
H	11.686671000	-16.253838000	-7.467879000
H	10.302516000	-15.193082000	-7.240378000
H	7.621224000	-13.977886000	-8.722352000
H	6.224093000	-12.959756000	-8.462335000
H	7.150030000	-11.296507000	-10.142591000
H	8.579707000	-12.304078000	-10.339250000
H	9.123083000	-12.033769000	-7.919570000
H	7.669865000	-11.057246000	-7.697314000
H	12.618079000	-15.439505000	-5.251644000
H	11.267370000	-14.318347000	-5.119066000
H	11.979695000	-13.252794000	-7.319578000
H	13.395551000	-14.296812000	-7.340499000
H	14.156075000	-13.317257000	-5.166511000
H	12.730060000	-12.276096000	-5.142161000
H	3.158836000	-14.214309000	-11.127625000
H	3.366976000	-15.456398000	-13.740673000
H	1.503584000	-14.607769000	-15.059659000
H	-0.192202000	-12.624238000	-13.904606000
H	2.628040000	-17.326649000	-12.350632000
H	1.385935000	-16.340243000	-11.590531000
H	1.804868000	-11.665202000	-16.017742000
H	0.362778000	-10.786401000	-15.514268000
H	2.283530000	-17.178354000	-15.205451000
H	0.585199000	-17.998979000	-16.839403000
H	-0.758961000	-16.917583000	-12.143476000
H	2.773332000	-11.407380000	-13.723644000
H	1.307715000	-10.635555000	-13.165689000
H	1.662633000	-8.762373000	-14.822438000
H	3.152706000	-9.521346000	-15.369761000

H	4.144008000	-9.287412000	-13.107326000
H	2.634628000	-8.607549000	-12.495853000
H	4.249125000	-6.902306000	-13.102514000
H	2.975658000	-6.790644000	-14.104777000
H	9.624034000	-9.686148000	-8.045334000
H	8.665008000	-9.512014000	-9.344274000
H	14.653352000	-11.147066000	-6.077930000
H	13.578644000	-11.365482000	-7.278877000
H	-17.919792000	-20.231281000	-20.988078000
H	-19.566270000	-19.897961000	-20.462572000
H	-18.764595000	-19.445446000	-18.150269000
H	-17.097047000	-19.681118000	-18.667916000
H	-18.079558000	-21.664756000	-17.647517000
H	-17.712076000	-21.975054000	-19.190560000
H	-1.956645000	-12.193958000	-15.381496000
H	-1.771166000	-12.962292000	-18.136946000
H	-4.049277000	-12.362025000	-19.115610000
H	-4.562837000	-9.634895000	-18.089389000
H	-2.388299000	-15.134910000	-17.237117000
H	-3.706893000	-14.455476000	-16.302221000
H	-5.504795000	-11.041861000	-20.650296000
H	-5.922161000	-9.392067000	-20.192525000
H	-2.627276000	-14.454116000	-19.954577000
H	-4.222262000	-14.836975000	-21.837636000
H	-5.851874000	-14.862978000	-17.106825000
H	-3.068928000	-10.422233000	-20.689386000
H	-3.468998000	-8.792082000	-20.169077000
H	-4.804045000	-8.448126000	-22.275994000
H	-4.380188000	-10.067558000	-22.818925000
H	-1.975583000	-9.473563000	-22.845674000
H	-2.339753000	-7.870910000	-22.201026000
H	-2.096357000	-7.896219000	-24.624051000
H	-3.630615000	-7.503893000	-24.251907000
H	-6.163878000	-12.599994000	-17.906716000
H	-16.481461000	-15.715580000	-20.544071000
H	-18.561218000	-15.604507000	-21.613737000
H	-14.208443000	-16.648053000	-22.022361000
H	-12.448119000	-17.196754000	-20.277889000
H	-13.315506000	-17.174476000	-17.536967000
H	-14.091572000	-14.241569000	-22.494836000
H	-14.180421000	-13.853276000	-20.774220000
H	-14.770699000	-18.952049000	-18.616040000
H	-13.309618000	-19.888894000	-18.947544000
H	-12.148326000	-13.511381000	-19.593476000
H	-9.745135000	-13.981035000	-19.229075000
H	-9.706457000	-16.507992000	-22.681927000
H	-12.079734000	-15.977068000	-23.114680000
H	-18.693886000	-14.920687000	-23.824687000
H	-18.343896000	-16.383514000	-24.394524000
H	-19.688174000	-17.822855000	-22.201008000

H	-18.114884000	-18.413812000	-22.731424000
H	-14.359624000	-19.061386000	-16.177066000
H	-12.893737000	-19.999328000	-16.421980000
H	-14.231906000	-21.813720000	-17.526546000
H	-15.704866000	-20.875798000	-17.312290000
H	-15.469287000	-20.986473000	-14.850854000
H	-13.950608000	-21.868620000	-15.012763000
H	-18.874172000	-17.530196000	-19.889013000
H	-17.227667000	-17.905670000	-20.353873000
H	-15.894894000	-23.308911000	-14.669624000
H	-15.239374000	-23.616710000	-16.119505000
H	-11.566646000	-18.049137000	-16.172180000
H	-9.152548000	-19.049682000	-17.432825000
H	-7.685286000	-19.850133000	-15.588052000
H	-8.724333000	-19.817218000	-12.925861000
H	-8.830498000	-16.588469000	-17.517730000
H	-9.183901000	-16.467678000	-15.786523000
H	-10.062583000	-21.712932000	-13.953174000
H	-8.541952000	-22.568065000	-14.246361000
H	-7.340790000	-16.447227000	-14.297293000
H	-5.001578000	-17.031034000	-13.729920000
H	-4.542549000	-18.923085000	-17.544629000
H	-6.835984000	-18.242349000	-18.168529000
H	-9.678562000	-21.731906000	-11.512904000
H	-8.099286000	-22.471705000	-11.709290000
H	-9.168238000	-24.508203000	-12.712659000
H	-10.763482000	-23.801286000	-12.476947000
H	-10.404303000	-23.726954000	-10.023043000
H	-8.758275000	-24.327578000	-10.224761000
H	-10.337423000	-26.081860000	-9.670415000
H	-9.762380000	-26.349315000	-11.161497000
H	-7.004127000	-20.355007000	-11.495053000
H	-4.406858000	-21.147052000	-12.620125000
H	-3.124756000	-22.294075000	-10.815490000
H	-4.673674000	-23.034186000	-8.474880000
H	-4.199744000	-18.794733000	-12.150861000
H	-4.935758000	-18.972030000	-10.541003000
H	-5.189784000	-24.899276000	-10.047412000
H	-3.463586000	-25.221244000	-10.240633000
H	-1.998530000	-20.214657000	-12.564695000
H	0.172254000	-20.852667000	-11.550598000
H	-1.306933000	-19.760247000	-7.675640000
H	-3.481057000	-19.162541000	-8.672562000
H	-5.012951000	-25.416343000	-7.591807000
H	-3.298634000	-25.736090000	-7.772966000
H	-3.822853000	-27.611524000	-9.379095000
H	-5.544614000	-27.325340000	-9.153389000
H	-3.595415000	-28.075192000	-6.916970000
H	-5.334820000	-27.842060000	-6.725920000
H	-4.175040000	-29.885868000	-8.478537000

H	-4.806449000	-30.164685000	-7.008377000
H	-0.667256000	-23.042753000	-8.940977000
O	0.542028000	-22.391271000	-8.234888000
H	0.098571000	-22.216322000	-7.388631000
O	-3.276526000	-20.087262000	-14.746400000
H	-4.182170000	-20.410069000	-14.865657000
O	-8.045619000	-17.310539000	-20.554990000
H	-8.868298000	-17.653379000	-20.171073000

$(AX)_3$-$(BX)_3$-ii

C	7.795771000	-16.889302000	-4.876879000
N	6.608976000	-16.326574000	-5.211009000
C	8.906726000	-15.886712000	-4.491300000
O	8.035750000	-18.095645000	-4.928093000
C	5.548400000	-16.995296000	-5.971765000
C	5.155933000	-15.955727000	-7.042417000
N	5.047256000	-16.373823000	-8.321939000
C	4.648384000	-15.485231000	-9.408623000
C	4.351136000	-17.400705000	-5.065223000
O	5.034049000	-14.771130000	-6.702808000
C	5.868772000	-14.837067000	-10.114163000
C	3.377075000	-18.324275000	-5.759751000
C	3.440383000	-19.704095000	-5.555005000
C	2.647089000	-20.599070000	-6.303519000
C	1.809068000	-20.085944000	-7.284112000
C	1.723310000	-18.681307000	-7.482838000
C	2.476007000	-17.804083000	-6.719897000
O	1.025955000	-20.738644000	-8.153838000
C	3.837665000	-16.321421000	-10.429988000
O	3.944346000	-17.549827000	-10.461385000
N	9.886579000	-16.470621000	-3.568999000
C	9.599338000	-15.444268000	-5.797943000
C	6.559288000	-13.732792000	-9.302302000
C	7.797930000	-13.152112000	-9.999826000
C	8.309965000	-11.887650000	-9.307769000
O	0.883538000	-18.385596000	-8.482573000
C	10.551477000	-14.252554000	-5.656410000
C	11.184053000	-13.871252000	-7.001658000
C	11.950852000	-12.547733000	-6.987318000
N	3.100943000	-15.570941000	-11.269153000
C	2.295999000	-16.033306000	-12.397253000
C	2.068291000	-14.770128000	-13.259027000
N	1.649043000	-14.954038000	-14.532551000
C	1.189041000	-13.830326000	-15.352811000
C	0.957937000	-16.681033000	-11.928065000
O	2.270242000	-13.646861000	-12.774317000
C	2.268116000	-13.317777000	-16.334787000
C	0.128721000	-17.241418000	-13.059926000

C	0.467061000	-18.464756000	-13.647524000
C	-0.283845000	-18.999637000	-14.715706000
C	-1.368724000	-18.276499000	-15.195016000
C	-1.698631000	-17.021273000	-14.621646000
C	-0.976937000	-16.511207000	-13.556338000
O	-2.197051000	-18.580795000	-16.200696000
C	-0.020923000	-14.258677000	-16.207129000
O	0.024543000	-15.291186000	-16.871369000
C	3.505834000	-12.713528000	-15.662626000
C	4.515995000	-12.168305000	-16.681297000
C	5.735860000	-11.520138000	-16.026149000
N	6.676485000	-11.018253000	-17.043045000
O	-2.734083000	-16.459867000	-15.257150000
N	9.598797000	-11.440858000	-9.874066000
N	12.456862000	-12.244707000	-8.331718000
C	-18.589724000	-18.535732000	-21.099046000
C	-18.203584000	-19.808362000	-20.339008000
N	-18.196084000	-20.979364000	-21.228726000
N	-1.056036000	-13.375970000	-16.200796000
C	-2.076156000	-13.312156000	-17.244329000
C	-1.663030000	-12.168487000	-18.205270000
N	-2.620558000	-11.690458000	-19.036739000
C	-2.322134000	-10.635763000	-19.980019000
C	-3.499787000	-13.217201000	-16.622671000
O	-0.513320000	-11.718246000	-18.230460000
C	-3.595107000	-10.225888000	-20.750280000
C	-4.668919000	-13.283117000	-17.602719000
C	-4.749169000	-14.312537000	-18.549842000
C	-5.819380000	-14.387386000	-19.461031000
C	-6.829794000	-13.437560000	-19.391990000
C	-6.784290000	-12.418146000	-18.414681000
C	-5.707550000	-12.314413000	-17.542440000
O	-7.927562000	-13.332104000	-20.158873000
C	-1.770038000	-9.400202000	-19.267567000
O	-2.129864000	-8.957314000	-18.201642000
C	-4.194267000	-11.331219000	-21.632159000
C	-5.510814000	-10.886747000	-22.281208000
C	-6.235158000	-11.997955000	-23.045136000
N	-7.537003000	-11.503076000	-23.523613000
O	-7.882977000	-11.630142000	-18.493572000
O	-0.855292000	-8.753520000	-20.045369000
C	-17.046025000	-14.395325000	-20.183714000
N	-16.373092000	-14.828939000	-19.087634000
C	-18.566428000	-14.676987000	-20.205891000
O	-16.515073000	-13.814013000	-21.130854000
C	-14.916443000	-14.925679000	-19.028926000
C	-14.630236000	-16.331332000	-18.465147000
N	-13.398154000	-16.848504000	-18.639105000
C	-13.111005000	-18.218495000	-18.213620000
C	-14.282778000	-13.789909000	-18.164984000

O	-15.526934000	-16.955199000	-17.876533000
C	-13.701654000	-19.228261000	-19.225022000
C	-12.862834000	-13.418295000	-18.542281000
C	-11.756793000	-13.783944000	-17.762478000
C	-10.466533000	-13.378651000	-18.118187000
C	-10.216362000	-12.587500000	-19.252036000
C	-11.337940000	-12.235891000	-20.023406000
C	-12.629471000	-12.642301000	-19.688032000
B	-8.713080000	-12.119775000	-19.671705000
C	-11.586022000	-18.363840000	-18.116851000
O	-10.868075000	-17.905844000	-19.005103000
N	-19.297399000	-13.569210000	-20.840034000
C	-18.846017000	-15.982800000	-20.985323000
C	-13.847224000	-20.657725000	-18.689004000
C	-14.601790000	-21.554986000	-19.680296000
C	-15.044845000	-22.897088000	-19.098869000
C	-18.484910000	-17.272503000	-20.233253000
N	-15.953773000	-23.584506000	-20.036009000
N	-11.135851000	-19.034130000	-17.035497000
C	-9.725975000	-19.250062000	-16.737675000
C	-9.702875000	-20.288471000	-15.599522000
N	-8.494327000	-20.785423000	-15.266846000
C	-8.318024000	-21.684041000	-14.129975000
C	-9.022054000	-17.915030000	-16.352056000
O	-10.748173000	-20.626305000	-15.026681000
C	-8.604643000	-23.152956000	-14.523733000
C	-7.508393000	-17.936505000	-16.367622000
C	-6.770064000	-17.736527000	-15.194318000
C	-5.382398000	-17.600218000	-15.239373000
C	-4.663331000	-17.661126000	-16.444415000
C	-5.413441000	-17.915876000	-17.604876000
C	-6.803038000	-18.046617000	-17.576894000
B	-3.073202000	-17.347202000	-16.468742000
C	-6.862951000	-21.509902000	-13.666730000
O	-5.974962000	-21.311037000	-14.489239000
C	-8.644949000	-24.124964000	-13.336619000
C	-8.893890000	-25.577489000	-13.762286000
C	-8.926910000	-26.544363000	-12.577478000
N	-9.153051000	-27.926881000	-13.035008000
N	-6.641617000	-21.586869000	-12.326632000
C	-5.302625000	-21.509616000	-11.769952000
C	-5.116201000	-22.673885000	-10.779150000
N	-3.821252000	-22.933713000	-10.456621000
C	-3.388369000	-23.892199000	-9.443636000
C	-5.047725000	-20.113146000	-11.117129000
O	-6.070703000	-23.295496000	-10.311950000
C	-1.846673000	-23.783077000	-9.356987000
C	-3.629938000	-19.938077000	-10.617252000
C	-2.553291000	-20.043473000	-11.509477000
C	-1.238350000	-20.002541000	-11.043425000

C	-0.921773000	-19.830827000	-9.684399000
C	-2.010043000	-19.692527000	-8.806385000
C	-3.338054000	-19.748783000	-9.256674000
B	0.630564000	-19.690988000	-9.238066000
C	-4.031785000	-23.652714000	-8.065840000
O	-4.385074000	-24.564197000	-7.353277000
C	-1.164774000	-24.534601000	-8.208490000
C	0.356403000	-24.326262000	-8.258245000
C	1.080032000	-24.785648000	-6.992734000
N	2.532873000	-24.612474000	-7.153539000
O	-4.102828000	-22.374821000	-7.647491000
H	6.509796000	-15.316707000	-5.196370000
H	8.461364000	-15.004626000	-4.010237000
H	5.975723000	-17.897253000	-6.417118000
H	4.948637000	-17.363368000	-8.538588000
H	4.014644000	-14.696233000	-8.988620000
H	4.784715000	-17.894295000	-4.187605000
H	3.867869000	-16.477335000	-4.717517000
H	6.580327000	-15.636850000	-10.359680000
H	5.529578000	-14.415587000	-11.069584000
H	4.136493000	-20.101105000	-4.817540000
H	2.710050000	-21.672736000	-6.139505000
H	2.392267000	-16.733135000	-6.889246000
H	9.436386000	-16.592140000	-2.660575000
H	10.033803000	-17.427326000	-3.902380000
H	10.139053000	-16.311998000	-6.202571000
H	8.825743000	-15.194880000	-6.536817000
H	6.840995000	-14.110589000	-8.314326000
H	5.832177000	-12.930106000	-9.114339000
H	7.559201000	-12.913362000	-11.048095000
H	8.604219000	-13.897468000	-10.026151000
H	8.471094000	-12.092381000	-8.241706000
H	7.525891000	-11.112738000	-9.364869000
H	11.324337000	-14.487239000	-4.914240000
H	9.989338000	-13.392161000	-5.260847000
H	10.392387000	-13.795502000	-7.761526000
H	11.858490000	-14.666300000	-7.345604000
H	12.807301000	-12.622550000	-6.301849000
H	11.288695000	-11.762409000	-6.571004000
H	3.067608000	-14.559550000	-11.165711000
H	2.863185000	-16.780341000	-12.962751000
H	1.334279000	-15.878178000	-14.816428000
H	0.919613000	-13.024536000	-14.662670000
H	1.223245000	-17.472659000	-11.221710000
H	0.394829000	-15.920844000	-11.372887000
H	2.555640000	-14.156632000	-16.981107000
H	1.789759000	-12.571563000	-16.983677000
H	1.294911000	-19.036856000	-13.234349000
H	-0.022413000	-19.955655000	-15.162562000
H	-1.252234000	-15.552627000	-13.121600000

H	3.991336000	-13.469074000	-15.032236000
H	3.196716000	-11.909005000	-14.981562000
H	4.017693000	-11.425233000	-17.323624000
H	4.858531000	-12.970153000	-17.348474000
H	6.266980000	-12.268910000	-15.423605000
H	5.390719000	-10.739673000	-15.322179000
H	7.444226000	-10.529415000	-16.582692000
H	6.200506000	-10.312993000	-17.606552000
H	9.807262000	-10.502233000	-9.533953000
H	9.502062000	-11.350715000	-10.886151000
H	12.928111000	-11.340329000	-8.320689000
H	11.655648000	-12.140874000	-8.962733000
H	-17.920092000	-18.425417000	-21.966381000
H	-19.603598000	-18.649302000	-21.506609000
H	-18.937698000	-19.995032000	-19.543081000
H	-17.238777000	-19.630002000	-19.830996000
H	-17.819376000	-21.790168000	-20.731882000
H	-17.528487000	-20.805723000	-21.981381000
H	-0.888308000	-12.504175000	-15.715991000
H	-2.013713000	-14.258967000	-17.788136000
H	-3.576195000	-12.019781000	-18.925398000
H	-1.550395000	-10.971994000	-20.682850000
H	-3.548807000	-14.054573000	-15.916522000
H	-3.569158000	-12.290595000	-16.035287000
H	-4.340837000	-9.896614000	-20.014733000
H	-3.351699000	-9.352008000	-21.369234000
H	-3.993628000	-15.093768000	-18.555171000
H	-5.874394000	-15.193932000	-20.187085000
H	-5.677235000	-11.513381000	-16.806623000
H	-4.382285000	-12.229982000	-21.032449000
H	-3.464439000	-11.618508000	-22.404221000
H	-5.345203000	-10.031787000	-22.952794000
H	-6.188034000	-10.536543000	-21.491173000
H	-6.324440000	-12.874718000	-22.384584000
H	-5.631443000	-12.301871000	-23.914402000
H	-8.106795000	-11.337142000	-22.684474000
H	-8.007669000	-12.272358000	-24.002751000
H	-0.603243000	-7.966006000	-19.528588000
H	-16.834708000	-15.462039000	-18.440626000
H	-18.943898000	-14.787655000	-19.180239000
H	-14.536437000	-14.832526000	-20.050385000
H	-12.655187000	-16.337373000	-19.106792000
H	-13.589703000	-18.368748000	-17.240704000
H	-14.934233000	-12.919065000	-18.303889000
H	-14.347968000	-14.066223000	-17.104680000
H	-14.697474000	-18.861629000	-19.495854000
H	-13.084635000	-19.208307000	-20.132325000
H	-11.909383000	-14.376467000	-16.860292000
H	-9.631047000	-13.675881000	-17.487746000
H	-11.183910000	-11.609846000	-20.898858000

H	-13.475774000	-12.343499000	-20.307878000
H	-19.186922000	-12.741916000	-20.250579000
H	-18.764121000	-13.337883000	-21.682494000
H	-19.913264000	-15.980901000	-21.239771000
H	-18.294576000	-15.935937000	-21.935261000
H	-14.408208000	-20.621384000	-17.743320000
H	-12.865809000	-21.088546000	-18.451053000
H	-13.979103000	-21.726984000	-20.571667000
H	-15.501696000	-21.034643000	-20.030190000
H	-15.606206000	-22.720253000	-18.172674000
H	-14.159888000	-23.497128000	-18.822276000
H	-19.143791000	-17.374099000	-19.357382000
H	-17.465504000	-17.206695000	-19.834477000
H	-16.235128000	-24.482373000	-19.643137000
H	-15.444179000	-23.805684000	-20.891975000
H	-11.765839000	-19.401632000	-16.328825000
H	-9.229914000	-19.658611000	-17.625374000
H	-7.642714000	-20.415057000	-15.684402000
H	-9.021466000	-21.383140000	-13.345094000
H	-9.375503000	-17.175065000	-17.077695000
H	-9.390500000	-17.603970000	-15.366290000
H	-9.571922000	-23.163515000	-15.039342000
H	-7.841762000	-23.464427000	-15.249066000
H	-7.296214000	-17.638591000	-14.244196000
H	-4.840357000	-17.389025000	-14.321130000
H	-4.896385000	-17.957091000	-18.560749000
H	-7.356182000	-18.170594000	-18.507884000
H	-9.439645000	-23.811795000	-12.642359000
H	-7.707012000	-24.075307000	-12.768857000
H	-8.098602000	-25.889407000	-14.457172000
H	-9.838492000	-25.661244000	-14.315919000
H	-9.758832000	-26.275631000	-11.913202000
H	-8.002488000	-26.419810000	-11.986525000
H	-9.144153000	-28.549776000	-12.227308000
H	-8.356297000	-28.213855000	-13.604902000
H	-7.363781000	-21.922862000	-11.701574000
H	-4.610437000	-21.621725000	-12.608389000
H	-3.112241000	-22.320082000	-10.846392000
H	-3.691894000	-24.904646000	-9.727483000
H	-5.279426000	-19.375552000	-11.895034000
H	-5.768467000	-19.967173000	-10.302473000
H	-1.439749000	-24.124405000	-10.318406000
H	-1.580163000	-22.720967000	-9.272584000
H	-2.736473000	-20.132253000	-12.579403000
H	-0.425199000	-20.069119000	-11.755322000
H	-1.820138000	-19.522946000	-7.747922000
H	-4.158446000	-19.608010000	-8.551130000
H	-1.413053000	-25.605075000	-8.244608000
H	-1.551695000	-24.162528000	-7.250933000
H	0.567393000	-23.257110000	-8.399552000

H	0.784253000	-24.852445000	-9.122507000
H	0.662236000	-24.232707000	-6.132040000
H	0.883581000	-25.852317000	-6.806776000
H	2.713980000	-23.649252000	-7.439312000
H	2.994149000	-24.723640000	-6.251015000
H	-3.741230000	-21.756711000	-8.318569000
O	1.482300000	-19.782319000	-10.393795000
H	2.316884000	-19.314354000	-10.236846000
O	-2.682201000	-16.721858000	-17.711758000
H	-1.734192000	-16.517081000	-17.642706000
O	-8.774715000	-11.062416000	-20.688365000
H	-8.137522000	-10.391646000	-20.405214000

ABA-BAB-i

C	9.184864000	-17.520274000	-6.604097000
N	7.915777000	-17.049607000	-6.542458000
C	10.260156000	-16.591526000	-5.997803000
O	9.511920000	-18.573525000	-7.151549000
C	6.792721000	-17.555505000	-7.340533000
C	6.164067000	-16.284091000	-7.939979000
N	5.965738000	-16.269563000	-9.275565000
C	5.381125000	-15.138940000	-9.986657000
C	5.799639000	-18.362651000	-6.472550000
O	5.956451000	-15.308619000	-7.208438000
C	6.446256000	-14.133268000	-10.494339000
C	4.707054000	-19.087018000	-7.238546000
C	5.023728000	-19.959310000	-8.284798000
C	4.027681000	-20.692231000	-8.960050000
C	2.709679000	-20.547282000	-8.554455000
C	2.374469000	-19.677702000	-7.488398000
C	3.356546000	-18.941163000	-6.839764000
O	1.616345000	-21.142744000	-9.053862000
C	4.621604000	-15.723116000	-11.196389000
O	4.996265000	-16.772232000	-11.719229000
N	11.408159000	-17.341232000	-5.475468000
C	10.715058000	-15.627534000	-7.113947000
C	7.100179000	-13.281610000	-9.398240000
C	8.179696000	-12.332345000	-9.938958000
C	8.657945000	-11.335732000	-8.881686000
O	1.050796000	-19.691252000	-7.257575000
C	11.594322000	-14.463493000	-6.646101000
C	12.001254000	-13.557452000	-7.815751000
C	12.656335000	-12.239829000	-7.398565000
N	3.596655000	-14.963754000	-11.640536000
C	2.625336000	-15.398189000	-12.647645000
C	1.851092000	-14.124585000	-13.017598000

N	1.481392000	-13.972158000	-14.309690000
C	0.613140000	-12.882281000	-14.743317000
C	1.694350000	-16.483630000	-12.036035000
O	1.612024000	-13.283109000	-12.143569000
C	1.398573000	-11.629709000	-15.208111000
C	-6.212845000	-18.261544000	-17.958473000
C	-6.899022000	-17.898021000	-16.794179000
C	-6.221701000	-17.902613000	-15.550696000
C	-4.896353000	-18.300764000	-15.509641000
C	-4.209116000	-18.678847000	-16.689805000
C	-4.860100000	-18.651480000	-17.916019000
O	-4.107670000	-18.424211000	-14.432338000
C	-0.208730000	-13.380672000	-15.947496000
O	0.292014000	-14.145227000	-16.771168000
C	2.245424000	-10.943958000	-14.129868000
C	2.898974000	-9.651227000	-14.636276000
C	3.720833000	-8.939317000	-13.561282000
N	4.328657000	-7.707020000	-14.092409000
O	-2.951221000	-19.051238000	-16.418545000
N	9.797827000	-10.532788000	-9.367804000
N	12.935809000	-11.419165000	-8.583595000
C	-18.578574000	-19.258675000	-20.075291000
C	-18.190241000	-19.795263000	-18.694033000
N	-18.346806000	-21.255483000	-18.623560000
N	-1.442641000	-12.840786000	-16.049396000
C	-2.308316000	-12.959590000	-17.214483000
C	-3.276536000	-11.758864000	-17.128092000
N	-4.060167000	-11.549947000	-18.220069000
C	-5.007019000	-10.451601000	-18.296024000
C	-3.017347000	-14.345817000	-17.290511000
O	-3.306787000	-11.024873000	-16.138028000
C	-5.218561000	-10.011218000	-19.757973000
C	-3.986947000	-14.496348000	-18.448932000
C	-3.580281000	-14.318019000	-19.776360000
C	-4.495477000	-14.423443000	-20.853343000
C	-5.818276000	-14.740711000	-20.580323000
C	-6.238322000	-14.932788000	-19.234324000
C	-5.348443000	-14.782058000	-18.174503000
O	-6.830527000	-14.936237000	-21.434776000
C	-6.380129000	-10.722822000	-17.639451000
O	-7.111529000	-9.793591000	-17.369787000
C	-3.959630000	-9.415757000	-20.400728000
C	-4.199444000	-8.905920000	-21.827121000
C	-2.954797000	-8.270827000	-22.449300000
N	-3.235668000	-7.788259000	-23.810233000
O	-7.525334000	-15.262871000	-19.183399000
O	-6.748042000	-11.987224000	-17.413325000
C	-16.683802000	-15.689401000	-22.109579000
N	-15.917517000	-15.409521000	-21.027077000
C	-18.210350000	-15.745772000	-21.868426000

O	-16.231063000	-15.895060000	-23.237615000
C	-14.467697000	-15.580463000	-20.990722000
C	-14.177653000	-16.342507000	-19.675945000
N	-13.023802000	-17.029780000	-19.592432000
C	-12.715932000	-17.850684000	-18.426180000
C	-13.733192000	-14.213695000	-21.110927000
O	-15.025993000	-16.346058000	-18.769949000
C	-13.524542000	-19.174422000	-18.474349000
C	-12.227646000	-14.349426000	-21.090257000
C	-11.475796000	-13.906769000	-19.996564000
C	-10.110823000	-14.191891000	-19.902222000
C	-9.442651000	-14.951785000	-20.875283000
C	-10.199479000	-15.334809000	-21.998696000
C	-11.556378000	-15.033488000	-22.117448000
B	-7.957999000	-15.573034000	-20.636899000
C	-11.199274000	-18.122426000	-18.433864000
O	-10.570630000	-18.102337000	-19.495515000
N	-18.943775000	-15.210206000	-23.026051000
C	-18.651766000	-17.205702000	-21.617060000
C	-13.731638000	-19.866378000	-17.120373000
C	-14.662417000	-21.080577000	-17.250954000
C	-15.166565000	-21.625673000	-15.915217000
C	-18.292289000	-17.758682000	-20.230055000
N	-16.222087000	-22.633914000	-16.140295000
N	-10.677921000	-18.424583000	-17.231518000
C	-9.293216000	-18.812569000	-16.983712000
C	-9.335825000	-19.680530000	-15.706588000
N	-8.212399000	-20.358181000	-15.387520000
C	-8.090647000	-21.079267000	-14.120003000
C	-8.370075000	-17.561041000	-16.852016000
O	-10.367101000	-19.732865000	-15.017389000
C	-8.652204000	-22.514687000	-14.239106000
C	0.617127000	-17.049048000	-12.930732000
C	0.818147000	-18.240875000	-13.641239000
C	-0.238790000	-18.854246000	-14.315640000
C	-1.534708000	-18.311713000	-14.316252000
C	-1.697764000	-17.078588000	-13.663534000
C	-0.652811000	-16.460426000	-12.978552000
B	-2.812347000	-19.118737000	-14.894747000
C	-6.596776000	-21.126526000	-13.731389000
O	-5.753601000	-21.432362000	-14.573510000
C	-8.798102000	-23.232365000	-12.889961000
C	-9.239621000	-24.694155000	-13.032077000
C	-9.364817000	-25.406993000	-11.684742000
N	-9.770957000	-26.812850000	-11.867311000
N	-6.338988000	-20.845874000	-12.431027000
C	-5.048203000	-21.000618000	-11.767342000
C	-5.258684000	-21.990918000	-10.601191000
N	-4.145864000	-22.594724000	-10.113698000
C	-4.171193000	-23.375844000	-8.875432000

C	-4.518711000	-19.614552000	-11.277822000
O	-6.389444000	-22.199479000	-10.143547000
C	-4.274143000	-24.887914000	-9.171240000
C	-3.203163000	-19.701311000	-10.531254000
C	-2.046559000	-20.167744000	-11.177398000
C	-0.877134000	-20.396604000	-10.449022000
C	-0.794830000	-20.171469000	-9.064015000
C	-1.936709000	-19.623067000	-8.454590000
C	-3.118465000	-19.399987000	-9.165868000
B	0.457576000	-20.718381000	-8.204094000
C	-2.927429000	-23.056072000	-8.033392000
O	-2.994187000	-22.743672000	-6.854469000
C	-4.350176000	-25.755559000	-7.908397000
C	-4.462156000	-27.254066000	-8.216713000
C	-4.472692000	-28.124920000	-6.960089000
N	-4.598133000	-29.551494000	-7.307408000
O	-1.809178000	-23.199752000	-8.728264000
O	0.037515000	-21.933745000	-7.412918000
O	-2.770316000	-20.491192000	-14.437314000
O	-7.942846000	-16.988583000	-20.907645000
H	7.734643000	-16.144307000	-6.122603000
H	9.827338000	-16.004283000	-5.175924000
H	7.214970000	-18.196774000	-8.116817000
H	6.005594000	-17.129364000	-9.817185000
H	4.691597000	-14.626515000	-9.306743000
H	6.413796000	-19.073154000	-5.900280000
H	5.355692000	-17.672909000	-5.744278000
H	7.206398000	-14.701031000	-11.047115000
H	5.961786000	-13.467572000	-11.222234000
H	6.063637000	-20.104065000	-8.574494000
H	4.278783000	-21.362128000	-9.777701000
H	3.087363000	-18.271281000	-6.026124000
H	11.109818000	-17.835563000	-4.633293000
H	11.574179000	-18.087675000	-6.156136000
H	11.245601000	-16.219655000	-7.872605000
H	9.823180000	-15.223249000	-7.612076000
H	7.534232000	-13.927205000	-8.627947000
H	6.318901000	-12.700359000	-8.888547000
H	7.786638000	-11.774540000	-10.803652000
H	9.041179000	-12.906256000	-10.305921000
H	8.993694000	-11.880976000	-7.990479000
H	7.800327000	-10.715608000	-8.567073000
H	12.477725000	-14.859185000	-6.130524000
H	11.037393000	-13.871927000	-5.902655000
H	11.106851000	-13.316277000	-8.408757000
H	12.679793000	-14.090607000	-8.494254000
H	13.606794000	-12.443060000	-6.884541000
H	12.002176000	-11.742444000	-6.654813000
H	3.255241000	-14.188549000	-11.080344000
H	3.161954000	-15.806668000	-13.508919000

H	1.569892000	-14.740990000	-14.967550000
H	-0.035318000	-12.612581000	-13.902907000
H	2.353489000	-17.287797000	-11.693933000
H	1.238284000	-16.037649000	-11.143676000
H	2.032012000	-11.926379000	-16.054713000
H	0.665218000	-10.911196000	-15.601829000
H	-6.717314000	-18.195156000	-18.919995000
H	-6.737349000	-17.627939000	-14.632404000
H	-4.330131000	-18.925334000	-18.824245000
H	3.020599000	-11.633751000	-13.776317000
H	1.618922000	-10.727910000	-13.255551000
H	2.116510000	-8.965341000	-14.999062000
H	3.548844000	-9.858167000	-15.497029000
H	4.536651000	-9.596672000	-13.232867000
H	3.080980000	-8.769495000	-12.675802000
H	4.831232000	-7.229593000	-13.344275000
H	3.582328000	-7.068717000	-14.370216000
H	9.970260000	-9.766303000	-8.717598000
H	9.540022000	-10.091801000	-10.251384000
H	13.333218000	-10.526419000	-8.291771000
H	12.044879000	-11.199730000	-9.040188000
H	-18.007430000	-19.807546000	-20.840594000
H	-19.637910000	-19.478133000	-20.267194000
H	-18.844442000	-19.349110000	-17.932135000
H	-17.167958000	-19.446574000	-18.462485000
H	-17.961355000	-21.600580000	-17.740231000
H	-17.753600000	-21.674556000	-19.341303000
H	-1.781649000	-12.179765000	-15.357050000
H	-1.692257000	-12.844816000	-18.114932000
H	-4.034172000	-12.249530000	-18.961563000
H	-4.590029000	-9.620526000	-17.720145000
H	-2.216693000	-15.092003000	-17.341242000
H	-3.541122000	-14.514144000	-16.343642000
H	-5.572921000	-10.869073000	-20.347089000
H	-6.026181000	-9.270697000	-19.758200000
H	-2.530038000	-14.133147000	-19.998211000
H	-4.161531000	-14.306574000	-21.881289000
H	-5.673248000	-15.005105000	-17.161369000
H	-3.159638000	-10.167614000	-20.410243000
H	-3.595813000	-8.588777000	-19.772512000
H	-5.012250000	-8.162484000	-21.814142000
H	-4.539839000	-9.723915000	-22.474072000
H	-2.160525000	-9.025020000	-22.522398000
H	-2.576513000	-7.482928000	-21.770012000
H	-2.400394000	-7.347964000	-24.194700000
H	-3.940541000	-7.052290000	-23.761655000
H	-6.091666000	-12.649278000	-17.729543000
H	-16.332540000	-15.429074000	-20.099252000
H	-18.474181000	-15.139660000	-20.991268000
H	-14.183002000	-16.200709000	-21.845225000

H	-12.286732000	-16.943247000	-20.288990000
H	-13.002685000	-17.292445000	-17.527854000
H	-14.088569000	-13.765461000	-22.048279000
H	-14.071577000	-13.565714000	-20.292737000
H	-14.511511000	-18.923236000	-18.877177000
H	-13.046012000	-19.853594000	-19.192644000
H	-11.974583000	-13.368955000	-19.190185000
H	-9.556456000	-13.868526000	-19.024839000
H	-9.718130000	-15.930902000	-22.771358000
H	-12.113061000	-15.365887000	-22.994893000
H	-18.716162000	-14.217429000	-23.108719000
H	-18.497678000	-15.628570000	-23.846790000
H	-19.738306000	-17.240659000	-21.765737000
H	-18.205658000	-17.835789000	-22.399960000
H	-14.186738000	-19.141705000	-16.428774000
H	-12.776957000	-20.168997000	-16.672587000
H	-14.148799000	-21.882154000	-17.803893000
H	-15.540719000	-20.808303000	-17.849294000
H	-15.616643000	-20.807403000	-15.338927000
H	-14.317969000	-22.003328000	-15.319617000
H	-18.851893000	-17.199292000	-19.464736000
H	-17.231846000	-17.582016000	-20.013384000
H	-16.536600000	-23.001811000	-15.242601000
H	-15.817394000	-23.430105000	-16.634371000
H	-11.266144000	-18.486226000	-16.406371000
H	-8.938551000	-19.408290000	-17.830862000
H	-7.353353000	-20.180510000	-15.901563000
H	-8.674634000	-20.532135000	-13.371577000
H	-8.574561000	-16.925788000	-17.718637000
H	-8.680147000	-17.003496000	-15.958279000
H	-9.631148000	-22.443687000	-14.727599000
H	-7.989612000	-23.079612000	-14.907308000
H	1.795696000	-18.722007000	-13.607794000
H	-0.070690000	-19.812883000	-14.802037000
H	-2.689201000	-16.634385000	-13.639609000
H	-0.837954000	-15.544474000	-12.416540000
H	-9.532011000	-22.690966000	-12.274010000
H	-7.854690000	-23.194639000	-12.331211000
H	-8.506356000	-25.231586000	-13.653693000
H	-10.199950000	-24.760098000	-13.561321000
H	-10.139985000	-24.913960000	-11.083074000
H	-8.417615000	-25.289414000	-11.129628000
H	-9.796442000	-27.270912000	-10.956022000
H	-9.036144000	-27.294420000	-12.387318000
H	-7.121361000	-20.788721000	-11.790290000
H	-4.341425000	-21.393050000	-12.501685000
H	-3.236001000	-22.284510000	-10.442762000
H	-5.045250000	-23.059062000	-8.302588000
H	-4.428892000	-19.000076000	-12.180413000
H	-5.286753000	-19.164702000	-10.633791000

H	-5.169995000	-25.040505000	-9.786491000
H	-3.408751000	-25.181720000	-9.778486000
H	-2.076939000	-20.370132000	-12.246310000
H	-0.004476000	-20.788079000	-10.965761000
H	-1.921680000	-19.401880000	-7.387029000
H	-3.997598000	-19.015961000	-8.648119000
H	-5.211860000	-25.441555000	-7.301210000
H	-3.462462000	-25.577615000	-7.286852000
H	-3.614605000	-27.555640000	-8.852032000
H	-5.371214000	-27.460242000	-8.797164000
H	-3.573224000	-27.895008000	-6.359886000
H	-5.338031000	-27.858002000	-6.338533000
H	-3.792078000	-29.819598000	-7.873183000
H	-4.532186000	-30.111793000	-6.457612000
H	-1.013137000	-22.776732000	-8.213947000
H	-0.573809000	-21.643986000	-6.715721000
H	-3.601787000	-20.918732000	-14.705266000
H	-8.718779000	-17.400136000	-20.493840000

I

C	-5.164567000	-0.515704000	2.323579000
C	-4.771580000	-0.518597000	0.974626000
B	-5.850767000	-0.392310000	-0.185637000
C	-8.056163000	0.211340000	-0.344417000
C	-7.287619000	1.183227000	-0.999985000
O	-5.952979000	0.891020000	-0.910102000
O	-7.239246000	-0.732990000	0.217945000
O	-5.428308000	-1.472081000	-1.333653000
C	-7.882177000	2.255544000	-1.646889000
C	-9.286758000	2.334440000	-1.618671000
C	-10.048817000	1.365950000	-0.965806000
C	-9.438005000	0.280061000	-0.312862000
C	-3.394493000	-0.599681000	0.701670000
C	-2.450796000	-0.668765000	1.726745000
C	-2.866690000	-0.665238000	3.060427000
C	-4.228180000	-0.589723000	3.357387000
H	-6.222982000	-0.452772000	2.564871000
H	-5.721736000	-1.170649000	-2.246007000
H	-7.279981000	3.013767000	-2.139355000
H	-9.780573000	3.167023000	-2.111511000
H	-11.131806000	1.448657000	-0.956195000
H	-10.023362000	-0.477155000	0.199904000
H	-3.055693000	-0.615144000	-0.331712000
H	-1.391620000	-0.728371000	1.487488000
H	-2.133869000	-0.721562000	3.861745000
H	-4.560371000	-0.586794000	4.392979000
O	-6.828115000	-3.417457000	-0.239008000
H	-7.311057000	-2.646203000	0.131601000
H	-6.315560000	-3.764698000	0.508893000

H	-5.848418000	-2.354244000	-1.091774000
O	-5.969031000	-0.140848000	-3.556808000
H	-5.682580000	0.600649000	-2.988082000
H	-6.916112000	0.032196000	-3.685440000

TS_{I-II}

C	-5.001298000	0.141950000	2.119884000
C	-4.705766000	-0.525035000	0.917436000
B	-5.721541000	-0.493825000	-0.308121000
C	-8.078739000	-0.000013000	-0.286811000
C	-7.373504000	1.049635000	-0.886298000
O	-6.027407000	0.851528000	-0.869335000
O	-7.195579000	-0.949080000	0.197202000
O	-5.350634000	-1.449389000	-1.384736000
C	-8.051331000	2.137179000	-1.421433000
C	-9.453661000	2.142613000	-1.342205000
C	-10.147859000	1.090173000	-0.745667000
C	-9.458407000	-0.006355000	-0.199719000
C	-3.475781000	-1.197223000	0.837369000
C	-2.577398000	-1.207820000	1.907618000
C	-2.894802000	-0.539292000	3.090261000
C	-4.112717000	0.138536000	3.194468000
H	-5.945952000	0.673325000	2.216901000
H	-5.396549000	-1.021117000	-2.277256000
H	-7.505190000	2.959042000	-1.875018000
H	-10.003180000	2.985270000	-1.752223000
H	-11.232218000	1.116117000	-0.693979000
H	-9.985039000	-0.828155000	0.276158000
H	-3.220176000	-1.715283000	-0.083417000
H	-1.630162000	-1.734836000	1.817407000
H	-2.198779000	-0.544022000	3.925796000
H	-4.366175000	0.663320000	4.112727000
O	-7.017615000	-3.109255000	-0.799501000
H	-7.314858000	-2.150240000	-0.206010000
H	-6.653604000	-3.761799000	-0.175659000
H	-6.172529000	-2.554178000	-1.231617000
O	-5.454233000	0.232011000	-3.539269000
H	-5.452110000	0.852268000	-2.782196000
H	-6.350998000	0.313873000	-3.900280000

II

C	-4.483857000	0.321601000	2.370606000
C	-4.365638000	-0.304516000	1.116924000
B	-5.423483000	-0.070961000	-0.005612000
C	-8.421717000	-0.133709000	-0.274264000
C	-7.560318000	0.971373000	-0.443891000
O	-6.329244000	0.969811000	0.157086000
O	-8.021562000	-1.152174000	0.540976000
O	-5.378773000	-0.844779000	-1.139963000
C	-7.963792000	2.072224000	-1.201783000

C	-9.216696000	2.072162000	-1.825544000
C	-10.063867000	0.969797000	-1.684761000
C	-9.669378000	-0.119879000	-0.904556000
C	-3.262749000	-1.151603000	0.904201000
C	-2.314654000	-1.368374000	1.903607000
C	-2.453467000	-0.736894000	3.142113000
C	-3.540154000	0.109664000	3.375040000
H	-5.330247000	0.977842000	2.553396000
H	-5.917625000	-0.526703000	-1.908756000
H	-7.284492000	2.914862000	-1.295506000
H	-9.526812000	2.932095000	-2.412729000
H	-11.036533000	0.962772000	-2.168269000
H	-10.324732000	-0.975235000	-0.767547000
H	-3.149091000	-1.638490000	-0.061167000
H	-1.467562000	-2.024658000	1.719496000
H	-1.715973000	-0.903635000	3.923569000
H	-3.650007000	0.601008000	4.338565000
O	-6.857563000	-3.201538000	-0.754161000
H	-7.816408000	-1.976830000	0.025256000
H	-6.477043000	-3.724150000	-0.030916000
H	-6.153554000	-2.555098000	-0.981997000
O	-6.735207000	-0.008509000	-3.377284000
H	-6.164422000	0.604541000	-3.865683000
H	-7.482639000	0.538651000	-3.076134000

III

C	-3.908621000	-0.366476000	1.240394000
C	-4.947371000	-1.294574000	1.446565000
B	-6.283948000	-1.191494000	0.684303000
C	-8.296834000	-1.662139000	-0.100004000
C	-7.899645000	-0.449641000	-0.658538000
O	-6.632966000	-0.134660000	-0.168304000
O	-7.302172000	-2.131690000	0.738048000
O	-7.427170000	3.094225000	-2.559934000
C	-8.681108000	0.264916000	-1.548025000
C	-9.923342000	-0.311191000	-1.857151000
C	-10.333302000	-1.528121000	-1.298971000
C	-9.520107000	-2.235323000	-0.401189000
C	-4.734406000	-2.339098000	2.365996000
C	-3.530148000	-2.450320000	3.058346000
C	-2.512421000	-1.518300000	2.840575000
C	-2.702219000	-0.476250000	1.929505000
H	-4.044984000	0.444999000	0.529608000
H	-7.080239000	3.318236000	-1.680935000
H	-8.348701000	1.210826000	-1.978415000
H	-10.580676000	0.205740000	-2.549947000
H	-11.302930000	-1.938065000	-1.566333000
H	-9.825577000	-3.179936000	0.035942000
H	-5.523232000	-3.067197000	2.535298000
H	-3.382526000	-3.262096000	3.765511000

H	-1.571874000	-1.604922000	3.378379000
H	-1.908913000	0.245960000	1.755800000
O	-4.731365000	2.405258000	-3.180861000
H	-4.759695000	1.458449000	-3.385849000
H	-4.704876000	2.436468000	-2.202458000
H	-6.597915000	2.922261000	-3.053712000
O	-5.441272000	2.442772000	-0.453541000
H	-5.913309000	1.597421000	-0.310346000
H	-5.121184000	2.713860000	0.419685000

2.15 Fluorescence Binding of A_3X_3 and B_3X_3

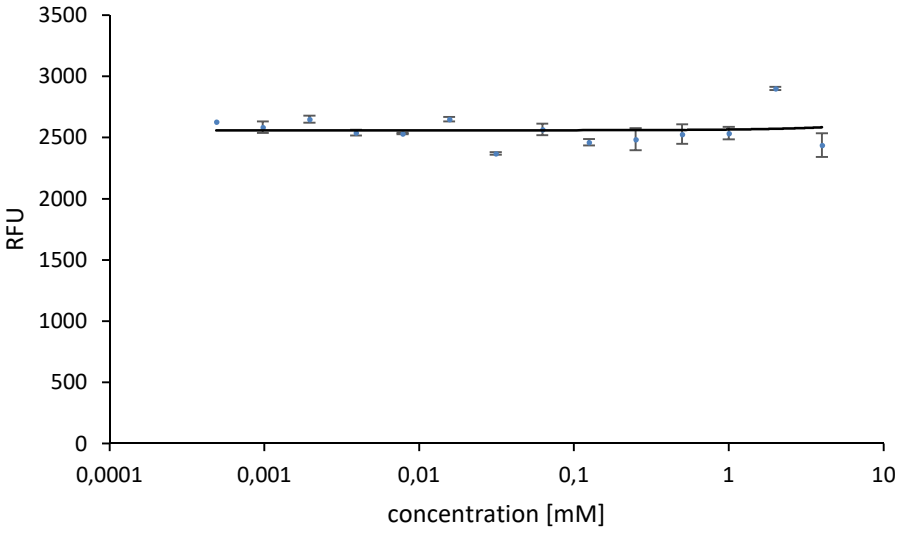

Figure S27. Fluorescence titration of **A_3X_3** against fluorescein labelled **B_3X_3** in 300 mM phosphate buffer, pH 7.4, using the same protocol detailed in Section 7.

2.16 Displacement experiment (Fluorescence Quenching Assay + FRET Assay)

Fluorescence spectra were recorded on an Infinite® M1000 PRO microplate reader (Tecan®). 15 µL of different concentrations of the Lys-Cat-Lys peptide was served (dilutions series with half-to-half concentrations beginning with 5.0 mM, phosphate buffer 300 mM, pH 7.4). To this a constant amount of the Fluorescein-Cys-AEEAc-Bor-Lys-Bor-Lys-Bor-Lys peptide (conc. 110 nM, vol. 15 µL) was added. After mixing for 1 h at 450 rpm, 26 µL of every mixture was placed in black UV Star® 384 microliter well-plates (Greiner bio-one). After 15 min of equilibration time, the fluorescence emission was recorded at 520 nm upon excitation at 488 nm with multiple reads per well (3x3).

After that a dilution series of a trivalent Catechol-tag (Dyelight650®-AEEAc-Cat-Lys-Cat-Lys-Cat-Lys) with 1/3 of the molar amount of the Lys-Cat-Lys peptide was made (26 µL each, phosphate buffer 300 mM, pH 7.4) and dropped into the mixtures. After that the mixtures were stirred for 2 h at 450 rpm and measured with an excitation wavelength of 488 nm and the emission was recorded from 280 nm to 850 nm.

2.17 Alizarin Red S Assay

Fluorescence spectra were recorded on an Infinite® M1000 PRO microplate reader (Tecan®). PEG_{5000}-**$(AX)_3$** (0.104 mM, 1 eq.) and Alizarin Red S (0.313 mM, 1 eq.) was mixed for 90 minutes in a phosphate buffer solution (pH 7.4, 300mM). After that CytC-**$(BX)_3$** was added resulting in a PEG_{5000}-**$(AX)_3$** concentration of 0.09 mM and an Alizarin Red S concentration of 0.27 mM.

The resulting concentrations of CytC-**$(BX)_3$** in the dilution serial is showed in the following table:

Dilution	c [mM]
1	0.09
2	0.045
3	0.0225
4	0.00562
5	0.00281
6	0.00141
7	7.03E-04

The resulting solutions were mixed for 12 h at room temperature. The excitation wavelength was 495 nm and the fluorescence intensity was measured at 556 nm.

2.18 Atomic Force Microscopy

AFM measurements were conducted on a Dimension FastScan Bio™ atomic force microscope from Bruker, which was operated in the PeakForce mode. AFM probes with a nominal spring constant of 0.25 Nm^{-1} were employed (FastScan-D, Bruker) for measurement in liquid. A circular mica disc (15 mm) was used as the substrate. Measurements were performed at scan rates between 0.8 and 2 Hz. Different areas of the mica substrate were scanned in order to ensure the integrity of the shown images. The images were finally processed by the software NanoScope Analysis 1.8.

For sample preparation, the initial sample (conc. **PEG_{5000}-$(AX)_3$**/**CytC-$(BX)_3$** mixture was 1 mM, solvent: phosphate buffer (150 mM, pH 7.4)) was diluted to 25 µM with 40 µL phosphate buffer (75 mM) and subsequently applied onto the freshly cleaved mica substrate. The solution was left to incubate for 15 minutes in order to deposit the desired species on the mica substrate. After successful adsorption, the supernatant was removed and fresh phosphate buffer (250 µL) was added for the measurement.

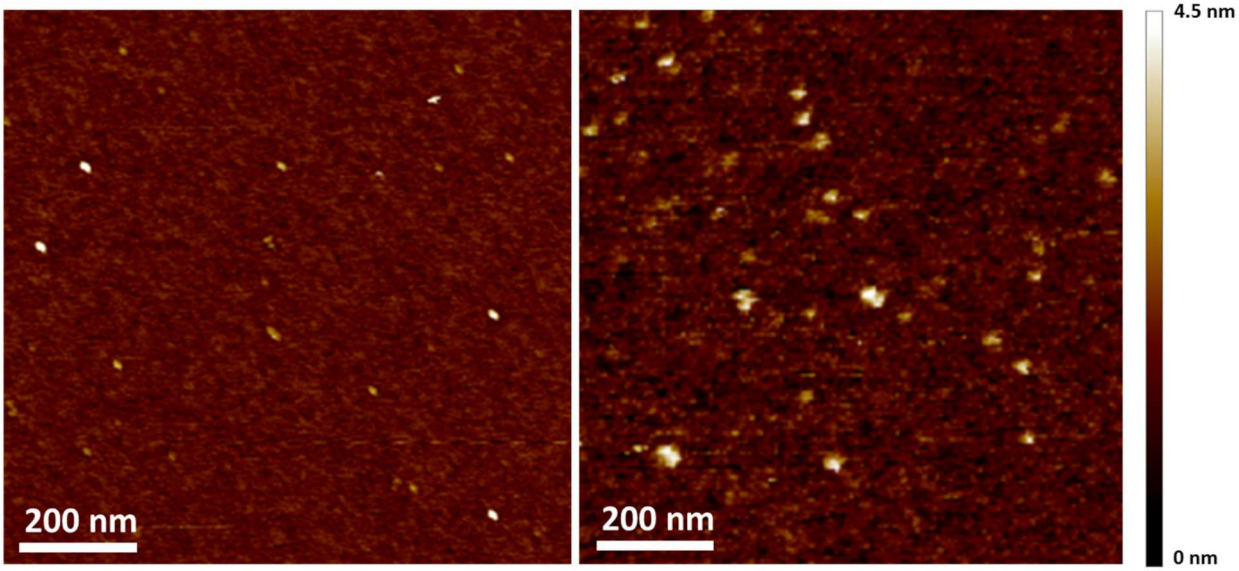

Figure S28. AFM micrograph of **PEG_{5000}-$(AX)_3$** (left) and **PEG_{5000}-$(AX)_3(BX)_3$-CytC** (right).

References:

[1] Lei, H.; Stoakes, M.S.; Schwabacher, A.W.; Herath, K.P.B.; Lee, J. *J. Org. Chem*. **1994**, *59*, 4206.

[2] Feng, Z.; Min, Q.-Q.; Xiao, Y.-L.; Zhang, B.; Zhang, X. *Angew. Chem. Int. Ed*. **2014**, *53*, 1669.

[3] Nakamura, H.; Fujiwara, M.; Yamamoto, Y. *Bull. Chem. Soc. Jpn.* **2000**, *73*, 231.

[4] Duggan, P.J.; Offermann, D.A. *Aust. J. Chem.* **2007**, *60*, 829.

[5] Harris, R. K.; Becker, E. D.; Cabral de Menezes, S. M.; Goodfellow, R.; Granger, P. *Pure and Applied Chemistry* **2001,** *73*, 1795.

[6] Lee, W.; Tonelli, M.; Markley, J. L. *Bioinformatics* **2014,** *31*, 1325.

[7] Bax, A.; Davis, D. G. *Journal of Magnetic Resonance (1969)* **1985,** *65* (2), 355-360.

[8] Frisch, M. J. et al. GAUSSIAN 09 (Revision D.01), Gaussian, Inc.: Wallingford CT, **2009**.

[9] Aitken, D. J.; Eijsberg, H.; Frongia, A.; Ollivier, J.; Piras, P. P., *Synthesis-Stuttgart* **2014,** *46*, 1.

[10] Chai, J.-D.; Head-Gordon, M., *Phys. Chem. Chem. Phys.* **2008,** *10*, 6615.

[11] (a) Cances, E.; Mennucci, B.; Tomasi, J., *J. Chem. Phys.* **1997,** *107*, 3032; (b) Cossi, M.; Barone, V.; Mennucci, B.; Tomasi, J., *Chem. Phys. Lett.* **1998,** *286*, 253; (c) Mennucci, B.; Tomasi, J., *J Chem Phys* **1997,** *106*, 5151; (d) Tomasi, J.; Mennucci, B.; Cammi, R., *Chem. Rev.* **2005,** *105*, 2999.
[12] Marenich, A. V.; Cramer, C. J.; Truhlar, D. G., *J. Phys. Chem. B* **2009,** *113*, 6378.

9 Curriculum Vitae

The content of this section was removed for privacy protection.

Publications

1. M. Pieszka, S. Han, C. Volkmann, R. Graf, I. Lieberwirth, K. Landfester, D. Y. W. Ng, T. Weil, *J. Am. Chem. Soc.* **2020**, *142* (37), 15780–15789.
2. J. Kockelmann, J. Stickdorn, S. Kasmi, J. De Vrieze, M. Pieszka, D. Y. W. Ng, S. A. David, B. G. De Geest, L. Nuhn, *Biomacromolecules* **2020**, *21* (6), 2246-2257.
3. M. Hebel, A. Riegger, M. M. Zegota, G. Kizilsavas,J. Gačanin, M. Pieszka, T. Lückerath, J. A. S. Coelho, M. Wagner, P. M. P. Gois, D. Y. W. Ng, T.Weil, *J. Am. Chem. Soc.* **2019**, *141* (36), 14026-14031.
4. M. Pieszka, A. M. Sobota, J. Gačanin, T. Weil, D. Y. W. Ng, *ChemBioChem* **2019**, *20*, 1376-1381.

Scientific Contributions to Conferences and Symposia

1. Talk at the Highlight's Colloquium of the Max Planck Institute for Polymer Research
   23. November 2020, Mainz (Germany)
2. Poster Presentation at the Poster Day of the Max Planck Institute for Polymer Research
   14. October 2019, Mainz (Germany)
3. Poster Presentation at the 47th World Chemistry Congress of IUPAC
   7.-12. July 2019, Paris (France)
4. Poster Presentation at the Twente / Mainz Mini-Symposium on 'Next Generation (Supra)Molecular Synthetic Materials'
   15. May 2019, Mainz (Germany)

10 Declaration of Originality in Academic Work

Ich versichere hiermit, dass ich diese Doktorarbeit selbstständig angefertigt habe und keine anderen als die angegebenen Quellen und Hilfsmittel benutzt sowie die wörtlich oder inhaltlich übernommenen Stellen als solche kenntlich gemacht habe.

Heidelberg, den 05.04.2021

The signature was removed for privacy protection.

Michaela Pieszka

I hereby declare that this thesis and the work reported herein was composed by and originated entirely from me. Information derived from the published and unpublished work of others has been acknowledged in the text and references are given in the list of sources.

Heidelberg, 05.04.2021

The signature was removed for privacy protection.

Michaela Pieszka

11 Acknowledgement

The content of this section was removed for privacy protection.